UNIVERSAL
LIBRARY

Advances in

ASTRONOMY AND ASTROPHYSICS

VOLUME 2

ADVANCES IN
ASTRONOMY and ASTROPHYSICS

edited by

ZDENĚK KOPAL

Department of Astronomy
University of Manchester
Manchester, England

Volume 2

ACADEMIC PRESS New York and London • 1963

ACADEMIC PRESS INC.
111 FIFTH AVENUE
NEW YORK 3, N. Y.

United Kingdom Edition
Published by
ACADEMIC PRESS INC. (LONDON) LTD.
BERKELEY SQUARE HOUSE, LONDON W. 1

Library of Congress Catalog Card Number 61-18299

PRINTED IN THE UNITED STATES OF AMERICA

CONTRIBUTORS TO VOLUME 2

(Numbers in parentheses indicate the page on which the authors contributions begin.)

J. B. EDSON (1), *Office of Advanced Research and Technology, National Aeronautics and Space Administration, Washington, D.C.*

R. P. KRAFT (43), *Mount Wilson and Palomar Observatories, Carnegie Institute of Washington, California Institute of Technology, Pasadena, California*

F. LINK (87), *Astronomical Institute of the Czechoslovak Academy of Sciences, Prague, Czechoslovakia*

W. J. LUYTEN (199), *Department of Astronomy, University of Minnesota, Minneapolis, Minnesota*

E. J. ÖPIK* (219), *Department of Physics, University of Maryland, College Park, Maryland*

A. D. THACKERAY (263), *Radcliffe Observatory, Pretoria, South Africa*

* Present address: *Armagh Observatory, Armagh, Northern Ireland.*

CONTENTS

CONTRIBUTORS TO VOLUME 2 v

CONTENTS OF VOLUME 1 xi

The Twilight Zone of Venus

J. B. EDSON

I. Introduction 1
II. Twilight Extentsions of the Venus Cusps: Observational Record . . 2
III. Color in the Twilight Cusp Extentions 22
IV. Interpretation of the Brightness Distribution along the Cusp Extention 23
V. Horizontal Refraction across the Twilight Zone at Solar Transit . 26
VI. Twilight Phenomena and the General Circulation of the Venus Atmosphere 29
VII. Relation of the Venus Ultraviolet Clouds to the Twilight Phenomena 30
VIII. Discrepancy between the Observed and Theoretical Times of Dichotomy 33
IX. Observational Methods and Aids 35
References 40

Cataclysmic Variables as Binary Stars

ROBERT P. KRAFT

I. Introduction 43
II. Examples of Well-Known Binaries in Groups (1) and (2) 45
III. Some Common and Related Properties of the Systems Discussed in Section II 54
IV. The Search for New Binaries Among U Geminorum Stars and Novae 56
References 84

Eclipse Phenomena

F. Link

I. General Relations 88
II. Eclipses of the Moon 100
III. Eclipses of the Artificial and Other Satellites 154
References 195

White Dwarfs

W. J. Luyten

I. Introduction 199
II. Historical 200
III. Discovery 201
IV. Magnitudes, Colors, Spectra 203
V. Spectra 206
VI. Motions 208
VII. Luminosities 209
VIII. Masses 210
IX. Red Shift 213
X. Frequency in Space 214
XI. White Dwarfs in Clusters 215
XII. Individually Interesting Stars 216
XIII. Conclusions and Suggestions for Future Work 217
References 217

The Stray Bodies in the Solar System. Part I. Survival of Cometary Nuclei and the Asteroids

Ernst J. Öpik

I. Introduction 220
II. Survival in Encounters 221
III. Dynamical Probabilities of Elimination for Comets and Related Objects 230
IV. Genetic Relationships of Comets and Asteroids 240
V. Capture of Comets into Terrestrial Space and Statistical Balance with Apollo Group 250
References 261

Recent Developments in Studies of the Magellanic Clouds

A. D. Thackeray

I. Introduction 264
II. Form, Brightness, and Distance of the Clouds 265
III. Nebulae and Clusters 275
IV. Variable Stars 280
V. General Stellar Content 288
VI. Dynamics of the Clouds 296
VII. Conclusions 301
References 302

Author Index 305

Subject Index 309

CONTENTS OF VOLUME I

The Shock-Wave Theory of Novae
JOHN HAZLEHURST

The Properties and Problems of T Tauri Stars and Related Objects
G. H. HERBIG

Meteorites and Cosmic Dust
D. W. PARKIN AND W. HUNTER

Distribution of Mass in Oblate Stellar Systems
L. PEREK

Polarization of Starlight
K. SERKOWSKI

The Twilight Zone of Venus

J. B. EDSON
National Aeronautics and Space Administration, Washington, D C

I Introduction 1
II Twilight Extensions of the Venus Cusps Observational Record . 2
III. Color in the Twilight Cusp Extensions 22
IV. Interpretation of the Brightness Distribution along the Cusp Extension 23
V. Horizontal Refraction across the Twilight Zone at Solar Transit . 26
VI. Twilight Phenomena and the General Circulation of the Venus Atmosphere . . 29
VII. Relation of the Venus Ultraviolet Clouds to the Twilight Phenomena 30
VIII Discrepancy between the Observed and Theoretical Times of Dichotomy 33
IX. Observational Methods and Aids 35
References 40

I

INTRODUCTION

The fair, veiled form of Venus moves in prudent nearness to the guardian sun. She is thus seen seldom, and never seen well, by the observers of the night. As her devotees well know, she is best pursued by day, or in bright twilight. And some of her best-kept secrets are reserved for those bold few who will gaze into the very eye of the sun, to find her at inferior conjunction, or at transit. There, her outer and diaphanous draperies gleam in the through-shining sunlight. There, the eye can find a spectacle of rare, delicate beauty. As she approaches within 15 degrees of the sun, out from the needle-pointed cusps of the slim crescent grow two faint, blue-white threads of light. Slender they are, beyond the resolution of any earthly instrument, yet their length makes them easily visible in the smallest of telescopes. As Venus approaches nearer to the sun, these bright threads extend themselves along the dark rim of the planet until at last the dark Cytherean disk stands encircled in a ring of light.

To this vision of the eye, the mind adds broader vision of its own, of high decked, sun-blazed cirrus floating in the clear, thin cytherean air above the dark shoulder of the planet; the twilit sky upon that distant world. Further, a skillful eye-estimate of the angular extension of those threads of light, plus

simple calculation, yields the height of that bright cloud sheet—with an accuracy of a few hundred meters across a distance of some 24,000,000 miles. Of such are the twilight phenomena of Venus. Like some others of Nature's best kept secrets, they lie open to the simplest of access; unseen because they are unsought.

II

TWILIGHT EXTENSIONS OF THE VENUS CUSPS: OBSERVATIONAL RECORD

In 1790, Johann Hieronymus Schroeter of Lilienthal discovered that the thin crescent of Venus near the sun could be seen extended far beyond the half-circle. The phenomenon was confirmed by William Herschel, who engaged

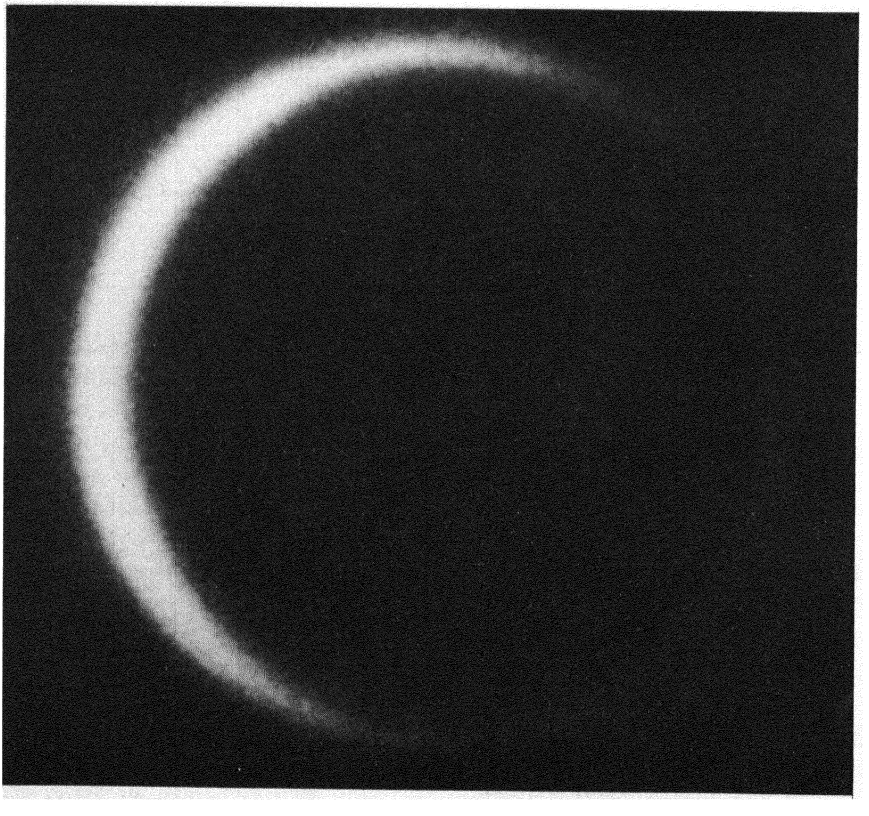

FIG. 1. Venus, 25 June 1940, showing the dark hemisphere outlined in light scattered from material suspended in the Venus atmosphere. Photographed by the Planet Group.

Schroeter in a spirited debate about the measurement and interpretation of it Guthrie in 1842 was the first to see the extensions coalesce into a complete ring (Fig. 1). Since that time, a number of people have seen and measured the cusp extensions. Their results are assembled in Table I.

TABLE I A

OBSERVATIONS OF VENUS CUSP EXTENSIONS, 1790-1898[a]

Observer	Date	Time	Elongation of Venus v'	Cusp extension angle p'	Angular extent of twilight zone s''	Height of scattering layer h(meters)	Minimum elongation at conjunction v_0	Conjunction date
Schroeter	1790 Mar. 12	Daylight	12 42′	15°19′	2 20′	5100	+ 8 4	Mar 18
	1793 May 21	Daylight	9 28	19 28	2 19	5040	1.4	May 27
	1794 Dec. 20	Daylight	19 04	11 56	2 27	5630	3 3	Dec. 30
	Dec 22	Twilight	16 24	13 58	2 33	6120		
	1795 Jan 10	Twilight	12 50	18 09	2 34	6260		
	1794 Dec 15	Twilight	25 20	12 10	3 31	11600	3.3	Dec 30
	17	Twilight	23 00	12 22	3 14	9750		
	18	Twilight	21 35	15 15	3 46			
	19	Twilight	20 24	14 29	3 20	10400		
	20	Twilight	19 04	17 23	3 44			
	22	Twilight	16 25	20 22	3 46			
	23	Twilight	14 42	22 07	3 38	12250		
Herschel	1793 May 20		11 42	15 00	1 54	3400	1 4	May 27
	20		11 42	24 07	3 12	9530		
Guthrie	1842 Dec			90			1 6	Dec. 17
Maedler	1849 May 9		6 16′7	10°	35′	300	− 3 2	May 12
	10		5 7 8	22 5	71	1300		
	11		3 57.1	27.5	65	1100		
	11		3 36 5	27 5	59	900		
	12		3 25 7	30	61	950		
	12		3 25 7	30	61	950		
	12		3 26 4	30	61	450		
	15		6 25 4	17.5	69	1220		
	16		7 36.9	15	71	1300		
Secchi	1857 May 8		4 18′	19 36′		600	+ 3 4	May 9

TABLE I A *(continued)*

Observer	Date	Time	Elongation of Venus v'	Cusp extension angle p°	Angular extent of twilight zone s°	Height of scattering layer h(meters)	Minimum elongation at conjunction v_0	Conjunction date
Lyman	1866 Dec 7		6 25	20	79	1630	+0.5	Dec 11
	10		1 24	90	46.4	550		
	12		1 52	90	65 5	1100		
	12		2 04	90	74	1850		
	14		5 06	25	77	2000		
	15		6 43	15	60	900		
	18		11 23	11	78	1150		
Winnecke	1871 Sept. 25			90 ?			8.2	Sept. 25
Lyman	1874 Dec. 8		0 32'5	90	11.1	100	Transit	Dec 9
	10		2 31 7	49° 41′	68 1	1200		
	11		4 02.5	26 38	63 3	1050		
	11	4 20 4	25 43	25 43	66.7	1100		
	12		5 58.3	17 41	63 4	1050		
Barnard	1890 Nov 29	(Note. S cusp extension longer, more slender than N extension)						
	Dec 1		5 28	45	105′	2800	−0 5	Dec 4
	5		3 28	80	79	1600		
	7			50 ?				
Russell	1898 Nov. 29		4°45′7	37	75	1500	−1 0	Dec 2
	Dec. 2		2 30 0	90	64	1100		
	7		13 11	11.3	66	1150		

[a] Based upon a tabulation by H N. Russell

Henry Norris Russell in 1899 observed the complete circle. He developed the correct concept of interpretation and gave the simple geometric theory required for the calculation of the angular size of the Venus twilight arcs as well as the maximum height h at which the scattering material can be seen above the opaque lower cloud deck of the planet. His approximate equations for those two quantities are:

$$s + 11' = \frac{r}{2\rho} \cdot v \sin p$$

$$h = (\sec s - 1)R$$

TABLE I B

OBSERVATIONS OF VENUS CUSP EXTENSIONS, 1906-1940[a]

Observer	Date	Time	Elongation of Venus ϵ	Cusp prolongation p'	Planetocentric angle of twilight s'	Scattering height h (meters)	Approx minimum elongation at conjunction ϵ'_0	Conjunction Date
Russell	1906 Nov. 27		4.55′	20″	58′	850	1°.2	Nov. 29
	Dec 4		7 23	10 5	45	500		
Daniel	1906 Nov. 27		1.83	90	62	1000	1.2	Nov. 29
Rabe	1913 Apr. 21		8 31	12 46	63 72	1080	1 5 3	Apr. 24
	22		7 24	13 91	61 51	1000		
	27		6.60	16 42	66 80	1150		
	29		8 68	14 09	77 12	1950		
	30		9,95	11 11	68 94	1200		
	May 2		12 60	7 20	54 82	780		
Campbell	1918 Mar. 2	3[h] GMT		N. 2 5 S 4.5			1 7 7	Feb 9
Graff	1921 Apr 12		16 98	5 50	56 77	800	1 5 6	Apr. 22
	13		15 75	7 42	73 88	1450		
	17		10 40	15 73	106 50	1500		
	21		6 57	13 16	51 31	680		
	22		6.06	20 94	79 45	1650		
	23		5 94	12 22	41.34	400		
	26		8 14	9 37	44 19	500		
	May 2		15.35	14 32	147 48	5600		
Richter	1937 Apr. 12		11 30	6 63	43 33	500	6 0	Apr 18
Richter	1940 June 14		18 17	1 72	11 8	100	2 8	June 27
	17		14 49	5 40	46.2	550		
	17		14 05	4 16	31 7	300		
	18		12 64	9 67	78 0	1600		
	19		11 18	11 79	84 8	1850		
	21		8 39	18 83	102 5	2600		
	July 1		8 00	20 94	108 8	3060		
	6		14 93	8 54	82 3	1700		

TABLE I B *(continued)*

Observer	Date	Time	Elongation of Venus ϵ	Cusp prolongation p	Planetocentric angle of twilight s'	Scattering height h (meters)	Approx. minimum elongation at conjunction ϵ_0	Conjunction Date
Rabe	1937 Apr. 12	625 GMT	11 17	13 40	96 87	2400	−6 0	Apr 18
	18	562	6 48	20 73	84.61	1850		
	20	640	7 37	15 62	71.69	1300		
	24	507	11 42	15 04	112 56	3250		
Rabe	1940 June 18	618 GMT	12 74	9 82	77 37	1600	2 8	June 27
	18	660	12 68	11 91	98 77	2500		
	20	615	9 83	18 60	120 48	5900		
	20	656	9 77	19 45	125 44	6300		
	21	592	8 50	16 40	89 64	2060		
	23	457	5 74	21 75	78 18	1600		
	23	468	5.73	28 78	104 69	2780		
Note.								
S. cusp measured →	23	475	5 73	34 56	125 29	4000		
	23	516	5 60	30 07	108 34	3050		
	23	520	5 67	30 47	109.56	3100		
	23	524	5.66	32 55	116 69	3450		
	25	452	3 28	45	86 22	1900		

[a] As collected by W Rabe

where s = twilight arc along the surface of Venus perpendicular to the terminator
$11'$ = allowance for the finite angular size of the sun as seen from Venus, which is $44'$
r = distance from earth to sun
ρ = distance from Venus to sun
ϵ = angle between Venus and sun as seen from earth
R = radius of Venus
p = angle of cusp prolongation beyond the theoretical cusp, as measured from the center of Venus.

Russell reviewed all observations to that date, and reduced those which gave sufficient data for the calculations of s and h. He estimated that for the "brighter

TABLE I C

OBSERVATIONS OF VENUS CUSP EXTENSIONS, 1938–1960

Observer	Date	Time	Elongation of Venus ϵ	Cusp extension angle p°	Angular extent of twilight zone s'	Height of scattering layer h(meters)	Minimum elongation at conjunction ϵ	Conjunction date
Slipher and Edson[a]	1938 Nov 16	15:30 MST	6.52	+ 31.5	2.164	4390	-2.8	Nov. 20
				12.0	0.759	549		
	17	14:30	5.15	+ 23.	1.209	1400		
				−11	0.494	479		
	17	15.30	5.00	+ 35.	0.794	3030		
				15.	0.709	479		
	18	11.40	4.06	+ 45.5	1.813	3080		
				−14	0.494	239		
	19	10:00	3.23	+				
				−90	2.044	3940		
	19	15:00	3.10	+				
				−90	1.953	3600		
	20	14.00	3.00	+ 90.				
				− 90	1.886	3320		
	21	12:00	3.40	+ 80	2.123	4180		
				−25	0.806	597		
	22	10:50	4.61	+ 63	2.699	5950		
				−17	0.796	525		
	24	09.50	7.37	+ 37	2.873	7690		
				16	1.216	1383		
Planet Group: Edson, Wright, Winget, Canright, and Meinel	1940 June	See separate tabulations of results; measurements from photographic record.						

[a] The Slipher-Edson data are the result of measurement of the first photographic record of the Venus cusp extensions (see Fig. 2). In the column headed p': + refers to the advancing cusp, − refers to the retreating cusp, as Venus moves past the sun. Venus passed south of the sun at this conjunction.

TABLE I C *(continued)*

Observer	Date	Time	Elongation of Venus $v°$	Cusp extension angle $p°$	Angular extent of twilight zone $s°$	Height of scattering layer h(meters)	Minimum elongation at conjunction $v_0°$	Conjunction date
Naef	1950 Jan. 22			N. Horn 15°			+7.2	Jan. 31
				S. Horn 15°				
	Jan. 30			N. Horn 23°				
				S. Horn 17°				
	Feb. 2			N. Horn 17°				
				S. Horn 18°				
Tombaugh (unpublished communication)	1950 Jan. 31		7.2°	E. Horn 25°	2°.0	3740	+7.2	Jan. 31
				W. Horn 5°	0.27	57		
Edson	1954 Nov. 14	1200 PST	4°	E. Horn 44°		2610	—3.7	Nov. 15
				W. Horn 19°		540		

portion" of the cusp extensions, that is, those seen by observers through the normal atmospheric haze prevalent at most observing stations, the angular extent s of the twilight zone is about 68′ of arc and the height h of the illuminated scattering layer is in the range of 800 to 1200 meters. For the longer, fainter cusp extensions seen by Schroeter and others in clearer air he calculates s at about 3°21′ and the height of the scattering layer h as around 11,600 meters.

In subsequent years there have been a few more observations as cataloged in Table I. However, the state of knowledge remained substantially unchanged until 1938, when the phenomenon was first photographed at Lowell Observatory.

TABLE I D

DISTRIBUTION OF h VS. POSITION ANGLE.[a] JUNE 1940 INFERIOR CONJUNCTION OF VENUS[b]

Position angle (deg)	No. of observations in 5° interval	h (meters)	Position angle (deg)	No. of observations in 5° interval	h (meters)
5	0	—	185	5	4610
10	0	—	190	4	8650
15	0	—	195	1	11000
20	0	—	200	0	—
25	0	—	205	0	—
30	0	—	210	0	—
35	0	—	215	0	—
40	1	1780	220	0	—
45	1	2830	225	0	—
50	4	2670	230	1	4030
55	2	1072	235	0	—
60	1	2693	240	2	3200
65	4	909	245	0	—
70	1	1460	250	1	2460
75	0	—	255	0	—
80	0	—	260	0	—
85	2	494	265	0	—
90	0	—	270	0	—
95	0	—	275	2	3030
100	0	—	280	0	—
105	1	1410	285	1	1950
110	2	1870	290	0	—
115	0	—	295	1	6970
120	0	—	300	1	6970
125	1	891	305	3	5470
130	2	1240	310	3	3845
135	0	—	315	1	1857
140	2	1670	320	1	1318
145	3	1930	325	0	—
150	2	2780	330	0	—
155	2	2760	335	0	—
160	5	3040	340	0	—
165	5	4520	345	0	—
170	7	3110	350	0	—
175	5	3110	355	0	—
180	3	3165	360	0	—

[a] Position angles measured eastward from the N. points.

[b] Composite histogram: Summary of all determinates of the height of the scattering lager in the Venus atmosphere by the Planet Group (Edson, Winget, Canright, and Meinel).

TABLE I E

DAILY AVERAGES FOR SCATTERING HEIGHT h IN FIVE COLOR BANDS: PLANET GROUP PHOTOGRAPHS, JUNE 1940

Date (1940)		Scattering height h (meters) + Cusp					− Cusp				
		Ultra-violet	Blue	Yellow	Red	Infra-red	Ultra-violet	Blue	Yellow	Red	Infra-red
June	22	—	2960	4080	1740	3420	—	2560	6100	1160	6880
	23	—	1340	—	1590	2680	—	5000	—	2990	4080
	24	915	1010	915	700	1460	2040	1860	4030	3660	4050
	25	1770	1950	1400	457	520	3350	3260	3350	3350	2980
	26	1220	1250	1590	885	1830	2440	2020	1890	1830	2200
	27	—	—	2440	2540	1460	2440	—	3450	2920	4020
	28	—	1040	3500	4020	—	—	1890	3230	2830	—
	29	—	—	—	—	—	—	—	—	—	—
	30	7320	7860	3840	7620	3510	3810	2200	4640	6950	1830
July	1	8540	>8540	2620	3660	—	5300	7900	1340	4020	—
Average		3950	3240	2550	2580	2120	3240	3339	3500	3300	3580
Average, + and −		3595	3285	3025	2940	2850					

Examples of these photographs are shown in Fig. 2. Results of this first photographic record were as follows:

1. Measurements of the photographs yielded values for the diameter of Venus. At inferior conjunction, the width of the cusp points is far below the limits of instrumental resolution. Consequently, irradiation effects are almost exactly symmetrical about the true edge of the planet. The measuring engine can be set to quite precisely bisect the image at the cusp points; the resulting diameter determinations have a small internal probable error. The usually troublesome irradiation systematic error is absent. The diameter determinations are at unit distance (one astronomical unit):

In red light, from 19 selected images, $16''.898 \pm 0''.015$.

In yellow light, from 9 selected images, $16''.938$.

In blue light, from 4 selected images, $16''.973$.

The slight increasing trend from red to blue is perhaps suggestive, but is probably not significant and should not be made the basis for the notion that the apparent diameter of Venus varies with the wavelength of the light in which it is observed..These measurements do offer a reliable and accurate value of the

diameter of Venus between points within a few hundred meters of the effective upper surface of the opaque cloud deck, this value being 16″919 ± 0″012.

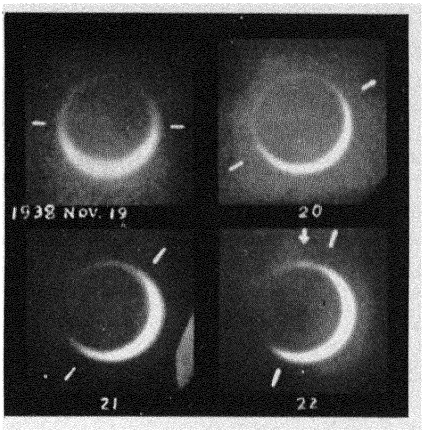

FIG. 2. Venus, 19-22 November 1938. Selection from the first series of photographs ever made of the Venus twilight cusp extensions—Lowell Observatory. On 20 November the dark rim of Venus was completely outlined by the twilight of her atomsphere. On the 22nd, a bright red segment appeared, as indicated by the arrow. Note the marked dissymmetry in length and brightness of the two cusp extensions on 19, 21, and 22 November.

2. The twilight cusp extensions are of very similar general appearance in the red, yellow, and blue photographs, as recorded against the light or the terrestrial sky near the sun. This agrees with the visual observation that the cusp extensions are generally bluish-white.

3. However, reddish bright spots appear in local areas along the twilight cusp extension. An exceptionally prominent one is shown on the image (taken in red light) of 22 November 1938, in Fig. 2. Photometry verifies that this spot represents an addition of red light with no appreciable absorption in the blue.

4. The distribution of the brightness along the cusp extensions in red and blue light was measured photometrically (Fig. 3). Interpretation of these photometric curves led to a model of the upper scattering layer that will be discussed later.

5. The cusp extensions are markedly unsymmetrical, as is evident in Fig. 2. As the planet moves past the sun, the illuminated crescent sweeps around the rim of the planet and the cusp extensions scan out most of the planetary rim. Calculation of the scattering height h, according to Russell's formula, and a plot of the results around the rim of the planet yielded the striking and suggestive

pattern shown in Fig. 4. At position angles in the southwest quadrant (as projected in our sky), the observed values of h ranged between 3000 and 7700 meters. The prominent red spot was also observed in this quadrant near the south point. In the northeast and northwest quadrants, the h-values were between 300 and 1400 meters, corresponding to relatively short twilight cusp extensions. This pattern is suggestive of some relationship to the meteorology of Venus, and perhaps to its rotation.

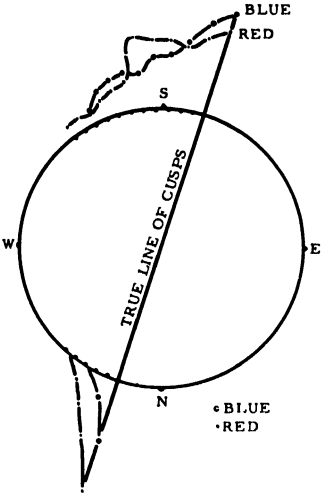

FIG. 3. Photometric curves of the cusp extensions, 22 November 1938. These Lowell Observatory curves are from photographs in red and blue light. Results for the two colors are similar except in the region of red brightening.

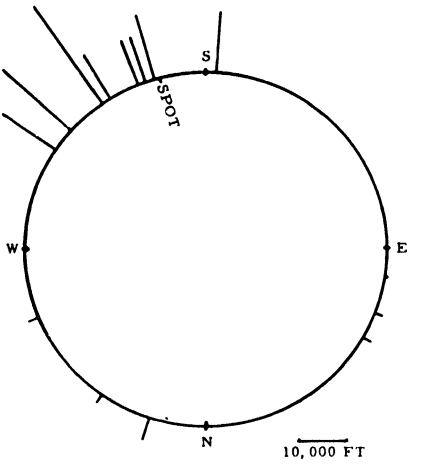

FIG. 4. Distribution of h, 16-24 November 1938. Distribution of scattering height h around the Venus rim, compiled from measurements of the Lowell Observatory photographs of 1938. Note the asymmetric height pattern which corresponds to the dissymmetry of the cusp extensions, $h + R(\sec s - 1)$.

The prospects thus opening up led to the formation of the Planet Group, a privately supported group of graduate students at the California Institute of Technology. The group consisted of E. Wright, R. Canright, J. Winget, A. Meinel, and J. Edson. With friendly assistance from many quarters they assembled at the Smithsonian Solar Observatory Station at Table Mountain, California a special set of equipment for the observation of the Venus inferior conjunction of 27 June 1940. A unique item of equipment was the sunshade, mounted on an aluminium mast and arranged so that it could be moved along by a system of ropes and pulleys to follow the sun across the sky. From its shade, the telescopes peered out at Venus. This observing setup is shown in

Fig. 5. The observing instruments were the Smithsonian Observatory's 6-in. refractor for visual and Roger Hayward's 6-in. reflector for photography.

The resulting photographic record contained more than 2000 Venus images in five colors bands taken in the interval 16-24 November 1938. Figure 6 is a

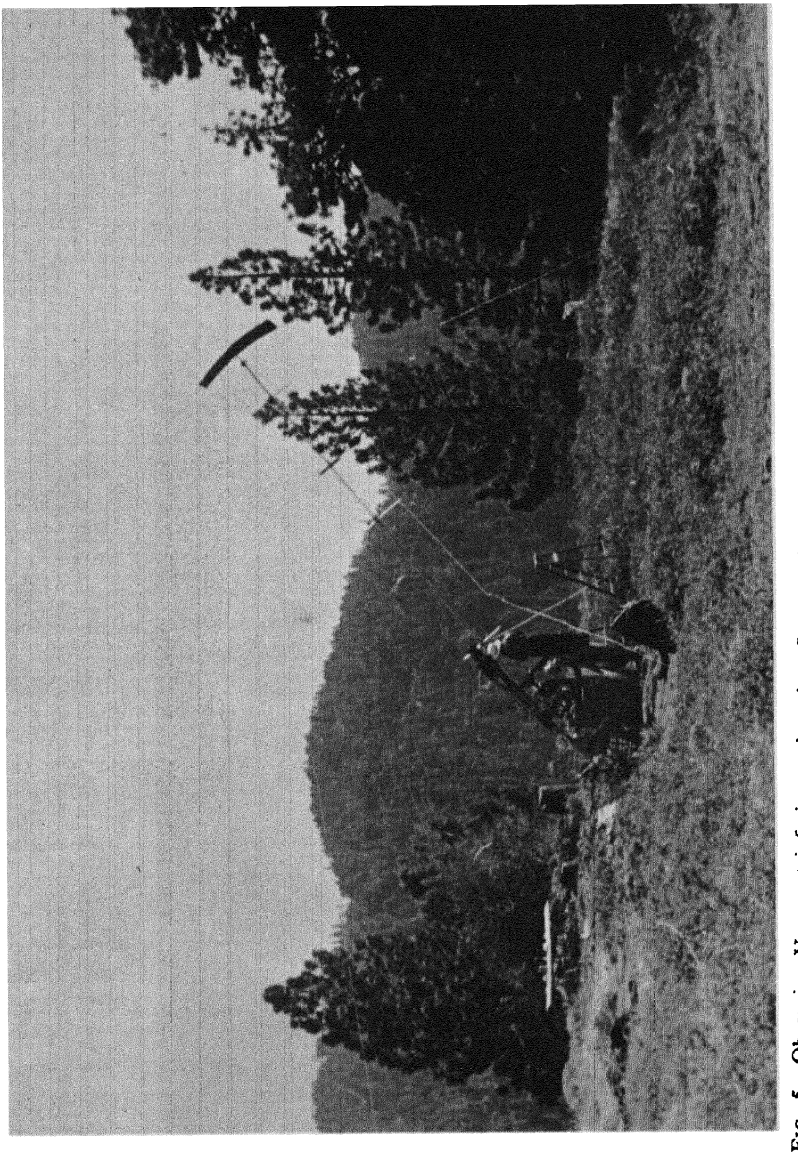

FIG. 5. Observing Venus at inferior conjunction, June 1940. The equipment of the Planet Group on the grounds of the Smithsonian Solar Observatory, Table Mountain, California. Note the special sunshade which was moved along by a system of ropes and pulleys to shield the telescopes from the sun's direct rays.

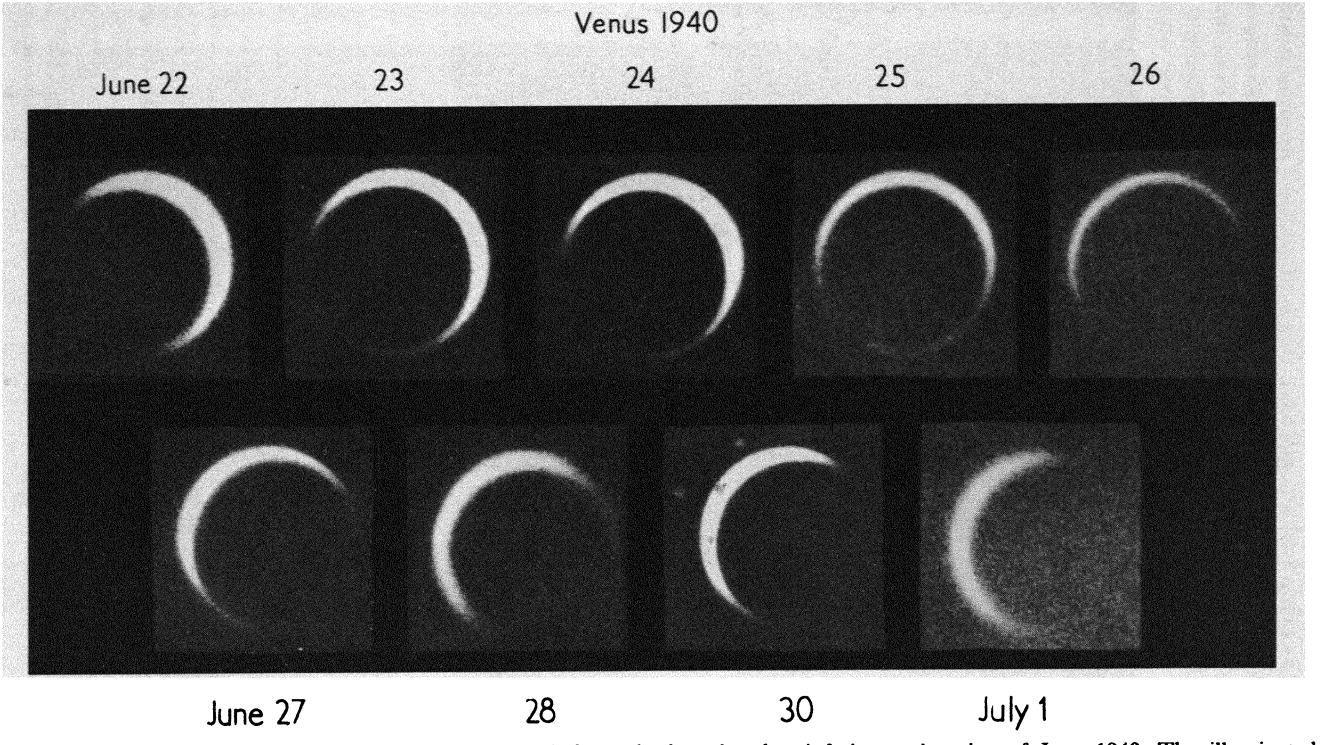

FIG. 6. Venus, 22 June-1 July 1940. One photograph for each observing day, inferior conjunction of June 1940. The illuminated crescent turns as Venus moves past the sun. The tips of the cusp extensions move around the rim of the planet, permitting the accumulation of data for h-distribution patterns like Fig. 4.

series containing one image for each day. Another series of images in the five color bands from ultraviolet to intrared is displayed in Fig. 7. The appearance of the cusp extensions is generally similar in all colors, again confirming the

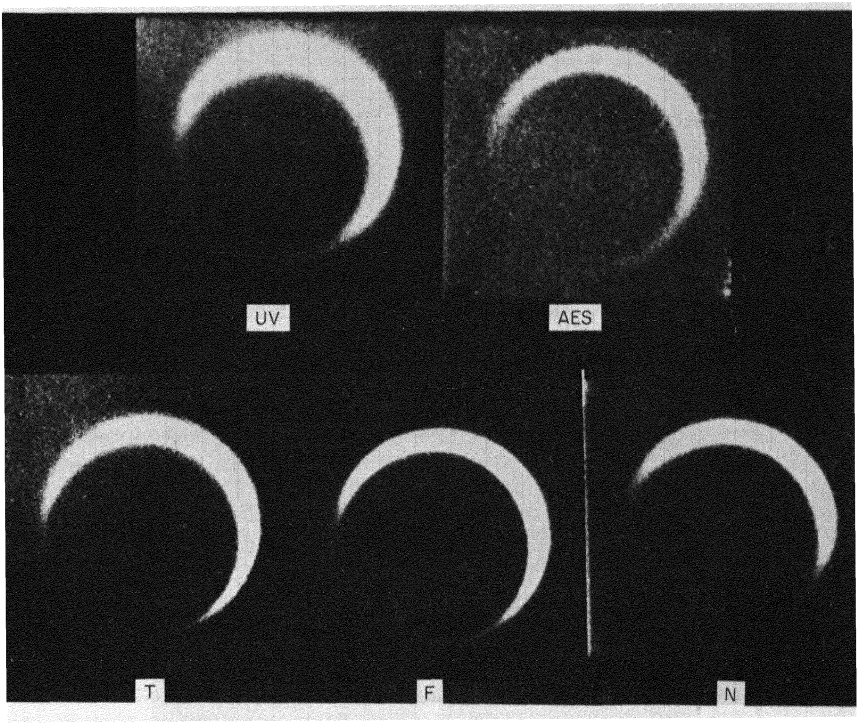

FIG. 7. The cusp extensions in five color bands, June 1940. UV = ultraviolet; Eastman lantern slide with ultraviolet filter. AES = blue; Eastman lantern slide with aesculine filter. T = yellow; Eastman 3*T* plate with Wratten K3 filter. F = red; Eastman 3F plate with red filter. N = infrared; Eastman 3N plate with infrared filter. One image for each color band, all taken on the same day, is here presented. Cusp extensions appear generally similar in all color bands.

blue-white appearance reported by visual observers. This bluish tinge is further substantiated by the fact that the average of measured h-values tends to increase slightly and progressively from infrared to ultraviolet, indicating that the cusp extensions could be seen and measured through a slightly greater angle in the shorter wavelengths, as shown in Fig. 8.

A check for gross polarization effects was made by photography through a polaroid filter in each of the five wavebands. As was expected, no detectable

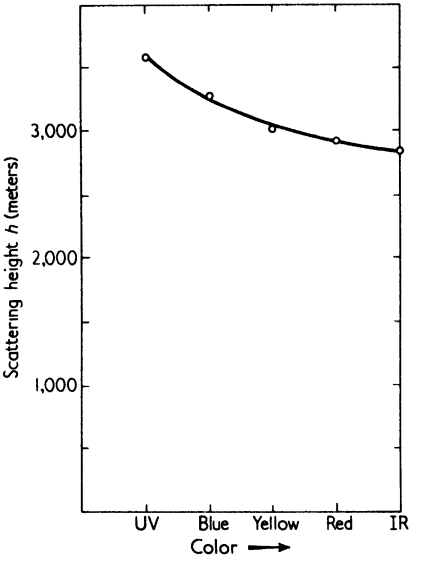

FIG. 8. Average h-value vs. color, 22 June-1 July 1940. Planet Group photographic data. UV = lantern slide, ultraviolet filter. Blue = lantern slide, aesculine filter. Yellow = 3T plate, K3 filter. Red = 3F plate, red filter. IR = 3N plate, infrared filter. Shows tendency for cusp extension tips to appear slightly brighter in comparison to sky background, hence slightly longer, in shorter wavelengths.

polarization was found. Figure 9 is a pair of images polarized at right angles to each other.

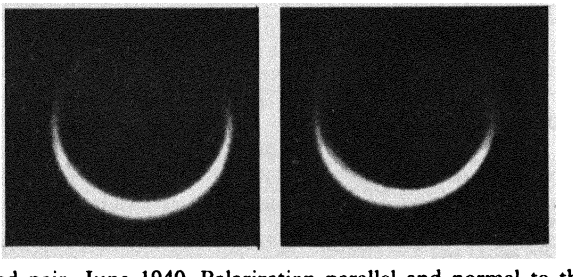

FIG. 9. Polarized pair, June 1940. Polarization parallel and normal to theoretical line of cusps, respectively. No appreciable polarization effects are shown.

Figure 10 displays the pattern of scattering layer heights h around the planetary rim in the five color bands. The patterns are all similar, and have been averaged together over ten degree intervals to produce the summary of the h-pattern around the Venus rim shown in Fig. 11. The Lowell Observatory

1938 results have been plotted in Fig. 11, along with a few other points, for comparison. This pattern, and the photographs shown in the several figures, display the same kind of dissymmetry of the cusp extensions that was observed at Flagstaff in 1938. Being more complete, it suggests even more strongly a systematic pattern connected with the general circulation of the Venus atmosphere.

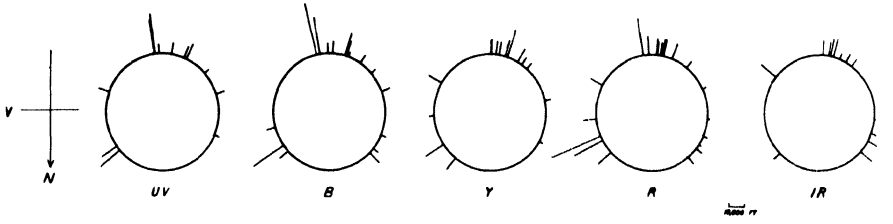

FIG. 10. Scattering height distributions in five colors, June 1940, showing the general similarity of h-distributions in all colors.

The scattering layer is high at the south point. Though data are lacking at the north point, the neighboring trends suggest a small value there. The fact that h is large at the south and small at the north in both the 1938 and the 1940 conjunctions is is interesting because the two conjunctions occurred in November and in June, respectively, on roughly opposite sides of the Venus orbit. There is more of similarity than of difference in these two atmospheric height patterns for very different Venus seasonal dates. This independence of seasonal date would be compatible with an axis of rotation nearly perpendicular to the Venus orbit plane, including the case in which the planet would keep the same face toward the sun. If the period of rotation is shorter than that of orbital revolution and in the same west-to-east sense as that of the earth, the east-west dissymmetry of the 1938 and 1940 scattering height patterns would indicate high clouds at dawn and low clouds or haze at sunset in the temperate and equatorial regions. However, the rather scanty evidence from observation of other inferior conjunctions does not support the assumption that the general 1938-1940 pattern is a permanent one.

Between 1940 and 1961 there appear to have been only a few sporadic observations. Two of them, one by C. W. Tombaugh on 31 January 1961 at the White Sands Missile Range and the other by J. Edson with a portable telescope near Mt. Wilson, California in 1954, showed cusp inequalities similar in character to those recorded in 1938 and 1940. Both of these yield scattering heights h in the NE and SE quadrants that are moderately higher than those found in 1938 or 1940. But both indicate very small values of h, about 100 meters at

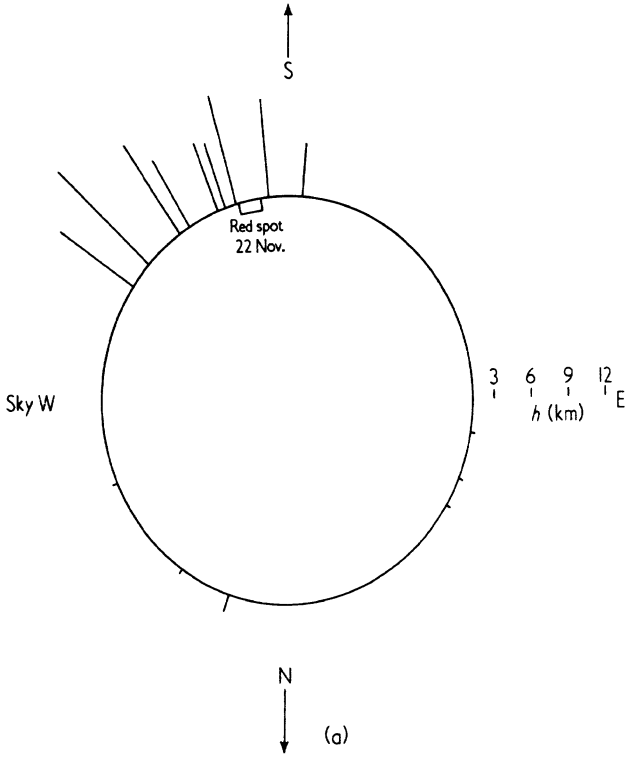

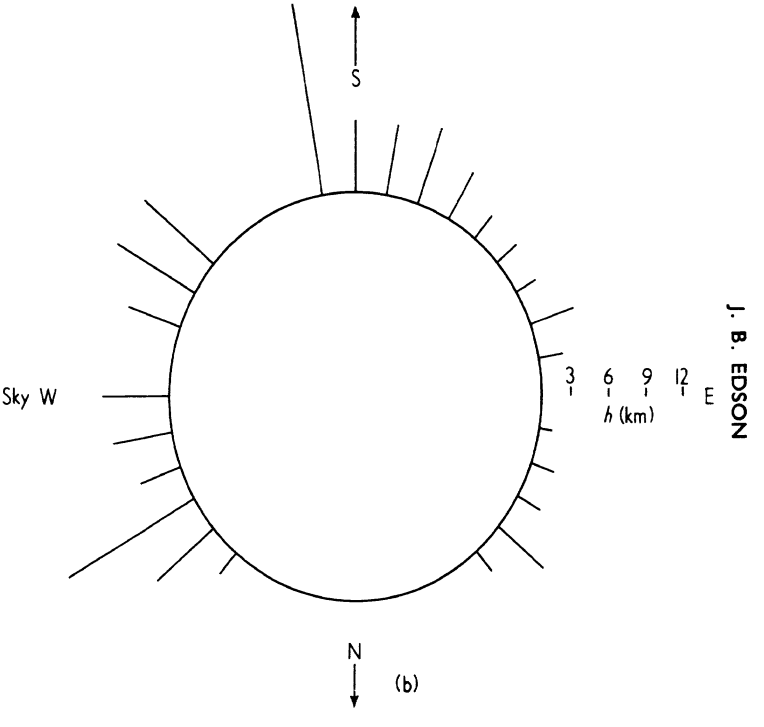

FIG. 11. Venus, height h of scattering layer (km): (a) measurements of Lowell Observatory photographs, November 1938; (b) composite of 83 measurements, June 1940 photographs, Planet Group data.

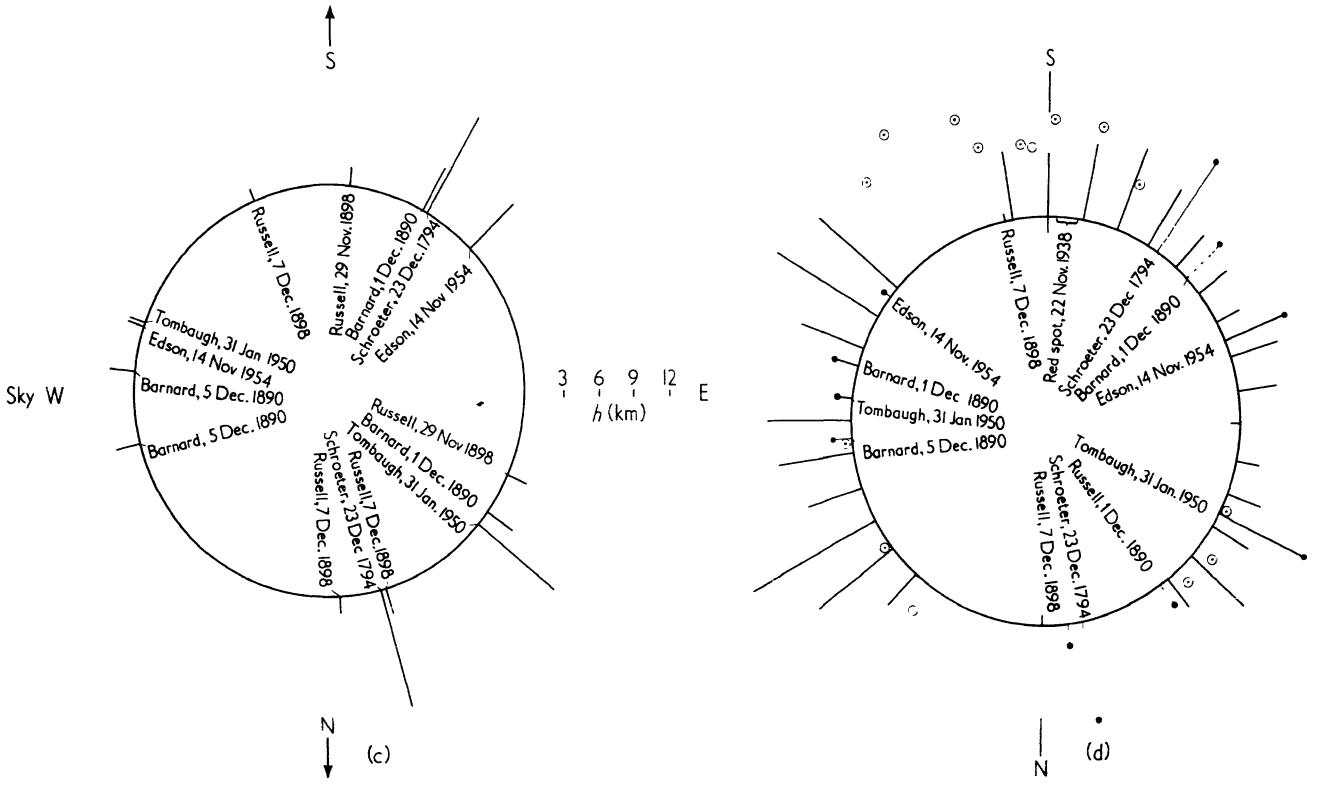

FIG. 11. Venus, height h of scattering layer (km): (c) collected from all sources, visual observations. (d) Observations referred approximately to the Venus orbit plane. "N" is the northward perpendicular to the Venus orbit, "S" is the southward perpendicular. Smooth radial lines = average of 1940 photographic data. ⊙ = November 1938 data, Lowell Observatory photographs. Others as labeled.

most, at a point about 20° south of west on the west rum where the height of the 1940 pattern would have been around 5000 meters (Fig. 11).

What can earlier observations contribute to knowledge of scattering height distribution around the rim? Unfortunately, not much at present. The observations, visual and photographic, in 1938, 1940, and since, indicate that inequalities in the cusp extensions are so common as to be the rule, and so conspicuous as to be obvious. Yet in the history of the observations there is little mention of these inequalities between the time of Schroeter, who often noted differences between the cusp extensions and discussed them at some length, in the 1790's and the conjunction of 1938. That so conspicuous and so significant a difference between the cusps should have been unnoted by a series of experienced observers engaged in the quantitative measurement of the cusp extension angles whould appear truly remarkable. Yet there is strong evidence that it can have happened. This is shown by Rabe's record of his 1940 visual observations. Observing the same conjunction as that recorded in the 1940 photographs, he measures and records in the traditional way, under the assumption that the cusp extensions are equal—except for one occasion, on 23 June. On that day, Rabe noticed that the south cusp extension appeared longer and stronger than the north extension. He made one separate measurement of the south extension, and this agrees with the values measured from the 1940 photographs. But the other measurements he made on the same day were on the usual assumption of cusp equality. He made no measurement of the north extension, but it can be correctly calculated on the assumption that Rabe was following the common practice of making a single angle measurement, namely, that of the angle around the unilluminated rim of Venus between the tips of the two twilight cusp extensions, subtracting that quantity from 180°, and assigning half of the remainder to each cusp. The degree of cusp inequality which attracted his notice to the extent of one measurement out of the six measurements he made on that day is portrayed in the photograph for 23 June in Fig. 6.

The modest amount of recoverable information about cusp inequalities, or of occasions on which the two cusps were specifically compared and found to have equal extensions, can be set forth in a brief space. Schroeter, as mentioned above, often noted and verbally described inequalities in length and brightness of the two cusp extensions, but recorded few numerical measurements. One set of his measurements at a time when he explicitly stated that the cusp extensions were equal are plotted in Fig. 11 and indicate that, at that time, 23 December 1794, the height of the scattering layer near the north point was around 10 km. This one old observation is in fair agreement with the 1940 pattern near the south point. But it is the only available quantitative measurement of high h-values near the north point. Schroeter summarizes his qualitative observations of the cusp inequalities with the statement that the north cusp extension

was longest in the conjunction of March 1790, and that the south cusp extension was longest in the conjunctions of May 1793 and December 1794.

Lyman on 12 November 1866 saw Venus as a complete ring of light when a passing cloud shaded his telescope objective against the direct rays of the sun. He says nothing about the distribution of brightness along the twilight side of the ring, but he saw the *sunlit* part of the crescent dim between 25° and 50° away from the crescent vertex toward the north cusp; that is, just north of the east point on the crescent rim. He reports that this dim spot had disappeared before the time of his next observation, on the 14th. Bright and dark irregularities were also observed along the sunlit part of the crescent on the photographs of 27 June 1940.

It is not certain how these observations of the sunlit side of the crescent should be related to the observations of irregularities in the twilight cusp extensions, but both must reflect some large-scale nonhomogeneities in the Venus atmosphere. In the 1940 case, the dim sector of the sunlit crescent appears at a position angle on the rim corresponding to a sector of relatively low scattering height values in the 1940 cusp extension pattern.

Barnard, at Lick Observatory, states that on 1 December 1890 the south cusp extension was longer than the north, but his measurements do not reflect the difference. Assuming that the south cusp was between 10° and 20° longer than the north, his measurements of that date can be roughly reconciled with the 1938-40 pattern. However, his observations of 5 December are about one-third of the 1940 values.

In 1898, Henry Norris Russell explicitly looked for inequalities in the cusp extensions, and found none. His assignment of equal extensions to the two cusps was thus meaningful, and his observations can be used to determine a pair of points in the Venus scattering height pattern, as shown in Fig. 4. Russell's measurements of the cusp extensions correspond to small height-values, probably because he observed through a relatively bright, hazy sky. The equal lengths and relative shortness of the cusp extensions as he observed them, and the smooth symmetry of the extensions as he saw them extended to a full circle on 2 December 1898, seem inconsistent with the patterns of 1938-40. However, the brighter parts of the cusp extensions, where the haze layers a kilometer or less above the opaque surface are illuminated by the sun and visible to the terrestrial observer, tend to be much more symmetrical; the major dissymmetries occur in the light from the fainter, higher regions as can be seen by inspection of the accompanying photographs. Both the shortness and the symmetry of the extensions as seen by Russell can probably be accounted for by the brightness of his sky.

In summary, the two photographically recorded and measured inferior conjunctions give generally similar and grossly unsymmetrical patterns of the

maximum height of the visible scattering layer above the opaque cloud surface as distributed around the rim of Venus. These patterns are suggestive of some connection with the general circulation and other large-scale phenomena in the Venus atmosphere. Most of the other observations and measurements reported between 1790 and 1940 were made on the assumption that the cusp extensions are symmetrical and in such a way that the dissymmetry cannot now be recovered from the recorded measurements. The records essentially state the angle of the illuminated arc between the tips of the visible cusp extensions.

Occasional reference in observers' notes to inequalities in brightness or length of the extensions, and a very few measurements, can be recovered from the century and a half of visual observations. Results of this gleaning of past and subsequent records do not fit the idea that the 1938-40 type of pattern is a permanent feature. Nor is the added evidence sufficient to indicate what the pattern might have been at other times, or to correlate the pattern with seasonal change or other parameters. It appears highly probable that observation of future inferior conjunctions and the scattering height patterns then displayed can provide valuable indications as to the general circulation, meteorology, climatology, and rotation of Venus. Perhaps the photographic record obtained by C. W. Tombaugh and his associates, covering the inferior conjunction of 11 April 1961, but as of this writing not reduced or published, will be helpful in these respects.

III

COLOR IN THE TWILIGHT CUSP EXTENSIONS

All observers agree in describing the color of the twilight cusp extensions as gray or gray-blue. This observation is, as noted above, substantiated by Fig. 8, which gives the average of all measures of the scattering height for each separate color band. It can be seen from the resultant plot that the cusp extensions were measured progressively as slightly longer (presumably because they were slightly brighter near their tips as seen against the sky) as the wavelength of the observation becomes shorter. This indicates that the cusp extension tip were slightly bluer than the blue-white of the terrestrial sky at the point of observation. The sky at Table Mountain, California (elevation 2.3 km), where these 1940 observations were made, is exceptionally clean and shows very little of white haze aureole near the sun. Thus indicates that the Venus cusp extension tips are almost as blue as the color produced by pure Rayleigh scattering and that the scattering particles are of colloidal size. It also strongly indicates that the reddening of the transmitted beam as it passes through the Venus atmosphere above the lower opaque cloud deck is small. This is consistent

with the determination of the horizontal refraction of the Venus atmosphere at the altitude of the upper surface of the opaque cloud deck as about 1 min of arc, corresponding to an atmospheric pressure, at the same level, of the order of 0.1 atm.

At times, red brightenings appear along the twilight cusp extensions. As noted earlier, an unusually conspicious one was seen and was recorded on color filter photographs at the Lowell Observatory on 22 November 1938. Several other red brightenings, very faint, were photographed by the Planet Group in 1940 at Table Mountain. Reference to the photometric curves of the cusp extensions in red and blue light, made at Lowell Observatory from the photographs of 22 November 1938 (Fig. 3), show the red spot as a brightening in the red, an *addition* of a source of red light, with little or no evidence of any influence at all in the blue. This could come about through the appearance of some red-only scattering material in the beam either (a) above and thus behind the blue-scattering layer, or (b) of such character as to intensely scatter red light while presenting negligible absorption to the blue, or (c) by a geometrical accident produce a blue scattering just sufficient to cancel the effects of its blue absorption. Alternative (a) above seems most plausible.

IV

INTERPRETATION OF THE BRIGHTNESS DISTRIBUTION ALONG THE CUSP EXTENSIONS

By photographic microphotometry it is possible to measure the brightness of the twilight cusp extensions as a function of the angular extension beyond the theoretical cusps. This was done for three Lowell Observatory plates. Reference to the red and blue pair, shown in Fig. 3, has already been made in the discussion of the bright red spot of 22 November 1938.

Such photometric curves as these, taken in various color bands and in sequence through a week or 10 days around inferior conjunction, are in principle capable of yielding a rather complete description of the optical characteristics and geometrical structure of the Venus atmosphere above the opaque layer. The general theory for such a reduction would be rather elaborate. With modern computing aids, it should be manageable.

Fortunately, the structure of the Venus atmosphere seems to be of a relatively simple character from the standpoint of the twilight scattering phenomena, and yields interesting results from an easy analysis.

Let us first examine the traditional picture of the Venus atmosphere as laden with a dust that thins with increasing height above some opaque layer whose upper surface represents the upper limit of a violently turbulent region. The

solar beam comes tangent to this upper surface of turbulent opacity and continues on to illuminate the "twilit" sky of Venus. A terrestrial observer sees that part of the Venus twilit sky which is above his Venus horizon, (that is, above the dark limb of Venus as seen from earth) and bounded by the tangent ray from earth past the opaque layer of Venus. When the total amount of scattered light from the Venus atmosphere above both of these tangent rays becomes great enough, the observer sees it as the tip of the twilight cusp extension. As one moves back along the prolongation toward the theoretical cusp point, these two rays intersect lower in the Venus atmosphere. And, at any given height above their intersection they include more horizontal miles of illuminated Venus atmosphere in the observer's view. The brightness of the extension, as one proceeds toward the cusp, should be increased by three causes.

First, the cross section of the Venus atmosphere illuminated by the sun and visible from the earth will increase. Second, lower layers of the illuminated atmosphere, which presumably carry more scattering material per unit volume, come into the observer's view. Finally, each volume of atmosphere of a given height which was previously seen will now be seen along a path through less dense portions of the Venus atmosphere, hence with less absorption. Consequently, if one assumes the brightness of the cusp extensions to be proportional to the cross sectional area of the illuminated and visible atmosphere below a certain height (this height being the assumed upper limit of any appreciable scattering power in the Venus atmosphere), then this model will indicate an increase in brightness along the twilight extension which must be less than the

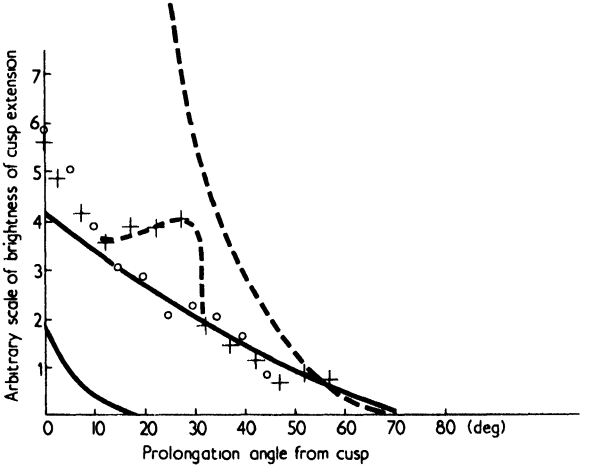

FIG. 12. Venus, 22 November 1938, 10:50 Mountain Standard Time. Relative intensities along twilight extension. ○, observed, blue light. +, observed, red light. ——, computed, "circus deck", simple model. — —, computed, simple "area of visible beam" model.

rate observed in a dust-filled atmosphere. Figure 12 shows the computed curve of illuminated and visible cross section of the scattering Venus atmosphere at various cusp extension angles compared with the observed red and blue data for 22 November 1938, One sees that the observed curve is of a totally different

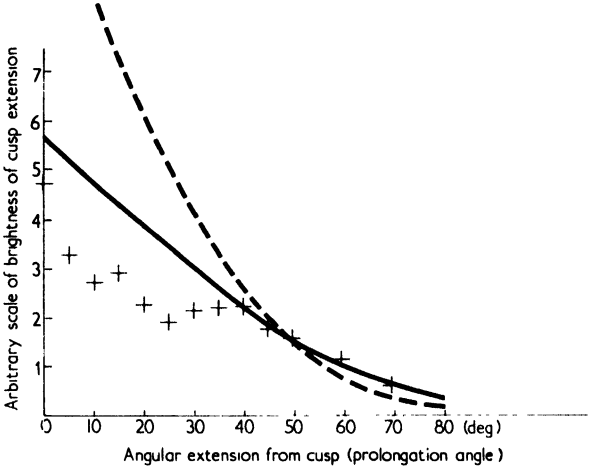

FIG. 13. Venus, 21 November 1938, 12:00 Mountain Standard Time. Intensity of twilight cusp extension. +, observed. ——, computed, simple "cirrus deck" model, deck height = 3.5 miles, — —, computed, "area of visible beam" model.

kind than the computed one. The observed brightness fails entirely to rise with the steep upward acceleration demanded by this computed "lower bound" theory for a dust-laden atmosphere. Observation in this case grossly fails to support the hypothesis of a dusty Venus atmosphere.

Now let us make another, even simpler, model. Let us assume a lower opaque cloud deck surmounted by a very thin, clear gas atmosphere. In this clear atmosphere, at the height h given by calculation from the measured cusp extension, let us assume the existence of a second, cirrus-like, very thin (a few hundred meters or less) and very bright scattering cloud deck. In this case the brightness of the cusp extension ought to be proportional to the horizontal length of the layer of cloud which lies in the solar beam and is visible from the Earth. In this model, both the absorption of and the scattered light from the Venus gaseous atmosphere are assumed small and, for the purposes of this estimate, are neglected.

The computed curve for this cirrus-deck model is also shown in Fig. 12. It provides a rather satisfactory fit to the observations. Near the theoretical cusp the observed curve accelerates upward away from this simple theoretical curve. The residuals form the curve displayed in the lower left corner of Fig. 12

and are qualitatively of the kind associated with the dusty atmosphere model earlier described. This feature can be explained by the hypothesis that the upper surface of the lower, opaque cloud deck is not smooth or abrupt, but that its upper part is a graduated haze layer with a height varying between a few hundred meters and about one kilometer. It would then be the relatively bright scattering from this shallow haze layer that was observed by Russell and other observers through bright terrestrial skies.

Figure 13 shows the comparison of observed points from a red photograph of 21 November 1938 (Lowell Observatory) with the models for the dust-filled atmosphere and for the "cirrus" cloud deck. Once more, the dusty atmosphere model cannot be reconciled with the observations, while the cloud deck model is consistent with them. The observations on this date suggest a high "cirrus" deck between 40° and 80° of angular prolongation from the theoretical cusp, with a "break" down to a similar deck at lower elevation from 35° or 40° on in to the cusp.

The break at the 35° point can also be explained as the result of a shift in the altitude of the lower, opaque layer at that place. In either case we have here some evidence of a "front" in the Venus atmosphere. The discontinuity is near the south point along the Venus rim, near the place at which the prominent red brightening appeared on the next day, the 22nd.

V

HORIZONTAL REFRACTION ACROSS THE TWILIGHT ZONE AT SOLAR TRANSIT

The variation of the scattering height h with time, and with position on Venus, raises the question whether the altitude of the upper scattering layer, or of the opaque cloud deck, or both, are responsible for the differences. This question cannot be readily answered from twilight extension data alone. Fortunately, another rare but simple observation of the Venus twilight zone, that of the horizontal refraction through the Venus atmosphere during ingress and egress at solar transits, is available. From the horizontal refraction we obtain the density. This, together with temperature estimates, in turn yields approximate differences in the altitude of the opaque cloud surface. For this purpose, F. Link has determined the horizontal refraction of Venus near the top of the opaque layer. A "diamond ring effect," generated by the refraction of the sun's image around the dark edge of Venus, was outlined theoretically by Russell and further investigated by Link. Link's study shows that the phenomenon begins only after the disk of Venus partially overlaps the disk of the sun during ingress at solar transits, or during egress. At such times, the portion of the Venus

rim which is outside the rim of the sun is seen partly or wholly outlined by a thread of light. In order to be seen in juxtaposition to the bright rim of the sun, it must be enormously brighter than the light seen along the twilight cusp extension at inferior conjunctions. It is in fact the refracted image of the solar surface seen through the Venus atmosphere. From analysis of the transit observations of the 18th and 19th centuries, Link finds that this thread of refracted light appears strongest near the north and south points on the Venus rim. It appears first near these points at ingress and disappears last near these same points at egress. This indicates that the horizontal refraction at these Venusan places is greater than elsewhere around the Venus rim.

Link states that the observations are consistent with Kuiper's estimate of the Cytherean axis of rotation, which has a tilt angle of about 32° with respect to the normal to the Venus orbit plane. Assuming the Kuiper axis, Link interprets his values for the Cytherean horizontal refraction as follows:

Pole in Venus winter:	1′.7
Pole in Venus summer:	1′.1
Venus equator:	0′.7

At the opaque cloud surface of Venus the horizontal refraction is related to the pressure and temperature by the expression

$$w = \frac{Ap}{T^{3/2}} \tag{1}$$

where w = total deflection of the beam; twice the horizontal refraction
A = effective deflection at unit pressure and temperature
p = pressure
T = absolute temperature.

The pressure is related to the altitude h by

$$p_h = p_0 e^{-h/H},\ H = RT/Mg \tag{2}$$

where R = gas constant
M = effective molecular weight of Venus atmosphere
g = acceleration of gravity on Venus around altitude h.

Substitution of (2) into (1) relates the refractive deflection to the altitude of the opaque layer by

$$w = \frac{Ae^{-h/H}}{T^{3/2}}$$

and from this may be derived the expression for the height difference that corresponds to a given ratio of deflection angles

$$h_2 - h_1 = H \log \left[\frac{w_1}{w_2}\left(\frac{T_1}{T_2}\right)^{3/2}\right]. \tag{3}$$

For conditions between the opaque cloud deck and the upper scattering layer we may estimate $T = 220°\text{K}$, $M = 40$, and $g = 860\text{cm/sec}^2$, yielding the scale height $H = 6.2$ km.

Radiometric measurements by Sinton and Strong indicate that the effective radiation temperature at the center of the Venus disk (near the equator?) is about 234°K and that near the cusps (polar regions?) it is about 210° or 220°K. Mintz finds evidence that these temperatures refer approximately to conditions not far above the top of the opaque layer. From these considerations we may estimate the decrease in altitude of the top of the opaque cloud deck between the "equator" and the "polar regions," winter and summer, respectively, assuming the Kuiper rotation axis to be roughly correct. Employing Eq. (3), we find for the decrease of the altitude of the opaque layer: from the "equator', to the "winter pole"—4.5 km; from the "equator" to the "summer pole"—2.26 km.

These results can now be compared with the variations of the height of the scattering layer around the Venus rim, as observed at inferior conjunctions. In the June 1940 pattern the h-values near the south point on the Venus rim were around 7 to 8 km, compared to values of about 3 to 6 km near the west point and 1 to 3 km near the east point in the "tropics." Link does not mention any evidence of an east-west dissymmetry in the brightness pattern of the refracted light, though a further discussion of the transit observations might possibly reveal it. For our present purposes of rough comparison, in June 1940 the south region can be regarded (following Kuiper and Lyman) as the "winter" pole. The average of east and west h-values in the "tropics" in 1940 is about 3 or 4 km, making an observed average difference from the "tropics" to the "south polar" region of about 4 km, in good agreement with the value of about 4.5 km depression of the opaque cloud deck over the winter pole as calculated from the refraction observations. It thus appears that, in this instance, the major part of the variation of the scattering height from "pole" to "equator" may be accounted for by a change in the level of the lower, opaque cloud layer. However, this simple relation fails when we compare the h-values of the north "polar" region with those for the south "pole" or the "tropics." The few available h-measurements around the north point for 1940 or 1938 have very small values. This situation seems best accounted for by the hypothesis that the upper, cirrus-like scattering layer simply did not exist over the northern region at these times. It should be noted that terrestrial June 1940 and terrestrial

November 1938 correspond to very different Cytherean seasonal dates. For this northern region, June corresponds to Kuiper's summer and November to Kuiper's winter. There is also some evidence that a high cloud deck is sometimes present in this northern region, as, for example, in Schroeter's observations of December 1794. It should also be pointed out that, around the south region in November 1938 (Kuiper's summer), the scattering heights h were about the same as those found in June 1940, but according to Link's results the south "polar" altitude of the opaque cloud surface should have been some 2.2 km higher in November than in June.

It may be concluded that variations in the height of the opaque layer are comparable to the vertical distance between the opaque layer and the cirrus deck, that the cirrus deck is probably very weak or absent over considerable areas at various times and places, and that an absolute height criterion for the various layers has not as yet been established.

VI

TWILIGHT PHENOMENA AND THE GENERAL CIRCULATION OF THE VENUS ATMOSPHERE

Behind the placid Cytherean mask of featureless uniformity there must lie a mighty thermal engine engaged in the endless mass transfer of heat-bearing substance across the twilight zone. Only thus can the thermal radiation of the night side be maintained within a few degrees of that prevailing at Cytherean noon. Some have reasoned that the Venus surface is composed of a substance of specific heat so great and effective thermal conductivity so high that the necessary stored heat is carried around the planet by its slow rotation; an ocean is usually invoked as the kind of surface required for this mechanism. In this concept, the atmosphere need play little role in the transfer of heat from day to night, and perhaps a modest one of supplement to ocean currents in carrying heat from the tropics to the poles. If this were so, the twilight zone might be a relatively tranquil place, so far as atmospheric phenomena are concerned.

But if surface heat transfer by rotation is not the dominant mechanism, then winds must do the job. In this case one might expect large jets of wind across the twilight zone, and strong fronts outlined against it. What might be the nature of such a circulation on a slowly rotating planet?

A circulation pattern offering symmetry about both the poles and the subsolar point of Venus is set forth by Yale Mintz (1960). The pattern is cellular in the sense that horizontal wind streams at lower and intermediate altitudes are arranged alternately around the twilight zone, one blowing from day to night

and its two neighbors blowing from night to day. Between neighboring cells at about 45° north and south latitudes at the twilight zone, convection and convergence occur along boundaries of oppositely directed horizontal winds. Inspecting the scattering height patterns (Fig. 4) we see that maxima in the *h*-values tend to occur at roughly corresponding places on the Venus rim, especially in the western side.

The Mintz pattern is unsymmetrical; air is carried by two parallel tropical currents off one side of the tropical zone and on at the other. If Venus rotates in the conventional direction, the Mintz pattern would indicate this flow as moving from right to left in Fig. 4, or off the daylight area on the dawn side and from night to day on the evening side. Thus, from our available data the larger equatorial *h*-values correspond to an evening flow of wind from the night side and the smaller equatorial scattering heights (perhaps indicating an absence of the cirrus deck) would be associated with a dawn flow of warmer air toward the night side. In the Mintz pattern the poles are near the centers of circulation cells where it looks as if quiet conditions might prevail. However, the Mintz model is clearly intended as a simple basis from which a more detailed model, taking into consideration the effects of polar tilt and the displacement of the pattern due to planetary rotation, may be evolved.

The Mintz circulation model for higher levels of the Venus atmosphere consists of a series of wind belts generally parallel to the equator. This upper pattern might, or might not be associated with the upper scattering cloud deck; the resemblance to some belted patterns seen on ultraviolet photographs of Venus seems closer.

VII

RELATION OF THE VENUS ULTRAVIOLET CLOUDS TO THE TWILIGHT PHENOMENA

Aside from the twilight cusp extensions, the only detailed features of Venus to be photographed to date are the ultraviolet "cloud" markings. These hazy, faint mottlings are in their form usually reminiscent both of belts and of spots. The beltedness patterns are, as a rule, roughly normal to the line of cusps Both beltedness and spottedness tend, on the average, toward a symmetry about the subsolar point, though there may be cases of quite pronounced dissymmetry.

There tend to be brightenings at or near the cusps. Sometimes these brightenings take the form of rather narrow, strong belts at right angles to the line of cusps and around 50° of north or south "latitude"; that is, they appear like belts around the "polar" regions near what, on the earth, would be the auroral

zones. The ultraviolet mottlings vary in their patterns within a few hours, in such a manner that the changes do not appear to represent the horizontal translation of wind-borne cloud across the planetary surface. Rather, these appear to be changes in the ultraviolet brightness of the atmosphere "in situ,"

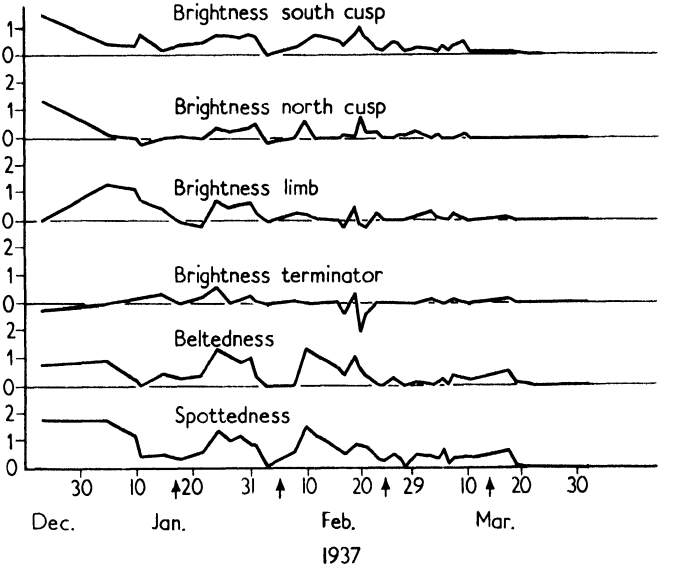

FIG. 14. Characteristics of the Venus ultraviolet cloud pattern; spring 1937. Eye estimates from inspection of original negatives by Edson, Lowell Observatory. Note that the terminator (twilight zone) is often neutral and sometimes darkened at the equator, while the cusps, particularly the south cusp, are often the regions of ultraviolet bright spots or belts. A set of similar observations in the interval 20 April—29 June 1938 yields similar results.

possibly due to vertical motions, so that bright or dark areas appear to develop, fade, and disappear. Any similarity of the patterns from one day to the next are vague and not very frequent. There are intervals of a few days when the ultraviolet markings are conspicuous, and other intervals in which they are virtually absent.

Figure 14 displays a series of subjective estimates of these various qualities of the Venus ultraviolet cloud pattern in the interval 23 December 1936 to 1 April 1937, made by J. Edson at the Lowell Observatory. Sketches of the cloud patterns for the same sequence are shown in Fig. 15. The form of these patterns frequently suggests the theoretical pattern for circulation in the intermediate levels of the Venus atmosphere as set forth by Yale Mintz and discussed above.

Can these ultraviolet cloud patterns be related to the height and brightness patterns shown by the twilight cusp extensions? There are some similarities; a tendency for brightenings in the polar regions, particularly near the south cusp, and the exhibition of changes within an interval of less than one day. However, the persistence of the general pattern of *h*-values over an interval of at least several days, and the suggestion of possibly permanent features, have no easily identifiable counterparts in the evanescent ultraviolet markings. The only evidence for more persistent causal factors in the case of the ultra-

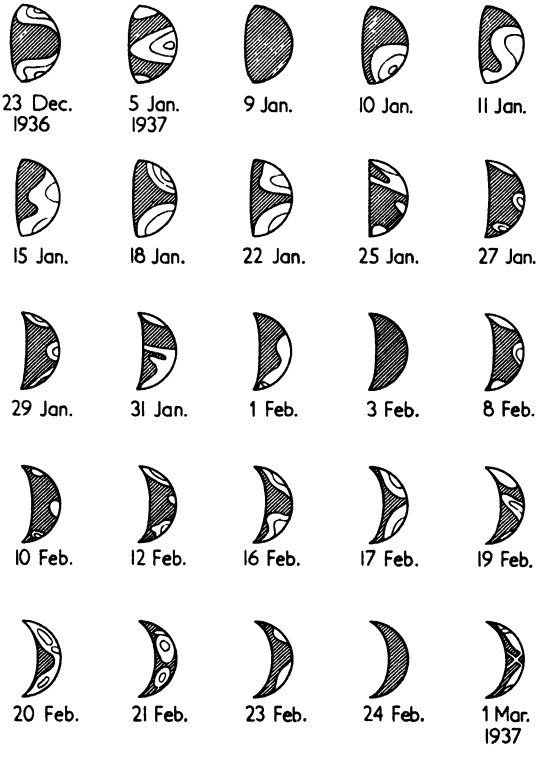

FIG. 15. Venus, schematic sketches from ultraviolet photographs, 1937. The ultraviolet cloud forms are difficult to print photographically because they are of low contrast compared to the strong gradation of brightness across the Venus disc from limb to terminator. However, on inspection of the original transparencies the eye readily differentiates the cloud patterns from the general light distribution over the planetary disk. The sketches in this figure are not intended to look like the original photographs. Rather, they are formalized diagrams to convey an impression of the various forms taken by the ultraviolet cloud patterns. The white areas on the diagrams appear brightened in the photographs. The contour lines within the white areas are rough estimates of iso-brightening lines.

violet markings must lie in the recurrence of certain general kinds of patterns. When this approach is applied to the region of the terminator (that is, the twilight zone) it is found that the ultraviolet brightenings reach the terminator more commonly in the higher Venus "latitudes," and that the terminator midway between the cusps is usually either neutral or darkened in the ultraviolet patterns. There are, however, exceptions to this rule; for example, in a pattern repeatedly seen in which a neutral or bright segment appears with its major axis centered on and normal to the midpoint of the terminator, and bounded by a darker, narrow band, the whole being much like Mintz's segmented pattern but with a bright segment, not a dark boundary, along the equator.

It should be remarked that, as the Venus crescent becomes more slender, that is, as the planet comes within a few weeks of inferior conjunction, the rapidly thinning crescent displays an even more rapid decrease of ultraviolet mottling. It may be that the increasingly oblique angles of illumination and view are not favorable for the display of the ultraviolet clouds. This suggests that the cause of the ultraviolet markings may be different from that of the twilight cusp extensions.

The best hint of a relationship, then, is the tendency for larger scattering height values to appear in those parts of the twilight zone which often appear brightened in the ultraviolet photographs.

VIII

DISCREPANCY BETWEEN THE OBSERVED AND THEORETICAL TIMES OF DICHOTOMY

Dichotomy is the situation of exact half-phase; on a diffuse-reflecting solid sphere illuminated by parallel light the terminator at dichotomy is a straight line connecting the two cusps, and the axis of the illuminating beam is precisely perpendicular to the observer's line of sight. In the case of Venus, dichotomy is generally observed to occur later than the theoretical time when the planet is waxing and earlier than the theoretical time when the planet is waning. In other words, at the theoretical time of dichotomy the terminator is generally observed not to be straight, but to be convex toward the illuminated side. The discrepancy has been reported by various observers to be in the range of 4 to 12 days. If one accepts 8 days as an average figure he finds (since the phase angle at that time is changing at the rate of about 0°55 per day) that the discrepancy of phase angle is around 4° or 5°.

One approach toward an explanation of this situation is to attribute it to the effect of the daylit sky background, which might so raise the threshold of visual perception as to blot out the outermost faint region of the terminator.

But, at dichotomy, photometry shows that near the terminator the isophotes in visible light are quite closely straight lines parallel to the terminator. To a good approximation, the terminator should still appear straight even though the faint outer fringes of it were lost in the glare of daylight. Also, at dichotomy time Venus is relatively far from the sun in our sky and can be observed against a relatively dark sky background in the later twilight.

What is needed is an effect operating differentially between the cusps and the midpoint of the terminator. One such possibility is that the effect is due, not to the obliteration of the terminator, but to an observation of the extended fringe of it, namely, the light from the high altitude scattering layer. The 1938-40 observations and other evidence suggest that this scattering layer is low, or at times absent, in the "equatorial" region midway between the cusps, and that it is often high at one or both of the cuspal, "polar" regions. Furthermore, the observer at dichotomy time looks directly down through this layer in the "equatorial" region, but views it edge-on, hence in much greater depth, at the cusps. The result might be a terminator roughly straight over much of the planetary diameter, but convex toward the daylight side near the cusps. The cusps might thus be seen extended by an amount roughly equivalent to the angular extent of the twilight zone as seen from the center of Venus. For scattering layer altitudes h prevailing near the south point in the 1938 and 1940 conjunctions, that is, around 6 or 7 km, the angle s subtended by the twilight zone is around 2°7. Evidently this effect is not large enough to account for the 4° or 5° involved in the discrepancy between theoretical and observed dichotomy, although it could possibly be a contributing factor, especially against a clean, dark sky with good atmospheric steadiness.

The dichotomy shift might also be produced if the opaque cloud deck of Venus had a downward slope of, say, about 5° across the twilight zone at the equator, and remained approximately level through the twilight zone near the cusps, or, more generally, if there were about a 5° increase in the slope of the cloud surface from the cusps to the center of the disk, in the sense of a downslope from the daylit to the dark side. This slope would have to continue for a distance of something like 5° of planetocentric angle normal to the terminator. The total altitude change of the cloud deck due to this slope would have to be around 40 km, corresponding to an atmospheric pressure change at the cloud surface amounting to about three orders of magnitude. Such a rapid physical change would probably be reflected in radiometric or other observational evidence; none is observed. This model does not appear very credible.

Further quantitative measurements of the character of the terminator near dichotomy, both photometric and geometric, are needed here. Meanwhile this phenomenon of the Venus twilight zone can not be discarded as an illusion, nor assigned a definite cause.

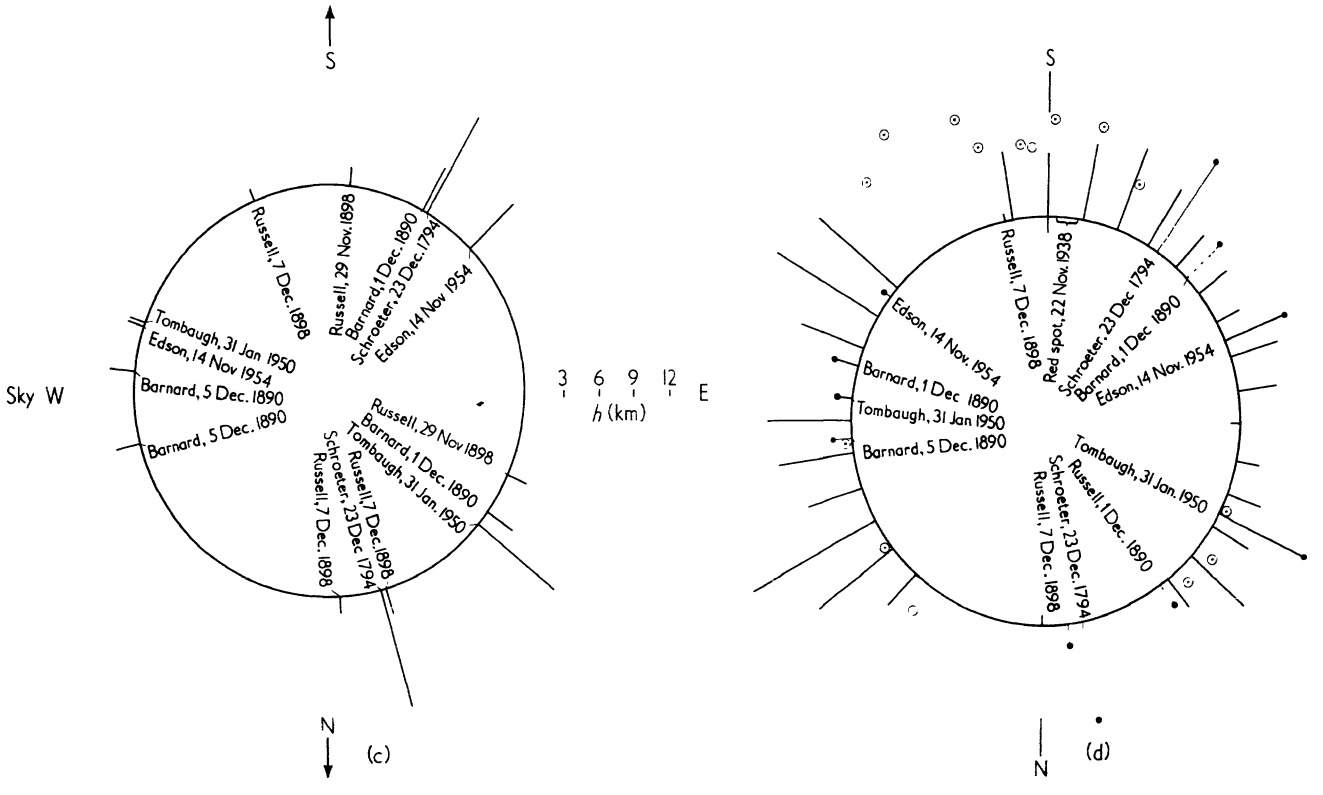

FIG. 11. Venus, height h of scattering layer (km): (c) collected from all sources, visual observations. (d) Observations referred approximately to the Venus orbit plane. "N" is the northward perpendicular to the Venus orbit, "S" is the southward perpendicular. Smooth radial lines = average of 1940 photographic data. ⊙ = November 1938 data, Lowell Observatory photographs. Others as labeled.

TABLE II

List of Inferior Conjunctions of Venus

Conjunction date	Angle of nearest approach	Conjunction date	Angle of nearest approach[a] (approx.)	Conjunction date	Angle of nearest approach[a] (approx.)	Conjunction date	Angle of nearest approach[a] (approx.)	Conjunction date	Angle of nearest approach[a] (approx.)
1769 June 3	Transit								
77 May 31	+0°.8								
85 29	1.1					1790 Mar. 18	+8°.4	1791 Oct. 17	−6°.8
93 27	1.4	1794 Dec. 29	+3°.3	1796 Aug. 2	−7°.0	98 16	8.5	99 15	7.0
1801 25	1.7	1802 27	3.0	1804 July 31	6.8	1806 13	8.5	1807 13	7.1
09 23	1.9	10 25	2.8	12 29	6.7	14 11	8.6	15 10	7.3
17 21	2.2	18 23	2.6	20 27	6.5	22 9	8.6	23 8	7.5
25 18	2.4	26 21	2.3	28 25	6.3	30 6	8.7	31 6	7.7
33 16	2.7	34 19	1.9	36 23	6.1	38 Mar. 4	8.7	39 4	7.8
41 14	2.9	42 17	1.6	44 21	5.9	46 Feb. 2	8.7	47 Oct. 2	7.9
49 12	3.2	50 15	1.2	52 19	5.8	54 27	8.7	55 Sept. 30	8.0
57 9	3.4	58 13	0.8	60 17	5.6	62 25	8.6	63 28	8.1
65 7	3.6	66 11	+0.5	68 15	5.4	70 23	8.5	71 Sept. 25	8.2
73 5	3.8	74 9	Transit	76 13	5.2	78 20	8.4	79 23	8.3
81 May 3	4.1	82 6	Transit	84 11	4.8	86 18	8.3	87 21	8.4
89 Apr. 30	4.4	90 4	−0.5	92 9	4.5	94 16	8.2	1895 19	8.5
97 28	4.7	98 Dec. 2	1.0	1900 7	4.2	1902 14	8.0	1903 17	8.6
1905 26	5.0	1906 Nov. 29	1.2	08 5	3.9	10 1212	7.8	11 15	8.7
13 24	5.3	14 27	1.5	16 3	3.7	18 9	7.7	19 12	8.7
21 22	5.6	22 24	2.2	24 July 1	3.4	26 7	7.5	27 10	8.7
29 20	5.9	30 22	2.5	32 June 29	3.1	34 5	7.4	35 8	8.7
37 18	6.2	38 20	2.8	40 26	2.8	42 Feb. 2	7.3	43 6	8.7
45 15	6.5	46 17	3.3	48 24	2.5	50 Jan. 31	7.2	51 4	8.7
53 13	6.8	54 15	3.7	56 22	2.3	58 29	7.1	59 Sept. 1	8.6
61 11	7.1	62 13	3.9	64 20	2.1	66 27	7.0	67 Aug. 30	8.6
69 Apr. 9	+7.3	70 Nov. 11	4.2	72 June 18	−1.9	74 Jan. 24	−6.8	75 Aug. 28	8.5

[a] + = Venus passes north of sun; − = Venus passes south of sun

does not require superb "seeing" because the image is a line of light and Venus appears relatively large at inferior conjunction, having then a diameter of about 1 min of arc, almost on the threshold of resolution of the naked eye.

Included herewith are some aids to the student or to the observer. Table II lists the inferior conjunctions from 1790 to 1972. It will be noted that they fall into five "families." The members of each "family" succeed each other by intervals of very nearly 8 years minus 2 days. Also listed is an approximate value of the angle of nearest approach of Venus to the sun as seen by the observer for each conjunction.

In the vicinity of inferior conjunction, Venus passes the sun at a rate of about 97 min of arc per day. If in Fig. 16 the sun is at the origin of coordinates,

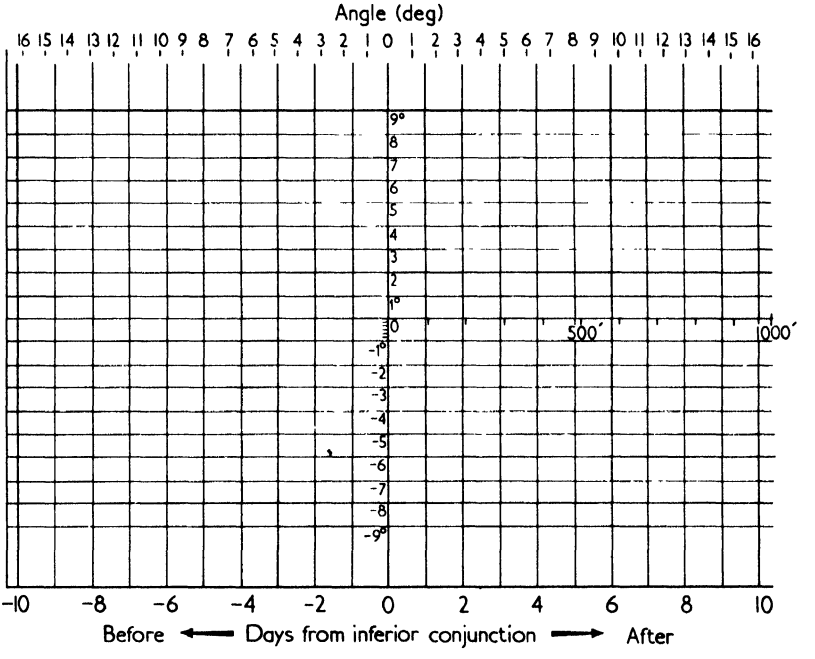

FIG. 16. Chart for determination of angle between Venus and the sun.

the approximate path of Venus past the sun can be plotted along the time axis on a line offset above or below the origin by the distance of nearest approach given in Table II. The path of Venus in the sky will be tilted away from the east-west line (line of constant declination) in the sky by an amount given roughly in Fig. 17, such that, if the angle given in Fig. 17 is positive, Venus will be moving southward relative to the sun. The angular distance between

the sun and Venus, as well as the approximate position angle of the line of cusps, can be estimated by measurements taken from the plotted Venus path. These plots are approximate guides only; precise circumstances of any specific inferior conjunction should be obtained by appropriate calculations using ephemeris data.

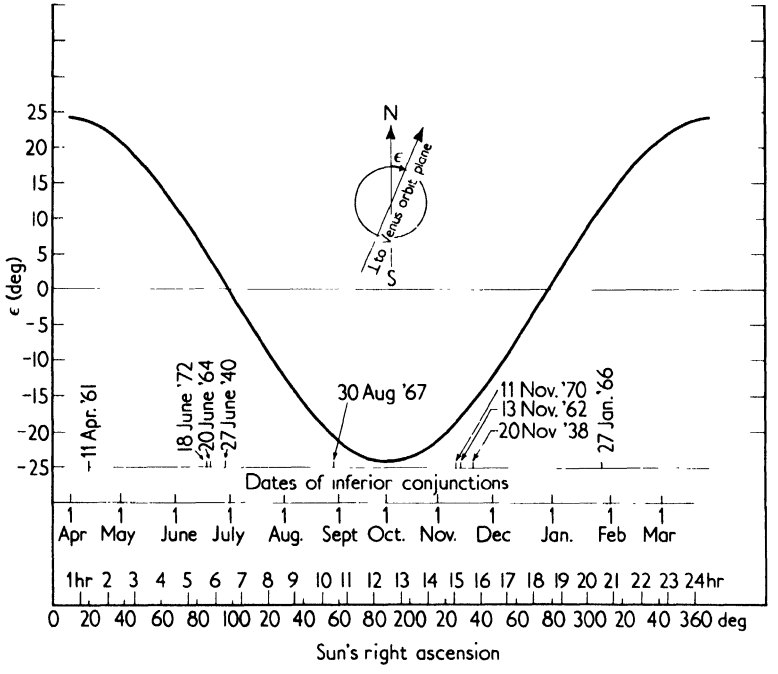

FIG. 17. (— = Angle between north and the normal of the Venus orbit plane as projected on the Venus disk at inferior conjunction.

Angular lengths of cusp extensions can be obtained by eye estimate recorded in sketches or, better still, by a protractor reticle in the eyepiece, or by some form of micrometer. Photographs can be measured by projection onto a suitable protractor chart, or by some kind of measuring engine. But be sure to measure the length or other characteristics *of each cusp extension separately*, and in relation to the true theoretical line of cusps, which is normal to the line from Venus to the sun.

Having measured the cusp extension angles and having found the angle v between Venus and the sun as seen by the observer at the time of observation, one may obtain the height h of the scattering layer at the tip of the cusp extension from Fig. 18. Figure 19 contains the same data as Fig. 18, but plotted in such

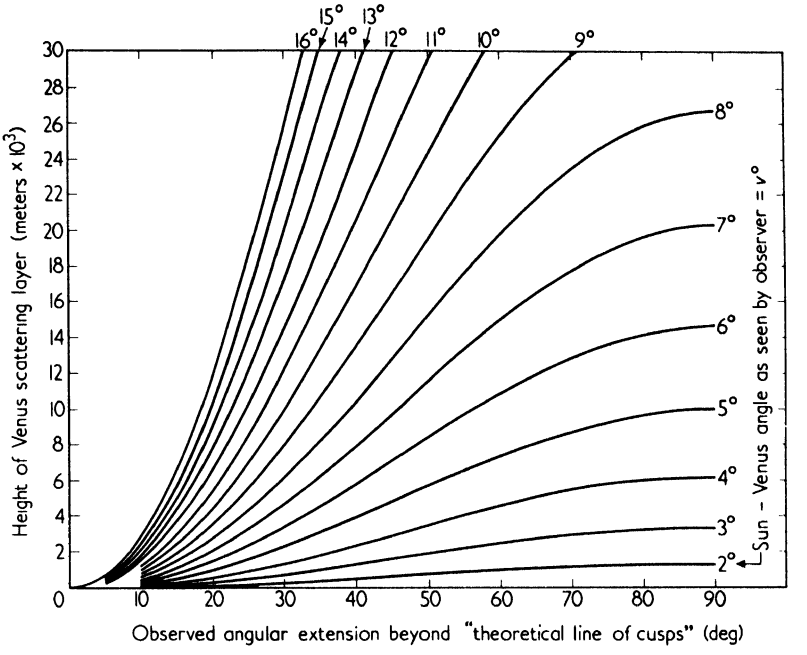

FIG. 18. Chart for determination of h = height of Venus upper scattering layer.

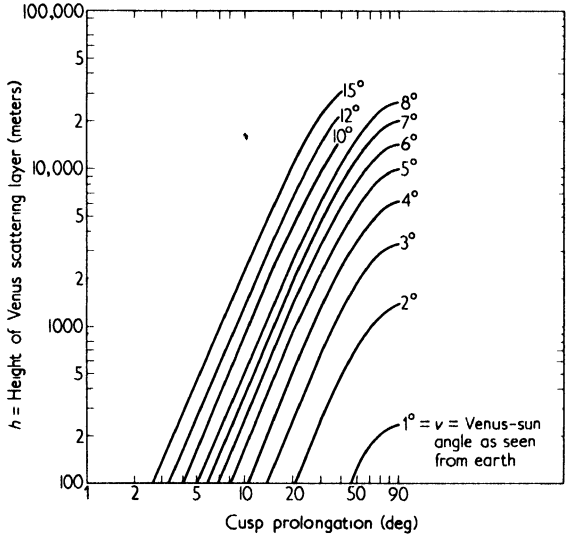

FIG. 19. Chart for determination of height of the scattering layer from Venus cusp prolongation at inferior conjunction (Russell's formula).

a form as to facilitate use with small angles of cusp prolongation p. The investigator is then in a position to plot his observed values of h at various position angles around the planetary rim and thus develop his own pattern for the height of the scattering layers in the atmosphere of Venus.

References

Barnard, E. E. (1891). *A. N.* **126**, 295. [Obs. at Mt. Hamilton, 28 Nov.-7 Dec. 1890; on 29 Nov. and 1 Dec., S. horn extended farther than N. horn. Two drawings, 5 Dec. and 7 Dec. Ring glimpsed complete on 5 Dec.]

Bartlett. (1953). *Strolling Astronomer* **7**, 30. (Strolling Astronomer is an amateur publication in Los Cruces, N. M.)

Brashear, J. A. (1882). *Sidereal Messenger* **1**, 269. [Description and drawing of refracted light around Venus rim external to solar disc between 1st and 2nd contacts.]

Baum, R. M. (1957). *J. Brit. astr. Ass.* **67**, 242. [The principal observations of the dark side of Venus 1643-1900. Several references to twilight cusp extension observations, but no measurements. Also mentions aurora-like glow sometimes seen near terminator.]

Campbell, W. W. (1918). *P. A. S. P.* **30**, 413. [Cusp prolongations on 2 March, 1918, 21 days from inferior conjunction of Venus.]

Danjon, A. (1951). *Bull. Soc. astr. Fr.* **65**, 249. [Geometry and times of inferior conjunctions, 1935-50.]

Denning, W. F. (1882). *M. N. R. A. S.* **42**, 109. [Discusses observations of cusp distortions.]

Edson, J. B., Wright, Winget, and Canright. (1940). *Amer. astr. Soc. Publ.* **10**, 125. [Short abstract of paper on 1940 observations by the Planet Group; photography of cusp extensions at inferior conjunction.]

Graff, K. (1921). *Hamburger Mitteilung* **5**, 29. [Data on twilight cusp extensions, conjunction of Apr.-May 1921.]

Guthrie, (1854). [Observation of Venus as a luminous ring.]

Hastings, C. S. (1883). *Sidereal Messenger* **1**, 273. [Observation of Venus refraction ring at the beginning of transit.]

Heath, M. B. B. (1955). *J. Brit. astr. Ass.* **66**. [Difference between theoretical and observed times of Venus dichotomy.]

Herschel, W. (1793). *Phil. Trans.* [Reports his observations of cusp extensions. Takes issue with some of Schroeter's results.]

Kuiper, G. (1954). *Ap. J.* **120**, 603. [Estimate of position of Venus pole of rotation from inspection of Venus ultraviolet belt patterns; $\alpha = 53° \pm 2°$, $\delta = 81° \pm 1°$.]

Link, F. (1948). *B. A. C.* **1**, 77 (in French). [Discusses cusp prolongations.]

Link, F. (1959). *B. A. C.* **10**, 105. [Key survey of literature and theoretical investigation of the refraction aureole around the Venus rim at beginning and end of transits.]

Lyman, (1867). *Amer. J. Sci.* **43**, 129. [Observations of Venus to within 22' of the sun's limb. Saw Venus as complete ring, and dim spot on sunlit side of crescent.]

Lyman, (1875). *Amer. J. Sci.* **9**, 47.

Maedler, J. H. (1849). *A.N.* **29**, 107. [Measurements of cusp extensions.]

Moore, P. (1958). "The Planet Venus." Macmillan, New York. [Nontechnical discussion of various Venus phenomena, by a long-time student of the planet.]

Mintz, Y. (1961). *Planet. Space Sci.* **5**, 141-152. [Structure and circulation models for the Venus atmosphere.]

Naef, R. A. (1950). *Orion* **27**, 91. [Cusp prolongation estimates.]

Rabe, W. (1913). *A. N.* **196**, 413. [Cusp extension measurements.]

Rabe, W. (1948). *A. N.* **276**, 111-117. [Key review article on cusp extension observations, 1790-1940, with list of observations.]

Richter, N. (1932). *A. N.* **246**, 235. [An observation of Venus cusp extensions, 1 July 1932.]

Richter, N. (1943). *A. N.* **274**, 119. [Observations of cusp prolongations, June 1940.]

Ruddy, H. E. (1954). *J. Brit. astr. Ass.* **64**, 304. [Personal diary of Lt. Cyril Corbett, RN; observations of Venus refraction halo at Kerguelen Island, transit of 1874.]

Russell, H. N. (1899). *Ap. J.* **9**, 284. [Reviews, tabulates and discusses cusp prolongation measurements to that date. Gives correct concept and theory for interpretation of the cusp prolongations.]

Russell, H. N. (1907). *Ap. J.* **17**, 69. [Cusp extension measurements, 1906.]

Sandner, W. (1960). *Mitt. Planetenbeobachter* (a) **11**, 20; (b) **12**, 62. [Discussion of Venus dichotomy times.]

Scharonow, W. W. (1952). *Dokl. Akad. Nauk. S. S. S. R.* **82**, 351 (in Russian); reviewed in *Astr. Newsletter* **62**, 9 (in English). [Analysis of refraction aureole of Venus at beginning and end of transits; estimates Venus horizontal refraction about 20".]

Scharonow, W. W. (19—). *Astr. Circ. Acad. Sci. U. S. S. R.* **125**, 8 (in Russian). [Discusses cusp extensions and horizontal refraction.]

Schoenberg, E., and Sandner, W. (19—). *Ann. Astrophysik* **22**, 839-889. [Discussion of dichotomy times.]

Schroeter, J. (1793). *Phil. Trans.* **73**, 201. [Schroeter reports to the Royal Society on cusp extensions and the detachment of a point of light from one cusp.]

Schroeter, J. (1795). *Phil. Trans.* **75**, 117. [Reports further observations and opinions about the cusp extensions and other phenomena.]

Schroeter, J. H. (1796). "Aphroditographische Fragmente." C. G. Fleckeisen, Helmstedt, 1796 (U. S. Naval Obs. has copy). [Describes and summarizes Schroeter's work, including discovery and study of cusp extensions.]

Sinton, W. M., and Strong, J. (1960). *Ap. J.* **131**, 470-490. [Radiometric observations of Venus.]

Slipher, E. C., and Edson, J. B. (1939). *Amer. astr. Soc. Publ.* **9**, 229. [Summarizes initial results of first photographic record of the cusp extensions.]

Sotkin, I. T., Edjuk, and Popowkina. (1949). *Bull. astr.-geodet. Soc. U.S.S.R.* **7**, 17 (in Russian). [Discusses cusp extensions. Six illustrations.]

Sotkin, I. T. (19—). *Bull astr.-geodet. Soc. U. S. S. R.* **12**, 9 (in Russian). [Discusses the cusp extensions.]

Struve, G. (1924). *A. N.* **222**. [Account of a stellar occultation by Venus.]

Tombaugh, C. W. (1950). *A. J.* **55**, 184.

Trouvelot, E. (1882). *Bull. Soc. astr. France* **6**. [Discusses cusp distortions.]

Vaucouleurs, G. de (1959). "A Survey of Physical Problems of the Nearer Planets," etc. Air Force Missile Development Center, Holloman Air Force Base, N. M. AFMDC-TN-59-37. [An excellent review, including Venus twilight phenomena.]

Ventosa, V. (1911). (a) *A. N.* **189**, 33; (b) *ibid.* **194**, 7.

Wolkow, W. W. (1941). *Bull. astr.-geodet. Soc. U. S. S. R.* **5**, 17 (in Russian). [Discusses Venus in 1940.]

Young, C. A. (1882). *Sidereal Messenger* **1**, 300-308. [Obs. of Venus refraction ring at beginning of transit , Princeton 24" refractor diaphragmed to 6", with excellent seeing. Says "This delicate ring appeared to have a width of about 2", and was made up of little filaments standing out from the planet like fine, short hairs close together, with here and there a brilliant knot".]

Cataclysmic Variables as Binary Stars

ROBERT P. KRAFT
Mount Wilson and Palomar Observatories,
Carnegie Institution of Washington, California Institute of Technology,
Pasadena, California

I. Introduction 43
II. Examples of Well-Known Binaries in Groups (1) and (2) 45
A. Dwarf Nova: SS Cygni 45
B. Recurrent Nova: T Coronae Borealis (1866, 1946) 46
C. Ordinary Nova: DQ Herculis (1934). 47
III. Some Common and Related Properties of the Systems Discussed in Section II 54
IV. The Search for New Binaries among U Geminorum Stars and Novae . 56
A. U Geminorum Stars 57
B. Novae 68
Appendix. 77
References 84

I

INTRODUCTION

The term "cataclysmic variable," as it will be used throughout this article, refers to an object in one of three classes: dwarf nova, nova, or supernova. The order of arrangement is one of increasing integrated outburst energy. Flare stars will not be included, but a few objects spectroscopically similar to the cataclysmic variables will be discussed, even though none are known to behave "impulsively."[1]

The dwarf novae, more often referred to as U Geminorum or SS Cygni stars, have integrated energies in the range 10^{38} to 10^{39} ergs. For any one star, the outbursts are quasi-periodic ($P \approx 10^{2}$ to 10^{-1} years) in the sense that the intervals between maxima average a certain value and are more or less normally distributed about that average. The rise in light is 2 to 5 magnitudes, depending on the star in question, and is the same within a few tenths of a magnitude from

[1] A comprehensive review of the properties of cataclysmic variables is found in C. P. Gaposchkin's book "The Galactic Novae" (1957), and in an article by D. B. McLaughlin (1960).

one outburst to another. Two subgroups of this class are recognized: SS Cygni stars and Z Camelopardalis stars. The latter differ from the former in that they do not always descend to minimum between outbursts, but may maintain a "minimum" position between true minimum and maximum for some months. Throughout this article, we shall speak of "U Geminorum star" as a term interchangeable with "dwarf nova," and reserve "SS Cyg star" and "Z Cam star" for the two subgroups. It should be noted that U Gem itself belongs to the SS Cyg subgroup.

Novae have ranges of 8 to 12 magnitudes and involve integrated energies of 10^{44} to 10^{45} ergs. The existence of a relation between the time needed to decay from maximum light to (say) half that rate of emission (known as the "lifetime") and the maximum brightness itself renders the novae useful for studies involving galactic and extragalactic distances. We distinguish between "ordinary" and "repeating" novae; the latter appear to have outburst intervals of order 10 to 100 years. Fast, i.e., short-lived novae, may be identifiable with the repeating variety (Arp, 1956; Kraft, 1958a).

Supernovae involve outburst energies of order 10^{49} to 10^{51} ergs; this is roughly equivalent to the total potential energy of a stellar configuration. Thus a star undergoing a supernova outburst must be altered profoundly and a recurrence of the phenomenon would not be expected. Supernovae of types I and II are recognized—the former involving perhaps 10 to 100 times the energy of the latter; these belong to Populations II and I, respectively (cf. Baade, 1958). Supernovae of type II are thought to be massive stars close to the limit of stability against radiation pressure. Blaauw (1961) has recently put forth a remarkable theory suggesting that certain early-type stars found to be "running away" from O-B associations are the former companions of type II supernovae, the latter being essentially "annihilated" during the explosion.

Thus the supernovae of type II may have been binary stars originally. However, since Population II systems, such as globular clusters, do not appear to contain eclipsing binaries, one would not expect duplicity to play a role in the development of supernovae of type I. On the other hand, a number of novae and dwarf novae are known to be eclipsing and/or spectroscopic binaries. For this reason, we shall restrict our attention in this paper to an examination of the following question:

Is membership in a certain kind of binary system (to be specified in more detail later) *a necessary condition for a star to become a nova or a dwarf nova?*

The observing astronomer might seek to answer this question by looking for eclipses or radial velocity changes. In order to assess the probability of the success of any such program, we need to consider what may be expected in terms of brightness, period, etc. Anticipating a little, we will be forced to

conclude that a very large telescope will be needed in order to make any real progress. Let us, therefore, consider in some detail the best-known binary stars in groups (1) and (2) as a guide to formulating a suitable observational program.

II

EXAMPLES OF WELL-KNOWN BINARIES IN GROUPS (1) AND (2)

A. *Dwarf Nova: SS Cygni*

According to Joy (1956), SS Cyg is a double-line spectroscopic binary of period 6^h38^m. The faint and sometimes rather fuzzy lines of a star classified as dG5 are seen superimposed on a blue continuum with wide bright lines of H, He I, and Ca II (sdBe); the velocity curve is shown in Fig. 1. The stars

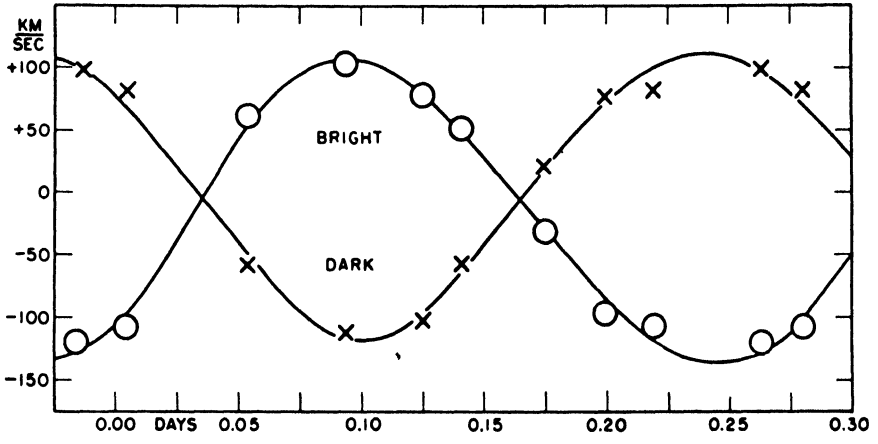

FIG. 1. The radial velocity of SS Cyg (courtesy A. H. Joy). Crosses and circles are normal points.

do not eclipse (Grant, 1955) and the minimum masses of the blue and red components are $\mathcal{M}_1 \sin^3 i = 0.18\odot$ and $\mathcal{M}_2 \sin^3 i = 0.20\odot$, respectively.[2] Corresponding minimum semimajor axes are $a_1 \sin i = 4.6 \times 10^{10}$ cm and $a_2 \sin i = 4.4 \times 10^{10}$ cm. No absorption lines attributable to a hot star are seen; it is clear that the emission lines correspond to a ring, disk, or shell surrounding the blue component.

[2] Throughout this paper the subscript 1 refers to the blue component in these systems, regardless of whether or not it is the more massive.

We define the characteristic minimum dimension $\mathscr{R} \sin i$ of a system by $[(a_1 + a_2) \sin i]/2$. Thus $\mathscr{R} \sin i = 4.5 \times 10^{10}$ cm. Unless i is unusually small, $\mathscr{R} \sin i$ is a number of the same order as the radius of a typical dG5 star, viz., 6.2×10^{10} cm. If so, it is probable that the spectrum described as "dG5" is affected by the nearby presence of the hot (subdwarf) companion and also by a reduction in surface gravity owing to centrifugal acceleration. Since the radii of stars decline slowly as one passes downward along the main sequence (e.g., $R_{\mathrm{dM5}} \approx \frac{1}{2} R_{\mathrm{dG5}}$), these remarks would no doubt be true even if the spectrum of late-type component, freed from these two influences, proved to correspond to a somewhat fainter and/or redder star than dG5.

B. *Recurrent Nova: T Coronae Borealis* (1866, 1946)

The spectrum of this star had been recognized as composite for some years prior to the 1946 outburst. At minimum light, an apparently normal spectrum of type gM3 is seen superimposed on a blue continuum with emission lines of H, He I, He II, Ca II, O III, [O III], [Ne III], etc. It was not until 1948, however, that Sanford (1949) discovered the variation in velocity of the red star with a period of 230 days and a semiamplitude of 21 km/sec. No variation in the emission-line velocities was found, however.

A subsequent investigation by Kraft (1958a) led to an improvement in period ($P = 227^{\mathrm{d}}6$) and to the detection of the velocity variation in the hydrogen emission lines. Velocities of the latter were estimated from reconstructed tracings of Hβ and Hα after the underlying gM3 spectrum had been allowed for. The emission lines are fairly wide ($\Delta V \sim$ 300 km/sec) and the velocity range small ($K_1 = 33.5$ km/sec) so that Sanford's failure to detect the motion is understandable. The forbidden emission lines do not share the motion and probably arise in a large envelope surrounding the system. It is assumed that the blue star follows the motion of the bright hydrogen lines. The velocity curve is illustrated in Fig. 2.

Minimum masses for the blue and red components are 2.1$\odot$ and 2.9$\odot$, respectively, and $\mathscr{R} \sin i = 6.4 \times 10^{12}$ cm. The radius of a gM3 star is about 9×10^{12} cm. The system may be expected to eclipse if $i \gtrsim 65°$. While eclipses are not known definitely to exist, there is some positive evidence on this point. An unpublished light curve obtained by D. C. Camp at the Goethe Link Observatory suggests a drop in blue light by 0.1 to 0.2 mag. for about 10 days, centered on superior conjunction for the blue star; not too much weight can be placed on the result, however, because of the known large, intrinsic fluctuations of light in T CrB (Walker, 1957). On the other hand, A. J. Deutsch has obtained spectra at similar phases showing striking enhancement of certain zero-volt lines of Ti II—lines normally very strong in shell spectra. A distinct

possibility exists that T CrB undergoes a grazing atmospheric eclipse similar to the well-known case of ϵ Aur.

If we then tentatively take 65° to 70° as a not unreasonable range of values for the inclination, the masses of the blue and red components become $\sim 2.6\odot$

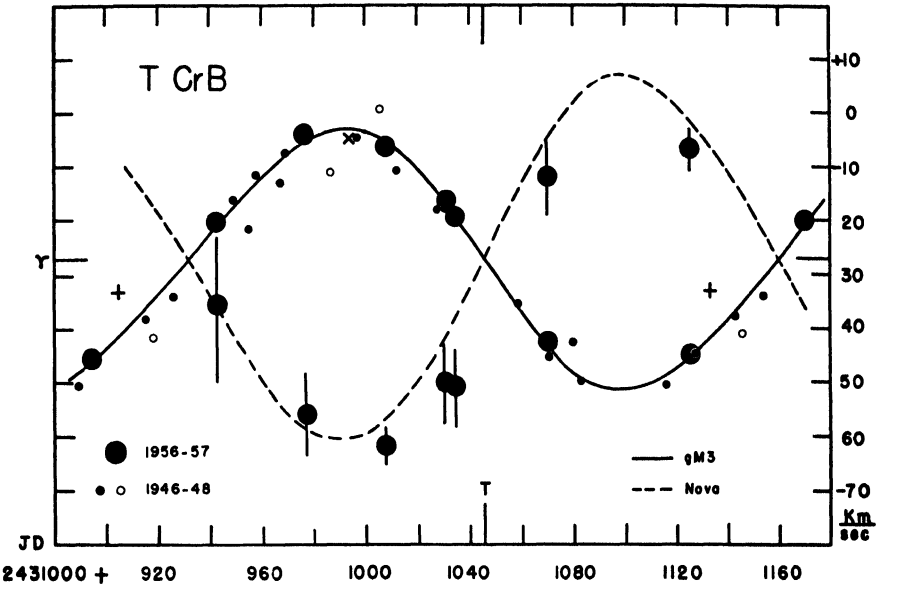

FIG. 2. The radial velocity of T CrB. Small circles and dots refer to velocities of the gM3 component obtained by R.F. Sanford. Vertical lines through the dots corresponding to velocity measures of Hβ and/or Hα in emission have lengths equal to twice the mean error of measurement.

and $\sim 3.7\odot$, respectively, and the characteristic dimension of the system $\mathscr{A} \cong 7.0 \times 10^{12}$ cm. As was the case for SS Cyg, $\mathscr{A}$ has a value of the same order as the radius of the red component. However, the combined effects of the presence of the hot star and of the centrifugal acceleration on the gM3 star should be much less pronounced here than on the red component of SS Cyg. The geometric dilution of blue-star radiation at the surface of the red star is $\sim 10^4$ times greater in the present case; moreover, the surface gravity of a gM3 star is already so low that placing the star in a rotating system would scarcely be expected to have much effect on the appearance of its spectrum.

C. *Ordinary Nova: DQ Herculis* (1934)

In 1954, Walker made the remarkable discovery that DQ Her is an eclipsing

binary of period 4^h39^m. Subsequent photometric investigations (Walker, 1956, 1958, 1961) revealed the following facts:

(a) The eclipse curve does not repeat from one epoch to another, and the photometric elements of the system derived in the usual way are unreliable (cf. Fig. 3).

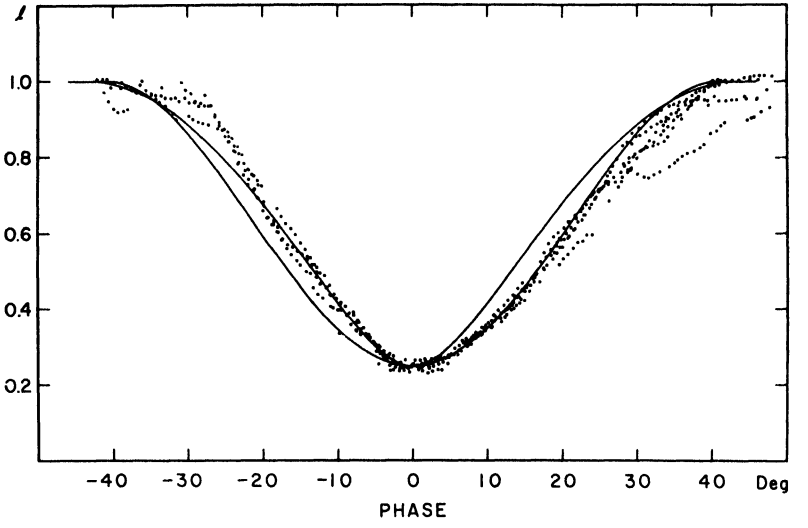

FIG. 3. The eclipse curve of DQ Her in 1956 (yellow light) (courtesy M. F. Walker). The descending and rising branches cannot be fitted by the same theoretical eclipse curve, as illustrated. The observed points are also different from those observed in 1954.

(b) The light "flickers" irregularly outside eclipse.

(c) Superimposed on these irregular variations, there is a strictly periodic oscillation having $P = 71$ sec and an amplitude in yellow light of 0.05 mag. The oscillation definitely disappears during eclipse.

(d) The average U — B, B — V colors of the nova, outside eclipse, are not like those of any normal star, viz., U — B $\approx$ —0.8 while B — V $\approx$ 0.0. These colors are, however, not unusual in comparison with other old novae and U Gem variables (Walker, 1957).

A series of low-dispersion spectrograms taken by Kraft (1958b) in 1956 with the 100-in. telescope revealed a velocity variation of the He II emission (λ 4686) with $K \sim 100$ km/sec; later a much better series was obtained by Greenstein with the Hale reflector which formed the basis of an extensive discussion of the spectrum as it changed during the cycle (Greenstein and Kraft, 1959;

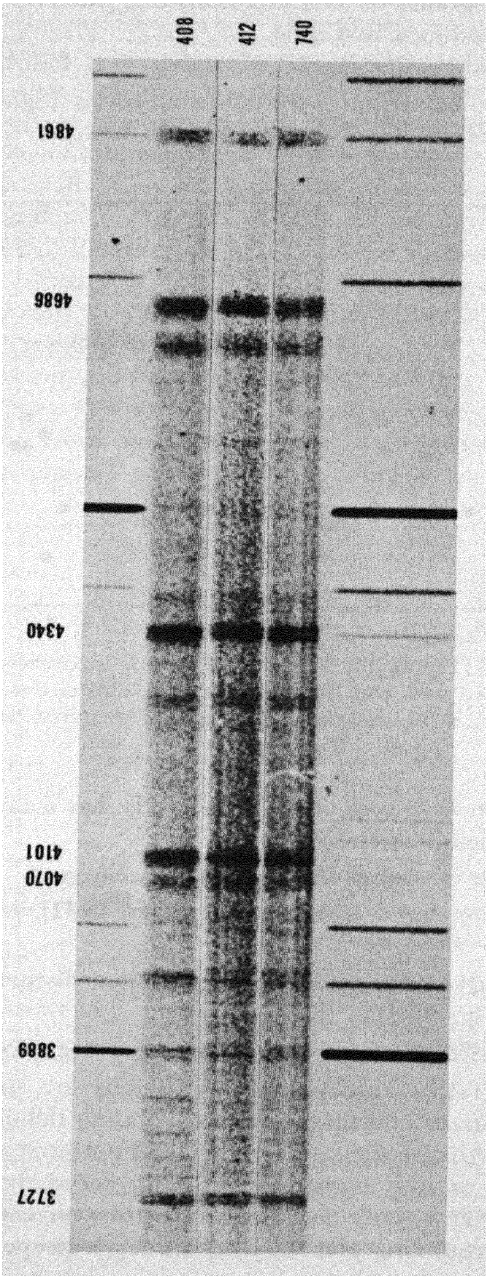

FIG. 4. The spectrum of DQ Her at opposite elongations. The spectra have been accurately aligned to show the radial velocity changes. Phases are: 408 at 0.32 P, 412 at 0.82 P, and 740 at 0.01 P. Notice the shift in λ 4686 and the higher members of the Balmer series. The forbidden emission lines $\lambda\lambda$ 3727, 4070 give no shift and Hβ, very little. The white streak in the bottom spectrum between λ 4101 and λ 4340 is a plate defect.

Kraft, 1959). A number of very short exposures were also made during the eclipse phases. Some spectrograms of DQ Her showing the velocity shift at opposite elongations are reproduced in Fig. 4.

The principal spectroscopic results can be summarized as follows:

(a) He II (λ 4686) and the members of the Balmer series higher than Hγ show a velocity variation interpretable as orbital motion with $K \sim 150$ km/sec (Fig. 5).

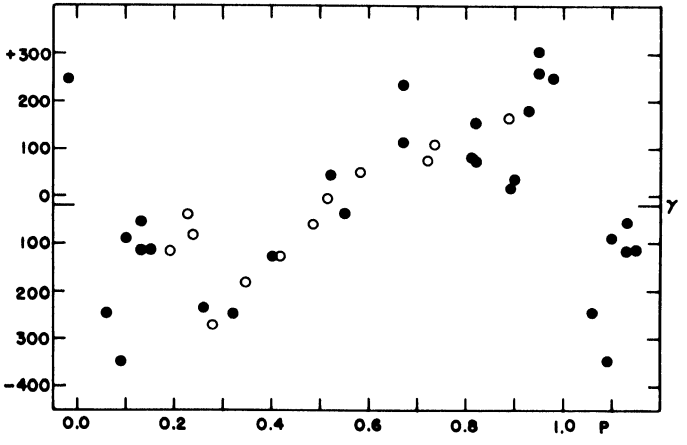

FIG. 5. Radial velocities of He II (λ 4686). The vertical scale is in km/sec. Open circles correspond to exposures obtained with the 100-in. telescope; solid circles, to exposures obtained with the 200-in. Notice the rotational disturbance centered on mid-eclipse (phase 0.0 or 1.0).

(b) Hβ shows no variation in excess of 25 km/sec; Hγ has a range between that of Hβ and the series members above Hγ.

(c) The Balmer decrement is steeper in than outside eclipse.

(d) The forbidden emission lines, namely, [O II] and [S II], have constant velocity.

(e) The He II velocity curve shows a classical rotational disturbance before and after mid-eclipse (cf. Fig. 5).

(f) No trace of the spectrum of the secondary star has been found.

These, to some extent, rather discordant observations are interpreted to mean that there are two sources of emission: the expanding nebular envelope, seen on direct photographs, that was ejected in the 1934 outburst, plus a small, rather dense, emitting disk or ring surrounding the nova and moving with it in the orbit. The latter is responsible for the He II emission and has a slow Balmer decrement. The surrounding planetary nebula has a steeper decrement;

thus Hβ is produced mostly in the outer envelope and the higher members in the dense disk.

However, the most important clue to the correct interpretation of DQ Her is the fact that the eclipse and the rotational disturbance begin and end together. This means that the disk, or ring, is itself responsible for a large, perhaps major, portion of the continuous emission in the form of free-bound and free-transitions of hydrogen. We would scarcely expect such a disk to be entirely stable geometrically, thus accounting for the small changes in shape and position of the eclipse curve. The disk is eclipsed partially; the underlying nova, presumably totally. The curious U − B, B − V colors also become interpretable qualitatively because B − V measures essentially the Paschen continuum and free-free emission, and U − B the Balmer jump in emission (which is observed, cf. Fig. 4). This is illustrated in Fig. 6.

The expansion parallax (Baade, 1940; Walker, 1956) leads to $M_V = +7.4$ (outside eclipse). Thus, if only a small portion of the visual light actually comes directly from the star itself (i.e., the light not arising from conversion of ultraviolet quanta), we have $M_{V_{(star)}} \sim +8$ to $+9$; hence the nova can be

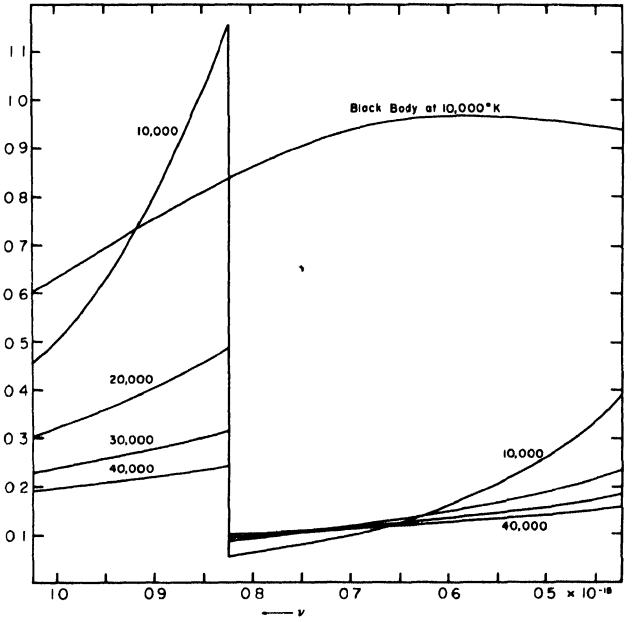

FIG. 6. The free-bound and free-free emission of hydrogen as a function of frequency. The vertical scale has an arbitrary zero point; the vertical position of the black-body curve is arbitrarily located relative to the other curves. The electron temperatures in °K are given.

regarded as a rather bright white dwarf—a view that may be strengthened by the fact that white-dwarf absorption lines are found in the spectrum of one other old nova, WZ Sge (Greenstein, 1957) (see Section IV, A, 2, however). The colors seem best represented by a black body (the white dwarf) with $T_c \sim 80{,}000°\text{K}$, giving only one-fourth the visual light, combined with a disk of electron temperature $T_e \sim 40{,}000°\text{K}$ emitting the balance in free-bound and free-free transitions of hydrogen. These numbers are, of course, rather uncertain, but they do account for the presence of He II in emission in about the right strength.

Walker (1958) suggested that the 71-sec oscillations might be pulsations of the nova; his recent discovery (1961) that the oscillations are not present during eclipse lends support at least to the idea that, whatever mechanism is responsible for them, they originate within the nova and not in the disk. If the pulsational interpretation is correct, one can estimate the mass of the nova because the $P\sqrt{\rho} = Q$ equation gives one relation between mass and radius, and the mass-radius relation from the theory of white dwarfs (Chandrasekhar, 1939) another. The fundamental pulsation frequency σ of white dwarfs was given by Mme Sauvenier-Goffin (1949) as

$$\sigma^2 = \frac{8A}{B} \frac{\int_0^{x_c} r^3 x^4 (x^2+1)^{-3/2}\, dx}{\int_0^R r^4 x^3 dx}$$

where r is the distance from the center of the star to some point in the interior, x is the Fermi threshold (P_0/mc) at that point, x_c is the central value of x, R is the radius of the star, and A and B are natural constants of the white dwarf theory. The equation was integrated (Kraft, 1959) for various degenerate stellar configurations (Chandrasekhar, 1939) with the result that, if the star contains no hydrogen except in a possible nondegenerate surface layer, the correct period is obtained when

$$R_1 = 1.4 \times 10^9 \text{ cm}; \qquad \mathcal{M}_1 = 0.22\, \mathcal{M}_\odot \tag{2}$$

If $i = 77°$, as found by Walker (1956), is approximately correct, $\mathcal{M}_1 \sin^3 i = 0.20 \mathcal{M}_\odot$, and we can find $\mathcal{M}_2$ from the velocity curve using the range of solutions tabulated in Table I. We obtain $\mu = 0.475$ and $\mathcal{M}_2 = 0.24 \mathcal{M}_\odot$. Because of the uncertainties already mentioned in the interpretation of the eclipse data, i is not accurately known, but it does not seem likely that $i < 60°$. In any case, a mass $\sim \frac{1}{4} \mathcal{M}_\odot$ is reasonable for the unseen companion.[3]

[3] According to Schatzman (1961), Mme. Sauvenier-Goffin's calculations are incorrect. Using his revision, I find that a white dwarf of pulsation period 71 sec is extremely close to a polytrope of index 3/2 (nonrelativistic degeneracy), in which case $R_1 = 1.74 \times 10^9$ cm, $\mathcal{M}_1 = 0.12\, \mathcal{M}_\odot$ and $\mathcal{M}_2 = 0.20\, \mathcal{M}_\odot$. The value of $\mathcal{M}_1$ is thus not significantly changed.

TABLE I

RANGE OF SOLUTIONS FOR MASS OF DQ HERCULIS

($K_1 = 149$ km/sec)

μ	$\mathcal{M}_1/\mathcal{M}_2$	K_1 (km/sec)	K_2 (km/sec)	$(\mathcal{M}_1 + \mathcal{M}_2) \times \sin^3 i$ ($\odot$)	$\mathcal{M}_1 \sin^3 i$ ($\odot$)	$\mathcal{M}_2 \sin^3 i$ ($\odot$)	$a_2 \sin i \times 10^{-10}$ (cm)
0.5	1.0	149	149	0.53	0.265	0.265	4.0
0.4	1.5	149	224	1.04	0.62	0.42	6.0
0.33	2.0	149	298	1.79	1.19	0.60	8.0
0.25	3.0	149	447	4.24	3.18	1.06	12
0.167	5.0	149	747	14.4	12.0	2.4	20
0.43	0.75	149	112	0.36	0.15	0.20	3.0
0.375	0.60	149	90	0.27	0.10	0.17	2.4
0.33	0.50	149	75	0.224	0.075	0.15	2.0
0.20	0.25	149	37	0.130	0.026	0.10	1.0
0.035	0.10	149	15	0.088	0.008	0.080	0.4

The characteristic dimension $\mathscr{R}$ is thus $\sim 3.5 \times 10^{10}$ cm for this system, since the mass ratio is close to unity. Unless the unseen star is a white dwarf (which cannot, of course, be ruled out), it would appear to be a star on, or near, the main sequence with $M_V > +9$ (the total light does not appear to be significantly redder during eclipse, according to Walker). A dwarf M-type star would have the appropriate mass and satisfy the magnitude limitation. Once again it would be true, as was the case for T CrB and SS Cyg, that the radius of the red star is of the same order as $\mathscr{R}$. As a check on this conclusion, we note that for any reasonable value of i the duration of eclipse is compatible with dM-star dimensions for the secondary.

III

SOME COMMON AND RELATED PROPERTIES OF THE SYSTEMS DISCUSSED IN SECTION II

Despite the rather large difference in orbital period between T CrB and the other two stars, a geometrical invariant emerges when the systems are compared; viz., the radius of the observed, or inferred, red component is of the same order as $\mathscr{R}$. Another way of stating this is to make the hypothesis that, in all cases, *the red component fills one lobe of the inner Lagrangian surface defined by the restricted problem of three bodies.* In that case material would be ejected by the

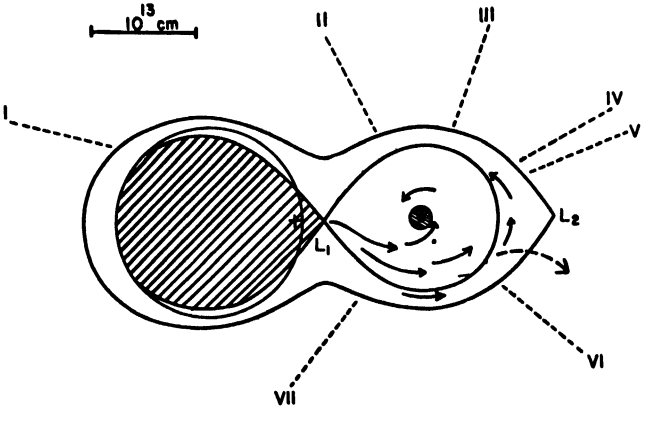

FIG. 7. Geometrical model for T CrB. Material flows out of the gM3 star at L_1 and circulates around the blue component. Some matter may be lost to the system near L_2. Dashed lines indicate aspects corresponding to the phases at which emission-line velocities were measured (cf. Fig. 2). This model, appropriately scaled, provides a schematic representation of SS Cyg, AE Aqr, DQ Her, etc., as well.

red star through the inner Lagrangian point and would take up an orbit around the blue companion in the manner of Kuiper's (1941) ejection of type A. This is illustrated in Fig. 7 for the case of T CrB.

A precise physical description of the flow of gaseous material has not been given primarily because the problem is hydrodynamical in character, the mean free path of a particle in the gas being many order of magnitude smaller than the dimensions of the system. Prendergast (1960) has obtained an approximate solution on the assumption that the pressure terms are small in comparison with the gravitational, centrifugal, and Coriolis forces. The material will take up the configuration of a rotating disk in the plane of the orbit and having a thickness $t = (kTr/\mu gH)^{1/2}$, where r is the distance from the hot star, g is the dynamical gravity at that point, μ is the mean molecular weight, H is the mass of the hydrogen atom, and T is the temperature—in this case, the "temperature" corresponding to the turbulent motions in the gas. It is still the case that one can speak of an "average" circulation radius r about the blue star (of mass $\mathcal{M}_1$) which rotates with a velocity v given by the energy integral of the two-body problem:

$$v = \sqrt{G\mathcal{M}_1/r}\,. \tag{3}$$

Moreover, Jacobi's integral possess a hydrodynamical analogy.

We can test observationally for the existence of such a disk. First of all, if the material really is flattened, then, regardless of its optical thickness, it will produce doubled emission lines when viewed edge-on. Thus the tendency for doubled emission lines should be associated with systems that eclipse. This is certainly the case in DQ Her. The emission lines of SS Cyg are "single" in appearance; the system does not eclipse. The most conspiciously doubled emission lines found so far in a U Gem variable are those of U Gem itself (Kraft, 1962) (cf. Section IV). W. Krzeminski (private communication) reports that U Gem is also an eclipsing binary.

A second observable consequence of our model is the possibility of a relation between the rotational velocity of the disk and the dynamical constants of the orbit. According to Jacobi's integral (Kuiper, 1941), angular momentum is approximately conserved as a particle falls from the inner Lagrangian point and takes up an orbit around the blue star. Thus, from the dimensions of the surfaces given by Kuiper and Johnson (1956), we can write

$$\frac{G\mathcal{M}_1 \sin^3 i}{v \sin i} = \lambda(a_1 \sin i)^2 \left(1.39 \frac{\mathcal{M}_1}{\mathcal{M}_2} - 0.39\right)^2 \frac{2\pi}{P} \tag{4}$$

where $v \sin i$ is the observed rotational velocity of the disk (taken as the half-half width of the emission lines), P is the orbital period, and λ is a constant of order unity (to be determined empirically) describing the fractional loss of

angular momentum. Since for any assumed mass ratio the orbit gives us also $\mathcal{M}_1 \sin^3 i$, the minimum masses of both components can be obtained if $v \sin i$ and λ are known, even though only one spectrum is visible.

We have evaluated λ from two U Gem variables in which both spectra are visible, viz., SS Cyg and RU Peg (cf. Section IV), for which $\lambda = 1.26$ and 1.36, respectively; thus $\langle\lambda\rangle = 1.31$ (cf. Kraft, 1962). Then for $i = 77°$, $v = 5.2 \times 10^7$ cm/sec, the equation can be balanced in the case of DQ Her if $\mathcal{M}_1/\mathcal{M}_2 = 0.91$, $\mathcal{M}_1 = 0.242\bigcirc$, and $\mathcal{M}_2 = 0.265\odot$. This value of $\mathcal{M}_1$ is remarkably close to the $\mathcal{M}_1 = 0.22\odot$ obtained from the pulsational argument, and this lends support to the view that the material circulating about the blue component is actually supplied by a red companion.[4]

A similar argument in the case of T CrB is inconclusive. Here, $v \sin i = 1.42 \times 10^7$ cm/sec (Kraft, 1958), and we take $i \approx 68°$ in accordance with the suggestion of Section II. It turns out that the equations involving $\mathcal{M}_1$ and $\mathcal{M}_2$, viz., Eq. (4) and Kepler's third law, do not have a point of intersection. A solution would be found for $\mathcal{M}_1/\mathcal{M}_2 \sim 0.9$ if $\lambda = 1.5$, about 25% larger than the value of $\langle\lambda\rangle$ derived from SS Cyg and RU Peg. Physically, this suggests that when the dimensions of the system become very large relative to the size of the ring or disk surrounding the blue star, the value of λ must change somewhat from that applicable when these two quantities are nearly of the same order of magnitude.

A third observable consequence of the existence of a rotating disk in these systems is the possibility that a portion of the blue and visual continuum radiation actually comes from the disk itself as a result of free-bound and free-free emission of hydrogen. This is clearly the case in DQ Her (Kraft, 1959) as we pointed out in Section II. Thus the location of old novae and U Gem variables (Walker, 1957) in the U − B vs. B − V diagram need not be compatible with any normal star, reddened or unreddened; effective temperatures based on colors for normal stars cannot, therefore, be assigned to cataclysmic variables.

IV

THE SEARCH FOR NEW BINARIES AMONG U GEMINORUM STARS AND NOVAE

Having described some of the invariant physical properties of known binary systems among novae and U Gem variables, we turn to a discussion of the requirements to be met by an observational program designed to detect binary motion among other stars in these groups. At minimum light, no known novae

[4] Compare, however, footnote 3.

(except η Car) are brighter than 10th magnitude; U Gem stars are all fainter than 12th. A search for eclipses by photoelectric techniques might be carried out with a telescope of moderate aperture, say 30 to 50 in. However, only a small fraction of the supposed binaries could be detected in this way, and the writer has preferred a search conducted spectroscopically. But the limitations are quite severe. A dispersion of not less than 150 to 200 A/mm is desirable, and since the periods may be short, a time resolution of at least 40 min is required. With the 200-in. prime focus spectrograph, the limiting magnitude for a 40 min exposure is about $m_{pg} = 15.5$; this yields a spectrum of $\frac{1}{3}$ mm widening and dispersion 180 A/mm on baked IIa-O plates. There are 22 novae and 25 U Gem stars brighter than $m_{pg} = 15.5$ at minimum light; of both kinds considered together, only 37 can be reached effectively from Palomar.

A. *U Geminorum Stars*

1. *Spectra: Known Binaries*

Of these, six are now known to be binaries with $P < 9$ hr (RX And, SS Aur, Z Cam, SS Cyg, U Gem, and RU Peg), one spectrum is composite (EY Cyg), and one other shows evidence of binary motion with an, as yet, undetermined period (SU UMa). Thus 44% of the U Gem variables that can be observed from Palomar (subject to the limitations discussed above) have been shown at

TABLE II

SUMMARY OF OBSERVATIONAL DATA FOR FIG. 8

Star	Plate no.[a]	Date (U.T.) (mid-exp.)	Length of Exposure (min)	Approx. dispersion (A/mm)	Remarks
U Gem	N1324a	1961 Feb. 10. 162	31	180	
EX Hya	B1607a	1960 Feb. 23. 443	101	180	Sharp emission lines
Z Cam	β1758b	1960 Dec. 19. 444	122	180	arise from Hg vapor
T Leo	B925a	1956 Mar. 5. 371	150	180	in Los Angeles city
RX And	N1156b	1960 Aug. 28. 320	16	180	lights
SS Aur	N1164	1960 Aug. 30. 494	29	180	
RU Peg	N1149a	1960 Aug. 26. 329	30	90	
	N1149b	1960 Aug. 26. 352	30	90	
	N1149c	1960 Aug. 26. 372	31	90	
EY Cyg	N1162a	1960 Aug. 30. 312	40	180	

[a] N = 200-in. prime-focus spectrograph; B = Mount Wilson Newtonian focus spectrograph operating at the 100-in.; β = same, operating at the 60-in.

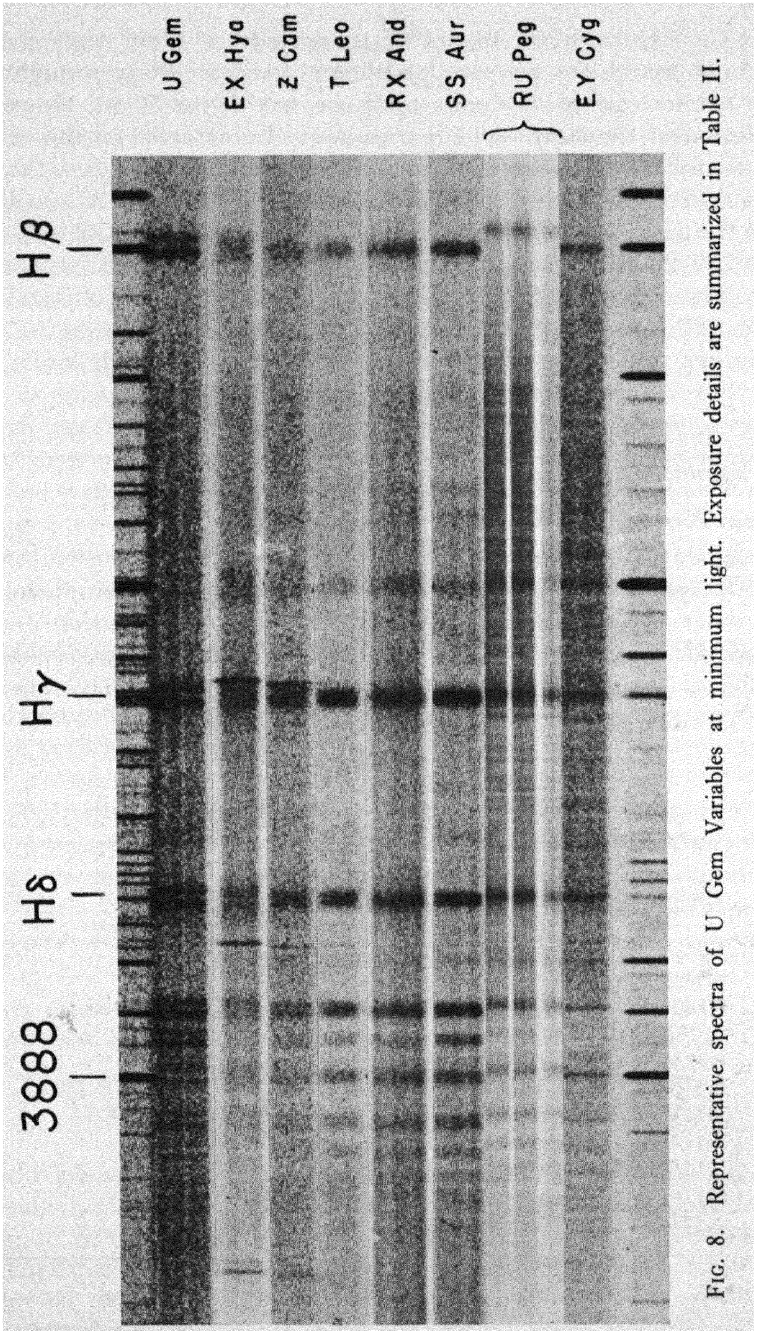

FIG. 8. Representative spectra of U Gem Variables at minimum light. Exposure details are summarized in Table II.

this writing (January 1962) to be binaries, and the presumption is strong that this is true of the others as well. A detailed discussion of the spectra of most of these stars is given in a paper by Kraft (1962) and a montage of representative spectra at minimum light is shown in Fig. 8; observational data relative to this figure are summarized in Table II.

The spectra reproduced in Fig. 8 confirm the results by Elvey and Babcock (1943) and give the following new information: (1) He II (λ 4686) is present in a few spectrograms of U Gem. When spectrograms of this star are lined up to show the variations around the cycle (see Fig. 9), one finds exceedingly

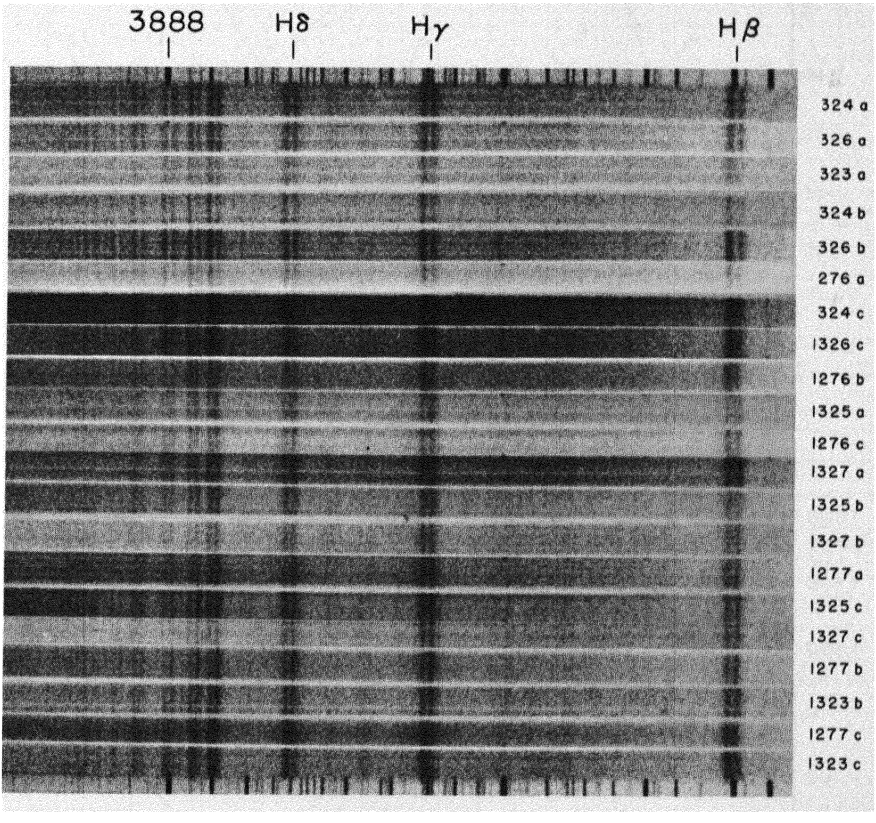

FIG. 9. The spectrum of U Gem around the orbital cycle. Elongation (1) with the blue star receding corresponds to plates near N 1324b and c; superior conjunction (blue star behind) to N 1276c; elongation (2) to N 1325c and N 1327c. Notice the change in visibility of the higher members of the Balmer series, and the change in the relative strengths of the violet and red components of the emission lines at opposite elongations. The spectra have *not* been aligned to show radial velocity changes.

feeble bright structures possibly identifiable with Fe II in emission. These may also be found in SS Aur. (2) A faint trace of the Balmer jump in emisson is present in SS Aur, T Leo, and Z Cam; the jump in emission is easily seen in RX And. However, in all the stars the Balmer lines converge long before

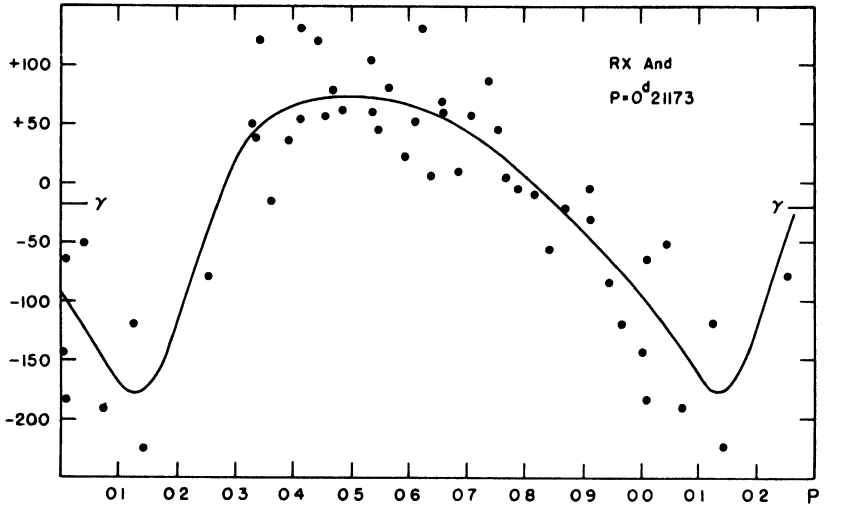

FIG. 10. The radial velocity of the bright lines in RX And. The vertical scale is in km/sec.

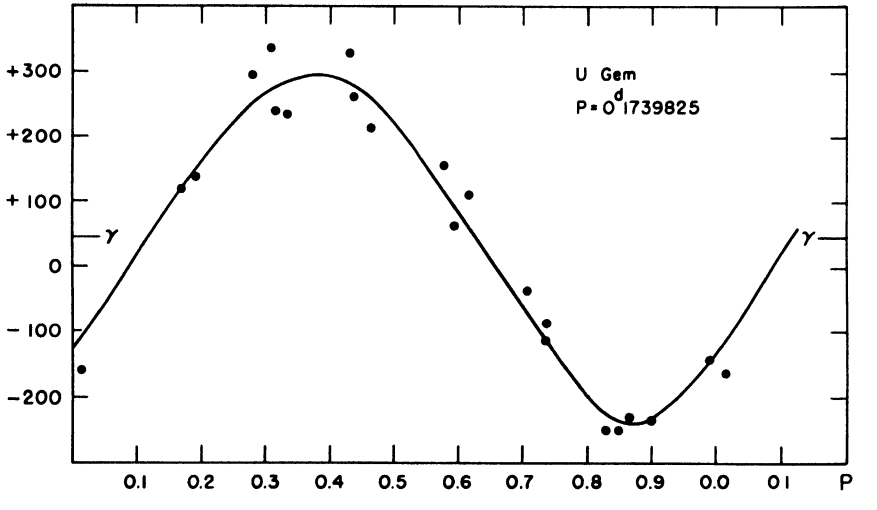

FIG. 11. The radial velocity of the bright lines in U Gem.

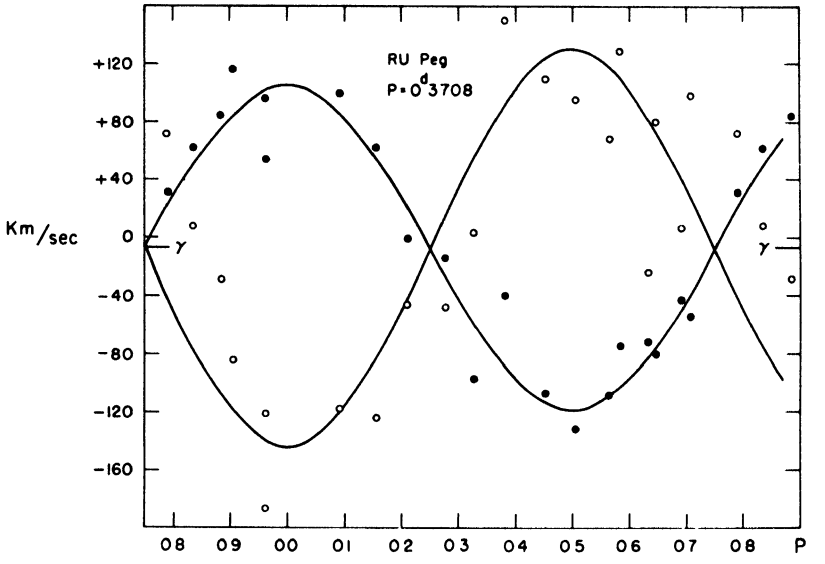

FIG. 12. The radial velocity of RU Peg. Open and solid circles refer to the bright and dark lines, respectively.

TABLE III

ORBITAL ELEMENTS FOR U GEMINORUM VARIABLES

	RX And	SS Aur	U Gem	EY Cyg[b]	SS Cyg	RU Peg
P (hr, min)	5 05	3 30(?)	4 10.5	—	6 38	8 54
P (days)	0.21173	0.15(?)	0.1739825	—	0.276244	0.3708
K_1[a] (km/sec)	77.5	~85	265	(?)	122	137
K_2 (km/sec)	—	—	—	—	115	112
γ (km/sec)	−18	~ + 45	+ 42	~ − 10	−9	−7
Sp. (1)	sdBe	sdBe	sdBe	sdBe	sdBe	sdBe
Sp. (2)	—	—	—	K0 V	dG5	G8 IVn[c]
$a_1 \sin i \times 10^{-10}$ (cm)	2.09	~0.88	6.31	—	4.63	7.02
$a_2 \sin i \times 10^{-10}$ (cm)	—	—	—	—	4.37	5.73
e	0.40	(?)	0.05	—	~0	~0
ω	220°	(?)	160°	—	—	—
$\mathcal{M}_1 \sin^3 i$ (⊙)	—	—	—	—	0.18	0.27
$\mathcal{M}_2 \sin^3 i$ (⊙)	—	—	—	—	0.20	0.32
$\mathcal{M}_1/\mathcal{M}_2$	—	—	—	—	0.90	0.85

[a] Subscript 1 refers to the blue star, regardless of whether or not it is the more massive.
[b] Probably viewed nearly pole-on..
[c] The luminosity class varies during the cycle, but averages MK class ~ IV.

the series limit is reached, and thus they effectively merge with the Balmer continuum. (3) The emission lines of U Gem, EX Hya, and occasionally Z Cam, are doubled—in the case of U Gem, very conspicuously so. (4) The absorption lines of a late-type dwarf star are present in the spectrum of EY Cyg as well as in SS Cyg and RU Peg.

Velocity curves for RX And, U Gem, and RU Peg are shown in Figs. 10, 11, and 12, respectively, and in Table III we summarize the orbital elements for these stars, including also the results from Joy's (1956) study of SS Cyg. In addition, preliminary results for SS Aur, Z Cam, and EY Cyg are given; we expect to obtain more spectrograms of the first two. EY Cyg may have a small velocity variation but it is close to the limit of detection and is most likely a system viewed "pole-on."

The main conclusions summarizing Table III are the following:

1. The mean period of the four best-studied stars is $\langle P \rangle = 0.25$ days.

2. In those cases in which a late-type spectrum is detected, the spectral type is dG or dK; the mass-ratio is near unity with the red star slightly more massive than the blue.

3. From the material at hand, it appears that the late-type absorption spectrum is most easily detected in stars having the narrowest emission lines.

4. In the cases of SS Cyg (cf. Section III) and RU Peg, a comparison of the probable radius of the late-type star and the size of the corresponding lobe of the inner Lagrangian surface (given as soon as $\mathcal{M}_1/\mathcal{M}_2$ and $a_2 \sin i$ known) indicates that the star fills that surface.

For RU Peg, however, there is some direct spectroscopic evidence that the late-type star acts as if it filled this surface. Classification on the MK system is possible since the dispersion is high enough to resolve the ratio λ 4254/λ 4260 and to permit a comparison of intensities of λ 4077 of Sr II and λ 4071 of Fe I. The lines are somewhat broadened by rotation and average during the cycle about G8 IVn. However, the luminosity appears to vary from class V to class III, depending on aspect! The highest luminosity corresponds to phases when the stars are in conjunction, red star behind. If we remember that the effective surface gravity of the red star, if it filled the inner zero-velocity surface, would be zero at the inner Lagrangian point, we can readily understand that the luminosity would appear brightest when that aspect of the star is presented to the observer; this is nearly the case at superior conjunction for the red star. (The effect would be more pronounced, of course, if i were nearer to 90° than is probably the case for RU Peg.)

2. *Masses for the Components*

We cannot make a direct determination of masses for the components of U Gem systems because neither of the two double-line binaries (SS Cyg and RU Peg) is known to eclipse; indeed, Grant (1955) has shown that SS Cyg does not eclipse. This is compatible with our hypothesis that only those stars showing doubled emission lines can be expected to be eclipsing binaries. With $\mathcal{M}_1/\mathcal{M}_2 = 0.90$ for SS Cyg, and with the red component filling its lobe of the inner Lagrangian surface, we have $i \leqslant 64°$, $\mathcal{M}_1 > 0.25\odot$, and $\mathcal{M}_2 > 0.27\odot$. Similarly, if RU Peg does not eclipse, $i \leqslant 64°$, $\mathcal{M}_1 > 0.37\odot$, and $\mathcal{M}_2 > 0.44\odot$.

On the other hand, U Gem, though known to eclipse (Krzeminski, private communication), presents only the spectrum of the blue component in the photographic region. However, we can make use of the measured width of the hydrogen emission lines, and, following the argument of Section III, write

$$\frac{G\mathcal{M}_1}{v} = 1.31\, a_1^2 (1.39 \frac{\mathcal{M}_1}{\mathcal{M}_2} - 0.39)^2 \frac{2\pi}{P} \tag{5}$$

where v is the rotational velocity of the ring, $a_1 = 6.31 \times 10^{11}$ cm, and $P = 1.50 \times 10^4$ sec. The value of v can be obtained from the half-width of the emission line; however, it depends on whether the emitting region is optically thick or thin—the latter leads to $v = 670$ km/sec. Equation (5) can then be balanced reasonably well (assuming the validity fo Kepler's third law) for $\mathcal{M}_1/\mathcal{M}_2$ lying between 0.8 and 1.9, implying $0.9\mathcal{M}_\odot < \mathcal{M}_1 < 5.5\mathcal{M}_\odot$. As we will show in the next subsection, $\langle M_V \rangle \sim +9.5$ for U Gem variables; thus a mass greater than $1.2\mathcal{M}_\odot$ is unlikely for the blue star because it must be a white dwarf (Schwarzschild, 1958). On the other hand, if the emitting region is optically thick, $v < 670$ km/sec and the value of $\mathcal{M}_1$ required to balance Eq. (3) is driven up. It seems likely that $\mathcal{M}_1$ lies in the range $0.9\odot < \mathcal{M}_1 < 1.2\odot$ and that the emitting region is optically thin. Masses of about $1\mathcal{M}_\odot$ for the components in these systems would certainly be compatible with the minimum masses required for RU Peg and SS Cyg.

Krzeminski's recent data for U Gem indicate that the eclipse is total and alsts 10 min in the stage of totality; ingress and egress take 3 min each. If $\mathcal{M}_1 = 1.0\odot$ and $i = 90°$, for example, then $\mathcal{M}_1/\mathcal{M}_2 \sim 0.9$ and the relative velocities of the two stars are 560 km/sec for circular orbits. If the size of the blue star is small compared with that of the red, the relative distance traveled by the red star during totality is the diameter of the red star, and the relative distance during ingress or egress is just the diameter of the blue star. For the former, we get $R_2 = 1.7 \times 10^{10}$ cm; the latter turns out to be $R_1 = 5.0 \times 10^9$ cm.

The given mass ratio and the value of a_2, however, show that $R_2 \sim 4.9 \times 10^{10}$ cm, about 3 times larger than our computed value. This

suggests that i is somewhat less than 90°. Further, the radius R_1 is about 7 times larger than would be expected from the mass-radius relation for white dwarfs (Chandrasekhar, 1939; Hamada and Salpeter, 1961). This may only mean that the inner portion of the rotating disk, the mean radius of which is $r = G\mathcal{M}_1/v^2 = 3.0 \times 10^{10}$ cm, is responsible for a portion of the emission in the blue region of the spectrum. On the other hand, the blue star in this particular system might be somewhat brighter than a white dwarf.

3. *Statistical Parallax*

The systemic velocities and corresponding peculiar radial velocities are listed in Table IV, along with the proper motions (Mannino and Rosino, 1950;

TABLE IV

MAGNITUDES, PROPER MOTIONS, PECULIAR RADIAL VELOCITIES, ETC., FOR U GEMINORUM VARIABLES

	V^a (km/sec)	μ^b (sec of arc/yr)	m_V (min)	Type	Outburst period (days)
RX And	−12	—	13.6	Z	14
SS Aur	+35	—	14.8	SS	54
U Gem	+37	0.078	14.0	SS	103
EY Cyg	~+13	0.062	15.0:	SS	~1000
SS Cyg	+16	0.116	12.1	SS	52
RU Peg	+11	0.070	13.1	SS	70

[a] Radial velocity with solar motion removed.

[b] Mean of values given by Mannino and Rosino (1950) and by Miczaika and Becker (1948).

Miczaika and Becker, 1948). A rough statistical parallax can be obtained, following Smart (1938), from the radial velocities and proper motions of four stars: U Gem, SS Cyg, RU Peg, and EY Cyg. We find $\langle M_V \rangle = +9.5 \pm 0.6$ (m.e.) at minimum light, where the quoted mean error is internal. A more realistic value would be ± 1 mag.

Despite the small number of stars used in the determination of $\langle M_V \rangle$, additional data are not expected to change this value significantly. The proper motions of eight additional U Gem variables for which no radial velocities are known do not differ appreciably from the four used; the radial velocities of RX And, SS Aur, and Z Cam (for which no proper motions are known) are also similar to those of the basic four.

There are additional checks, however, on this value of $\langle M_V \rangle$. Strand's (1948)

well-determined parallax for SS Cyg gives $M_V = +9.5$ at minimum light. From a study of the color of UZ Ser, Herbig (1944) concluded that the star is in front of an absorbing cloud not more distant than 200 pc. This led to $M_V \sim +10$ at minimum. A further indication that $\langle M_V \rangle = +9.5$ is roughly correct is found from a consideration of the colors at maximum light, at which time the spectra of U Gem variables appear to be continuous (or nearly so) (Elvey and Babcock, 1943). Wallerstein (1961) has shown that the U − B, B − V colors of SS Cyg and U Gem fit the black-body trajectory (Arp, 1961) in the color-color diagram. Thus no interstellar reddening is required to explain the observed colors; this is what one would expect since $\langle M_V \rangle \sim +9.5$ leads to a mean distance of only 66 pc for the four basic stars.

4. *Evolutionary Considerations*

A result of $\langle M_V \rangle_{min} = +9.5$ for U Gem variables seems incompatible with a spectral type of dG5-dK5 and $\mathcal{M} \sim 1.0\odot$ for the red components of these systems; in other words, the red components are underluminous for their masses by about 4 or 5 magnitudes. Further, the small peculiar velocities indicate that the stars belong to the galactic disk. The only other binaries of comparably short period which also belong to the galactic disk are the W UMa stars. These too have the property that the primary is underluminous (by 3 or 4 mag.) for its mass. In both cases, however, the underluminous component overflows its Lagrangian surface (Kitamura, 1959; Kraft, 1962). Sahade (1959) and the writer have independently advanced the view that the U Gem variables represent a later stage in the evolution of a W UMa star.

Supporting evidence for this hypothesis is found in Table V, where the

TABLE V

PHYSICAL PROPERTIES OF U GEM AND W UMa STARS COMPARED

Property	U Gem	W UMa
$\langle P \rangle$	0.25	$0^d.37$
$\langle \mathcal{M}_1/\mathcal{M}_1 + \mathcal{M}_2 \rangle$	~1/2	~1/3
$\langle \mathcal{M}_1 + \mathcal{M}_2 \rangle$	~1.5 − 2.0⊙	~1.2 − 2.5⊙
$\langle M_V \rangle$	+9.5	+4.5
$\langle z \rangle^a = \langle r \sin b \rangle$	37 pc	40 pc
$\langle V \rangle$	+16 km/sec	−8 km/sec
σ_V	18 km/sec	26 km/sec
No. stars[b]	6	10

[a] For U Gem and W UMa stars to apparent magnitude limit, $m_{pg} = 17.5$ and $m_{pg} = 12.5$, respectively.

[b] Used in determination of $\langle V \rangle$ and σ_V only.

physical properties of U Gem (Kraft, 1962) and W UMa (Kitamura, 1959) systems are compared. The $z = r \sin b$ distributions are compared in Fig. 13. Here we have considered only U Gem variables brighter than $m_{pg} = +17.5$ at minimum; the corresponding limit for W UMa stars is $+12.5$. It is important

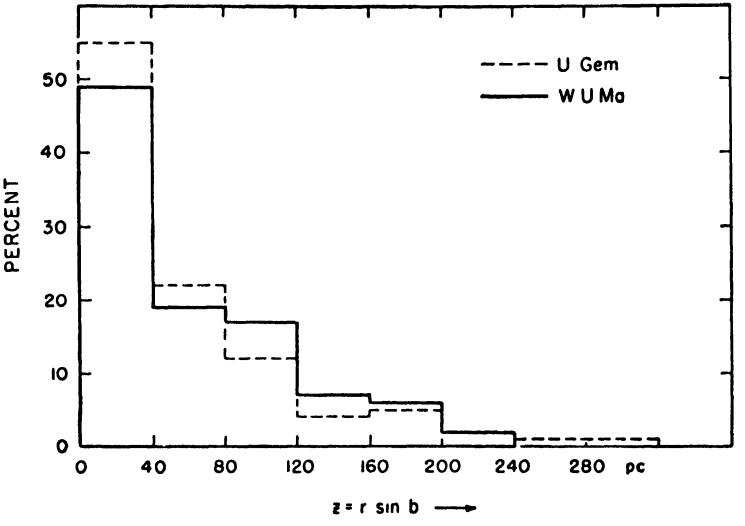

FIG. 13. The $|z|$-distribution of U Gem and W UMa systems compared. Limiting magnitudes are $m_{pg} = 17.5$ and $m_{pg} = 12.5$ for U Gem and W UMa stars, respectively.

to note that $\langle z \rangle$, in the sense used here, does not reflect the true z-distribution because of the faint-magnitude cutoff. The table and figure show that the z-distributions are comparable, the space motions are similar, and the total masses are roughly the same. If our evolutionary pattern is correct, we must simultaneously satisfy the following conditions: (1) the total mass remains nearly constant or perhaps slightly decreases; (2) the mass ratio decreases from about 2 to 1; (3) the period decreases from an average value of 0.37 days to 0.25 days. Huang (1956) has shown that, if a component of a binary star loses mass to its companion, the period will decrease, but if it loses mass into space, the period will increase. Thus our evolutionary picture can be satisfied qualitatively, for if the primary of a W UMa system loses $\sim$50% of its mass to the secondary, the mass ratio will approach unity while the period decreases—in accordance with the hypothesis. We imagine that, during the process, the evolution of the primary is speeded up so that it becomes a white dwarf. Later the secondary begins to overflow its lobe of the Lagrangian surface, giving rise to the conditions now observed for U Gem variables. Kraft (1962) has computed

some elementary examples to show how appropriate combinations of mass transfer and mass loss in a W UMa star can "manufacture" a U Gem system.

Actually, a fairly sharp upper limit to the total masses of systems from which U Gem variables (on the average) can evolve can be set at $\mathcal{M}_1 + \mathcal{M}_2 = 4.2\odot$. If we consider arbitrary pairs of main sequence stars as possible projenitors, those that are in contact will have the shortest periods. For stars of the main sequence, we have roughly $R/R_\odot = (\mathcal{M}/\mathcal{M}_\odot)^{2/3}$. Combining this with Kepler's third law, we have the following condition on the period of a contact binary:

$$P^2 = 0.99 \times 10^8 \frac{(\mathcal{M}_1^{2/3} + \mathcal{M}_2^{2/3})^3}{\mathcal{M}_1 + \mathcal{M}_2} \tag{6}$$

where $\mathcal{M}_1$ and $\mathcal{M}_2$ are in solar units and P is in seconds. (We take $a = R_1 + R_2$, and ignore the distortion of the stellar surfaces.) For all possible divisions of the total available mass between $\mathcal{M}_1$ and $\mathcal{M}_2$, the one leading to the shortest period is that for which $\mathcal{M}_1 \gg \mathcal{M}_2$, i.e., $\mathcal{M}_2 \to 0$. The longest period corresponds to $\mathcal{M}_1 = \mathcal{M}_2 = \frac{1}{2}(\mathcal{M}_1 + \mathcal{M}_2)$. Thus for $\langle P \rangle = 0^d.25$, one finds $\mathcal{M}_1 + \mathcal{M}_2 \cong 4.2\odot$ when $\mathcal{M}_2 \to 0$. This simply means that no pair of main sequence stars in contact can, on the average, evolve into a U Gem variable if the total mass exceeds about $4\odot$. This overly strong condition exceeds only by a factor of 2 the total masses for W UMa stars. Thus it is very unlikely that the projenitor of the blue component in any U Gem system could originally have been earlier than about dA0; this is certainly an observed upper limit for primaries of W UMa systems.

Despite the qualitative success of some of these arguments, a number of important questions are left unanswered. Of greatest importance is the mysterious relation between cataclysmic outbursts and the binary characteristic. One may also ask why the U Gem phenomenon is observed only when the mass ratio is near unity. Indeed, why do we not observe intermediate cases between W UMa and U Gem variables? Finally, one may ask how a star losing mass can have a spectrum corresponding to a mass of order $1\odot$, yet have a luminosity 5 mag. fainter than expected for this mass. As a general rule, we are forced to the conclusion that *spectroscopic parallaxes are meaningless in both W UMa and U Gem systems*, and may be quite meaningless in other close binaries as well.

Some properties of our evolutionary picture can be tested in the case of TX Cnc, a W UMa star that is a member of Praesepe (Haffner, 1937; Eggen, 1961). Morton (1960) has shown that loss of mass for a member of a close binary proceeds on the Kelvin time scale. This is about 1.5×10^6 years for the primary of present mass $1.6\odot$ (Kitamura, 1959) in TX Cnc; this is two orders of magnitude shorter than the age of Praesepe (Sandage, 1957). This presumably means that the components of TX Cnc have only recently begun

the activity presently identified with the W UMa characteristic. The masses of stars presently breaking off the main sequence in Praesepe are about $2\odot$; thus if the lifetime of TX Cnc (as a W UMa star) is significantly less than the age of the cluster, one could imagine that the original system consisted of an A or F type primary of mass $\sim 2\odot$ together with a less massive and much fainter secondary. At first neither star filled its lobe of the Lagrangian surface. As evolution proceeded, the primary expanded to fill its lobe in a time of order 10^8 years; loss of mass has brought it rapidly to its present position in the HR diagram. However, in order to maintain this scheme, one would have to explain how the primary and secondary can evolve down and up, respectively, along a line nearly parallel to the main sequence itself. Calculations related to such considerations would no doubt have to take into account the fact that part of the stellar flux of the primary is in the form of particle, as opposed to photon, emission. The effect of possible accretion on the luminosity of the secondary would also have to be considered (cf. Kitamura, 1960).

B. *Novae*

A spectroscopic search for binaries among old novae, comparable to that already described for U Gem variables, is underway at the time of writing (February 1962); only a few results have been obtained. However, if we compare the spectra of typical old novae with that of U Gem stars at minimum, we find that, as a group, the novae are characterized by a decidedly smaller ratio of emission-line to continuum intensity (Greenstein, 1960); however, we must exclude here old novae still showing strong emission lines produced by the expanding nebulosity of the most recent outburst, T CrB, DQ Her, and GK Per, for example. But the nebulous material does not share the sought-for binary motion, in any case. Thus failure to detect binary motion in some old novae might only reflect serious observational limitations—the emission lines may be too feeble to be measured with confidence for radial velocities, or they may be masked by more powerful nebular emission. A montage of recently obtained spectra of old novae is shown in Fig. 14.

1. *The Spectra of Some Old Novae*

a. DI Lac (1910). A single spectrogram (dispersion 180 A/mm) has been obtained with the star trailed continuously over a long slit for 1^h36^m. The wide, shallow absorption lines of hydrogen seen earlier by Greenstein (1960) are recorded; their profiles are decidedly "dish-shaped"—more like a rapidly rotating star than a white dwarf. Superimposed on the wide absorption lines are feeble, centrally-placed narrow emission lines. Weak, narrow emission is

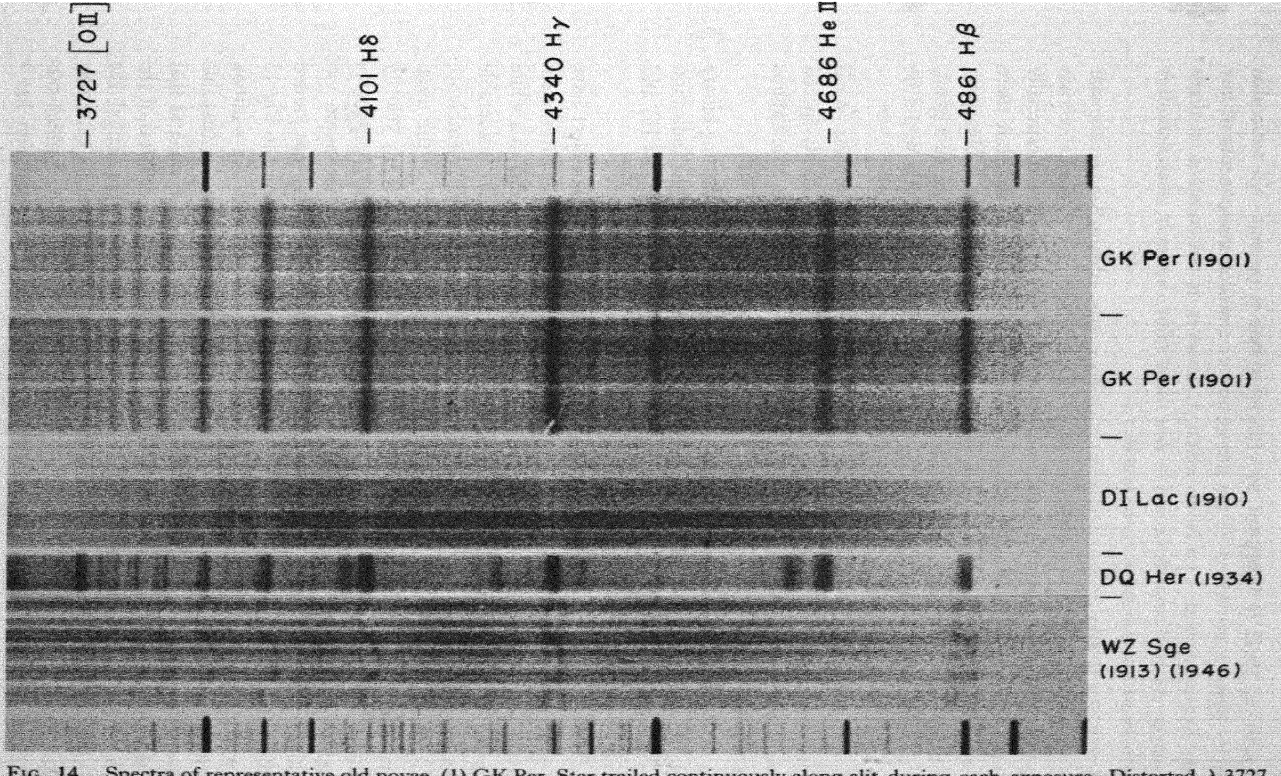

FIG. 14. Spectra of representative old novae. (1) GK Per. Star trailed continuously along slit during each exposure. Distorted λ 3727 results from bringing different portions of outer nebulosity onto slit during trailing. Notice λ 4226, g-band and other absorption features. (2) DI Lac. Star trailed continuously along slit from lower to upper edge; the rate of trailing was increased three times during the exposure. Changes in appearance of He II (λ 4686) are marginal. (3) DQ Her. The spectrum has been discussed in detail in the text. (4) WZ Sge. Spectrum taken by J. L. Greenstein; star was continuously trailed, time runs up. Horizontal streaks are

also seen at He II (λ 4686) but no absorption line is present. No noticeable velocity changes are found in the absorption or emission components of any of the hydrogen lines. The He II emission, however, is not constant, at times appearing doubled and shifted. The line is so faint, however, that definitive results must await further observations.

b. GK Per (1901). Several spectrograms have been obtained when the star was fainter than $m_V \sim 15.0$. All show the absorption lines of a K-type spectrum in addition to strong emission lines of H, He I, and He II; the last is especially intense. The plates have not yet been measured for radial velocity, but there are certainly no large changes. Thus the star may be regarded as a binary on the basis of its composite spectrum. If the K-star should prove to be a giant, the object might be similar to T CrB, in which case the amplitude would be too small to detect velocity changes at 180 A/mm dispersion.

c. V 603 *Aql* (1918). Greenstein (private communication) reports small velocity changes of the hydrogen emission lines in several closely-spaced 35 A/mm spectrograms obtained with the Palomar coudé. More observations are needed.

d. T Aur (1891). Walker (1962) reports that the object is an eclipsing binary with $P = 4^h54^m$. The eclipse is partial and there may be a slight indication of a secondary dip. The star is quite faint photographically ($m_{pg} \sim 16$) and spectra have not been obtained.

e. WZ Sge (1913, 1946). The hydrogen emission lines of this object have for some time been known to be double (McLaughlin, 1953), but Greenstein (1957) discovered as well wide, shallow absorption lines attributable to a white dwarf. The writer observed the star early in his program, despite its considerable faintness, because the doubled emission lines showed a superficial resemblance to those of DQ Her and U Gem. Several spectrograms obtained in the usual way (repeated passes of the image over a short slit) failed to reveal any velocity changes, but indicated that the V/R intensity ratio of the emission components reversed sharply in a time of about an hour. The observational technique was changed and, in order to gain increased time resolution, the star was guided continuously down a long slit without retracing. The results are shown in Fig. 15 in which time runs upward; the spectrum was recorded in 1^h28^m. In addition to the double emission and white dwarf absorption lines, there is an unmistakable "S-wave" emission component. The total amplitude is about the same as that of the separation of the stationary emission lines; evidently the reversal of the V/R intensity ratio on conventionally guided spectrograms represented the reinforcement of the stationary components by this oscillation at its extremes. The "S-wave" has now been detected on four spectrograms, one of which was obtained by Greenstein. Interpreted as binary motion, the oscillation has *e*

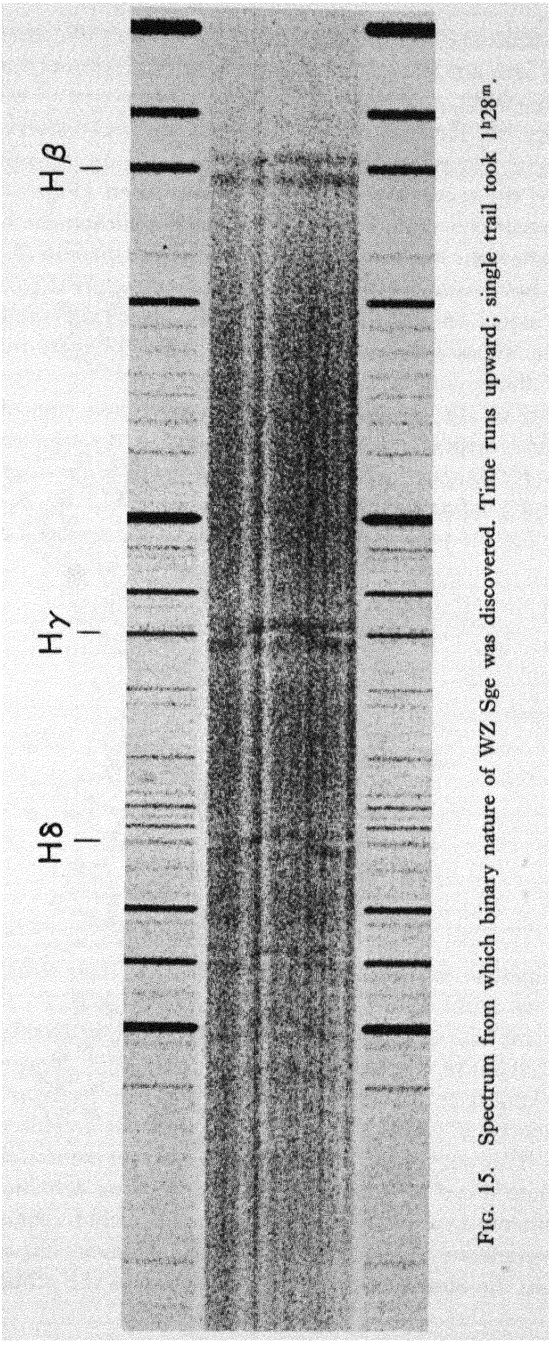

FIG. 15. Spectrum from which binary nature of WZ Sge was discovered. Time runs upward; single trail took 1^h28^m.

small, $2K \sim 1200$ to 1400 km/sec, and $P \sim 80$ min. The exact values of $2K$ is not easy to estimate, however, because of the interference of the stationary emission components.

Subsequently, W. Krzeminski, working with the Lick Observatory's Crossley (36-in.) reflector, discovered that WZ Sge is also an eclipsing binary with $P = 81.5$ min; the secondary eclipse is readily seen (Fig. 16) (Krzeminski, 1962). This result is a remarkable observational achievement not only because of the star's faintness, but also because a nearby companion (8″ away) must be "scooped-in" by the photometer diaphragm. Fortunately the companion, while of brightness equal to WZ Sge in the yellow, is considerably fainter in the ultraviolet; the eclipse information obtained so far therefore refers to the combined light of the two stars in the ultraviolet.

On the basis of the presently available information, the object is difficult to interpret and evidently somewhat unique. For definiteness, take $i = 90°$. Then if $K \sim 650$ km/sec, we have $\mathcal{M}_1 + \mathcal{M}_2 = 1.62/(1 - \mu)^3$ in solar units, where subscript 1 refers to the "seen" oscillation and $\mu = \mathcal{M}_1/(\mathcal{M}_1 + \mathcal{M}_2)$. In Table VI, we list the total and individual masses for assumed mass ratios. The

TABLE VI

μ	$\mathcal{M}_1$ (⊙)	$\mathcal{M}_2$ (⊙)	$10^{-10}\,a$ (cm)
0	0	1.62	5.08
0.01	0.017	1.65	5.15
0.1	0.22	2.00	5.64
0.2	0.63	2.53	6.35
0.3	1.42	3.30	7.26
0.4	2.99	4.49	8.47
0.5	6.46	6.46	10.2

white dwarf lines do not appear to move. However, their structure is so diffuse it is unlikely we could detect a velocity variation with $K_2 < 350$ km/sec. If we go to the extreme case of $\mathcal{M}_2 \to 0$, the mass of the white dwarf would be $1.62\odot$, a value still well above the theoretical white dwarf limit. However, if we reduce K_1 from 650 km/sec to 580 km/sec, the limiting case leads to $\mathcal{M}_2 = 1.2\odot$, an acceptable theoretical value. This is close to, but not outside the observational uncertainties. This suggests a model (Herbig, private communication) in which we have a white dwarf surrounded by a rotating ring containing a (essentially massless) condensation. In its favor, this model would require $2K$ to be the same as the separation of the stationary emission components, which is certainly the case within the observational errors. Against it is the problem of the origin

of the ring, the maintenance of the condensation, and the dissimilarity of this picture to that advanced for other old novae and U Gem stars.

However there is one observed fact that suggests a related, but different interpretation. The phasing of the radial velocities and the ultraviolet light

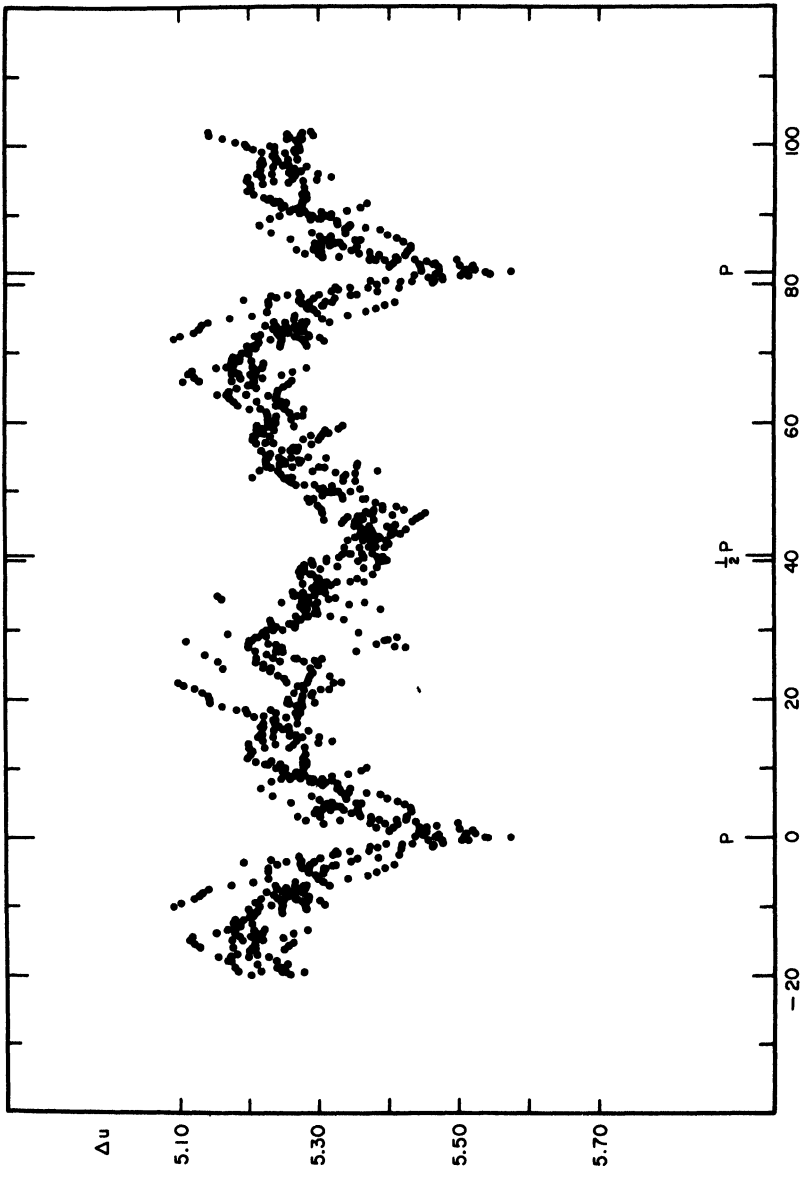

FIG. 16. The light curve (in the ultraviolet) of WZ Sge (courtesy W. Krzeminski). The period is 81¼ min.

variations indicate that the condensation itself is being eclipsed at primary minimum. This means that the condensation is responsible for a large fraction of ultraviolet continuous radiation, and one is reminded of the ring surrounding the blue component of DQ Her. We recall that this ring shines by fluorescence of ultraviolet quanta, has a radius r of about 2×10^{10} cm, and rotates with a velocity v of 500 km/sec (Kraft, 1959). Suppose there were a condensation, or "lump," in this ring. It would have a period of $2\pi r/v = 40$ min. This is a number not unlike the 81.5 min period of WZ Sge. One wonders if, for reasons difficult to explain, a condensation is maintained in a ring surrounding the blue (white dwarf) component of WZ Sge; this moves with a period of 81.5 min, alternately eclipsing, and being eclipsed by, the white dwarf. The material of the ring is supplied by a faint, as yet undetected, red companion moving with the white dwarf in an orbit, with a period of the order of hours. An additional eclipse might be expected which has not yet been detected. A velocity variation of the whole Be-type emission in WZ Sge should consequently be sought.

2. *Hypotheses on the Origin of the Outbursts; Evolutionary Considerations*

The preceding observational material coupled with our prior knowledge of the nature of T CrB and DQ Her now makes highly tenable the hypothesis that all novae are close binary stars. However, some years ago it has appeared reasonable to suppose that single stars, on the way to becoming white dwarfs, might pass through the nova stage. For, if in the age of the universe all stars more massive than about $1.5\mathcal{M}_\odot$ should have evolved off the main sequence because of hydrogen burning, and if only a relatively short time were spent in the red giant stage, all such stars would rapidly have become white dwarfs. Greenstein (1958) has shown, from the theory of degenerate stellar configurations (Chandrasekhar, 1939), that white dwarfs have an average mass of $0.6\mathcal{M}_\odot$. The mechanism for loss, then, of *at least* several tenths of a solar mass per star was presumably provided by the nova phenomenon. Greenstein's (1957) discovery that WZ Sge has a white dwarf spectrum seemed to provide confirmation for this picture. Naturally, the hypothesis required that all novae are in fact recurrent. But there are several arguments against this hypothesis. First, according to Salpeter (1955), the Galaxy contains about as many main-sequence stars below the solar luminosity as the total of all stars that are now in the white dwarf graveyard. Thus the Galaxy contains perhaps 5×10^{10} totally evolved stars. From Arp's (1956) work on the novae in M 31, the frequency is 26 per year; estimates of the Galactic frequency as comparable. Surely in the last 10^9 years ($\sim$1/10 the age of the Galaxy), we cannot have expected the population of Galactic stars to have changed significantly, and the frequency of 26/yr can be taken as constant over that time. Thus we find

26×10^9 explosions in 10^9 years, so that no evolved star can have had more than one or two outbursts. Since a nova explosion involves the ejection of only 10^{-4} to $10^{-5}\mathcal{M}_\odot$, we cannot account in this way for a loss of several tenths or more of a solar mass. This argument would still be true even if Salpeter's result were in error by one or two orders of magnitude.

Second, because they are members of many systems, estimates of mass can be made for T CrB, SS Cyg, and DQ Her; the blue stars have masses of about $2.5\odot$, $1\odot$, and $0.25\odot$, respectively. Though these numbers are not known with precision better than perhaps 50%, we note that the range is quite large and thus the tendency for outbursts (if the binary nature is only accidental and not generic) cannot have much to do with the total mass of the star. The case of DQ Her is especially puzzling. If the blue component of this system already has fallen well below the mass limit for white dwarfs, why need the object explode at all? Once again, it would seem that the binary nature, in some way, must play the leading role in generating the outbursts.

But the main prop supporting the argument that the nova phenomenon provides a significant mass-loss mechanism for massive stars was knocked out with Deutsch's (1956, 1960) discovery of large-scale secular mass loss from red giants. The process appears to be operative in the evolution of all massive stars and takes place with adequate efficiency.

If it is true, therefore, that a necessary condition for a star to become a nova is that it is a member of a close binary system, what processes are envisaged by which the outbursts can be generated? Schatzman (1958, 1959) suggests that, for both U Gem stars and novae, nonradial oscillations are set up in one component by the orbital motion. If resonance conditions are reached between the period of the orbital motion and the period of one of the modes of nonradial oscillation, the amplitude may grow without bound if the damping constant is negative or vanishes. It is supposed that, at some time in the evolution of the nova component, the energy sources lie close enough to the surface that the damping constant can vanish. In favor of the argument is the result that matter can be ejected along the polar caps and in certain belts and zones. This would be in agreement with the observations by Weaver and others that nova shells are ejected in "cones" and not in a spherically symmetrical fashion.

On the other hand, it is known that "flickering" in the light of novae and U Gem stars is associated with the blue component—in most cases, a white or near-white dwarf. This component has generally been regarded as the nova, though it must be admitted direct observational evidence in support of this identification is lacking. A white dwarf has a density distribution lying between polytropes of indices 3/2 and 3; for the latter, Cowling (1941) has computed the fundamental period of nonradial oscillation, which for a typical white dwarf is of the order of 10 sec. It is difficult to understand then how a typical

orbital period of a few hours can resonate with a nonradial oscillation having $P \gtrsim 10$ sec. If the red component were really the nova, this difficulty could be overcome. But then one wonders what source of energy generation near the surface could be invoked which would lead to small damping. It seems to the writer more likely that the blue star raises tides on the red component which may aid in the ejection of material by the latter through L_1—but possibly nothing more spectacular than this.

An alternative picture is based on the assumption that the white dwarf component accretes material from the ring of matter ejected by the red star, an hypothesis already advanced in the interpretation of AE Aqr (Crawford and Kraft, 1956). A degenerate or near-degenerate stellar configuration presumably has exhausted its hydrogen supply except for a possible nondegenerate envelope of thickness $\sim$100 km. If material should be accreted onto the surface of such an object, the hydrogen-rich envelope would be depressed gradually into the degenerate zone; if the core temperature is high enough, hydrogen burning begins. A remarkable property of degenerate material is that the equation of state does not involve the temperature. Thus the increased energy generation is not accompanied by a corresponding increase in pressure leading to expansion of the material; the matter simply heats up, giving rise in turn to increased energy generation, etc. Because of the high power dependence in the hydrogen-burning energy-generation laws, an explosion may result. An argument of this kind was first advanced by Mestel (1952) in his accretion theory of supernovae. A critical factor would seem to be the rate at which electrons in the core can conduct away the heat of any localized "hot-spots." If this were important, one would have to wait for the heating of the entire core. The critical factor must be a comparison of the rate of local heating (a factor presumably proportional to the accretion rate) at the outer edge of the core with the rate of cooling by electron conduction.

This picture has the advantage of making necessary the presence in the system of a star which overflows its Lagrangian surface and thereby acts as a source for the material ultimately accreted by the blue star—a requirement in harmony with present observations. It also leads naturally to recurrence of outbursts (so does the model advanced by Schatzman), separated by a characteristic induction time, and to a location for the explosions which is not deep-seated. However, the present remarks are entirely qualitative, and the way in which the frequency and amplitude of the outbursts are related to the accretion rate and to the core temperature of the white dwarf has not been worked out.

We conclude this section with a few remarks on the possible evolution of such objects as DQ Her. Here we are confronted with the problem that the *total* mass of the system may be no more than $\frac{1}{2}\mathcal{M}_\odot$, yet, if evolutionary arguments for single stars apply, one component must surely once have had

$\mathcal{M} \gtrsim 1.5\mathcal{M}_\odot$. Significant mass loss must have occurred. Huang's (1956) treatment of the problem has already been discussed in connection with the evolution of U Gem variables. Here we integrate his equations of mass transfer and/or mass loss for a binary system in the case that the ejection velocity is small (compared with the relative velocities of the components) and $e \sim 0$. We find then

$$\frac{P}{P_0} = \left[\frac{(\mathcal{M}_p + \mathcal{M}_s)_0}{(\mathcal{M}_p + \mathcal{M}_s)}\right]^2 \left[\frac{(\mathcal{M}_s)_0}{\mathcal{M}_s}\right]^3 \tag{7}$$

where subscript "0" refers to the initial values, and "p" and "s" refer to the *original* primary and secondary (by mass).

We notice that the two factors in Eq. (7) refer, left to right, to the loss of mass by the system (tending to increase the period) and to loss of mass from primary to secondary (tending to decrease the period). Because of the cubic dependence in the second factor, it seems possible to decrease the period despite considerable total mass loss. Thus, for example, suppose we begin with $(\mathcal{M}_p)_0 = 1.5\odot$, $(\mathcal{M}_s)_0 = 0.1$, and $P_0 = 1.0$ days. Then, if we lose $\mathcal{M} = 1.0\odot$ from the system (i.e., from the primary), and in addition transfer $0.2\mathcal{M}_\odot$ from primary to secondary, we find $\mathcal{M}_p = 0.3\odot$, $\mathcal{M}_s = 0.3\odot$, and $P = 0.26$ day, values not greatly different from those of DQ Her. While it is easy to make such calculations, it is still not at all obvious how a star can lose 80% of its own mass, becoming a white dwarf in the process.

Even more puzzling is the case of T CrB. Here the blue component has a mass of perhaps $2.5\odot$, very much above the white dwarf limit. If the spectroscopic luminosity of the gM3 companion can be relied upon, then the blue star is not far from the position it should have in the H-R diagram if it were burning helium in equilibrium (Cox and Giuli, 1961; Cox and Salpeter, 1961). The star must therefore still lose considerable mass to become a white dwarf and the stellar configuration can scarcely be degenerate. This star appears to provide an exception to our accretion hypothesis for the explosions, but the very long orbital period is inconsistent with resonance oscillations of the blue star. The outbursts repeat; in 10^6 years, we find a mass $\sim 1\mathcal{M}_\odot$ might well be ejected. Perhaps this star is the "old-fashioned" exception to our arguments—an object that really must have outbursts to reach the white dwarf stage! For this reason, we must be prepared for the possibility that nova explosions arise from more than one set of physical circumstances.

APPENDIX

Some "Nonexplosive" Close Binary Systems

We will consider briefly in the Appendix some binary systems similar in physical characteristics to the cataclysmic double stars, but which are not

known to be members of the nova or U Gem groups. Almost all are found, however, to have "activity" at minimum light.

a. VV Pup. This remarkable object was for some years considered to be an RR Lyr star with $P = 100$ min. The mean photographic light curve determined by Alden (1931) is shwon in Fig. 17. One notes that the rise to maximum

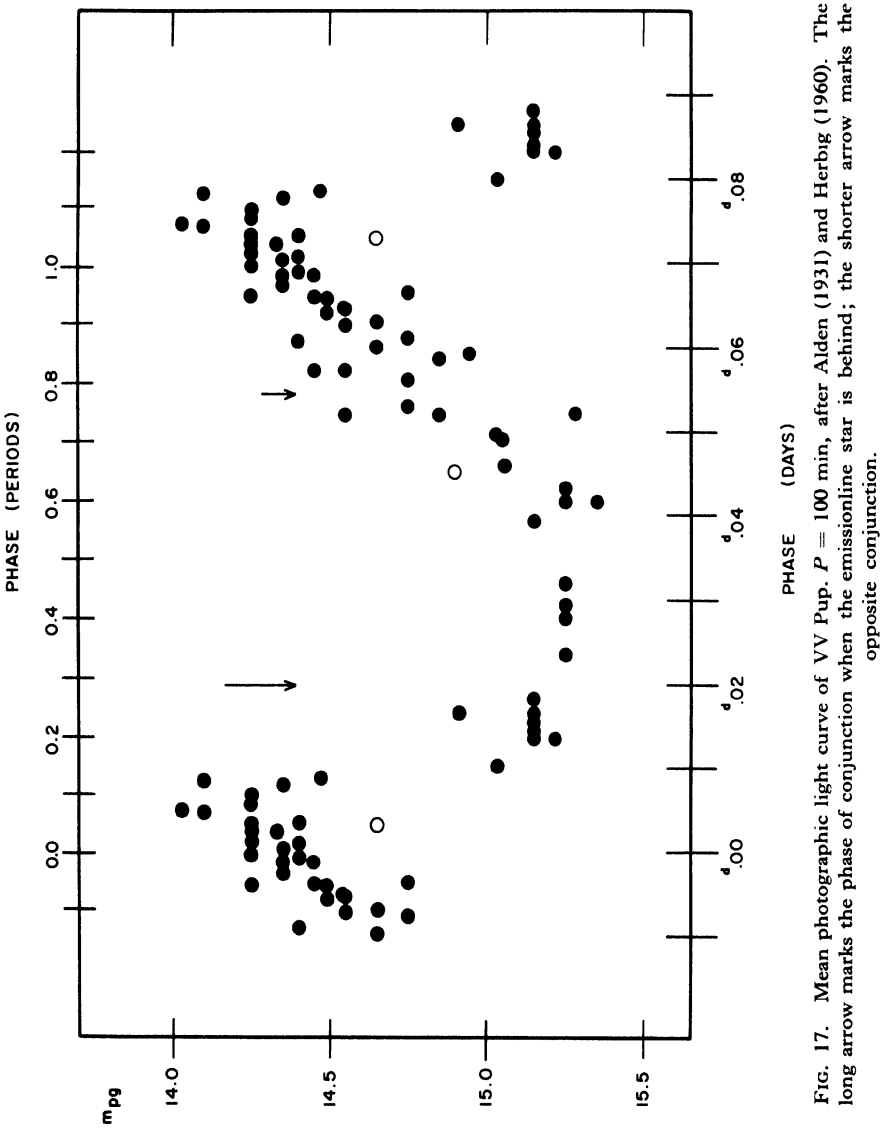

FIG. 17. Mean photographic light curve of VV Pup. $P = 100$ min, after Alden (1931) and Herbig (1960). The long arrow marks the phase of conjunction when the emissionline star is behind; the shorter arrow marks the opposite conjunction.

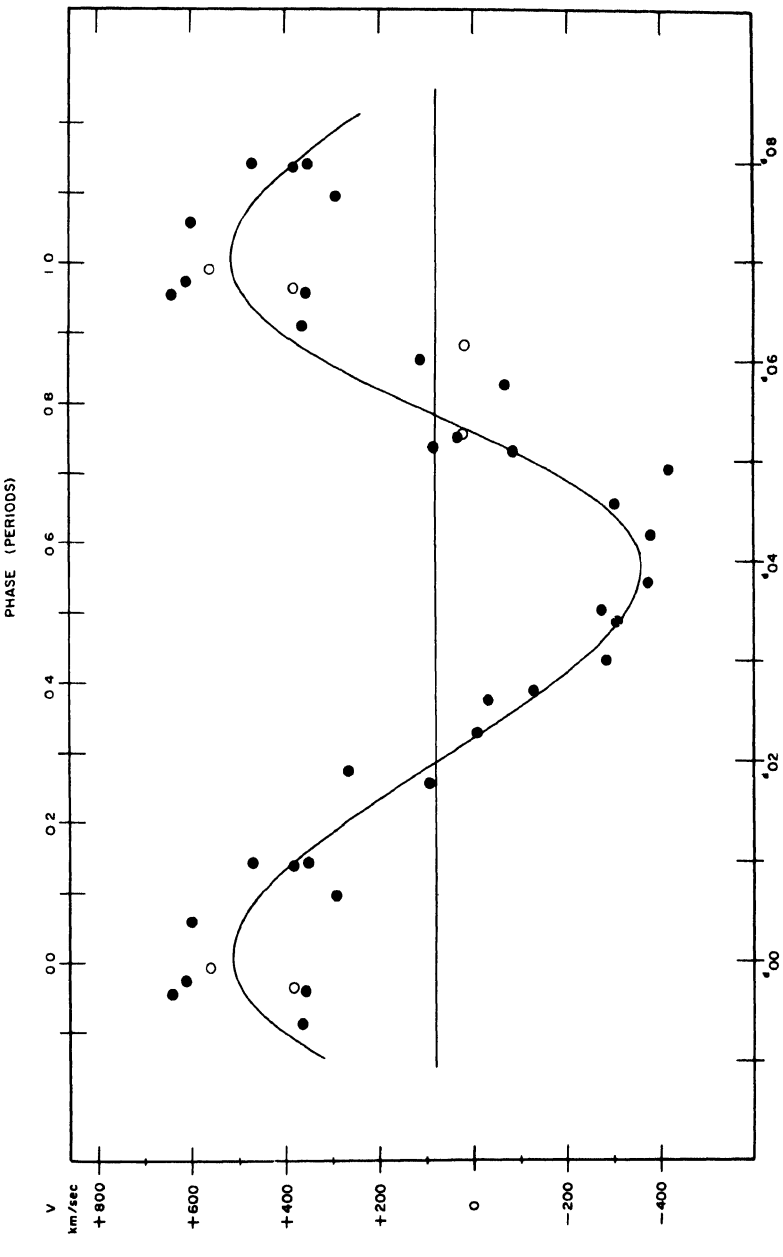

FIG. 18. The radial velocity of the emission lines of VV Pup (courtesy G. H. Herbig). Open circles refer to observations of low weight.

light is much slower than the decline to minimum, a feature not characteristic of RR Lyr stars. Another peculiarity is the existence of a secular fluctuation in brightness. The star was as faint as 17th magnitude at minimum in 1948-1949, though at the time of discovery (Van Gent, 1931) $m_{pg(min)} \sim 14$. But most curious of all, the 100-min variations disappeared altogether for hundreds of cycles in 1948-1949. Yet, when they reappeared they occurred in the same phase relationship that had been established prior to their disappearance!

Herbig (1960) discovered that the spectrum consisted of strong bright lines of H and He II (λ 4686), totally unlike that of any RR Lyr variable. The emission line velocities varied in a fashion interpretable as orbital motion with $P = 100^m$, $K = 437$ km/sec, e small, and $a \sin i = 2 \times 10^{10}$ cm; the object is clearly an eclipsing variable with a seriously distorted light curve. The radial velocity curve, derived from spectrograms made with the Lick Observatory Crossley reflector, is shown in Fig. 18; the spectrum of the secondary was not recorded. Spectroscopic conjunction, in which the star carrying the emission lines is behind, takes place at the beginning of minimum light. Thus the very slow rise to maximum is an exaggeration of similar effects found in DQ Her and UX UMa (see below).

A schematic diagram representing Herbig's interpretation of the system is shown in Fig. 19. Because the emission lines are carried with the star observed to be eclipsed, and because these lines are roughly constant in intensity, Herbig assumes that the larger (eclipsed) star is the brighter. The distribution of temperature over the face of this star is such that a hot spot is presented "full face," so to speak, at maximum light. This is quickly eclipsed by the smaller, dark companion, after which the dimmer, cooler face of the larger star is presented. The secular changes in light are thus interpreted as resulting from disappearance of the hot region, in which case the maxima disappear, and from changes in brightness of the fainter hemisphere. This model would predict that when the star was very faint (as it was in 1948-1949), eclipses of a regular sort, centered on spectroscopic conjunction, should occur. This picture, while explaining the main photometric and spectroscopic features, probably should not, as Herbig remarks, be taken too literally. In particular, one wonders how the "hot spot" is maintained, and how it is that, in similar systems (UX UMa, DQ Her) having a shoulder on the light curve before the drop to minimum, the hot spot is always in the same relative geometric position.

A somewhat different model can be advanced in the light of properties of DQ Her. We recall that a major portion of the emitted *continuous* radiation of DQ Her is provided by free-bound and free-free emissions of hydrogen in a rotating disk surrounding the blue component. We advance a picture for VV Pup in which the hot star is smaller than, or at least does not exceed in size, the dark companion. Material flows out of the dark star toward the *following*

hemisphere of the hot one and circulates around the latter; a concentration is built up along the following hemisphere in a position similar to that of Herbig's hot spot. We postulate that the major proportion of the blue and visual continuum light comes from this concentration in the form of free-bound and

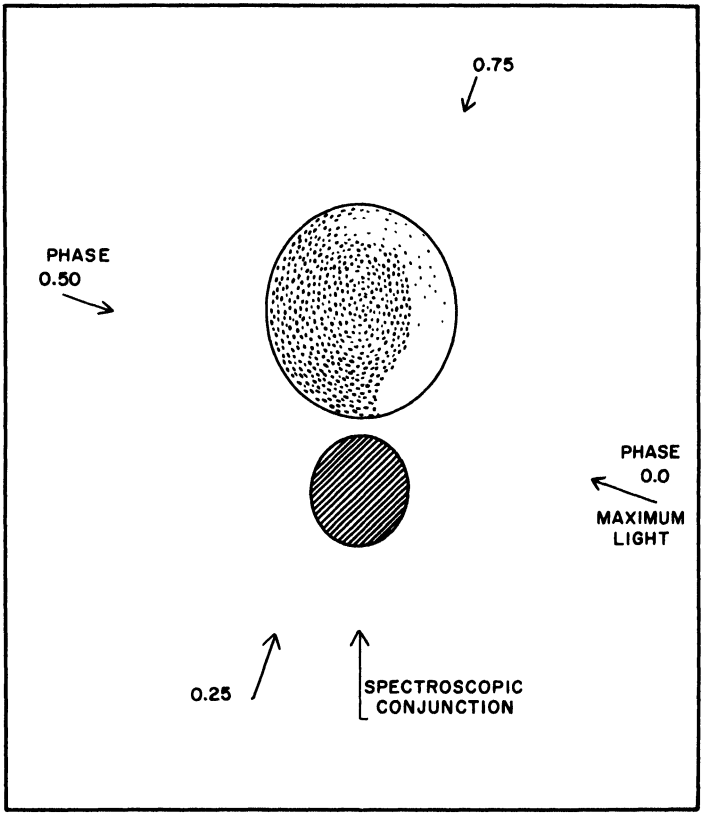

FIG. 19. Schematic model of VV Pup (after Herbig). The smaller star is dark and the "hot-spot" on the larger star is indicated by the absence of shading.

free-free emission; thus the ultraviolet quanta of the hot star appear by fluorescence in the blue and visual portions of the spectrum. If the properties of this region are like those of the ring in DQ Her ($T_e \sim 40{,}000°K$, $N_e \sim 10^{13}$ cm^{-3}, $T_{star} \sim 80{,}000°K$), which is likely since the line spectra are very similar, self-absorption plays a role in the formation of the hydrogen lines. Thus the lines are cut down relative to the continuum in the concentration in comparison to the situation in which lines and continua are both optically thin. On the

preceding side of the hot star, however, the density is lower and self-absorption in the lines is less important. Thus the emission lines might be produced with nearly equal intensity all around the hot star, but the continuous radiation would be concentrated near the following hemisphere. In this picture, the decline in brightness in 1948-1949 is attributable to a decline or stoppage of flow from the dark star. This hypothesis seems to the writer slightly more natural than Herbig's because it invokes properties known to exist in stars of similar type, but it also requires some rather special conditions—viz., those required to separate the center of light from the center of mass. At the present time, we must agree with Herbig and admit there is no entirely satisfactory model for VV Pup, but several critical observations and measurements might be made. Continuum colors are needed to test the hypothesis of the presence of Paschen and Balmer continua; measurements of the Balmer decrement will show whether or not self-absorption is significant; and a rotational disturbance surrounding eclipse should be looked for.

b. UX UMa. The star is a well-known eclipsing binary of Algol type (Linnell, 1950; Walker and Herbig, 1954; Johnson, Perkins, and Hiltner, 1954) with a period only four minutes longer than that of DQ Her. Considerable

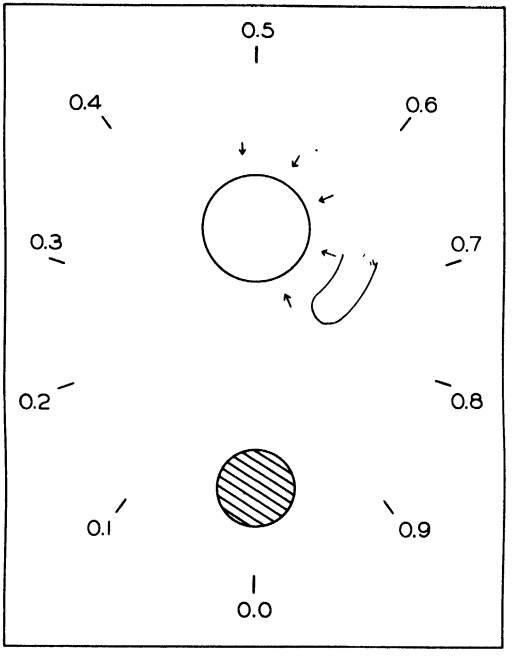

FIG. 20. The Walker-Herbig model for UX UMa. The lower star is the fainter.

photometric "activity" outside eclipse has been noted, especially in the ultraviolet, but the fluctuations are less pronounced than those of DQ Her or T CrB. The star is anomalously bright just before eclipse, and there is a delay in recovery from eclipse (phase 0.0) between phases 0.03 and 0.10 P. This is similar to the behavior of VV Pup, but is much less pronounced.

Spectroscopically, the star is quite disappointing, and the spectrum is somewhat reminiscent of Nova (DI) Lac. Herbig (Walker and Herbig, 1954) finds wide, very shallow absorption lines at Hγ, Hδ, and Hϵ though Hβ is weakly and variably in emission. These wide absorption lines are crossed by narrow absorption features seen in about half the cycles observed by Herbig. They are present only in the phase interval 0.5 P to 1.0 P, and are displaced longward by a constant amount of 350 to 400 km/sec. Owing to the absence of strong features, either in emission or absorption, no certain velocity variation during the cycle has been detected.

A possible working model advanced by Walker and Herbig (1954) is shown in Fig. 20. A cloud of luminous material is concentrated near the hot star in such a position that it is projected on the disk near phase 0.75 P; this accounts for the rise in light just before eclipse. An appendage of cooler material is seen projected on the hot star between phases 0.50 P and 0.75 P; this is responsible for the sharp absorption lines seen in the higher Balmer lines. In the present case, it is clear that the gas cloud must be relatively closer to the surface of the hot star than is presumably the case in DQ Her or perhaps in VV Pup. The general similarity of the picture advanced by Walker and Herbig for UX UMa and the models proposed by the writer for VV Pup and DQ Her is clear, particularly in the fact that the cloud is found along the following hemisphere of the hot star, and is responsible for some of the continuous radiation of the system. If the latter were true, then a photometric analysis of the eclipse data (Linnell, 1950) is, in principle, somewhat meaningless, assuming as it does essentially spheroidal or elliptical stars (cf. Kraft's discussion of DQ Her, 1959). Thus the relative sizes and separations of the two components remains in doubt.

c. AE Aqr. Joy (1954) discovered that this "flaring" variable is a spectroscopic binary with $P = 16^h49^m$. The spectra of both components (types dK and sdBe) are seen; there is evidence that the red component overflows its lobe of the inner Lagrangian surface (Crawford and Kraft, 1956), the ejected material forming a ring or disk around the blue companion. The mass ratio is near unity, and the minimum masses are close to $1\mathcal{M}_\odot$. The evolutionary pattern for this object may be similar to that advanced for the U Gem variables (Kraft, 1962) except that the masses of the components are probably larger than those found in typical U Gem systems.

Using the evolutionary models of Sandage and Schwarzschild (1952), Crawford

and Kraft showed that the red star could lose mass at a rate ($\sim 10^{25}$ gm/yr) sufficiently fast to insure continuity of gas flow around the blue star, assuming that all the material of the ring is eventually accreted by the latter. It was also suggested that the accretion rate might be sufficiently high to account for a substantial fraction of the radiant energy emitted by the blue component.

References

Alden, H. L. (1931). *A. J.* **41**, 89.
Arp, H. C. (1956). *A. J.* **61**, 15.
Arp, H. C. (1961). *Ap. J.* **133**, 874.
Baade, W. (1940). *P. A. S. P.* **52**, 386.
Baade, W. (1958). *In* "Stellar Populations" (D. J. K. O'Connell, ed.), p. 165. North Holland Publ., Amsterdam.
Blaauw, A. (1961). *B. A. N.* **15**, 265.
Chandrasekhar, S. (1939). "An Introduction to the Study of Stellar Structure," p. 412, Univ. of Chicago Press, Chicago, Illinois.
Cowling, T. G. (1941). *M. N. R. A. S.* **101**, 368.
Cox, J. P., and Giuli, R. T. (1961). *Ap. J.* **133**, 755.
Cox, J. P., and Salpeter, E. (1961). *Ap. J.* **133**, 764.
Crawford, J. A., and Kraft, R. P. (1956). *Ap. J.* **123**, 44.
Deutsch, A. J. (1956). *Ap. J.* **123**, 210.
Deutsch, A. J. (1960). *In* "Stellar Atmospheres" (J. L. Greenstein, ed.), p. 543. Univ. of Chicago Press, Chicago, Illinois.
Eggen, O. J. (1961). *Roy. Obs. Bull.* No. 31.
Elvey, C. T., and Babcock, H. W. (1943). *Ap. J.* **97**, 412.
Gaposchkin, C. P. (1957). "The Galactic Novae." North Holland Publ., Amsterdam.
Grant, G. (1955). *Ap. J.* **122**, 566.
Greenstein, J. L. (1957). *Ap. J.* **126**, 23.
Greenstein, J. L. (1958). *In* "Handbuch der Physik" (S. Flügge, ed.), Vol. 50, p. 161. Springer, Berlin.
Greenstein, J. L. (1960). "Stellar Atmospheres," p. 676. Univ. of Chicago Press, Chicago, Illinois.
Greenstein, J. L., and Kraft, R. P. (1959). *Ap. J.* **130**, 99.
Haffner, H. (1937). *Z. Ap.* **14**, 285.
Hamada, T., and Salpeter, E. (1961). *Ap. J.* **134**, 683.
Herbig, G. H. (1944). *P. A. S. P.* **56**, 230.
Herbig, G. H. (1960). *Ap. J.* **132**, 76.
Huang, S.-S. (1956). *A. J.* **61**, 49.
Johnson, H. L., Perkins, B., and Hiltner, W. A. (1954). *Ap. J. Suppl.* **1**, 91.
Joy, A. H. (1954). *Ap. J.* **120**, 377.
Joy, A. H. (1956). *Ap. J.* **124**, 317.
Kitamura, M. (1959). *Publ. astr. Soc. Japan* **11**, 216.
Kitamura, M. (1960). *Publ. astr. Soc. Japan* **12**, 1.
Kraft, R. P. (1958a). *Ap. J.* **127**, 625.
Kraft, R. P. (1958b). *P. A. S. P.* **70**, 598.
Kraft, R. P. (1959). *Ap. J.* **130**, 110.

Kraft, R. P. (1962). *Ap. J.* **135**, 408.
Krzeminski, W. (1962). *P. A. S. P.* **74**, 66.
Kuiper, G. P. (1941). *Ap. J.* **93**, 133.
Kuiper, G. P., and Johnson, J. R. (1956). *Ap. J.* **123**, 90.
Linnell, A. P. (1950). *Harv. Circ.* No. 455.
McLaughlin, D. B. (1953). *Ap. J.* **117**, 279.
McLaughlin, D. B. (1960). *In* "Stellar Atmospheres" (J. L. Greenstein, ed.), p. 585. Univ. of Chicago Press, Chicago, Illinois.
Mannino, G., and Rosino, K. (1950). *Padua Publ.* No. 14.
Mestel, L. (1952). *M. N. R. A. S.* **112**, 598.
Miczaika, G., and Becker, W. (1948). *Heidelberg Veröff.* **15**, No. 8.
Morton, D. C. (1960). *Ap. J.* **132**, 146.
Prendergast, K. H. (1960). *Ap. J.* **132**, 162.
Sahade, J. (1959). "Liege Symposium: Modèles d'étoiles et évolution stellaire," p. 76.
Salpeter, E. (1955). *Ap. J.* **121**, 161.
Sandage, A. R. (1957). *Ap. J.* **125**, 435.
Sandage, A. R., and Schwarzschild, M. (1952). *Ap. J.* **116**, 475.
Sanford, R. F. (1949). *Ap. J.* **109**, 81.
Sauvenier-Goffin, E. (1949). *Ann. d'Ap.* **12**, 39.
Schatzman, E. (1958). *Ann. d'Ap.* **21**, 1.
Schatzman, E. (1959). *Ann. d'Ap.* **22**, 436.
Schatzman, E. (1961). *Ann. d'Ap.* **24**, 237.
Schwarzschild, M. (1958). "Structure and Evolution of the Stars," p. 233. Princeton Univ. Press, Princeton, New Jersey.
Smart, W. M. (1938). "Stellar Dynamics," p. 208. Cambridge Univ. Press, London and New York.
Strand, K. A. (1948). *Ap. J.* **107**, 106.
Van Gent, H. (1931). *B. A. N.* **6**, 93.
Walker, M. F. (1954). *P. A. S. P.* **66**, 230.
Walker, M. F. (1956). *Ap. J.* **123**, 68.
Walker, M. F. (1957). *I. A. U. Symp.* No. 3, 46.
Walker, M. F. (1958). *Ap. J.* **127**, 319.
Walker, M. F. (1961). *Ap. J.* **134**, 171.
Walker, M. F. (1962). *Konkoly Obs. Bull.* No. 2.
Walker, M. F., and Herbig, G. H. (1954). *Ap. J.* **120**, 278.
Wallerstein, G. (1961). *Ap. J.* **134**, 1020.

Eclipse Phenomena

F. LINK

Astronomical Institute of the Czechoslovak Academy of Sciences, Prague, Czechoslovakia

I. General Relations 88
A. Introduction 88
B. Action of the Planetary Atmospheres 90
C. Basic Relations between the Illuminating and the Illuminated Plane 91
D. Relation between the Auxiliary and the Actual Shadow. 93
E. General Transmission Coefficient 94
F. High Absorbing Layers 96
G. Luminosity of the Elementary Segments of the Sun 98
II. Eclipses of the Moon. 100
A. Description of the Eclipses of the Moon 100
B. The Path of Rays in the Terrestrial Atmosphere 104
C. Auxiliary Shadow 106
D. Normal Densities of the Shadow 108
E. The Lunar Eclipse on the Moon 113
F. Geographic Circumstances of the Eclipses 115
G. Illumination by Diffusion 120
H. Hepperger's and Seeliger's Theories of Lunar Eclipses 122
I. Other Theories of Lunar Eclipses 123
J. Photometry of Lunar Eclipses 124
K. Comparison of the Theory with Observations 128
L. Ozone Layer 129
M. High Absorbing Layer 130
N. Increase of the Terrestrial Shadow 135
O. Methods of Determining the Increase of the Shadow and their Results 136
P. Flattening of the Shadow 137
Q. Explanation of the Increase of the Shadow 139
R. Origin of the High Absorbing Layer 141
S. Tropospheric Influences on the Eclipses 145
T. Changes in the Brightness of the Eclipses 150
III. Eclipses of the Artificial and Other Satellites. 154
A. Comparison with the Eclipses of the Moon 154
B. Computation of the Solar Illumination 155
C. Photometry of Eclipses of Artificial Satellites 157
D. Topocentric Brightness of the Satellite 158
E. Comparison of the Theory and Observation 159
F. Eclipse of the Sun Observed from the Artificial Satellites of Other Planets 160
G. Eclipses of the Jovian Satellites 164

IV. Transits of Planets 166
A. Introduction 166
B. Refraction in the Atmosphere of Venus 167
C. Formation of the Solar Image 168
D. Results Obtained during Earlier Transits 172
E. Other Phenomena Accompanying the Transits 174
F. Extent of the Cusps of Venus 174
G. Explanation of the Extension of the Cusps 176
V. Occultations of Stars by Planets 179
A. Basic Equations 179
B. Course of the Occultation 181
C. Occultation of Regulus by Venus, July 7, 1959 183
D. Influence of the Diffraction of Light 184
VI. Eclipse Phenomena in Radio Astronomy 185
A. General Remarks 185
B. Occultations of Radio Sources by the Moon 186
C. A Numerical Example 188
D. Occultations of Radio Sources by the Solar Corona 190
E. Course of the Occultation 192
F. Results of Observations 194
References 195

I

GENERAL RELATIONS

A. *Introduction*

Eclipses and allied phenomena have so far been of the utmost importance in the investigations of planetary atmospheres. They have provided us with a number of interesting facts on the structure and composition thereof at relatively small costs. In the near future the data will be supplemented, amplified, and corrected by means of direct astronautical investigation. It may be assumed, however, that for some time to come both methods will coexist; since rocket investigations of planetary atmospheres, due to their great demands upon technical equipment and costs, can be only of a sporadic character and, moreover will have to be limited to a few nations of this planet, unless the desired international collaboration in the field of space investigations of the cosmos is brought about. In these circumstances it should be of interest to give an account of eclipse observations, the subject being treated in its entirety and from a uniform point of view, in order to unfold the results as well as the further potentialities of such observations.

In all the phenomena in question three heavenly bodies appear, all three to be found temporarily and approximately on one straight line (Fig. 1). The body A is the source of the radiation that passes through the atmosphere of

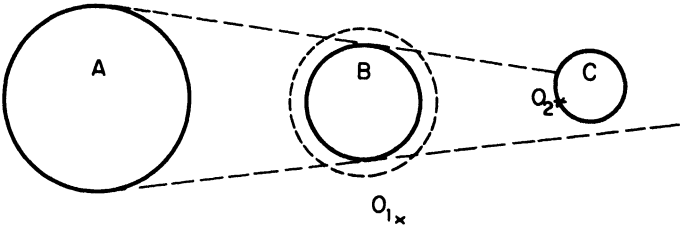

FIG. 1. Different types of eclipse phenomena.

the body B and falls on the body C, which is the target. The following cases may occur:

1. *Eclipse*

The observer O_1 is anywhere in the space, from where he sees the illuminated part of the body C. An example would be the eclipse of the moon as observed from the earth or the eclipse of the old satellites of Jupiter.

2. *Transit*

The observer O_2 is on the body C, so that he can see the transit of the body B across the luminous body A. An actual example would be the transit of Venus across the sun or, in the near future, the observation of the eclipse of the sun from the moon.

3. *Occultation*

A particular case of transit occurs when the luminous body A is in practice at infinity and the observer O_2 is again on the body C. An example would be occultation of a star by a planet.

In all the above-mentioned phenomena an important part is played by the atmosphere of the body B, which modifies the direction and the intensity of the rays. In practice this facilitates the investigations.

Even though a geometrical configuration adequately describing the above phenomena is lacking, ample use of them can be made for the investigation of planetary atmospheres due to the great sensitivity of the method. In the course of these events the rays pass tangentially through the observed atmosphere in contrast to the approximately radial direction met in other investigations. The path of the rays in the atmosphere is thus multiplied by the factor 10 and more,

which increases the sensitivity of the method. Another reason for the increased sensitivity is provided by the lens-like action of the atmosphere multiplied by the distances between the bodies A and C. These circumstances will be dealt with in more detail in the following account.

In the original classic conception, our problems would be concerned only with the light radiation and with the natural heavenly bodies. We shall see further that, in the present state of radioastronomy and astronautics, our considerations can be extended to these new possibilities—i.e., to domain of the radio waves and of the artificial satellites.

All that has been said so far implies that an important part will be played by the atmosphere of the body B. In what follows, we shall therefore concentrate on this aspect which we shall discuss generally at first, proceeding to individual special cases later.

B. *Action of the Planetary Atmospheres*

Let us consider a simplified case in which rays emanating from the luminous point M (Fig. 2) pass through the atmosphere of the body B and fall upon the plane II, in which the body C is situated. Rays within the pencil 0-1 (only a part of the picture above the axis MBC being considered) are stopped by the opaque body B, which accordingly casts upon the plane II an actual shadow with a diameter CU. Rays outside the pencil, e.g., ray 2, traverses the atmosphere of the planet and falls upon the plane II at the point N. On its direction by the action of the atmosphere, the angle ω traced being negative, representing the refraction of the rays of light, or positive, as in the case of ray 3, representing the refraction of the radio beam below.

Another action of the atmosphere is connected with the intensity. The molecules and atoms of gases or, as the case may be, the solid or the liquid particles floating in the atmosphere, produce the absorption or the diffusion of the radiation in all directions and along the entire spectrum. Losses of intensity will affect the original ray. Further changes in intensity are caused by the changes in the divergence of the ray, be it loss as it is indicated with the ray 2 or gain as with the ray 3.

Accordingly, the atmosphere of the planet casts upon the plane II a shadow, the density of which we define as

$$D = \log \frac{E}{e} \tag{1}$$

where E is the illumination at the point N in the absence of the atmosphere and e is the illumination modified by its presence.

Strictly speaking, to the factors exerting an influence on the illumination of

the atmosphere of the plane II one more can be added: namely, the illumination by the atmosphere of the planet shining with diffused light which passes through it. This influence, however, is negligible in most cases.

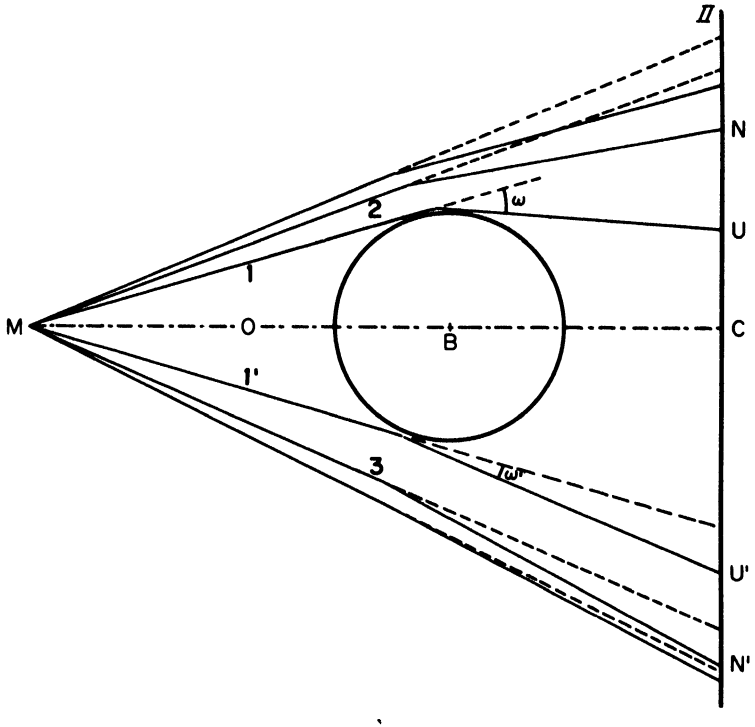

FIG. 2. Action of the planetry atmosphere. *Above*: optical rays. *Below*: radio rays.

The shadow defined and simplified in this way will hereafter be referred to as the *auxiliary shadow*. We shall also show below how one can proceed from the auxiliary shadow (i.e., the shadow cast by a point source) to the *actual shadow* cast by an extended source.

C. *Basic Relations between the Illuminating and the Illuminated Plane*

From the optical point of view all our problems can be reduced to the diagram in Fig. 3. The luminous body A is represented by the illuminating plane I, the illuminated body C by the plane II, and between them there is the acting body, e.g., the planet B, which, by its presence, in particular by its atmosphere, brings about the modification of the rays.

The ray 1 emanating from the point M in the illuminating plane I will pass through the atmosphere of the acting body, in which it is deflected by the angle ω and falls upon the point N in the illuminated plane II. The position

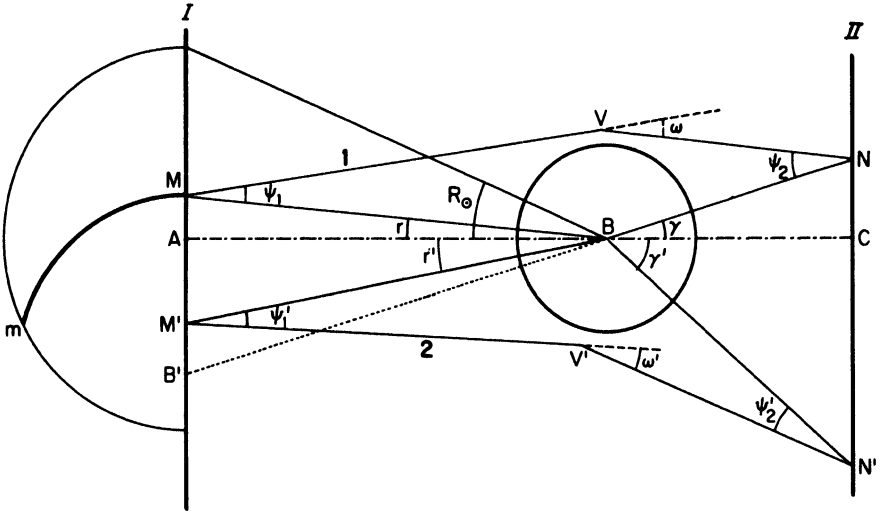

FIG. 3. Relation between the illuminating (I) and the illuminated (II) plane. *Above*: optical rays. *Below*: radio rays. One-half of the plane I is rotated on the left in the plane of the picture.

of the points M and N is given by the geocentric angles r and γ. From the quadrangle MVNB (above the axis AB) we obtain

$$\gamma = \psi_1 + \psi_2 - \omega - r \tag{2}$$

where

$$\sin \psi_1 = \frac{a + h'_0}{L}, \qquad L = \overline{MB}$$
$$\sin \psi_2 = \frac{a + h'_0}{l}, \qquad l = \overline{NB}. \tag{3}$$

This relation is true for the luminous path which is concave with respect to the acting body (planet), which is the case of the refraction of the rays of light in the atmosphere. A similar relation (in the lower half of Fig. 3)

$$\gamma' = \psi'_1 + \psi'_2 + \omega' + r' \tag{4}$$

obtains for the radio waves 2 whose paths are convex and which pass through the ionosphere of the planet. In various special cases these relations are simplified, as we shall see further.

With the observer at the point N observing the transit of the body B across the sun, for instance, the required relation between the angle r (object angle) and the angle ψ_2 (image angle) can be obtained from

$$\begin{aligned} \psi_2 &= \gamma - \psi_1 + \omega + r \qquad \text{for the ray of light} \\ \psi_2' &= \gamma' - \psi_1' - \omega' - r' \qquad \text{for the radio ray.} \end{aligned} \tag{5}$$

From the photometric point of view, we shall always seek the illumination of the plane II by means of the luminous formations in the plane I. For the sake of simplicity we shall assume, initially, a point source of light in the plane I, which casts upon the plane II the auxiliary shadow. The actual shadow will then be obtained as the superposition of an infinite number of auxiliary shadows cast from various point sources in the plane I, which define the luminous body —for instance, the sun.

D. *Relation between the Auxiliary and the Actual Shadow*

In all the applications we have in mind, the illuminating body A will be at a sufficient distance from the acting body B, which enables us to effect the orthogonal projection of the body A upon the plane I—in other words, to reduce the luminous body to a luminous disk in the plane I. The transition from the auxiliary shadow to the actual shadow is easy. The ray 1 issuing from the illuminated point N falls upon the illuminating plane I at the point M (Fig. 3). Along its path it suffers a certain loss of light, which can be expressed in terms of the general transmission coefficient T, the magnitude of which is only a function of the minimum altitude of the ray h_0. If we proceed to rotate the ray round the axis NB, its end will describe a circle m in the plane I, and all the luminous elements along this circle m will illuminate the point N with the same losse of light. A part of this circle is covered by the luminous disk A. If the luminosity of this elementary ring is denoted by di, its contribution to the illumination at the point N will be

$$de = T\, di\,.$$

The total illumination at the point N from the whole disk A (the sun) will be

$$e = \int_{\gamma - R_\odot}^{\gamma + R_\odot} T\, di \tag{6}$$

in which the integral extends over the whole solar disk.

In the absence of the eclipsing body and its atmosphere, we should have $T = 1$, and the illumination at N would be given by

$$E = \int_{\gamma - R_\odot}^{\gamma + R_\odot} di, \tag{7}$$

and the density of the actual shadow would be (1)

$$D = \log_{10} \frac{E}{e}. \tag{1}$$

The computation of the density of the actual shadow will then require, besides the knowledge of the auxiliary shadow structure determined by the values T, the knowledge of di, i.e., the luminosity of the elementary solar ring. The luminosity is dependent upon the distribution of brightness on the solar disk.

E. *General Transmission Coefficient*

The passage of the ray through the atmosphere entails losses of several kinds. In the ideal atmosphere containing only the molecules and atoms of the gases, losses of light arise partly due to the molecular diffusion according to the Rayleigh-Cabannes law (Cabannes, 1929), and partly due to the real absorption accompanied by the appearance of absorption lines and bands. The first of the two factors is usually more important. The aerosols floating in the atmosphere cause a diffusion of light which is governed by relatively complex laws. Finally, the losses of light caused by differential refraction in the atmosphere are due to the change in the natural divergence of the rays issuing from the source of light. In such a case, however, gains in light may also occur, due to the concentration of the pencil of rays.

In an ideal atmosphere—the so-called Rayleigh's atmosphere— we may take into account the effect exerted by molecular diffusion by the transmission coefficient

$$t = 10^{-AM} \tag{8}$$

where A is the absorption coefficient of 1 km of the normal density air and M is the air mass or the equivalent path traversed by the ray of light when traveling in the atmosphere. The coefficient A can be computed theoretically from the relation

$$A = 5.71 \times 10^{-13} \frac{(\mu - 1)^2}{\lambda^4} \tag{9}$$

where λ is the wavelength and μ the index of the refraction.

The actual absorption can be expressed by the formula analogous to (8) with the only difference being that for M we shall have the corresponding quantity for the absorbing gas whose absorption coefficient we know, for instance, from the laboratory measurements. This applies, for instance, to the case of the atmospheric ozone.

The influence of the aerosols is complex, not only because of their dependence on the magnitude and the composition of the particles, but also because of their distribution in the atmosphere. In many cases, therefore, we shall limit ourselves to models consisting of a homogeneous layer, either a very thin one at the altitude h, or a thick one extending from the surface of the earth up to that altitude. The corresponding expressions for the paths of the rays will be given below.

Finally, we must compute the attenuation by differential refraction. We shall derive a general expression which we shall simplify later for individual applications. Let us consider a flux of light emanating from the point M (Fig. 4) between

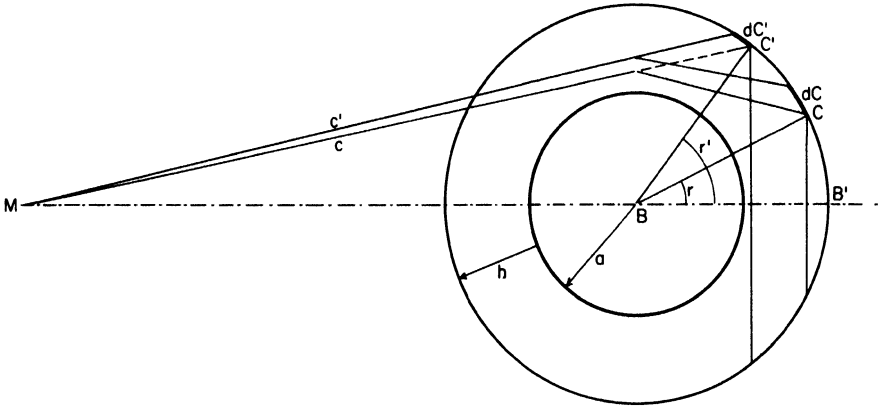

FIG. 4. Attenuation of the illumination by differential refraction.

two cones c and c' lying close to each other, which illuminates the sphere described by the radius $a + h$ from the center of the acting body B. For the sake of generalization this sphere takes the place of plane II. Were it not for the refraction, the flux of light would reach the sphere in the zone dC'. Because of the refraction, the pencil will deviate and reach the sphere in the zone dC. The attenuation by refraction expressed by the coefficient p will be given by the ratio

$$p = \frac{1}{\phi} = \frac{dC'}{dC} \tag{10}$$

We shall determine first the spherical caps CB' and $C'B'$:

$$\begin{aligned} C &= 2\pi(a + h)^2 (1 - \cos r) \\ C' &= 2\pi(a + h)^2 (1 - \cos r') \end{aligned} \tag{10a}$$

where

$$\begin{aligned} r &= \pi_0 \left(1 + \frac{h_0'}{a}\right) + \psi_2 - \omega \\ r' &= \pi_0 \left(1 + \frac{h_0'}{a}\right) + \psi_2 \end{aligned} \tag{10b}$$

from which we may obtain by differentiation

$$dC = 2\pi(a + h)^2 \sin r \left[\frac{\pi_0}{a} + \frac{1}{(a + h)\cos\psi_2} - \frac{dw}{dh_0'}\right] dh_0'$$

$$dC' = 2\pi(a + h)^2 \sin r' \left[\frac{\pi_0}{a} + \frac{1}{(a + h)\cos\psi_2}\right] dh_0'$$

which ultimately yields the general expression

$$\phi = \frac{dC}{dC'} = \frac{\sin\{\pi_0(1 + h_0'/a) + \psi_2 - \omega\}}{\sin\{\pi_0(1 + h_0'/a) + \psi_2\}} \left[1 - \frac{a(a + h)\cos\psi_2 \, d\omega/dh_0'}{\pi_0(a + h)\cos\psi_2 + a}\right]. \tag{11}$$

Accordingly, the general transmission coefficient in Rayleigh's atmosphere will be

$$T = \frac{t}{\phi} \tag{12}$$

and to this coefficient further factors may be added, such as the coefficient p_1, p_2, etc., arising from the actual absorption or from the diffusion on the aerosols.

F. *High Absorbing Layers*

When interpreting the observed phenomena we shall find an assumption of Rayleigh's atmosphere hardly sufficient, and shall be compelled to add to it an assumption of a high absorbing layer. To begin with we shall consider two simple models.

(a) *A thin absorbing layer* between the altitudes h_1 and h_2 (Fig. 5). The ratio

of the horizontal path in the layer for the altitude of the ray h_0 to the similar path for $h_0 = 0$ is given by the expression

$$\frac{G(h_0)}{G(0)} = \frac{\sqrt{h_2 - h_0} - \sqrt{h_1 - h_0}}{\sqrt{h_2} - \sqrt{h_1}}. \tag{13}$$

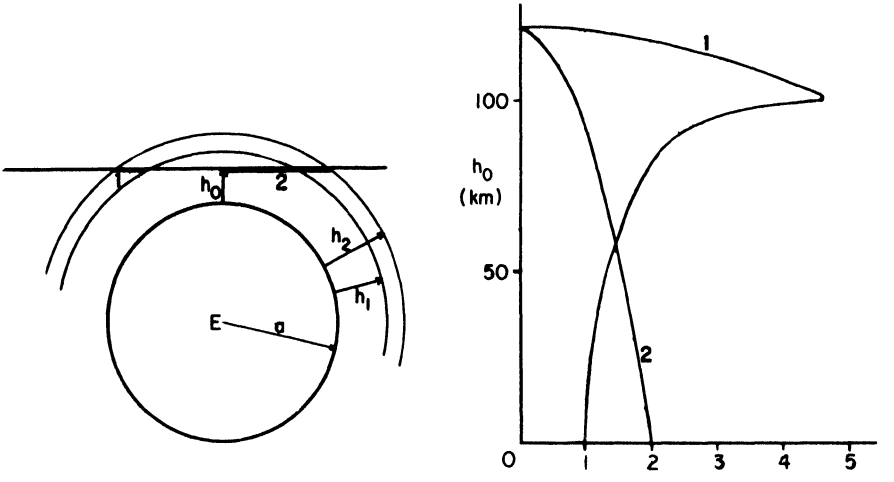

FIG. 5. High absorbing layers: curve 1-thin layer, curve 2-thick layer.

With the rising altitude h_0 the ratio is at first only a little larger than 1 (Fig. 5) and only near the lower limit of the layer (i.e., for $h_0 = h_1$) does it rapidly rise up to its maximum and, after reaching the maximum for $h_0 = h_1$, rapidly drops to zero at the upper limit of the layer $h_0 = h_2$.

If we designate the optical density of the layer in the zenith as B, the optical density of the layer for the ray $h_0 = 0$ will equal

$$G(0) = 2B\sqrt{\frac{a}{2h_1}} \tag{14}$$

(b) *A thick absorbing layer* between the terrestrial surface and the altitude h_2. Our above ratio will equal the expression

$$\frac{G(h_0)}{G(0)} = \sqrt{1 - \frac{h_0}{h_2}} \tag{15}$$

which behaves as before (Fig. 5). The optical density for $h_0 = 0$ will then be

$$G(0) = 2B\sqrt{\frac{2a}{h_2}} \tag{16}$$

i.e., twice as large as before.

To these two simple models a third one may be added, in which the density of the layer is a function of the altitude, as, for instance, in the case of the ozone layer. If we designate this function as $o(h)$ the equivalent path in the layer will be given by the expression

$$O(h_0) = \sqrt{2a} \int_{h_0}^{\infty} \frac{o(h)\, dh}{\sqrt{h - h_0}}. \tag{17}$$

This formula will be used in the problem of the ozone layer (Section II, L). Here, also, from the qualitative point of view, the behavior of the ratio $O(h_0)/O(0)$ is analogous to what it has been previously.

For the inclined rays emanating from a spot on the terrestrial surface and for the zenith distances $z < 75°$ all the layers behave similarly and give an optical density $B \sec z$. Closer to the horizon this quantity changes more slowly than $\sec z$ and at the horizon it reaches a maximum, the value of which is represented by one-half of the expressions (14) and (16).

G. *Luminosity of the Elementary Segments of the Sun*

Another general factor in our considerations is represented by the luminosity of certain elements of the solar disk—e.g., the rings or the bands and the like. Before computing the corresponding expressions we shall note the change in brightness of the solar ring with the distance R from the center. As a rule we represent it by the function

$$b(R) = 1 - \kappa + \frac{\kappa}{R_\odot} \sqrt{R_\odot^2 - R^2} \tag{18}$$

$$\kappa < 1$$

where κ is a constant dependent on the wavelength of the light. This relation will prove true up to 97% $R_\odot$. Closer to the limb the actual brightness decreases more rapidly as was shown for instance by Heyden (1954) in his measurements during the eclipse of the sun.

In various cases mentioned below we shall need the luminosity of the following elementary parts of the sun (Fig. 6):

(a) An elementary ring described from the center of the sun by the radius R. Its luminosity will be

$$di = 2\pi R b(R)\, dR_\odot \tag{19}$$

(b) An elementary ring described by the radius r from the center B' lying at a distance γ from the center of the sun for $\gamma \geqslant R_\odot$ (Fig. 6)

$$di = 2 \int_0^{\epsilon_0} (1 - \kappa) r\, dr\, d\epsilon + 2 \int_0^{\epsilon_0} \frac{\kappa r}{2R_\odot} \sqrt{2r\gamma} \sqrt{\cos\epsilon - \cos\epsilon_0}\, dr\, d\epsilon$$

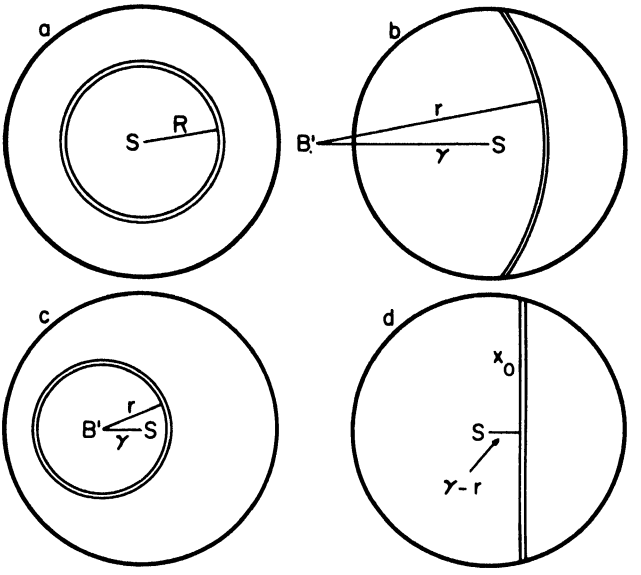

FIG. 6. Different kinds of solar elements.

or

$$di = 2\left[(1 - \kappa)\epsilon_0 r + \frac{\kappa r}{R_\odot}\sqrt{r\gamma}\; Y(m)\right] dr \tag{20}$$

where

$$\begin{aligned} y(m) &= \frac{\pi m\sqrt{2}}{8}\left(1 + \frac{m}{32} + \frac{3m^2}{1024} + \ldots\right) \\ m &= 4\sin^2\frac{\epsilon_0}{2} = \frac{(R_\odot + \gamma - r)(R_\odot + r - \gamma)}{r\gamma}. \end{aligned} \tag{21}$$

(c) An elementary ring of analogous properties, for $\gamma < R_\odot$ and $r < R_\odot - \gamma$ (Fig. 6)

$$di = 2\pi r(1 - \kappa)dr + \frac{2n}{R_\odot}\sqrt{R_\odot^2 - (\gamma - r)^2}\int_0^\pi \sqrt{1 - \frac{4r\gamma}{R_\odot^2 - (\gamma - r)^2}\sin^2\frac{\epsilon}{2}}\, d\epsilon\, dr \tag{22}$$

where the integral on the right-hand side is an elliptic integral of second kind

$$\begin{aligned} \int_0^\pi \sqrt{1 - \frac{4r\gamma}{R_\odot^2 - (\gamma - r)}\sin^2\frac{\epsilon}{2}}\, d\epsilon &= 2E\left(\vartheta, \frac{\pi}{2}\right) \\ \sin^2\vartheta &= \frac{4r\gamma}{R_\odot^2 - (\gamma - r)^2}. \end{aligned} \tag{23}$$

(d) An elementary band m (Fig. 6) at a distance $\gamma - r$ from the center of the sun. Its luminosity will be a limiting case of (a) for

$$r \to \gamma \to \infty \qquad m \to \epsilon_0^2$$

$$\epsilon_0 r \to x_0 = \sqrt{R^2{}_\odot - (\gamma - r)^2}$$

and

$$di = 2(1 - \kappa)x_0\, dr + \frac{\pi\kappa}{2R_\odot} x_0^2\, dr\,. \tag{24}$$

All the above-mentioned cases may be expressed formally by the same formula

$$di = P - \kappa Q \tag{25}$$

in which the quantities P and Q are defined as follows:

Case	P	Q	
(a)	$2\pi R$	$P - \frac{2\pi R}{R_\odot}\sqrt{R_\odot^2 - R^2}$	
(b)	$2\epsilon_0 r$	$P - \frac{\sqrt{r\gamma}\; y(m)}{R_\odot}$	(26)
(c)	$2\pi r$	$P - \frac{4}{R_\odot}\sqrt{R_\odot^2 - (\gamma - r)^2}\, E\left(\vartheta, \frac{\pi}{2}\right)$	(27)
(d)	$2\sqrt{R_\odot^2 - (\gamma - r)^2}$	$P - \frac{\pi}{R_\odot}[R_\odot^2 - (\gamma - r)^2]$	(28)

Also see Tables I and II.

II

ECLIPSES OF THE MOON

A. *Description of the Eclipses of the Moon*

The common tangents of the sun and the earth (Fig. 7) form a convergent cone of umbra and a divergent penumbral cone. In the lunar plane II these cones intercept circles with apparent semidiameters

$$\begin{aligned} \sigma_1 &= \pi_\odot + \pi_\leftmoon + R_\odot \qquad \text{for the penumbra} \\ \sigma_2 &= \pi_\odot + \pi_\leftmoon - R_\odot \qquad \text{for the umbra,} \end{aligned} \tag{29}$$

TABLE I

LUMINOSITY OF SOLAR ELEMENTS [Cases (b) AND (c)]

	$\gamma = 0'$		$\gamma = 5'$		$\gamma = 10'$		$\gamma = 20'$		$\gamma = 30'$		$\gamma = 36'$		$\gamma = 40'$		$\gamma = 45'$		$\gamma = 50'$		$\gamma = 58'$		$\gamma = 68'$	
$r-\gamma$	$P/2$	$Q/2$	$P/2$	$Q/2$	$P/2$	$Q/2$	$P/2$	$Q/2$	$P/2$	$Q/2$	$P/2$	$Q/2$	$P/2$	$Q/2$	$P/2$	$Q/2$	$P/2$	$Q/2$	$P/2$	$Q/2$	$P/2$	$Q/2$
+16	50.3	50.3	0.0	0.0	0.0	0.0	0.0	0.0	0.0	0.0	0.0	0.0	0.0	0.0	0.0	0.0	0.0	0.0	0.0	0.0	0.0	0.0
15	47.1	30.7	11.3	8.2	8.8	6.4	7.9	5.9	6.8	5.0	6.6	4.8	6.5	4.7	6.4	4.6	6.3	4.6	6.2	4.5	6.1	4.5
14	44.0	22.7	15.5	9.6	12.1	7.5	10.1	6.3	9.4	5.8	9.1	5.7	9.0	5.6	8.9	5.5	8.8	5.4	8.6	5.3	8.5	5.3
13	40.8	17.0	18.5	10.1	14.4	7.8	12.0	6.5	11.2	6.1	10.9	5.9	10.8	6.0	10.6	5.7	10.5	5.6	10.3	5.5	10.2	5.4
12	37.7	12.8	20.8	10.2	16.0	7.7	13.5	6.5	12.6	6.0	12.2	5.9	12.1	5.8	11.9	5.7	11.8	5.7	11.6	5.6	11.5	5.5
11	34.6	9.5	22.6	10.0	17.3	7.5	14.6	6.3	13.7	5.9	13.3	5.7	13.2	5.7	13.0	5.6	12.8	5.4	12.7	5.3	12.5	5.3
10	31.4	6.9	24.2	9.9	18.3	7.2	15.5	6.0	14.5	5.6	14.2	5.5	14.0	5.4	13.8	5.3	13.7	5.3	13.5	5.2	13.4	5.2
9	28.3	4.9	25.5	9.7	19.0	6.8	16.1	5.7	15.2	5.3	14.9	5.2	14.7	5.2	14.5	5.1	14.4	5.0	14.2	5.0	14.1	4.9
8	25.1	3.4	26.9	9.9	19.5	6.4	16.6	5.3	15.7	5.0	15.4	4.9	15.2	4.9	15.1	4.8	14.9	4.8	14.8	4.7	14.6	4.7
7	22.0	2.2	28.6	10.6	19.8	6.0	17.0	4.9	16.1	4.7	15.8	4.7	14.7	4.6	15.5	4.6	15.4	4.5	15.2	4.5	15.1	4.4
− 6	18.8	1.4	34.6	14.2	20.0	5.6	17.2	4.8	16.4	4.3	16.1	4.4	16.0	4.4	15.8	4.3	15.7	4.3	15.6	4.2	15.4	4.2
5	15.7	0.8	31.4	9.9	20.1	5.4	17.3	4.5	16.6	4.2	16.3	4.2	16.2	4.1	16.1	4.1	15.9	4.0	15.8	4.0	15.7	4.0
4	12.6	0.4	28.3	7.2	20.0	5.2	17.3	4.2	16.7	4.0	16.5	4.0	16.3	3.9	16.2	3.9	16.1	3.8	16.0	3.8	15.9	3.8
3	9.4	0.2	25.1	5.1	19.8	4.9	17.3	4.0	16.6	3.8	16.5	3.8	16.4	3.8	16.3	3.8	16.3	3.8	16.2	3.7	16.0	3.7
2	6.3	0.0	22.0	3.6	19.5	4.8	17.0	3.8	16.6	3.6	16.4	3.6	16.4	3.6	16.3	3.6	16.2	3.6	16.1	3.6	16.1	3.6
+ 1	3.1	0.0	18.8	2.5	19.0	4.6	16.8	3.7	16.4	3.6	16.3	3.6	16.3	3.5	16.2	3.5	16.1	3.5	16.1	3.5	16.1	3.5
0	0.0	0.0	17.7	1.7	18.5	4.6	16.5	3.6	16.2	3.5	16.1	3.5	16.1	3.5	16.1	3.5	16.0	3.4	16.0	3.4	16.0	3.4
− 1			12.6	1.1	18.0	4.6	15.8	3.6	15.9	3.5	15.9	3.5	15.9	3.4	15.9	3.5	15.8	3.4	15.8	3.4	15.9	3.4
2			9.4	0.7	17.5	5.0	15.5	3.5	15.5	3.5	15.6	3.5	15.6	3.5	15.6	3.5	15.6	3.4	15.6	3.4	15.6	3.5
3			6.3	0.4	17.1	5.5	15.0	3.5	15.1	3.5	15.2	3.5	15.2	3.5	15.3	3.5	15.2	3.5	15.3	3.5	15.4	3.5
4			3.1	0.2	16.8	5.2	14.3	3.5	14.6	3.5	14.7	3.6	14.8	3.6	14.9	3.6	14.8	3.6	14.9	3.6	15.0	3.6
5			0.0	0.0	15.7	5.0	13.6	3.5	14.0	3.7	14.2	3.6	14.3	3.7	14.4	3.7	14.4	3.7	14.5	3.7	14.6	3.7
7					9.4	2.5	12.0	3.6	12.7	3.8	13.0	3.8	13.1	3.9	13.3	3.9	13.3	3.9	13.5	4.0	13.6	4.0
8					6.3	1.5	11.1	3.6	12.0	3.9	12.3	3.9	12.5	4.0	12.6	4.0	12.7	4.1	12.9	4.1	13.0	4.2
9					3.1	0.7	10.2	3.6	11.2	3.9	11.5	4.0	11.7	4.1	11.9	4.2	12.0	4.2	12.1	4.4	12.3	4.3
10					0.0	0 0	9.1	3.6	10.3	4.0	10.7	4.2	10.9	4.2	11.0	4.3	11.2	4.3	11.4	4.4	11.6	4.5
11							7.8	3.4	9.3	4.0	9.7	4.2	9.9	4.3	10.1	4.4	10.3	4.3	10.5	4.4	10.7	4.5
12							6.9	3.3	8.3	4.2	8.7	4.2	8.9	4.3	9,1	4.3	9.2	4.4	9.4	4.5	9.6	4.6
13							5.6	3.0	7.1	3.8	7.5	4.1	7.7	4.2	7.9	4.3	8.0	4.3	8.2	4.4	8.4	4.5
14							4.3	2.7	5.7	3.5	6.0	3.7	6.3	3.9	6.4	4.0	6.6	4.1	6.7	4.2	6.9	4.3
15							2.8	2.0	3.9	2.9	4.3	3.1	4.4	3.2	4.5	3.3	4.6	3.4	4.8	3.5	4.9	3.6
−16							0.0	0.0	0.0	0.0	0.0	0.0	0.0	0.0	0.0	0.0	0.0	0.0	0.0	0.0	0.0	0.0

TABLE II

LUMINOSITY OF SOLAR ELEMENTS [CASE (d)]

$\frac{\gamma - r}{R_\odot}$	$\gamma - r$			P	Q
	☿ (deg)	♂ (deg)	♀ (deg)		
0.000	0.000	0.000	0.000	2.000	0.429
0.062	0.017	0.011	0.023	1.995	0.434
0.125	0.033	0.022	0.046	1.984	0.437
0.188	0.050	0.033	0.069	1.965	0.449
0.250	0.067	0.044	0.092	1.935	0.464
0.312	0.083	0.055	0.115	1.900	0.483
0.375	0.100	0.066	0.138	1.853	0.504
0.438	0.117	0.076	0.161	1.798	0.529
0.500	0.133	0.087	0.184	1.734	0.554
0.562	0.150	0.098	0.207	1.654	0.580
0.625	0.167	0.110	0.230	1.561	0.604
0.687	0.183	0.120	0.253	1.453	0.624
0.750	0.200	0.131	0.276	1.321	0.635
0.812	0.217	0.142	0.299	1.167	0.633
0.875	0.233	0.153	0.322	0.968	0.599
0.938	0.250	0.164	0.435	0.696	0.506
1.000	0.267	0.175	0.368	0.000	0.000

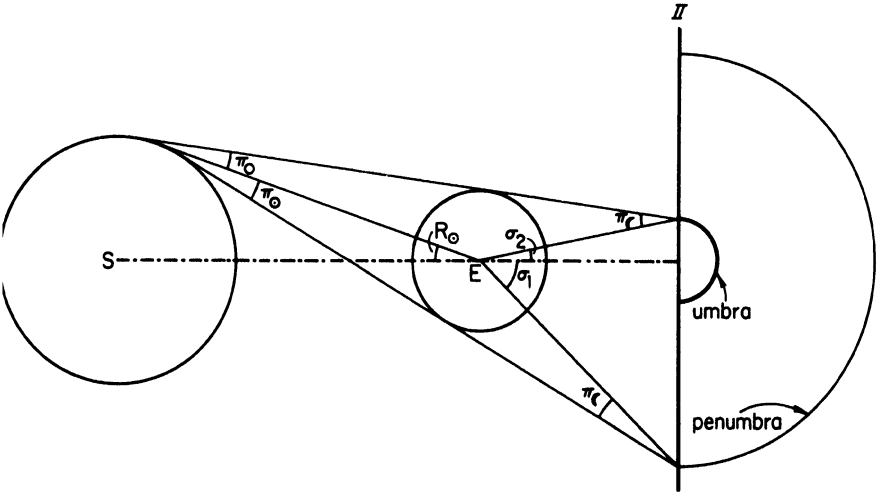

FIG. 7. Umbra and penumbra during lunar eclipses. Half of the plane II is rotated on the right into the plane of the picture.

TABLE III

FUTURE ECLIPSES OF THE MOON (Oppolzer, 1887)[a]

(1)	(2)			(3)		(4)		(5)	(6)	(7)	(8)	(9)
4905	1963	VII	6	2438	217	22^h	0^m	8.6	88^m	—	+ 31°	−22°
4906	1963	XII	30	2438	394	11	7	16.2	107	42	−166	+23
4907	1964	VI	25	2438	572	1	7	18.8	110	49	− 16	−23
4908	1964	XII	19	2438	749	2	35	14.2	104	32	− 40	+23
4909	1965	VI	14	2438	926	1	51	2.4	50	—	− 28	−23
4910	1967	IV	24	2439	605	12	7	16.0	107	41	+178	−13
4911	1967	X	18	2439	782	10	16	13.7	103	28	−158	+10
4912	1968	IV	13	2439	960	4	49	13.6	103	28	− 72	− 8
4913	1968	X	6	2440	136	11	41	14.1	104	31	−178	+ 5
4914	1970	II	21	2440	639	8	31	0.6	26	—	−124	+11
4915	1970	VIII	17	2440	816	3	25	5.0	71	—	− 50	−14
6916	1971	II	10	2440	993	7	42	15.6	107	39	−112	+14
4917	1971	VIII	6	2441	170	19	44	20.7	112	51	+ 65	−17
4918	1972	I	30	2441	347	10	53	12.9	102	21	−160	+18
4919	1972	VII	26	2441	525	7	18	6.9	80	—	—108	−20
4920	1973	XII	10	2442	027	1	48	1.2	36	—	− 29	+23
4921	1974	VI	4	2442	203	22	14	9.9	93	—	+ 26	−22
4922	1974	XI	29	2442	381	15	16	15.5	106	38	+128	+21
4923	1975	V	25	2442	558	5	46	17.5	109	45	− 87	−21
4924	1975	XI	18	2442	735	22	24	13.1	102	23	+ 20	+19
4925	1976	V	13	2442	912	19	50	1.7	43	—	+ 62	−18
4926	1977	IV	4	2443	238	4	21	2.5	51	—	− 64	− 6
4927	1978	III	24	2443	592	16	25	17.5	109	45	+115	− 2
4928	1978	IX	16	2443	768	19	3	16.0	107	41	+ 73	− 3
4929	1979	III	13	2443	946	21	10	10.5	94	—	+ 45	+ 3
4930	1979	IX	6	2444	123	10	54	13.4	103	26	−164	− 7
4931	1981	VII	17	2444	803	4	48	6.9	80	—	− 71	−21
4932	1982	I	9	2444	979	19	56	16.2	107	42	+ 63	+22
4933	1982	VII	6	2445	157	7	30	20.6	112	51	−112	−23
4934	1982	XII	30	2445	334	11	26	14.4	105	33	−171	+23
4935	1983	VI	25	2445	511	8	25	4.1	65	—	−126	−23

[a] (1) The number of the eclipse according to Oppolzer; (2) the civil date; (3) the Julian day; (4) the middle of the eclipse in G.M.T.; (5) the magnitude of the eclipses in inches (12 inches = the moon's diameter); (6) the semiduration of the partial phase; (7) the semiduration of the total phase; (8) the geographical longitude; and (9) the geographical latitude of the sublunar point at the time of the conjunction.

where $\pi_{\odot}$ and $R_{\odot}$ are the parallax and the apparent semidiameter of the sun and $\pi_{\mathbb{C}}$ the parallax of the moon. When the ephemeris of the eclipse is being computed, the above geometrical values are empirically increased by 2% for reasons to be expounded further on (Section II, N-II, R).

In the projection on the plane II we can observe from the earth the ingress of the moon into the penumbra P_1 which is imperceptible to the naked eye the ingress into the umbra U_1, the beginning of the total eclipse T_1, the center of the eclipse M, and, in reverse, the end of the totality T_2, the exit from the umbra U_2, and the exit from the penumbra P_2. At times the phases T_1 and T_2 are missing, so that we speak of a partial eclipse instead of the total eclipse; at times even the moon passes through the penumbra only. The latter phenomenon is as a rule not included among the eclipses.

Standard methods of spherical astronomy permit the computation of lunar eclipses if the positions of the moon and the sun are known, these positions being supplied by the theory of their motions. This was the method used by Oppolzer (1887) who computed all the eclipses of the moon in the interval from 1207 BC to AD 2163. The future eclipses of the moon within the next 20 years may be found in Table III.

According to the geometrical trajectory of the rays plotted in Fig. 7 the direct light of the sun should not penetrate into the umbra and the moon should disappear there completely. Actually, owing to refraction, solar rays penetrate into the geometrical umbra too, as was first shown by Kepler (Frisch, 1958). They are, however, considerably attenuated and reddened by the action of the terrestrial atmosphere, which lends lunar eclipses a picturesque appearance and makes them indeed one of the most beautiful astronomical phenomena.

Lunar eclipses can occur only at the full moon, when the latter stands in close proximity to the intersection of the lunar orbit with the ecliptic. This explains why eclipses occur only at some full-moons. There may be at most three eclipses per year; however, there are years in which no eclipse occurs, as may be seen from the table. In contrast to the solar eclipses, lunar eclipses are visible from all the points of the terrestrial hemisphere at which the moon happens to be above the horizon.

B. *The Path of Rays in the Terrestrial Atmosphere*

The photometric theory of the lunar eclipses leading to the computation of the density of the shadow must be based, as the above general relations have shown, on the knowledge of the path of the rays of light in the terrestrial atmosphere. In order to determine it, the refraction ω and the air mass M will have to be computed as functions of the minimum altitude of the ray h_0.

This computation is based upon the structure of the terrestrial atmosphere,

i.e., on the dependence of the density of the air ρ on the altitude h. Physical reasons (i.e., change of temperature or composition with altitude) show that it is not possible to find a simple form of the function $\rho = f(h)$, which is known only under the tables of numerical values ρ, such as are for instance the tables Rocket Panel (1952) and others. Such a table will indeed be taken as the basis of the computation of ω and M.

The classical theory of refraction leads to the formulas (Link, 1933):

$$\begin{aligned} \omega &= 2\int_0^2 K\,dZ \qquad & K &= \frac{c\rho\beta}{1 - c\rho\beta} \\ M &= 2\int_0^1 L\,dZ \qquad & L &= \frac{\rho}{1 - c\rho\beta} \end{aligned} \tag{30}$$

where β denotes the gradient of the density with the altitude h

$$\beta = \frac{1}{\rho}\frac{d\rho}{dh} \qquad c = 293.2 \times 10^{-6} \qquad (\text{for } \lambda = 5400\ \text{Å})$$

and the independent variable

$$Z = \cos\psi \tag{30a}$$

depends on the angle ψ subtended at a general point on the trajectory by its radius vector with the ray (Fig. 8). This angle will be obtained from the invariant theorem (32).

These formulas are well suited to the numerical integration of ω and M.

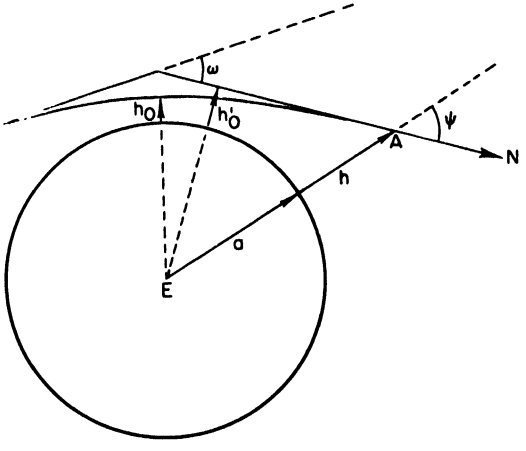

FIG. 8. Path of the optical ray in the terrestrial atmosphere.

It is known from experience that the interval of integration from h_0 to infinity is, in practice, reduced to the interval from h_0 to $h_0 + 30\text{-}50$ km. If, for instance, we stop the integration at the altitude of $h_0 + 12$ km, the integral ω and M will be decreased by only about 5%, so that the knowledge, however inaccurate, of the upper layers has but a limited influence on the values of our integrals. Modern rocket soundings provide reliable values of ρ up to the altitudes about 100 km, which will suffice for the computation of ω and M in the whole range of the umbra and the penumbra.

C. *Auxiliary Shadow*

If we know the refraction ω and the air mass M as the function of the altitude h_0 of the ray, the magnitude of the general transmission coefficient T may be computed by means of the formulae (8-12) valid for Rayleigh's atmosphere. The expression for the attenuation by refraction can be simplified,

TABLE IV

AUXILIARY SHADOW FOR $\pi_{\mathbb{C}} = 57'$ AND $\lambda = 5400$ Å

h_0 (km)	$\frac{a + h_0'}{a}$	ω (min)	$a\frac{d\omega}{dh_0'}$ (min)	M	r (min)	d_1	d_2	D
2	1.0005	55.72	45350	60.64	1.36	1.30	2.79	4.09
3	7	49.96	38930	53.75	7.13	1.94	2.48	4.41
4	8	45.08	33300	47.51	12.02	2.09	2.18	4.27
5	9	40.52	29700	41.88	16.58	2.18	1.92	4.11
6	11	36.56	25120	37.02	20.55	2.20	1.70	3.90
7	12	33.38	22380	32.52	23.74	2.22	1.50	3.71
8	14	30.42	19310	28.44	26.71	2.20	1.31	3.51
9	15	27.79	17340	24.83	29.34	2.20	1.15	3.34
10	17	25.19	17600	21.39	31.96	2.24	0.98	3.22
11	18	22.50	16430	18.37	34.65	2.24	0.84	3.09
12	20	19.66	18120	15.60	37.50	2.32	0.75	3.07
13	21	16.77	18590	13.38	40.40	2.36	0.62	2.98
14	23	14.27	15700	11.43	42.91	2.32	0.53	2.84
15	24	12.15	13440	9.75	45.04	2.24	0.45	2.69
16	25	10.37	10860	8.40	46.82	2.20	0.39	2.58
17	27	8.88	9180	7.14	48.32	2.14	0.33	2.46
18	28	7.59	7760	6.09	49.62	2.08	0.28	2.36
19	30	6.47	6590	5.23	50.75	2.01	0.24	2.25
20	31	5.58	5550	4.45	51.65	1.95	0.20	2.15

TABLE IV (*continued*)

h_0 (km)	$\frac{a + h_0'}{a}$	ω (min)	$a\frac{d\omega}{dh_0'}$ (min)	M	r (min)	d_1	d_2	D
21	33	4.75	4780	3.80	52.49	1.89	0.18	2.07
22	35	4.04	4080	3.25	53.21	1.83	0.15	1.98
23	36	3.46	3473	2.79	53.80	1.76	0.13	1.89
24	38	2.96	2969	2.38	54.31	1.70	0.11	1.81
25	39	2.56	2536	2.04	54.71	1.64	0.09	1.73
26	41	2.19	2158	1.76	55.09	1.57	0.08	1.65
27	42	1.87	1836	1.50	55.42	1.51	0.07	1.58
28	44	1.62	1571	1.28	55.68	1.44	0.06	1.50
29	46	1.36	1342	1.10	55.95	1.38	0.05	1.43
30	47	1.16	1138	0.94	56.16	1.31	0.04	1.36
31	49	0.99	977	0.81	56.34	1.25	0.04	1.29
32	50	0.85	834	0.69	56.49	1.19	0.03	1.22
33	52	0.73	712	0.60	56.62	1.12	0.03	1.15
34	53	0.62	601	0.51	56.73	1.06	0.02	1.08
35	55	0.53	507	0.44	56.83	0.99	0.02	1.01
36	56	0.46	424	0.38	56.91	0.92	0.02	0.94
37	58	0.39	356	0.33	56.99	0.86	0.02	0.88
38	59	0.33	297	0.28	57.06	0.79	0.01	0.80
39	61	0.29	251	0.24	57.11	0.73	0.01	0.74
40	63	0.24	204	0.21	57.17	0.66	0.01	0.67
26[a]	41	2.14	2143	1.72	55.26	1.57	0.08	1.65
27	42	1.82	1807	1.47	55.57	1.50	0.07	1.57
28	44	1.55	1520	1.28	55.86	1.43	0.06	1.49
29	46	1.34	1309	1.08	56.07	1.37	0.05	1.42
30	47	1.14	1108	0.94	56.28	1.30	0.04	1.34
35	55	0.53	524	0.45	56.93	1.01	0.02	1.03
40	63	0.24	229	0.22	57.26	0.70	0.01	0.71
45	71	0.12	100	0.11	57.42	0.44	0.00	0.44
50	78	0.06	47.1	0.06	57.53	0.26	0.00	0.26
60	94	0.02	12.8	0.02	57.66	0.09	0.00	0.09
70	110	0.00	0.0	0.00	57.77	0.02	0.00	0.02
80	125	0.00	0.0	0.00	57.86	0.00	0.00	0.00
90	141	0.00	0.0	0.00	57.95	0.00	0.00	0.00
100	157	0.00	0.0	0.00	58.04	0.00	0.00	0.00

however, as the angles ψ are small. The expression (11) is replaced by the following expression:

$$\phi = \left[1 - \frac{\omega}{\pi_{\mathbb{C}} + \pi_{\odot}}\left(1 - \frac{h_0'}{a}\right)\right]\left[1 - a\frac{d\omega}{dh_0'}\frac{1}{\pi_{\odot} + \pi_{\mathbb{C}}}\right]. \qquad (31)$$

The ratio $d\omega/dh'_0$ can be best derived from the numerical values ω. The altitude of the asymptote h'_0 (Fig. 8) may be computed from the invariant theorem

$$a + h'_0 = (a + h_0)\mu_0 = (a + h)\mu \sin \psi . \tag{32}$$

$$\mu = 1 + c\rho, \qquad \mu_0 = 1 + c\rho_0.$$

The general absorption coefficient is determined from $T = t/\phi$ [Eq. (12)]. The angle r will be denoted by the simple expression (2) with $\gamma = 0$

$$r = (\pi_\odot + \pi_\mathbb{C}) \left(1 + \frac{h'_0}{a}\right) - \omega . \tag{33}$$

The structure of the auxiliary shadow has thus been determined. An example is given in Table IV for the green light $\lambda = 5400$ Å ($A = 0.0460$) and for $\pi_\mathbb{C} = 57'$. In the table, basic quantities ω, $a\, d\omega/dh'_0$, and M and derived quantities r, $d_1 = \log \phi$, $d_2 = \log t$, and $D = d_1 + d_2$[1] are given.

From the numerical values d_1 and d_2 all the changes and mutual ratio in dependence on the altitude follow easily. For low rays, i.e., at the center of the auxiliary shadow, absorption d_1 prevails over the attenuation by refraction d_2. As d_1 is strongly dependent on the wavelength, the auxiliary shadow will be colored red at the center. However, the absorption d_1 decreases rapidly with altitude, while d_2 at the beginning still rises up to the altitude circle 13 km and then gradually decreases. The attenuation by refraction is practically independent of the color, from which it follows that the auxiliary shadow in the outer parts (where the attenuation by refraction is absolutely predominant) will be neutral. At the center of the auxiliary shadow for $r = 0$ the focusing of the rays (i.e., $\phi = 0$) occurs, so that theoretically the illumination may increase there toward infinity.

These properties of the auxiliary shadow are conserved by the actual shadow, being considerably blurred, as the illumination is a resultant of the integration in a wide range ($2R_\odot = 32'$) in the auxiliary shadow. Nevertheless, the actual shadow is grey at the limb, grows reddish towards the center, and at the center, there is a particular brightening up noticeable at times. This is dependent, of course, on the transparency of the lowest layer of the atmosphere ($h_0 < 2$ km), where cloudiness as well as general pollution by aerosols often exerts a disturbing influence.

D. *Normal Densities of the Shadow*

The transition from the auxiliary shadow to the actual shadow is now made possible by means of the formulas of Section I, D. In this way the normal

[1] Above 26 km also according to the Rocket Panel (1952) data.

densities of the shadow have been computed for three colors and for three moon's parallaxes to hold good in Rayleigh's atmosphere. The results are presented in Table V and are also represented graphically in Fig. 9. From

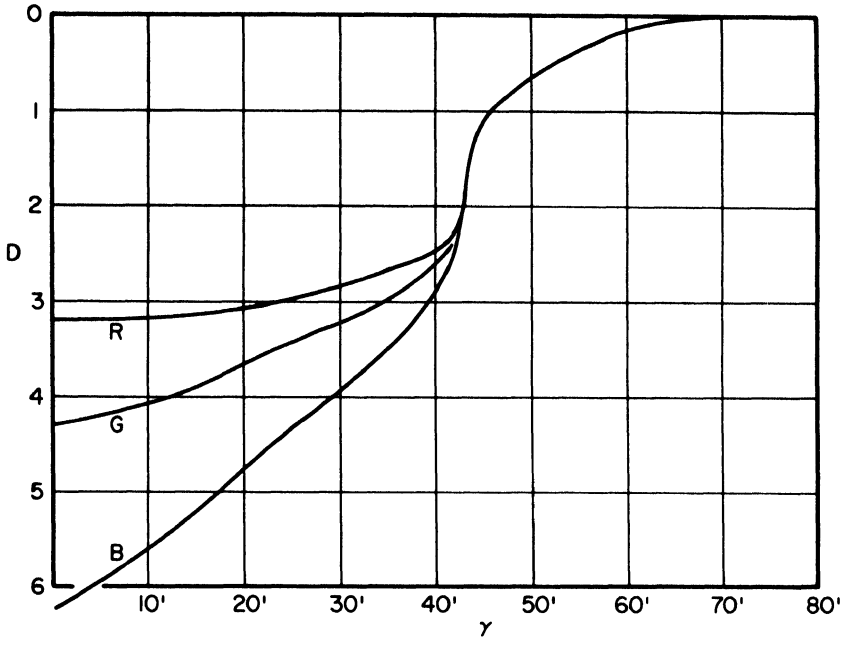

FIG. 9. Normal densities of the shadow ($\pi_{\mathbb{C}} = 57'$).

these numerical data the properties of the shadow in different parts are most readily seen. In practice it is important to note too that at the edge of the geometrical shadow the density depend only little on the parallax if we select as argument the distance from the edge of the geometrical shadow

$$\gamma' = \pi_{\mathbb{C}} - R_{\odot} - \gamma . \tag{34}$$

This circumstance is made use of in another table of normal densities of the shadow, Table VI.

The graphical form of the integral of illumination in the shadow is also not without interest. In Fig. 10 some such forms are given, in which the maximum altitude is standardized to 100. The curves clearly indicate the resolving power in altitude of the illuminating pencil of rays falling upon the moon. It is relatively favorable especially in the upper parts of the atmosphere—i.e., in the outer parts of the shadow—as shown by the sharp maximum of the curve at the

TABLE V

NORMAL DENSITIES OF THE SHADOW

		Densities, $\gamma' =$:						Mean air masses, $\gamma' =$:					
	$\pi_{\mathbb{C}}$	$\gamma = 0'$	5′	10′	20′	30′	35′	0′	5′	10′	20′	30′	35′
	54′	3.10	3.09	3.06	2.97	2.76	2.58	49.5	48.4	43.5	27.8	17.5	11.8
	55′	3.14	3.13	3.10	3.01	2.79	2.62	50.3	49.5	44.4	28.7	18.9	13.1
	56′	3.18	3.16	3.14	3.05	2.81	2.66	51.2	50.6	45.3	29.8	20.1	14.3
$\lambda = 0.62\ \mu$	57′	3.21	3.20	3.17	3.09	2.83	2.70	52.2	51.7	46.3	31.1	21.2	15.5
	58′	3.25	3.24	3.21	3.12	2.85	2.73	53.4	52.6	47.4	32.3	22.1	16.5
	59′	3.29	3.27	3.24	3.16	2.87	2.76	54.5	53.4	48.7	33.7	22.8	17.5
	60′	3.32	3.31	3.27	3.18	2.90	2.78	55.5	54.2	50.0	35.2	23.5	18.4
	61′	3.36	3.35	3.31	3.20	2.92	2.80	56.7	54.9	51.8	36.8	24.1	19.3
	54′	4.10	4.04	3.91	3.49	3.09	2.79	44.9	43.3	37.8	24.7	15.3	9.9
	55′	4.17	4.11	3.97	3.53	3.13	2.86	45.8	44.0	38.6	25.5	16.2	11.0
	56′	4.24	4.18	4.03	3.58	3.17	2.91	46.9	44.9	39.6	26.5	17.1	12.1
$\lambda = 0.54\ \mu$	57′	4.30	4.24	4.09	3.63	3.21	2.97	48.0	46.1	40.8	27.7	18.1	13.2
	58′	4.36	4.31	4.15	3.68	3.25	3.02	49.2	47.6	42.2	29.0	19.0	14.2
	59′	4.43	4.37	4.22	3.74	3.29	3.07	50.5	49.2	43.8	30.2	19.9	15.2
	60′	4.49	4.43	4.28	3.80	3.33	3.12	52.0	50.8	45.5	31.5	20.8	16.1
	61′	4.55	4.49	4.35	3.87	3.37	3.16	53.3	52.7	47.3	32.9	21.7	17.0
	54′	5.86	5.69	5.30	4.46	3.68	3.18	42.0	37.6	32.1	20.9	12.5	7.7
	55′	5.98	5.77	5.40	4.55	3.76	3.28	43.3	39.2	33.0	21.7	13.2	8.5
	56′	6.10	5.87	5.50	4.63	3.85	3.38	44.8	40.8	34.1	22.7	14.1	9.5
$\lambda = 0.46\ \mu$	57′	6.23	5.98	5.60	4.72	3.93	3.48	46.3	42.4	35.2	23.7	15.1	10.5
	58′	6.36	6.11	5.72	4.82	4.01	3.57	47.8	43.8	36.6	24.8	16.2	11.4
	59′	6.49	6.25	5.84	4.93	4.09	3.66	49.3	45.4	38.1	25.9	17.4	12.4
	60′	6.63	6.40	5.97	5.05	4.17	3.75	50.8	47.0	39.5	27.1	18.8	13.3
	61′	6.76	6.56	6.11	5.16	4.24	3.84	52.3	48.4	41.1	28.3	20.3	14.1

TABLE VI

NORMAL DENSITIES OF THE SHADOW[a]

	$\pi_{\mathbb{C}}$	$\gamma' = 0'$	1′	2′	3′	4′	5′	6′	7′	8′	9′	10′
	54′	2.37	2.46	2.53	2.58	2.63	2.67	2.70	2.73	2.76	2.79	2.81
		7.3	9.2	10.7	11.8	13.0	14.0	15.2	16.3	17.5	18.5	19.5
$\lambda = 0.62\ \mu$	57′	2.35	2.46	2.52	2.58	2.63	2.67	2.70	2.73	2.75	2.78	2.81
		7.3	8.8	10.2	11.7	13.0	14.5	15.5	16.7	17.8	19.0	20.1
	61′	2.33	2.42	2.49	2.55	2.60	2.64	2.67	2.71	2.75	2.77	2.80
		7.3	8.3	9.5	10.6	11.7	13.1	14.5	15.7	17.0	18.4	19.3
	54′	2.50	2.62	2.72	2.79	2.86	2.93	2.99	3.04	3.08	3.13	3.17
		6.0	7.4	8.8	9.9	11.1	12.1	13.2	14.3	15.3	16.4	17.4
$\lambda = 0.54\ \mu$	57′	2.48	2.61	2.70	2.78	2.85	2.92	2.97	3.02	3.07	3.13	3.17
		5.7	7.1	8.4	9.7	11.0	12.1	13.2	14.3	15.3	16.3	17.2
	61′	2.46	2.58	2.68	2.76	2.83	2.90	2.95	3.01	3.07	3.12	3.16
		5.9	7.2	8.4	9.7	11.0	12.1	13.2	14.3	15.2	16.2	17.0
	54′	2.73	2.91	3.06	3.18	3.29	3.39	3.49	3.59	3.68	3.77	3.85
		4.1	5.4	6.6	7.7	8.6	9.5	10.5	11.4	12.5	13.4	14.4
$\lambda = 0.46\ \mu$	57′	2.71	2.89	3.04	3.16	3.28	3.38	3.48	3.58	3.67	3.76	3.84
		4.1	5.4	6.6	7.7	8.6	9.5	10.5	11.4	12.4	13.3	14.2
	61′	2.69	2.86	3.01	3.16	3.26	3.37	3.46	3.56	3.65	3.75	3.84
		4.3	5.4	6.4	7.5	8.5	9.5	10.5	11.4	12.4	13.3	14.1

[a] Numbers which appear as heads of columns 3-13 are values of γ'.

edge of the shadow. The curves indicate further the effect exerted by various atmospherical layers on the density in the different parts of the shadow. The outer parts of the shadow at a distance of 5-10′ from the edge are affected

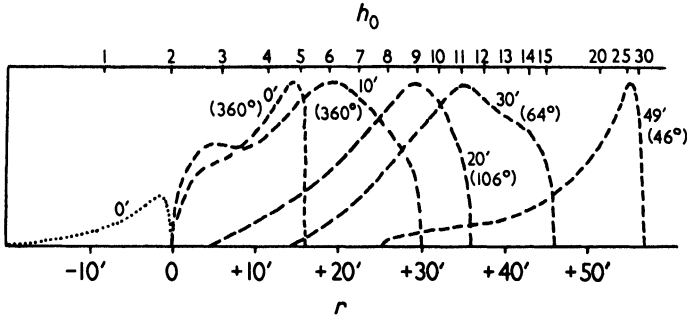

FIG. 10. Forms of the illumination integrals for $\pi_{\mathbb{C}} = 57°$. The maxima are normalized to 100. The figures at the curves indicate distances γ and angular amplitudes $2\Delta P$ of the terminator. [Eq. (40).]

mostly by the upper layers, above 11 km, only where there is no disturbance caused by cloudiness or atmospheric pollution. The inner parts of the shadow are subject to these influences to a greater extent, which lessens their significance for investigation of the upper atmosphere.

Some of the integrals of the illumination near the center extend to the negative values of the angle r. This is due to the double illumination of the corresponding point of the lunar plane (Fig. 11) by higher rays a, on the one hand, and by lower rays b, on the other, passing at the antipodes. The latter rays, however, pass through very low layers of the atmosphere (Fig. 10), from which it follows that they are greatly attenuated and also obscured by cloudiness.

In Table V, another important quantity, the so-called air mass M_0, is listed. The illumination in the shadow

$$e = \int 10^{-AM} \phi^{\,1}\, di\, dr \tag{34a}$$

is dependent substantially on the adopted value of the absorption coefficient A. A small change dA will cause a change of the illumination

$$\frac{de}{dA} = -2.30 \int 10^{-AM} M \phi^{\,1}\, di\, dr$$

and a change of the density

$$\frac{dD}{dA} = M_0 = \frac{\int 10^{-AM} M \phi^{-1}\, di\, dr}{\int 10^{-AM}\, di\, dr}. \tag{35}$$

This expression has the dimension of the air mass and, therefore, we call it the mean air mass. We shall later use this quantity when discussing the differences between the measured and the computed density of the shadow.

E. *The Lunar Eclipse on the Moon*

In the days when Proctor and Raynard (1892) carried out researches to find out what the lunar eclipse looked like from the moon, their work had but a theoretical meaning. In our days, however, when rockets are being sent towards the moon and men round the earth, the problem assumes a much more definite significance.

The observer N on the moon (Fig. 11) at an angular distance γ from the center of the shadow will see the dark disk of the earth under the angle

$$\psi_0 = \pi_{\mathbb{C}}(1 + c\rho^*) \qquad \rho^* = 1 \tag{36}$$

and the projected distance of the center of the sun S from the center of the earth will be γ''; the apparent diameter of the solar disk being $R''_{\odot}$. All this can be expressed by

$$\gamma'' = \frac{\pi_{\mathbb{C}}}{\pi_{\mathbb{C}} + \pi_{\odot}}\gamma\,, \qquad R''_{\odot} = \frac{\pi_{\mathbb{C}}}{\pi_{\mathbb{C}} + \pi_{\odot}}R_{\odot}\,. \tag{37}$$

The ratios γ''/γ or $R''_{\odot}/R_{\odot}$ can differ from unity only by amounts of the order of 0.25%.

The geometrically invisible solar disk becomes visible due to refraction as a considerably deformed refraction image. The ring m on the solar disk appearing under the geocentric angle (33)

$$r = \left(\pi_{\mathbb{C}} + \pi_{\odot}\right)\left(1 + \frac{h'_0}{a}\right) - \omega$$

will be observed from the moon as the ring m' under the angle

$$\psi = \frac{a + h'_0}{l} = \pi_{\mathbb{C}}\left(1 + \frac{h'_0}{a}\right), \tag{38}$$

or at the distance of

$$\psi - \psi_0 = \pi_{\mathbb{C}}\left(1 - c\rho^* + \frac{h'_0}{a}\right) \tag{39}$$

from the limb of the earth (right-hand side of Fig. 11).

In this manner the whole refraction image of the sun can be gradually built-up

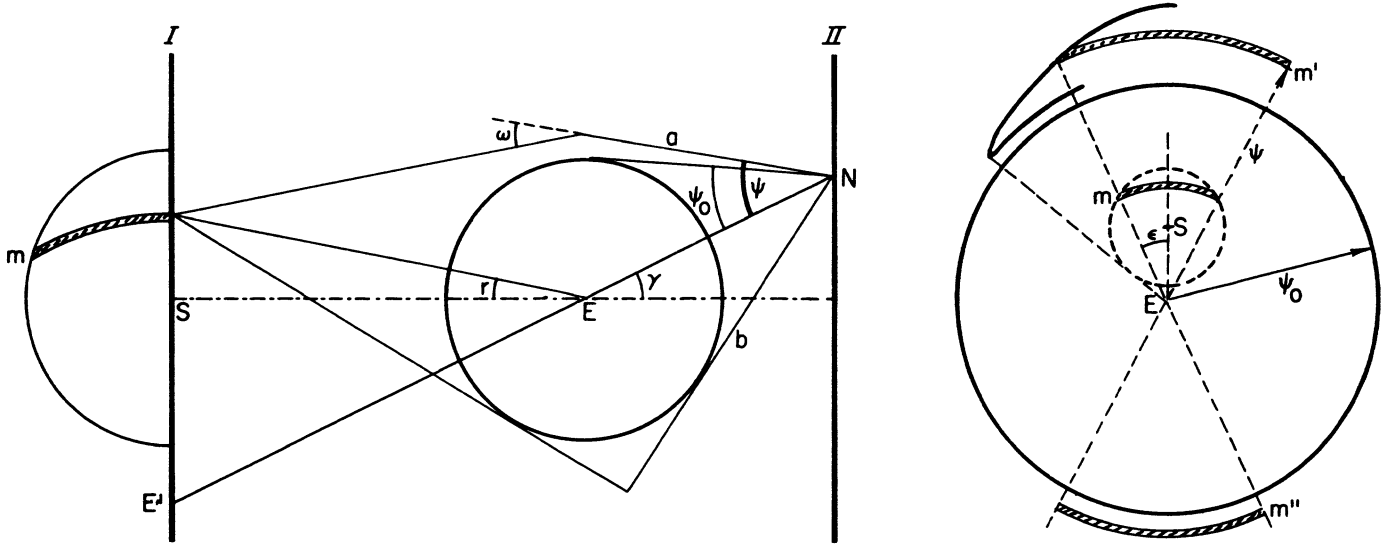

FIG. 11. Lunar eclipse on the moon. *Left*: optical scheme of rays. *Right*: Formation of the solar image.

from the individual rings. Up to now we have considered only the ray a illuminating the point N. In reality, the ray *b* can come to the point N from the antipodes of the spot traversed by the ray *a*. This is the reason why a second refraction image m'' can arise on the side opposite to the image m'. When we approach the center of the shadow, the two images are broadened along the limb of the earth, and at the distance of $\gamma = R_{\odot}$ they blend into one continuous ring surrounding the whole earth.

Were it not for the absorption in the terrestrial atmosphere, the solar image would possess the original brightness of the sun. The ratio of the surface of the refracted image to the geometrical surface of the solar disk would provide the attenuation by refraction. Actually, because of atmospheric absorption, the brightness of the refraction image will rapidly decrease from the outer edge to the inner edge; and in the total light the color will change from the initial yellow to the deep red.

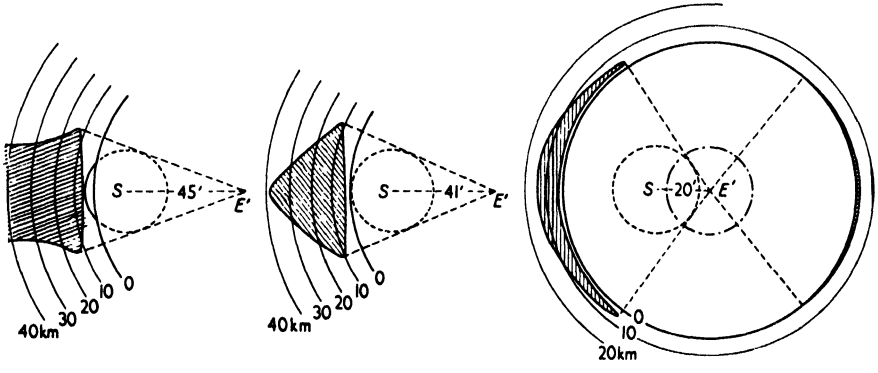

FIG. 12. Some aspects of refraction images of the sun. The distances from the limb of the earth are amplified 100 times.

Figure 12 presents some aspects of the solar eclipse as observed from the moon. To make the refraction image more distinct its distance $\psi - \psi_0$ from the limb of the earth are exaggerated. At the same time, for the sake of simplicity, the independence of the refraction upon the geographic latitude has been assumed. This does not need to be fulfilled in reality, and further deformations of the solar image at various geographic latitudes may be expected.

F. *Geographic Circumstances of the Eclipses*

The density of the shadow depends on the structure of the atmospere, which itself depends on geographic latitude. In other words, the density of the shadow

will not only depend on the distance from the center of the shadow, but also on the position angle. This induces us to examine the geographical circumstances of the eclipse—i.e., to consider places on the earth above which the rays of light forming a shadow on the moon are passing.

The terminator of the shadow according to the current astronomical ephemerides represents all the places on the earth at which the upper limb of the sun rises or sets at the same time. These regions accordingly lie on the adjacent circle at a distance $90° - \omega/2 - R_\odot$ from the antisolar point. The terminator defined in this way is related to the ray which touches the surface of the earth. As far as the higher rays are concerned, the refraction will decrease and the terminator will be approaching the circle $90° - R_\odot$. If we consider further that the refraction as well as the air mass depends mostly on the structure of the atmosphere in the first ten kilometers above the top of the path of light (which corresponds to the geocentric angle around 8°) we see that the effective terminator will actually be a band of a certain width along the ephemeris terminator. Provided that no really detailed investigation of the course of the rays is required, we shall limit ourselves to the ephemeris terminator, which will prove sufficient for current information.

Its course is given by the table to be found, for instance, in the "Nautical Almanac" or "American Ephemeris," where for certain days in the year the rising and the setting of the sun in various geographic latitudes is listed. Converting these times into angles, we obtain directly the corresponding longitudes of the terminator, the longitudes being positive eastward of the meridian of Greenwich: namely, for midnight U.T. At a determined hour H of universal time the terminator of the shadow will be shifted westward by H. In this way the course of the terminator of the shadow on the surface of the earth can be plotted for any moment during the eclipse. Figure 13 shows the terminators for certain eclipses.

The whole terminator does not always take part in the formation of the shadow, but only the part dependent on the position of the considered point N of the lunar plane, where we measure the density of the shadow. If we effect measurements at a place defined by the distance γ from the center of the shadow and by the position angle P, the span of the position angles to be taken into account is $P \pm \Delta P$, where (Fig. 15)

$$\sin \Delta P = \frac{R_\odot''}{\gamma''} = \frac{R_\odot}{\gamma} \tag{40}$$

The place on the terminator corresponding to the position angle P is yet to be determined. Figure 14 represents a view of the sun and the earth from space. The terminator t of the shadow is marked by a dashed line, V being

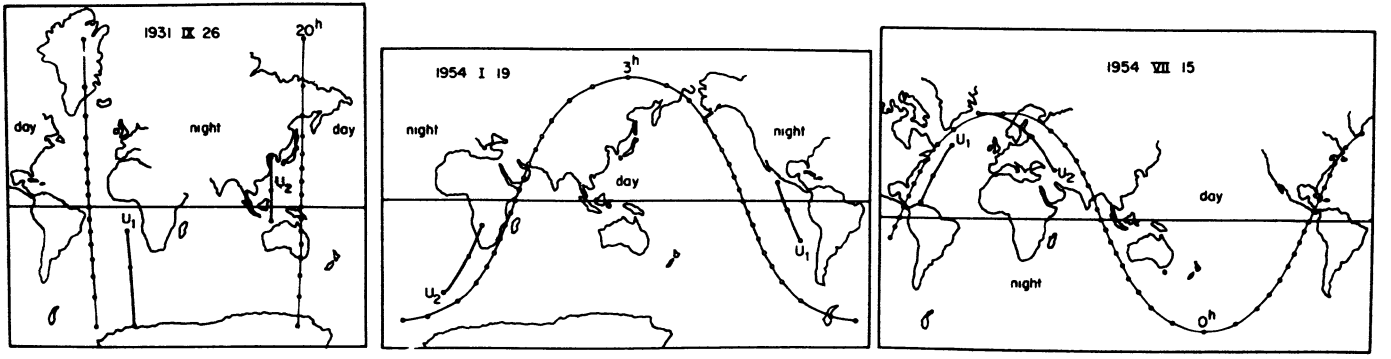

FIG. 13. Shadow terminators at different eclipses. U_1—the beginning, U_2—the end of partial eclipse. The whole terminators at the designated hours of the GMT are divided in position angles from 10° to 10°.

the place in question on the terminator, S′, the antisolar point, and P_N, the North Pole on the earth. From the spherical triangle P_N V S′ we find

$$\cos P = \frac{\sin \varphi}{\sin [90° - (\omega/2) - R_\odot] \cos \delta_\odot} - \cot [90° - (\omega/2) - R_\odot] \tan \delta_\odot ;$$

and since the angle $(\omega/2) + R_\odot$ is small, with a satisfactory precision

$$\cos P = \frac{\sin \varphi}{\cos \delta_\odot}. \tag{41}$$

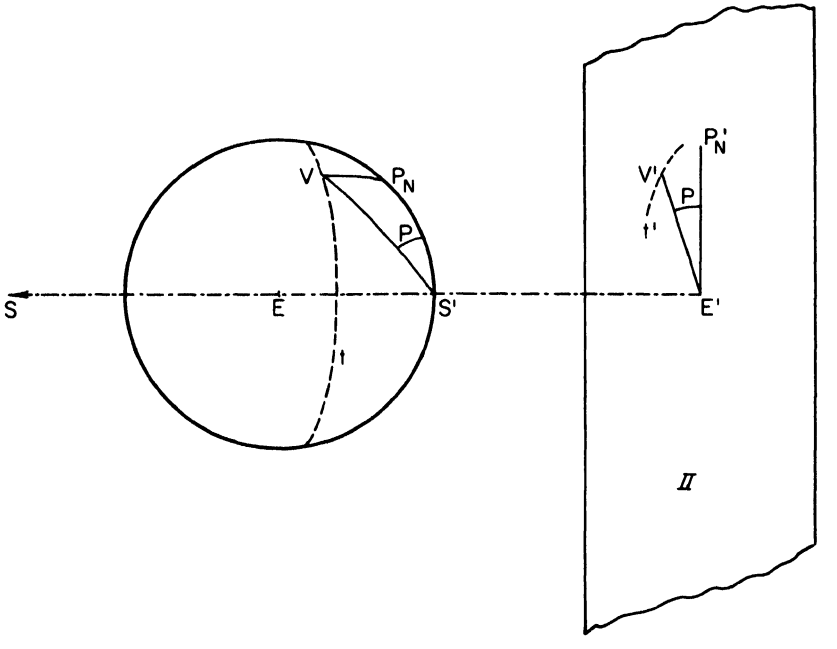

FIG. 14. Relation between the position angle P and the latitude of the point V on the terminator.

Both extreme ends of the effective terminator will, accordingly, possess the following geographic latitudes

$$\sin \varphi_{1,2} = \cos \delta_\odot \cos (P \pm \Delta P) \tag{42}$$

The length of the arc of the effective terminator is on the edge of the penumbra 0°. In the outer penumbra, where the illumination for the most part comes from

the uneclipsed part of the solar disk (Fig. 15 showing the position of the solar center S_1 and S_2), the length of the arcs $2\Delta P$ are alone of importance. In the inner penumbra, where the influence of the refraction image of the sun (position S_3) also makes itself felt, it is better to take into account the length of the

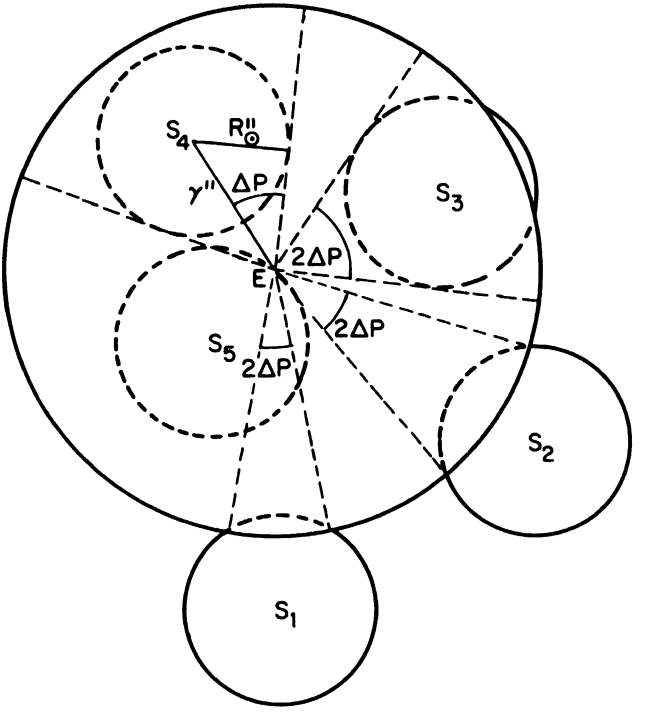

FIG. 15. Different amplitudes $2\Delta P$ of the position angles on the terminator viewed from the moon.

arc according to Eq. (40), which holds good only in full shadow. There the length of the arc rapidly increases and finally subtends an angle of 180° at the distance of $\gamma = R_{\bigcirc}$ from the center of the shadow.

In the above considerations we have disregarded the presence of the second refraction image of the sun. This may be found opposite the first image, and the corresponding part of the terminator lies within the position angle $P + 180° \pm \Delta P$. The geographic latitudes of its terminal points will correspond to $\varphi'_{1,2} = -\varphi_{1,2}$. When $\gamma = R_{\bigcirc}$ the two arcs of the terminator will be complements of 360°. From this point up to the center of the shadow the whole 360° long arc of the terminator proves effective.

G. *Illumination by Diffusion*

The lunar plane is illuminated not only by direct sunlight, but also by the terrestrial atmosphere shining with the diffused light of the sun. The influence of this parasitic illumination was suggested by Rougier and Dubois (1944).

First of all we shall make an estimate of the upper limit of the parasitic illumination (Link, 1950a). The surface brightness of the volume element of the diffusing medium will be

$$db = E \frac{dD}{4\pi} \tag{43}$$

where E is the illumination and dD the optical density of the element, an orthotropic diffusion being assumed. At the point K (Fig. 16) the brightness

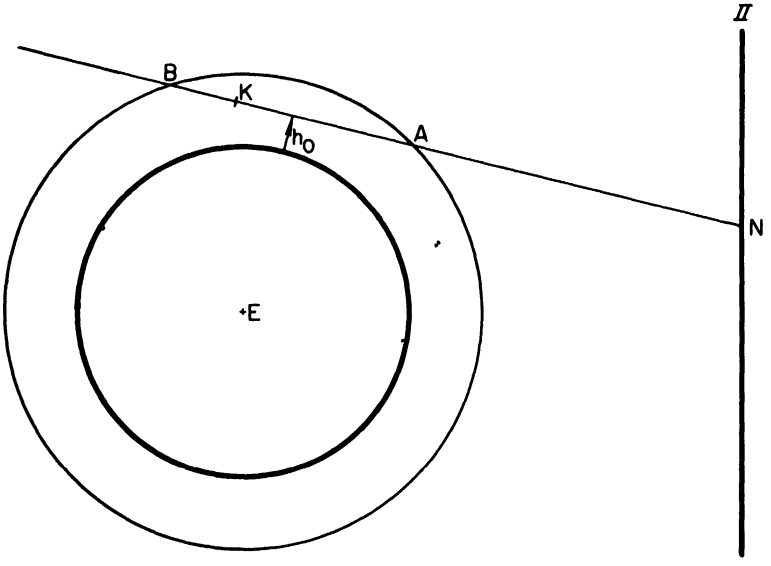

FIG. 16. Illumination by the diffusion in the earth atmosphere.

of the medium observed from the lunar point N will be given by the expression

$$db = \frac{E}{4\pi} \exp\left[-(D_1 + D_2)\right] dD \tag{44}$$

where D_1 denotes the optical density between B and K, D_2 the same quantity between K and A. Let us further set

$$D(h_0) = D_1 + D_2 ,$$

so that

$$db = \frac{E}{4\pi} \exp\left[-D(h_0)\right] dD\,. \tag{45}$$

The parasitic illumination $d\eta$ from the ring of radius $a + h_0$ and width dh_0 will be

$$d\eta = b\, d\Omega \tag{46}$$

where the solid angle of the ring observed from N is

$$d\Omega = \frac{2\pi[1 + (h_0/a)]\pi_{\mathbb{C}}^2}{a}\, dh_0\,. \tag{47}$$

The total illumination is computed by integrating

$$\eta = \frac{E\pi_{\mathbb{C}}^2}{2a} \int_0^H \left(1 + \frac{h_0}{a}\right) \exp\left[-D(h_0)\right] D(h_0) dh_0 \tag{48}$$

up to the limit of the atmosphere H. The upper limit of the illumination will therefore, be

$$\eta < \frac{E\pi_{\mathbb{C}}^2}{2a}\, 0.368 \left(H + \frac{H^2}{a}\right); \tag{49}$$

or, with $\pi_{\mathbb{C}} = 57'$,

$$\frac{\eta}{E} < 7.9 \times 10^{-9} H - 1.2 \times 10^{-12} H^2\,. \tag{50}$$

This process, moreover, can be made more precise by means of numerical integrations (Švestka, 1948), which give

$$\frac{\eta}{E} = 1.9 \times 10^{-7} \quad (\lambda = 7000\,\text{Å}) \quad \text{or} \quad 2.1 \times 10^{-7} \quad (\lambda = 4500\,\text{Å}) \tag{51}$$

whereas our estimate yielded

$$\frac{\eta}{E} < 8 \times 10^{-7} \tag{52}$$

For the center of the shadow, the measurements yield

$$\frac{b}{E} = 6 \times 10^{-5} \quad (\lambda = 6300\,\text{Å}) \quad \text{or} \quad 10^{-6} \quad (\lambda = 4600\,\text{Å}) \tag{53}$$

so that the parasitic illumination by diffusion can prove disturbing only in proximity to the center of the shadow and in the blue part of the spectrum, where direct solar illumination is the weakest.

A very drastic estimate of the upper limit of the parasitic illumination may be added to the above quantitative computations. Viewed from the moon at the center of the shadow, the earth will be surrounded, besides the refraction image of the sun, also by a narrow bright fringe caused by the diffusion of light in the terrestrial atmosphere. This is the very phenomenon, noted first by Gagarin in his flight round the earth (1961), which to some extent bears analogy to Venus (Section IV). When the surface brightness of the ring is denoted by b and the solid angle by Ω, the illumination on the moon yields

$$\eta = b\Omega\,. \tag{54}$$

If we consider the upper limit of the ring in the altitude of 120 km ($2\%a$) and its surface brightness $b = 10^4$ cd/m^2, the parasitic illumination will be

$$\eta < 0.3 \text{ lux}$$

or in the ratio to the direct illumination on the moon beyond the eclipse $E = 1.3 \times 10^5$ lux

$$\frac{\eta}{E} < 2 \times 10^{-6} \tag{55}$$

in conformity with the previous results.

H. *Hepperger's and Seeliger's Theories of Lunar Eclipses*

These theories were based on imaginary observations of eclipses on the moon (Hepperger, 1895; Seeliger, 1896). In terms of the modern nomenclature they may be summed by up saying the illumination at the point N of the lunar plane by the elementary ring dm' is given by the product of the average surface brightness b of the ring and the solid angle under which it appears from the point N—i.e.,

$$de = kb\ 10^{-AM} dm' \tag{56}$$

where dm' is the solid angle of the ring.

The total illumination is then given by the integral

$$e = k \int b\ 10^{-AM} dm'\,, \tag{57}$$

in which the whole refraction image of the sun will be involved; with Hepperger setting $b = 1$ and Seeliger taking account of the variable brightness on the solar disk.

These theories appear to have disregarded the attenuation by refraction which is, however, implicitly comprised within the solid angle dm'. The latter

is reduced for attenuation by refraction, unlike the solid angle of the ring dm, as may be proved by means of simple substitution for these quantities. For we have (Fig. 11)

$$\begin{aligned} dm' &= 2\epsilon\psi \, d\psi \\ dm &= 2\epsilon r \left(\frac{L}{L+l}\right)^2 dr \end{aligned} \tag{58}$$

so that the ratio

$$\frac{dm}{dm'} = \frac{r\,dr}{\psi\,d\psi}\left(\frac{L}{L+l}\right)^2 \tag{59}$$

by substituting becomes

$$\frac{dm}{dm'} = \left[1 - \frac{\omega}{\pi_\odot + \pi_\leftmoon}\left(1 - \frac{h_0'}{a}\right)\right]\left[1 - a\,\frac{d\omega}{dh_0'}\,\frac{1}{\pi_\odot + \pi_\leftmoon}\right] \tag{60}$$

which is identical with the expression (31) for the attenuation by refraction.

I. *Other Theories of Lunar Eclipses*

Beside the theory (Link, 1933) expounded in the preceding sections and those of Hepperger and Seeliger, another theory of lunar eclipses was worked out by Fesenkov (1932, 1937). In his earlier work there was no mention of the full expression for the attenuation by refraction, the second term only being considered, which implies that the validity of his theory is limited only to the edge of the shadow where ω is negligible in comparison with $\pi_\leftmoon$. Only in his subsequent work did Fessenkov make use of the full expression equivalent to our formula (31). He also set $\pi_\odot = 0$, which is a tolerable approximation.

Fesenkov also integrated in the solar plane (Fig. 17), but for the element of integration he adopted the elementary ring described from the center of the Sun, thus losing the advantage of one analytical integration and compelling him to carry out from the very beginning both integrations for the illumination numerically in the form

$$e = k \iint T(r)\, b(R)\, R\, dR\, d\varphi \tag{61}$$

Among other theories of the photometric circumstances in the lunar plane let us mention that of Saussure. Actually it represents but a further elaboration of Seeliger's theory, adding only another set of rather problematic approximations (Saussure, 1931).

In principle, all these theories can be divided into two categories. Some integrate in the solar plane (Fesenkov, Link), others integrate from the point of view of the observer on the moon, i.e., in the terrestrial atmosphere (Hepperger, Seeliger). Apart from this difference, all are formally equivalent. Differences

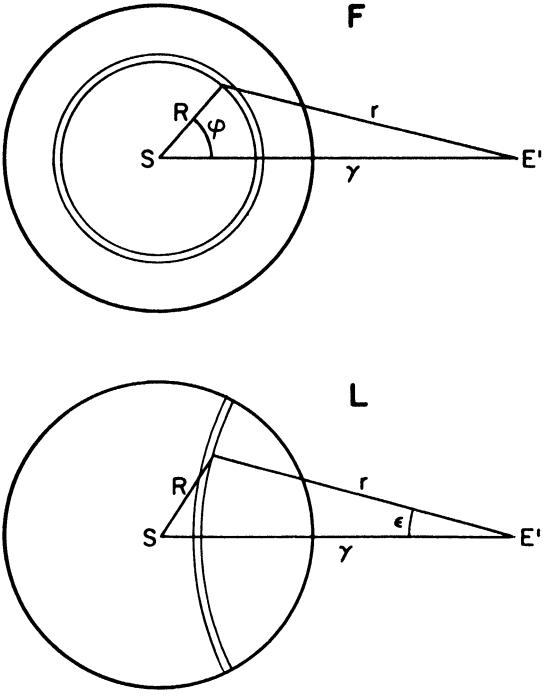

FIG. 17. Integration of the solar illumination according to Fesenkov (F) and Link (L).

arise only when numerical applications are carried out, which must be based upon a specific structure of the terrestrial atmosphere. The obvious great disadvantage of older investigations is that they could not have known the conditions in the atmosphere to the extent we know them now; and their refraction theories as well as the values of ω and M represented only rather rough approximations.

J. *Photometry of Lunar Eclipses*

The measurement of the density of the shadow according to Eq. (1) consists of two measurements of the brightness of the same area on the moon—the first before the eclipse and the second during the eclipse, when this area is

at the distance γ from the center of the shadow. Though this can be done by many photometric methods, we encounter several difficulties of a specific character, due to the influence of the diffused parasitic light on the optical surfaces of the apparatus, in the atmosphere itself, and to the variations of extinction in the course of the measurements. During the partial phase, when the part of the lunar disk in the penumbra may be 100 times brighter than that in the shadow, the parasitic light originating from the first part can considerably reduce the densities of the shadow in the second. The comparison of the brightness at the measured spot before and during the eclipse must be carried out at different times; and the change in the position of the moon above the horizon as well as the general changes in the atmospheric conditions may give rise to disturbing extinction changes. Therefore, the photometry is to be carried out in such a way that these influences should, if possible, be excluded.

An example of such a method is provided by Danjon's cat's-eye photometer. This photometer gives (Fig. 18) a double image of the moon (Danjon, 1928),

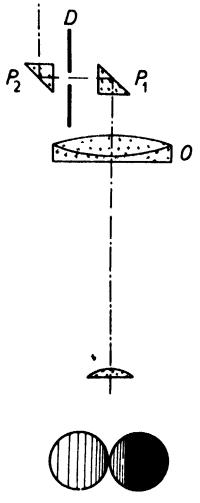

FIG. 18. Danjon's cat's-eye photometer. *Below*: view of the moon during measurements.

enabling us to compare the brightness of the two opposite limbs of the moon, along the median line on which the greatest as well as the least brightness occurs. By means of the changeable cat's-eye diaphragm of the photometer the brightness of the two parts can be adjusted and sets of two points each in the shadow (for which the difference of the distances from the center of the shadow is $2R_{\mathbb{C}}$) can be linked up photometrically. By means of the gradual linking up, beginning with the ingress into the penumbra, the whole curve of the density of the shadow, as it is indicated in Fig. 19, can be measured.

This method automatically eliminates the influence of the diffused parasitic light, both measured images being projected on the common background. The influence of the extinction is as a rule quite negligible, as we compare two spots lying near each other. The necessity for continuous measurements is, however,

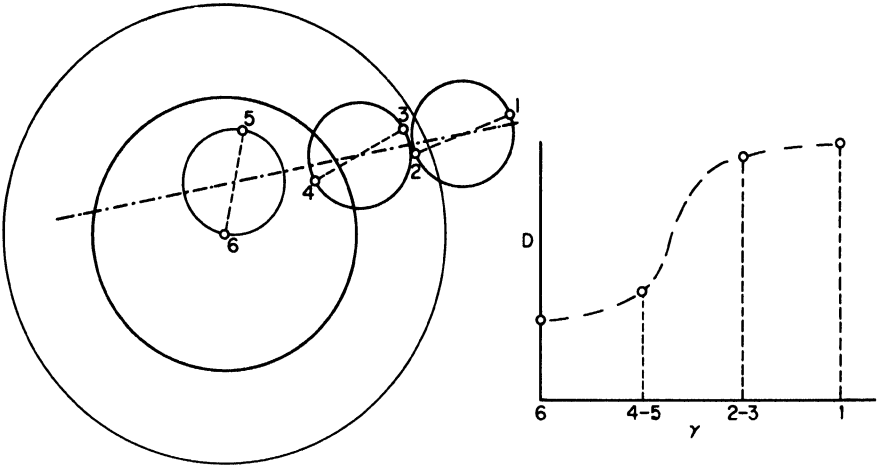

FIG. 19. Technique of measurements with the cat's-eye photometer. *Left*: positions of measured couples of points. *Right*: their positions on the light curve $D = f(\gamma)$. In practice the number of couples is much greater.

a disadvantage, as these are at times impeded by cloudiness. Besides, the measurements are limited only to some areas of the shadow lying on the line joining the centers of the moon and the sun. Measurements can be made without any difficulty by means of color filters, as the comparison with the theory requires. By means of this method, a long series of lunar eclipses has been measured by Danjon and his followers since 1921. The results were uniformly reduced, as it will be shown below (Section II, K).

Guth and Link (1936) applied Danjon's method partly to photography. Close to the photographic plate (Fig. 20) there is a thin gelatin filter of density about 2 and circular in shape. The curvature of the image of the edge of the shadow in the focus of the photographic camera corresponds to the curvature of the filter, and during the partial phase we place the image of the moon in such a way that a part of the penumbra is attenuated by the filter. With the differences between the shadow and the penumbra greatly diminished in intensity, the two may be easily related by standard methods of photographic photometry. For this purpose a photometric scale illuminated by a constant electric bulb is projected round the image of the moon, and the exposure is taken

through a colored filter. The influence of the diffused parasitic light must be taken into consideration and the veil round the image of the moon measured. For the total eclipse the circular filter need not, of course. In other respects the measuring procedure is similar to that employed by Danjon. The methop has the advantage of permitting a determination of the isophotes of the shadow in all its parts traversed by the moon.

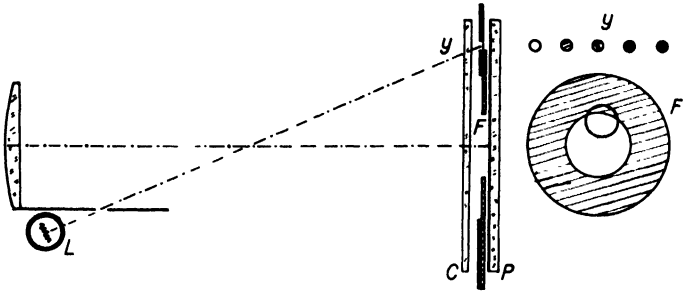

FIG. 20. Link's photographic photometer. C—color filter, F—neutral filter, I—intensity scale, P—photographic plate.

The photoelectric method has also recently been used. There is some difficulty, however, with the elimination of the parasitic light. Walker and Reaves (1957) therefore measured only the part of the moon which at a given time is at the greatest distance from the center of the shadow. It is bound to be the brightest, and the influence of the diffused parasitic light the smallest. Cimino and Fresa (1958), on the other hand, linked up two distant spots on the moon, which eliminates the extinction changes.

In special cases, e.g., investigations of the ozone, spectral photometric measurements were carried out in such a way that the image of the eclipsed moon was projected onto the slit of the spectrograph (Barbier and Chalonge, 1942; Paetzold, 1950; Vigroux, 1954). The considerable length of the exposure ($\sim$10 min) and the disturbing influence of the diffused light, impairing the results, constitute a serious handicap.

There are also a number of measurements effected by one of the standard photometric methods—unfortunately, without any regard to the above-mentioned disturbing influences. These results do not, therefore, lend themselves to any comparison with the theory. The measurements of the total brightness of the moon during the eclipse, providing a kind of average density of the shadow on the whole lunar disk (a density greatly affected by the differences of albedo) are also devoid of much significance.

K. *Comparison of the Theory with Observations*

When it comes to compare observations with the theory, the measurements carried out by Danjon's method are most suitable, as they furnish shadow densities free from any systematic errors. A general reduction of these measurements since 1921 has been carried out in the *Catalogue of Lunar Eclipses II* (Link, 1956a) where, apart from the measured and theoretical values of the shadow, other data of great importance to the analysis of the results have been listed—such as the mean air masses, the positions of the terminator of the shadow, and the detailed ephemerides of the eclipse.

Generally we find certain differences $O - C = \Delta$ between the observation and the computation, and these differences are usually positive, i.e., the measured density of the shadow is greater than the density computed for the case of the ideal Rayleigh atmosphere. A trivial explanation of these differences would be provided by the atmospheric pollution of the troposphere. This explanation does not, however, stand the test of a closer analysis. Let us plot the differences Δ as a function of the mean air mass (Fig. 21): we obtain a number of points usually lying along a curve or a slightly inclined straight line. If we want to explain the differences Δ by the increase of the absorption coefficient over the theoretical value, the inclination of the curve would give the desired correction. The latter is relatively small and the shape of the curve of the differences appears

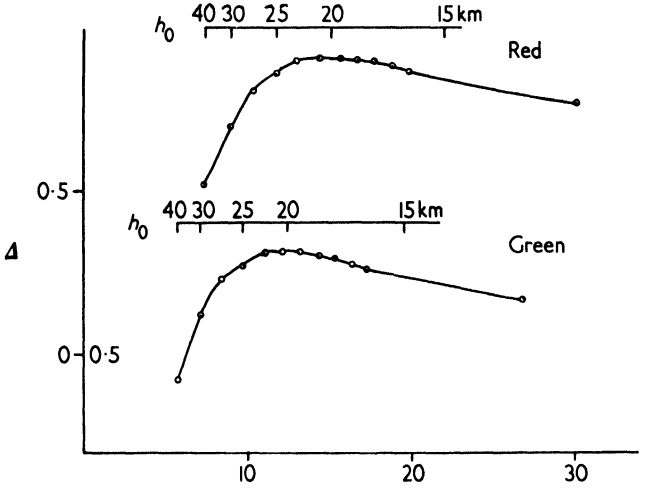

FIG. 21. Differences O-$C = \Delta$ during the eclipse of October 16, 1921. *Above*: the scale of altitudes of rays corresponding to the upper limit of the illumination integral. *Below*: mean air masses.

to be due to the constant absorption, which changes little within the altitudes of the rays between 0 and 25 km. Such is the property of the high absorbing layer, as we have shown above in Section I, F.

L. *Ozone Layer*

The greater part of the above-mentioned differences Δ can be explained by the absorption of light in the ozone layer, these results having greatly contributed to a better investigation of its structure. A considerable part of the measurements have been carried out in the green part of the spectrum (5400 Å), where the ozone exhibits a quite distinct absorption. In earlier days the opinion prevailed (Cabannes and Dufay, 1927) that the atmospheric ozone was concentrated in a layer at an altitude of about 50 km. The eclipses of the moon proved beyond doubt (Link, 1933) that the ozone layer must lie far lower—somewhere between 20 and 30 km—which was proved later by direct ascents to these altitudes (Regener and Regener, 1934).

The circumstances are described in an analysis of the eclipse of 16.X.1921 (Link, 1933). In Fig. 21 the differences are plotted so as to represent the functions of the mean air mass; there is also the altitude scale for the upper limit of the integral of the illumination h_2, which lies close to the maximum of the function of the integral of the illumination (Fig. 10). The differences begin to fall sharply as soon as the altitude reaches approximatly 20 km. This indicates, in conformity with the results of Section I, F, that the lower limit of the ozone layer has been reached, which is thus found to lie lower than had previously been thought.

This method enables us to investigate the behavior of the ozone layer in various geographic latitudes, it being dependent on the position angle in the shadow in which the measurements are taken (Section II, F). There appeared conspicuous differences (Link, 1946d) with the geographic latitudes. Measurements taken in higher latitudes yielded greater values of the differences than those close to the equator. This points to the dependence of the quantity of ozone on the geographic latitude in the same sense as obtained from extensive measurements carried out at various parts of the terrestrial globe (Dobson, 1929). Lunar eclipses provide these results almost simultaneously, and at much lesser cost (Fig. 22).

Close analysis of the distribution of the ozone in the atmosphere by means of lunar eclipses was carried out by Paetzold (1950, 1951, 1952). He started from the general equation (17)

$$O(h_0) = \sqrt{2a} \int_{h_0}^{\infty} \frac{o(h)}{\sqrt{h - h_0}}\, dh \tag{62}$$

where the unknown is the desired function $o(h)$, which we obtain as the solution of Abel's integral equation (17)

$$o(h) = \frac{1}{\pi\sqrt{2a}} \int_h^\infty \frac{d\,O(h_0)/dh_0}{\sqrt{h - h_0}}\, dh_0 . \tag{63}$$

The measurements, however, do not yield the function $O(h_0)$ appropriate for one single ray at the altitude of h_0, but another function $O^*(\gamma')$ relevant to a wide pencil of rays (32′). Instead of h_0 we shall therefore substitute the altitude $h_0{}^*$, for which the air mass is equal to the average air mass of the whole pencil. Some of Paetzold's results are represented in Fig. 23. They confirm the low altitude of the maximum of the ozone layer (about 20 km).

To illustrate these facts we have prepared a table of values $o(h)$ and $O(h)$ true for mean latitudes (Guth and Link, 1941) with the zenith quantity of ozone 2.7 mm, which represents the behavior of the ozone layer during the eclipse—i.e., a practically constant value up to the altitude of 20 km and then a rapid decline to zero above 40 km (see Table VII).

TABLE VII

MEAN OZONE LAYER

h_0 (km)	$o(h_0)$ (10^3 cm km^{-1})	$O(h_0)$ (cm)
0	3.3	8.7
5	4.1	8.8
10	5.5	9.1
15	7.2	9.0
20	9.1	8.7
25	10.3	7.8
30	9.1	4.7
35	4.6	1.9
40	1.5	0.3

M. *High Absorbing Layer*

The ozone may explain only the greater part of the differences $\Delta = O - C$. This is shown by the comparison of the measured differences with the differences computed from

$$\Delta_1 = \alpha G(0) \tag{64}$$

where the path $G(0)$ through the ozone layer was computed from the average structure of the layer in the mean latitudes (Guth and Link, 1941) and the absorption coefficient was taken from laboratory measurements (Table VIII).

TABLE VIII

CONSTANT OZONE ABSORPTION DURING LUNAR ECLIPSES

$\lambda(\mu)$	0.46	0.54	0.58	0.62	0.68	0.70	0.76
Δ_1	0.034	0.33	0.53	0.43	0.15	0.086	0.017

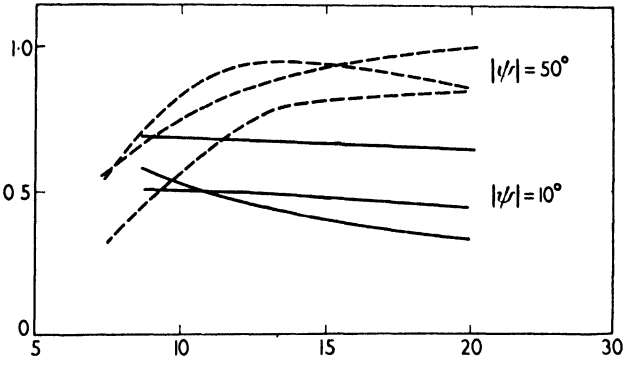

FIG. 22. Curves of the differences Δ for several eclipses from higher and lower latitudes as functions of the mean air mass M_0.

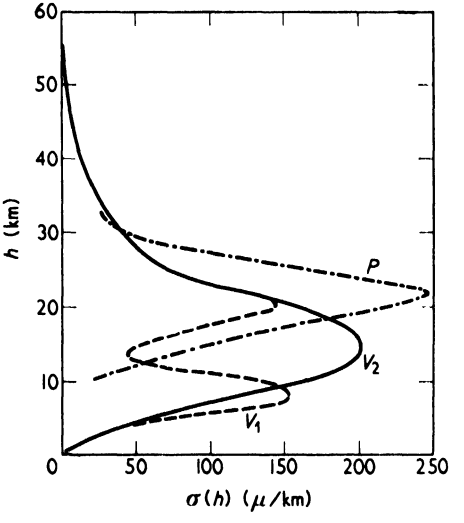

FIG. 23. Curves of ozone distribution, according to results of eclipse January 29, 1953, V_1 equatorial, V_2 polar (Vigroux, 1954), Paetzold October 16, 1921.

The measurements will often give values twice as large (Fig. 22). If we wanted to explain these differences by means of false assumptions about the structure of the ozone layer, we would have to double the vertical quantity of the ozone ($= 2.7$ mm O_3), which is hardly admissible.

The remaining differences $\Delta' = \Delta - \Delta_1$ cannot, therefore, be explained by the ozone absorption and have to be attributed to the high absorbing layer. The fact that such a medium exists in the high atmosphere had already been demonstrated before its identification during eclipses (Link, 1933) by other proofs— however indirect or unconvincing they may have seemed.

First of all, attention has to be paid to the measurements of the atmospheric absorption by means of Bouguer's straight lines. The logarithm of brightness $\log I$ of the extraterrestrial body (e.g., the sun) is measured at various zenith distances z and plotted in the graph as a function of the air mass $M(z)$ (Fig. 24).

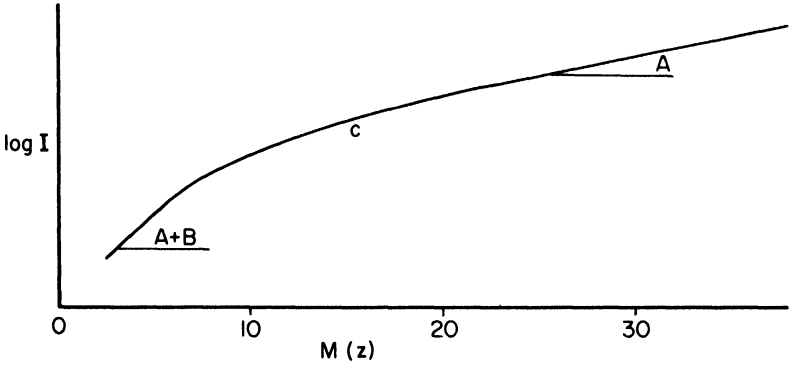

FIG. 24. Bouguer's graph.

The points lie approximately along the straight line, the inclination of which gives the requisite absorption coefficient. Two effects transpire, which may be explained by the presence of a high absorbing layer. Actually the points do not lie along a straight line, but rather along the curve c. At small zenith distances, when the path in the layer is changing with the air mass $M(z) \sim \sec z$, the following equation may be used

$$\log y = \log y_0 - (A + B) \sec z\,, \tag{65}$$

in which B is the absorption coefficient of the layer (i.e., its optical density at the zenith).

Close to the horizon the air mass $M(z)$ changes very quickly with the zenith

distance, whereas the path in the layer is practically constant and equals $G(0)$ (Section I, F); the equation of this part of the curve is then

$$\log y = \log y_0 - AM(z) - B\sqrt{\frac{2a}{h_2}} \tag{66}$$

The occurrence of the curvature is thus an effect pointing to the possibility of a high absorbing layer. Such an effect was found at first in Müller's (1883) measurements at Potsdam; and Hausdorff (1895) was the first to offer the explanation by means of a high absorbing layer. Later on similar results were arrived at by Bauer and Danjon (1923) on the basis of measurements taken on Mt. Blanc, and by Link on Pic-du-Midi and elsewhere (Link, 1929). The results give the value of absorption at the zenith $B = 0.015$-0.045 and the altitude of the layer above 100 km. The use of the method is rather delicate, for the construction of Bouguer's straight line or curve requires very stable conditions in the atmosphere, which seldom occur even in high mountains.

Another method leading to the existence of the high absorbing layer is based upon the Rayleigh-Cabannes formula for the absorption coefficient of the ideal atmosphere. According to that formula (9) in the logarithm shape

$$\log A = \text{const} + \log \frac{(\mu - 1)^2}{\lambda^4} \tag{67}$$

a representation of the dependence should be a straight line inclined at the 45°. If, however, we plot on a graph the results of measurements carried out in various elevations above sea level at different stations of the Astrophysical Observatory at the Smithsonian Institution, we obtain curves (Link, 1943) which considerably deviate from theoretical straight lines. If we overlook the undulation in the middle of the spectrum caused by the ozone (Fig. 25), certain differences depending little on the wavelength and changing but little from station to station are to be found even on the days of greatest sky transparency. The absorption of our high layer may be contained precisely in those differences ranging from 0.004 to 0.01.

The absorption, however, shows up best during the eclipses of the moon. According to the structure explained in Section I, F for two simple cases, the absorption for horizontal rays becomes 20 times as large as that at the zenith. This absorption is practically constant within a certain range of altitudes h_0 of the solar rays, corresponding to a rather important interval in the auxiliary shadow and the actual shadow. The remaining $O - C$ differences, which cannot be attributed to the ozone, can be explained in this manner.

As far as the lunar eclipses are concerned, it is difficult to decide between the thin and the thick absorbing layer. Measurements of the brightness of the sky at the zenith taken at twilight will, however, prove useful. The brightness

is due to molecular diffusion of light in the layers of air at altitudes which depend on the actual altitude of the sun. The absorption in our high layer should bring about the diffusion of light too. Between the optical density at the zenith B,

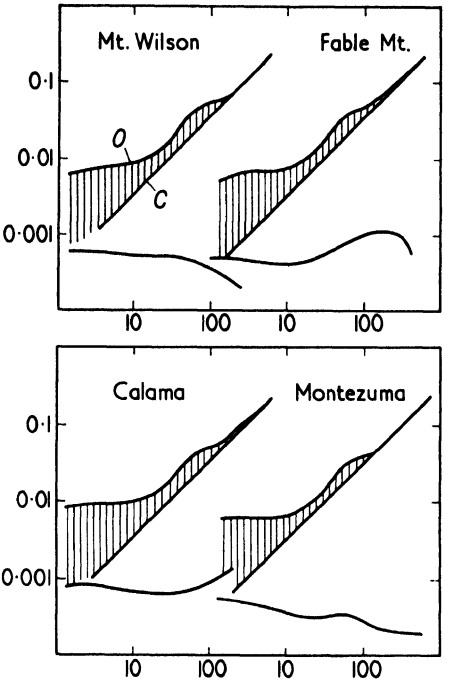

FIG. 25. Link's diagram. Logarithm of the optical density in zenith as function of log c^2/λ^4. The inclined line gives the theoretical relation in Rayleigh's atmosphere. Below the logarithms of O-C. The curves are valid for days of perfect transparency.

the surface brightness of the sun $b_{\odot}$, and the sky b the following relation holds (Link, 1948)

$$b = 1.2 \times 10^{-5} B b_{\odot} . \tag{68}$$

At a time when the sun is approximately 5° below the horizon, the air layers at an altitude over 30 km are still illuminated, and the measurements yield

$$b = 10^{-9} b_{\odot} . \tag{69}$$

If, however, our layer of optical density $B = 0.005$ was to be found above this altitude it should give the surface brightness

$$b = 6 \times 10^{-8} b_{\odot} . \tag{70}$$

about 60 times larger than we see.

This implies that the high absorbing layer is thick and not all concentrated in higher altitudes. Its upper limit is revealed both by the measurements of the increase of the shadow (Section II, O) and by the measurements at dusk. The curve of the twilight brightness of the sky depending on the depression of the sun displays a certain discontinuity in its course (Brunner, 1935; Link, 1946a; Neužil, 1961) at altitudes of about 100 km, and this discontinuity might signify the upper limit of the layer.

As far as the origin of the layer is concerned, a connect ion with micrometeorites may prove very likely. The whole matter, however, will be explained together with the increase of the shadow.

Recently our absorbing layer was directly observed by Glenn (1962) during his three revolutions round the earth, approximatively in the position assigned by the astronomical observations (Link, 1963).

N. *Increase of the Terrestrial Shadow*

At the beginning of the 18th century the method of determining geographic longitudes or, strictly speaking, their differences, by means of lunar eclipses grew to be used extensively. The simultaneous observation of a lunar eclipse from two or more places provided at various phases (e.g., the transits of the edge of the shadow through individual craters) time signals, which, compared with local times, yielded the differences of geographic longitudes. This very old method, mentioned as far back as the second century B.C. by the Greek astronomer Hipparchos, facilitated the determination of the difference of geographic longitudes to a fraction of the minute of time.

On this occasion it was noticed by the astronomers that the radius of the shadow as computed by the geometric formula

$$\sigma_2 = \pi_\odot + \pi_\mathbb{C} - R_\odot \tag{29}$$

did not correspond exactly to the observation, and with an increase of the shadow were found discrepancies as large as 1 to 2 min between theory and observations.

The first attempt to determine this increase of the geometrical shadow was made by Lahire (1707), who established the value 1/41 for the increase the shadow. Subsequently, J. D. Cassini (1740) explained the increase of the shadow attributing it to the influence of the terrestrial atmosphere. Others, such as Lemonnier (1746), and Lalande (1782) set forth the values of the increase of the shadow, within the range of 1/25 and 1/123, failing, however, to describe the methods of determining the value.

O. *Methods of Determining the Increase of the Shadow and their Results*

In practice, the methods based on the observation of the transits of lunar craters across the edge of the shadow have proved most successful. The observer determines the time of the transit of a certain crater across the assumed edge of the shadow, and from the known position of the crater and the ephemeris of the moon and the sun the corresponding increase of the shadow may be determined. To effect the reduction two fundamental methods have been used. The first method, due to Maedler (1838), requires the determination of the ingress and the egress of the crater. This determines the length (Fig. 26) of

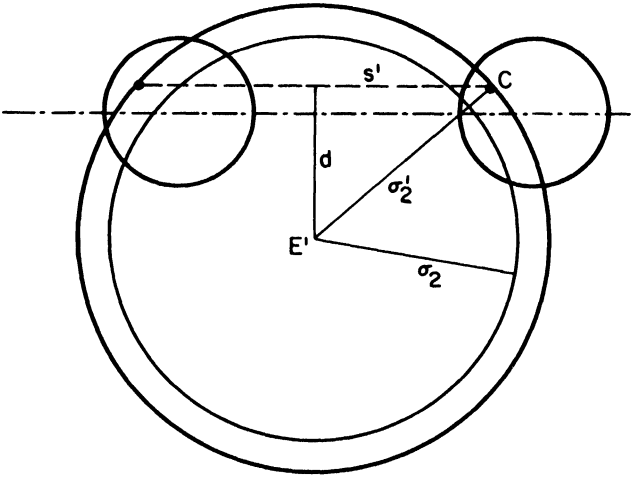

FIG. 26. Determination of the increase of the shadow.

the path $2s'$ described by the crater in the shadow, and from the minimum distance d of the path computed from the ephemeris the radius of the shadow σ_2' is also derived. The difference $\sigma_2' - \sigma_2$ gives the increase of the shadow. Maedler's method offers one advantage: it is to a great extent independent of the exact ephemeris of the moon, the weak point of which is the longitude of the moon (on which the computation depends but little). On the other hand, we may consider the necessity to determine the times of the ingress and egress a disadvantage, since it is often made impossible by the weather or by the position of the moon below the horizon. It is also not possible to determine the increase of the shadow separately from the ingress and the egress, which take place on various spots of the shadow and hence can differ (Section II, P).

Hartmann's method (1891) makes use of the ingress and the egress of the craters separately. For every moment the positions of the crater and the center

of the shadow are known, from which it is possible to determine the distance, i.e., the radius of the shadow σ_2'. Here the knowledge of the exact ephemeris of the moon is necessary. However, the method offers advantages which do not obtain in Maedler's method.

Hartmann treated his problems in terms of the ecliptical spherical coordinates, which are less in use these days. Therefore, Kosik (1940) introduced equatorial coordinates, making use of the rectangular system of coordinates. This rendered the computations easier to survey, though shortened them only slightly. The method of determining the increase from the transits of the craters is well suited for amateur observations, and it would be desirable to set up an adequate organization of observer to this end.

Other experiments have been undertaken to determine the increase in the shadow. Wirtz (1906, 1917) measured micrometrically the distance of the two corners of the shadow during partial eclipse, and such measurements were repeated by Arend (1942). A photographic determination by means of photographs was taken up by Donitsch (1900) and Malsch (1923). There have appeared, however, systematic differences depending upon the exposure and the treatment of the negatives. The photoelectric determinations of the density near the limit of the shadow would prove ideal, but have not yet been carried out during any eclipse.

So far only a few series of observations have been reduced, as is shown by the following survey:

1776-1888	20 eclipses	(Brossinsky, 1889)
1802-1889	28 eclipses	(Hartmann, 1891)
1889-1936	23 eclipses	(Link and Linková, 1954a)

Moreover, some eclipses have been reduced by Kosik (1940, 1955) Bouška (1948, 1949, 1950, 1956, 1958, 1960), Bouška and Růžičková (1953), and Koebcke (1951, 1954). From the total material collected so far, e.g., from 57 eclipses in the last 150 years (Link and Linková, 1954b) it may be derived that the average increase of the terrestrial shadow amounts to 2.3%, which represents a number close on the conventional value 2% used for the computation of the ephemerides.

P. *Flattening of the Shadow*

The limit of the terrestrial shadow is not exactly circular, but it is slightly flattened in the same sense as the geoid (Kosik, 1940). The value of the flattening is, however, greater than that of the geoid, as is shown by the following examples

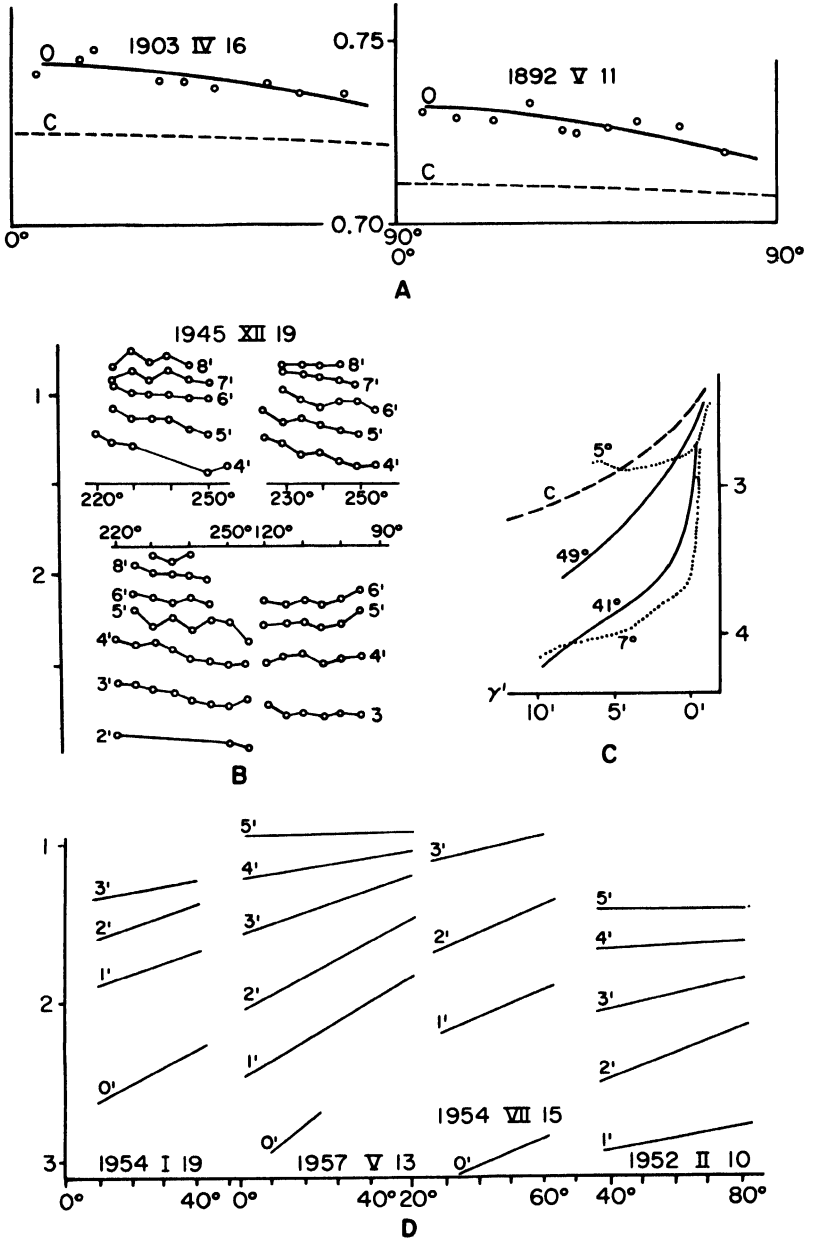

FIG. 27. Different manifestations of the shadow flattening. A—the flattening by passages of craters. B—isophotes of the penumbra for differents distances γ' as function of the position angle (90°, 270° equator). C—curves $D = F(\gamma)$ for different latitudes; curve C—the mean computed curve. D—schematic variation of the density in the penumbra at different distances γ' as function of the latitude.

of the radius of the shadow in its dependence on the position angle P on both sides of the equator:

1938 XI 7	$43.67' - 0.353 \sin^2 P$	Observed	
	$42.95 - 0.183 \sin^2 P$	Calculated	
	$0.72' - 0.170 \sin^2 P$	Flattening	(71)
1939 V 3	$42.90 - 0.456 \sin^2 P$	Observed	
	$42.12 - 0.183 \sin^2 P$	Calculated	
	$0.78 - 0.273 \sin^2 P$	Flattening	

The flattening of the shadow has been confirmed also for other eclipses, whenever sufficiently exact observations were available (Fig. 27). The flattening is shown by the shadow as well as the penumbra. In the latter, at the same distance γ' from the limit of the shadow the density increases from the pole to the equator (Link, 1946c, 1958) as is shown in Fig. 27. In the shadow the conditions are similar (Link, 1960). The density curves in the neighborhood of the equator are much steeper than the curves at higher geographic latitudes, and their bends on the equator are further away from the center of the shadow.

Q. *Explanation of the Increase of the Shadow*

If we omit the first attempts to interpret the increase of the shadow by means of the influence of the atmosphere (dating back to the 17th century), the first serious attempt to establish a theory of the shadow increase was made by Hepperger (1895) and Seeliger (1896). Using their theories (Section II, H) and the incomplete knowledge of the atmosphere at the time, they computed a detailed course of the density of the shadow in the surroundings of its geometric limit. Both attempts now possess but a historic value, as they have been based on incorrect premises.

Hepperger located the optical limit of the shadow at a distance where the change in the density of the shadow with the distance was the greatest, i.e., where $dD/d\gamma$ was maximum. According to his computations this was to be found at approximately 52″ from the geometric limit of the shadow, which agreed fairly well with the observations. For Seeliger, this criterion led to an increase by 70″, which is contradicted by the facts.

Seeliger, however, proceeded to investigate the phenomenon of the increase of the shadow by means of experiments. From the shape of his curve $D = f(\gamma)$ he constructed a disk (Fig. 28), the bright part of which at every distance had a central angle corresponding to the illumination in the shadow. The disk was made to spin rapidly, and when observed from a greater distance it appeared

to have a hazy border. By means of a suitable micrometer its diameter was measured, and from the results by several observers Seeliger obtained an increase in the shadow of about 50″. This may have led Seeliger to the conclusion that the increase of the shadow was a purely physiological matter which did not depend on the course of the density $D = f(\gamma)$, and that the structure of the

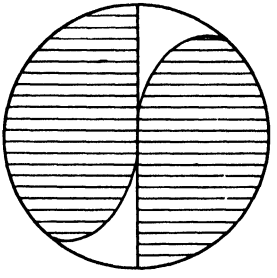

FIG. 28. Seeliger's sector simulating the density of the shadow.

atmosphere had no perceptible influence upon the phenomenon. In support of this thesis he asserted that the absorption of light at altitudes that corresponded to the increase of the shadow was negligible. Seeliger must have failed to realize the existence of the attenuation of the light by refraction (which, however, was implied in his theory) and could not have anticipated the existence of the high absorbing layer.

Another test carried out by M. de Saussure (1931) and based upon Seeliger's theory was not conclusive, as the fundamental elements of the computation (e.g., the 45–50 km altitude of the ozone layer and the actual structure of the atmosphere) were incorrect.

Seeliger's experiments have been recently repeated and improved upon by Paetzold (1953). According to Kühl's (1928) theory of contrast the estimated limit of the shadow should lie where the function $D = f(\gamma)$ has its point of inflection (i.e., where the relative change in the illumination reaches its maximum value). Paetzold started from several curves of the shadow based on the modern theory of the eclipse, taking for granted Rayleigh's atmosphere itself, with the ozone layer and finally with the high absorbing layer at the altitude of 90 km and the zenith absorption 0.012. Rotating sectors were constructed accordingly, and the limits of the shadow were measured; the outcome of which indicated that only the high absorbing layer had a substantial influence on the increase of the shadow, while the lower layers exerted little or no influence. This implies that the location of the variations in the increase of the shadow must be sought in the high absorbing layer.

With the above-mentioned parameters of the layer Paetzold obtained an

increase of the shadow of 3.2%. The accepted absorption, however, represents the maximum value, the average values being about 0.004–0.006, which means that the increase of the shadow would also turn out to be less.

R. *Origin of the High Absorbing Layer*

The increase of the terrestrial shadow and the deviations in its density can both be explained by the existence of a high absorbing layer composed of meteoric dust. We have shown how the average increase of the shadow can be explained by the existence of a high absorbing layer, with an upper limit at

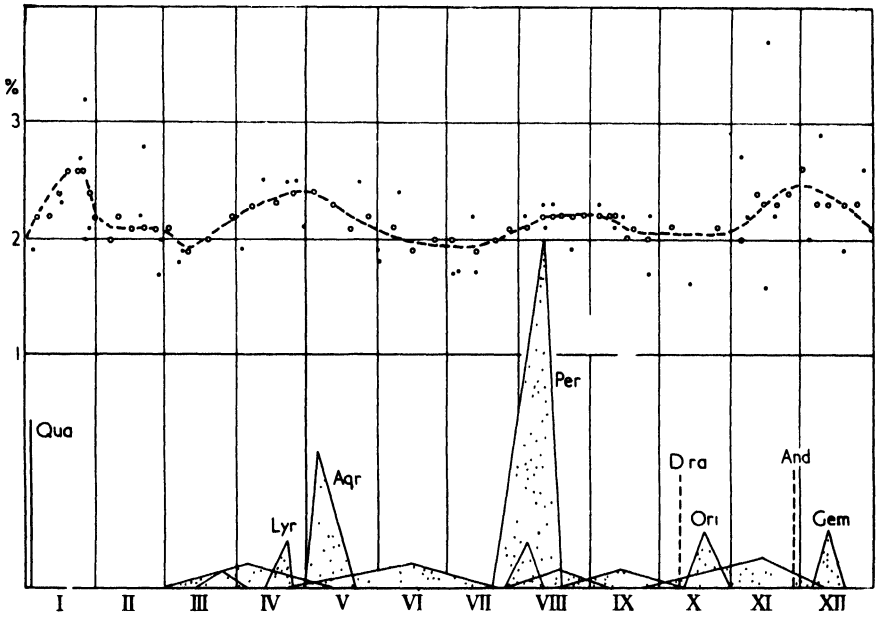

FIG. 29. Increase of the earth's shadow in relation to the meteoric activity (Link and Linková, 1954b).

about 100 km. Furthermore, we have shown that the increase in density of the shadow, which cannot be explained by means of known causes, has its origin in the high absorbing layer. We shall now demonstrate, in conformity with observations and theory, that the origin of the high absorbing layer can be attributed to the meteoric material which keeps impinging into the high atmosphere and falls thereafter to the terrestrial surface, its downward fee fall being slowed down by air resistance.

The increase of the shadow varies yearly, as was shown first by Bouška and Švestka (1950) and later, on the basis of a more extensive material from the years 1804–1950, by Link and Linková (1954a, b). The seasonal change in the increase corresponds closely to the activity of the meteoritic showers familiar from visual observations (Fig. 29). Furthermore, Švestka (1950) found from the method of the zero'th day that the brightness of the eclipse in Danjon's scale (Section II, Q) falls off sharply after the maximum of the showers (Fig. 30)

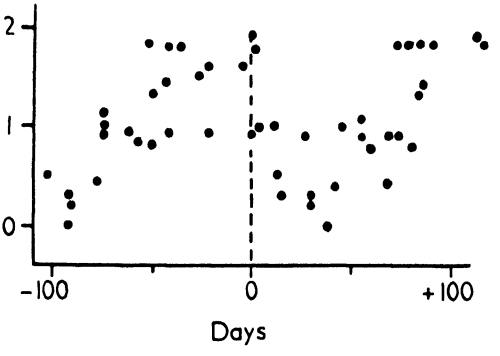

FIG. 30. Luminosity of lunar eclipses following the maximum of meteor swarms (Švestka, 1950).

to a minimum in about one month, and only after another two months will the brightness recover its original value. Both phenomena can be explained in the following way: near the maximum activity of the shower, the atmosphere is invaded by an increased number of meteors or meteoric dust, which at high altitudes of about 100–150 km (where the air resistance will commence to make itself felt) forms a layer falling slowly towards the terrestrial surface. The fall takes approximately one month or more, in conformity with the curve in Fig. 30. Similar results are also arrived at on the basis of other phenomena. Zacharov (1952) reduced the measurements of optical density at the zenith, made at Mt. Wilson in the years 1908 to 1920 at the time of the maximum activity of the Perseids. He found a noticeable rise in the density, persisting for 24 days at most after the maximum of the swarm. In the collections of the meteoric dust on the terrestrial surface we come across a similar delay. Hansa and Zacharov (1958) collected meteoritic dust at three stations in Czechoslovakia at intervals of two weeks. The proportion of nickel to iron present in the collections was determined by means of spectral analysis, the ratio rising to double the value at an interval 14–42 days after the maximum of the Perseids or Orionids. A sharper time-selectivity has so far been impossible due to the length (14 days) of the collection period. Finally, the well-known work of

Bowen (1953, 1956a, b) and his collaborators (Bigg, 1957; Hefferman and Bracewell, 1959) seems to suggest that the number of condensation nuclei rises to sharp maxima for 30 days on the average after the maximum of various meteoritic swarms. Bowen's phenomenon was confirmed by Dmitrijev and Czili (1958) by means of a quite independent statistical method, which takes into consideration the objections of Bowen's critics. These phenomena point to the connection with the activity of the meteor showers as well as to the duration of the fall of meteoric particles, which is close to 30 days.

From the theoretical point of view (Link, 1950b) it is possible to demonstrate the connection between the optical density and other properties of the layer and the duration of the fall and the meteoric accretion. Let us consider that about m_0 gm/cm^2 sec impinge upon the atmosphere at about 100 km. This material is changed into spherical particles with the semidiameter a and the density δ, falling toward the earth through a resisting medium. The duration of the fall T can be computed from the known structure of the atmosphere as the function of the radius and of the density of the particle (Fig. 31). Because of the continuity of the flux of the particles, the total mass contained in the vertical column from the terrestrial surface to the 100 km surface will be equal to

$$M = m_0 T\,; \tag{72}$$

and its optical density

$$B = k(a) m_0 T\,, \tag{73}$$

where the coefficient $k(a)$ was computed by Greenstein (1937).

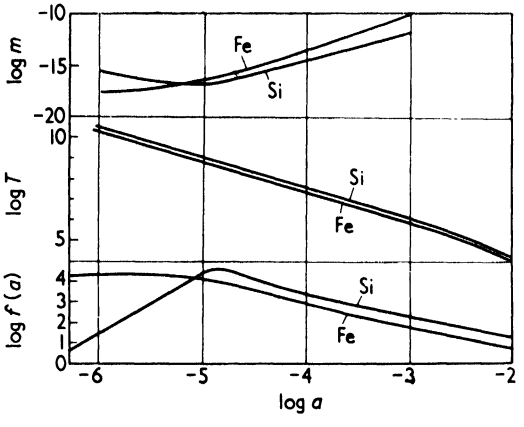

FIG. 31. Regime of the high absorbing layer. *Above*: meteoric accretion required for the density in zenith $\Delta = 0.004$. *Center*: time of fall of meteoric particles. *Below*: Greenstein's absorption coefficients $f(a)$. All as functions of the composition (Fe = iron, Si = silicates) and of the radius a of the meteoric particle.

The above relation is of fundamental importance to the theory and the regime of the high absorbing layer. Its graphical representation is shown in Fig. 31. The system of curves for the iron and stone particles shows the duration of the fall necessary for the optical density to be reached at the zenith $B = 0.004$, which is in dependent of the radius of the particle a for various accretions m_0 Moreover, the duration T of the fall of the particles is shown to be dependent on the radius of the particles. As the duration of the fall, according to the data obtained from the eclipses, is at most 10^7 sec, the accretion of at least $5 \cdot 10^{-13}$ particles of radii between 1 and 10 μ is required for the observed density B to be reached at the zenith. The particles with such dimensions produce neutral absorption, which corresponds to the results in Fig. 31. Though the estimated

TABLE IX

METEORIC ACCRETION (Zacharov, 1961)

No.	Author	Year	Accretion (gm/cm² 5cc)	Method
1	Th. Oppolzer	1884	5×10^{-10}	Upper limit according to the celestial mechanic
2	Hanza-Zacharov	1958	3×10^{-11}	Ni in terrestrial dust collections
3[a]	Petterson	1958	1×10^{-12}	Ni in terrestrial dust collections
4	Zacharov	1961	7×10^{-12}	Ni in terrestrial dust collections
5	Link	1955	5×10^{-13}	Optical density of the atmosphere
6	Petterson-Rotschi	1950	2×10^{-13}	Ni on the bottom of the Pacific
7	Petterson	1958	6×10^{-14}	As No. 3
8	Petterson	1960	4×10^{-14}	As No. 6
9	Petterson-Rotschi	1950	2×10^{-14}	As No. 6
10	Watson	1956	2×10^{-14}	All interplanetary matter, upper limit
11	Kreiken	1959	2×10^{-14}	Only magnetic spherules in collection.
12	Kizilirmak	1960	2×10^{-14}	Magnetic particles in collections
13	Petterson	1960	2×10^{-14}	Air filtration, preliminary value
14	Thompsen	1953	1×10^{-14}	Magnetic spherules in collections
15	Van de Hulst	1947	4×10^{-15}	Zodiacal light
16	Watson	1956	2×10^{-15}	As No. 10, lower limit
17	Öpik	1956	2×10^{-15}	As No. 15
18	Norris-Hogg	1949	2×10^{-15}	Spherules
19[b]	Dubin	1960	1×10^{-15}	Space probes
20	Schwinner	1936	1×10^{-15}	Geological evidence, max. value
21	Schwinner	1936	3×10^{-16}	Geological evidence, min. value
22	Watson	1939	7×10^{-17}	Meteors and meteorites
23	Wylie	1935	2×10^{-17}	Meteors and meteorites
24	Watson	1939	7×10^{-19}	Only meteors

[a] No. 3, the value of No. 7 reduced to the fall time of 30 days.
[b] No. 19, only a partial accretion, total accretion is 2×10^{-14}.

accretion $m_0 = 5 \times 10^{-13}$ is greater than the accretions obtained by direct findings on the earth or by means of the rockets and artificial satellites, it is very far from the values obtained from visual observations of the meteors (cf. Table IX). The question concerning the presence of meteoritic dust in the atmosphere, its fall to the earth, and its influence upon precipitations is far from being definitely clarified. It is connected with the physics of the clouds, the atmospheric circulation, and interplanetary matter—all of which exceeds the scope of our present paper in which we have confined ourselves to a discussion of lunar eclipses.

S. *Tropospheric Influences on the Eclipses*

The analysis of the tropospheric influences on the brightness of the eclipses should be included in any theory on lunar eclipses. Even though these phenomena do not add much to the investigation of the high atmosphere, we shall survey them briefly in order to bring out the scope of the photometric theory of the lunar eclipses.

The structure of the troposphere determines the density of the interior parts of the shadow, as it is shown in Fig. 10. It is not, of course, the local structure of the troposphere that matters, but the structure along the whole effective terminator of the shadow which for the distances $\gamma < 16'$ involves the whole terrestrial periphery, i.e., the length of 40,000 km. Small local deviations from the normal state will thus be evened out and only extensive changes of the troposphere can appear in the central parts of the shadow. Characteristic examples are as follows:

(a) A *brightening up in the center of the shadow* can be observed in a number of curves of the eclipses (Fig. 32). Several causes combine to exert an action in the same sense. The attenuation by refraction (Table IV) begins to decrease towards the center of the auxiliary shadow where, by Eq. (31), $\phi = 0$, for $r = 0$, i.e., the focusing of rays emanating from the luminous element of the sun is at its best. This phenomenon was known already to Laplace. According to (31) the focusing is subject to the following condition

$$\omega = \left(\pi_{\mathbb{C}} + \pi_{\odot}\right)\left(1 + \frac{h_0'}{a}\right) \tag{74}$$

which, in the mean latitudes, leads to the altitude of $h < 2$ km. Of course, at such altitudes the rays are often obstructed by cloudiness reaching these heights. At higher latitudes, where the refraction is greater, the condition is fulfilled at altitudes of 3–4 km; in winter, when there is less cloud, it is lower, especially at higher latitudes. An extension of the effective terminator to higher latitudes, greater refraction, and a lower level of clouds at these latitudes all combine to

form a kind of "polar window," through which light penetrates into the center of the shadow, causing it to brighten.

(b) *The disappearance of the moon* during the eclipse, or, rather, considerable attenuation of its light bordering on invisibility, is a rare phenomenon, but it has been recorded. Table X lists the principal cases of very dark eclipses:

TABLE X

DARK LUNAR ECLIPSES (Link, 1961)

No.	Date	Degree	Observers	Observations and volcanic explosions
1	1601 XII 9	11	Kepler	Eclipsed part invisible
2	1620 VI 15	18	Kepler	Moon invisible, stars visible
3	1620 XII 9	19	Cysat at Ingolstadt	Moon invisible
4	1642 IV 14	19	Many observers	Very dark or invisible. Explosion Avoe 1741 I, 1 km³ ashes
5	1761 V 18	18	Many observers	Very dark or invisible. Explosion Jorullo 1759 IX 28??
6	1816 VI 16	15	Lee at London, Eule at Dresden	Moon invisible. Explosion Tambora 1815, spring, 150 km³ ashes!!
7	1884 X 4	18	Many observers	Very dark and colorless. Explosion Krakatoa 1883 VIII, 18 km³ ashes
8	1902 X 16	18	Barnard and others	Very dark. Explosions 1902 V Mt. Pelée and St. Vincent, 1 km³; Santa Maria 1902 X 5 km³
9	1903 IV 11	12	Many observers	Very dark. Explosions as above
10	1913 III 22	19	Many observers	Very dark and colorless. Explosion
11	1913 IX 15	17	Many observers	Mt. Katmai 1912 VI-X, 21 km³

In order to explain these phenomena we need to know if the disappearance of the moon during the eclipse is theoretically possible at all. To have the illumination in the center of the shadow ($\gamma = 0$) reduce to zero, the illumination in the auxiliary shadow (Table IV) must vanish up to the distance $r = R_{\odot} = 16'$ which, according to the parallax of the moon, requires the opacity of the atmosphere up to the altitudes of 4 to 6 km, all over the terrestrial circumference of 40,000 km. The cloudiness can cause a local opacity of the atmosphere up to these altitudes along a limited part of the terminator, but not along its full length. The extension of cloudiness on a greater or smaller scale can, therefore, be expected to produce certain fluctuations of brightness, but not a complete disappearance.

Apart from cloudiness, the general atmospheric pollution by the volcanic dust can causes a conspicuous increase of the density of the shadow leading almost to the disappearance of the moon. This idea was expressed on several occasions (Dufour, 1899; Flammarion, 1884), but only recently was it supported by numerical data and new observational material (Link, 1961).

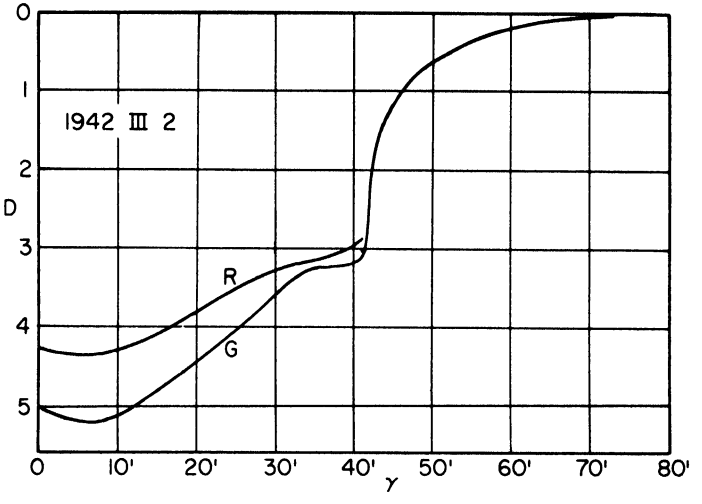

FIG. 32. Curves of the density of the shadow for the eclipse 1942 III 2.

Experience based upon various volcanic eruptions (Symons, 1888) has shown that, during great eruptions, volcanic dust will spread by the general atmospheric circulation round the whole earth and also practically to all geographic latitudes. The altitude of the polluted layer attains at first some tens to a hundred kilometers, followed by only a gradual down fall, which implies that the atmosphere does not clear up until after a number of months or a year. In this way the condition for influencing the brightness lunar eclipses by volcanic eruptions is indeed fulfilled. A sufficient absorption of the layer is yet another condition. Great volcanic eruptions produce from ten to a hundred cubic kilometers of ash and it may be presumed that at least 0.1 km^3 of it is the form of a fine ash whose particles (according to the size of Bishop's ring) have a mean radius a of approximately 10^{-4} cm.

We shall adopt as basis of our considerations the following model layer: altitude—20 km; range—half of the surface of the earth (i.e., for instance between the latitudes 30°N to 30°S); the ejected mass—0.1 km^3 (i.e., 2×10^{14} gm) From the equations for the high absorbing layer in Section II, R it is possible now to compute the path of the horizontal rays s in the layer, the total mass m

of the dust along this path, and the corresponding optical density D_V, which are listed in Table XI in comparison with the optical density D_R in Rayleigh's atmosphere (for green light).

TABLE XI

VOLCANIC DUST LAYER

h_0 (km)	s (km)	m (10^{-3} g)	D_V	D_R
0	1100	4.4	4.4	—
5	920	3.6	3.6	4.1
10	740	3.0	3.0	2.2
15	514	2.0	2.0	2.7

If we consider that the surface brightness of the full moon is 0.25 cd cm^{-2}, the same surface brightness subjected to the combined effect of pure atmosphere and volcanic dust can diminish to 10^{-8} of its value, which is less than the surface brightness of the night sky (10^{-8} cd cm^{-2}). To express if in a different way, a great volcanic eruption can bring about an effective disappearance of the eclipsed moon.

The influence of the volcanic pollution of the atmosphere was actually measured on several occasions. After the eruptions relating to Krakatoa, 1883, St. Vincent, Mt. Pelée, Santa Maria, 1902-3, and after the Katmai eruption, 1912, the optical density at the zenith rose by 0.06 to 0.09, which corresponds to our model with an increase by 0.08.

In Table XI volcanic eruptions could be associated with a number of subsequent eclipses, for which the evidence is by now complete. Older eclipses, of course, are not accompanied by reports on volcanic activities. The low intensity of the moon during the eclipse of 1761 V 18 was however, probably not due to the eruption of the volcano Jorullo of 1759 IX 28, but must have been connected with the solar activity (Section II, T) in conformity with Danjon's relation.

(c) *Meteorological influences* on eclipses were closely observed on the occasion of the eclipse 1938 XI 7 (Guth and Link, 1941). Photographic photometry of the eclipse (Guth and Link, 1939) showed isophotes of the shadow distinctly flattened in the inner part of the shadow and variable in time (Fig. 33). The explanation of this particularity lies with the changing synoptical situation along the terminator of the shadow, analyzed by Sekera on the basis of the weather maps of the nights 7–8 November, 1938. Figure 34 represents the synoptic situation along the terminator of the shadow set down for three

moments at which isophotes of the shadow were determined (Fig. 33). It appears that the parts of the terminator (both equatorial and central parts) were greatly affected by the cloudiness, whereas the polar area was relatively clear. This brought about a distinct extension of isophotes along the equator. In the course of time the cloudiness gradually increased, which is reflected in the increase

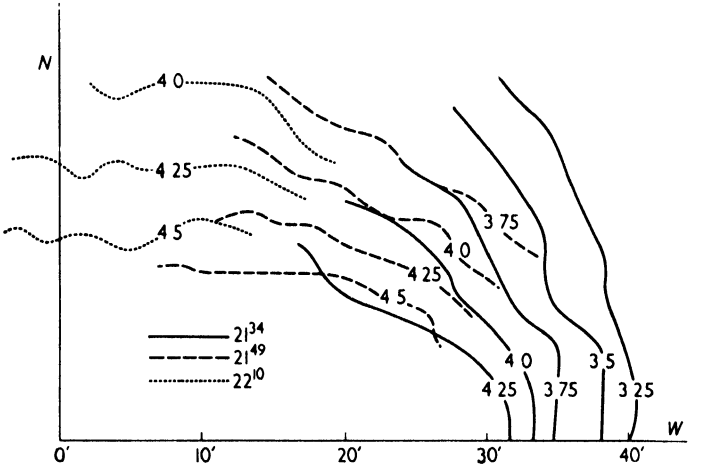

FIG. 33. Isophotes of the shadow during the eclipse November 7, 1938.

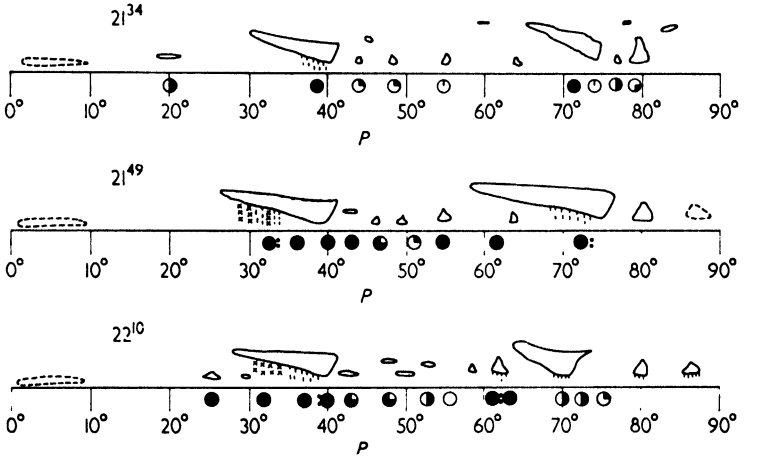

FIG. 34. Meteorological situation on the terminator corresponding to the three moments of the Fig. 33.

in density of the shadow in those spots in which the adjacent systems of isophotes are in contact.

An average flattening of isophotes within the inner parts of the shadow may be foreseen, of course, in synoptical situations (namely, in Rayleigh's atmosphere). By aerological investigations we have learned the average composition of the atmosphere up to approximately 25 km in various latitudes and at various times, which enables us to compute the isophotes of the auxiliary shadow may be deduced from which the densities of the shadow at different position angles by means of graphical methods. The results of these computations (Bouška and Link, 1947; Letfus, 1953) show but small deviations of 0.1 in the densities against normal values contained in Tables V and VI. These circumstances are clearly shown in Fig. 35.

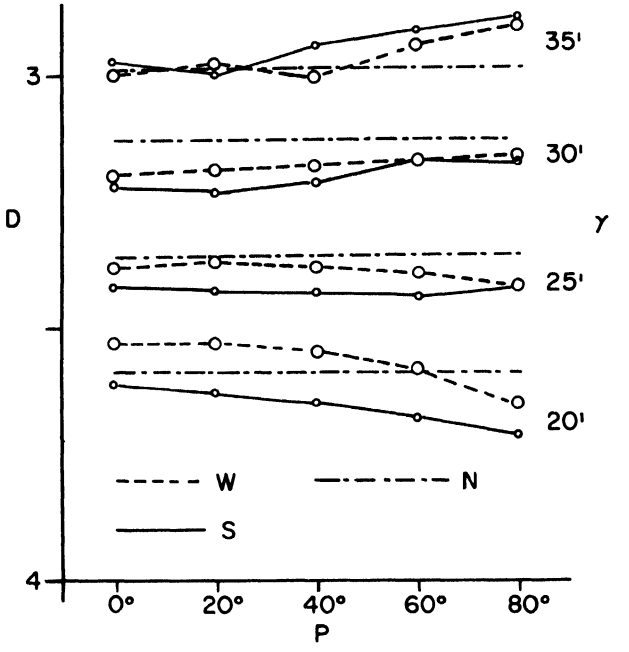

FIG. 35. Variation of the density of the shadow with position angle P (latitude) in the case given by $\delta_{\odot} = 16°$, $A = 0.04$/km, $\pi_{\mathbb{C}} = 59'$. W = winter, S = summer, N = mean conditions for the latitude 45—50°.

T. *Changes in the Brightness of the Eclipses*

In Section II, S we mentioned some abnormally dark and hardly visible eclipses, many of which can be accounted for by the pollution of the atmosphere

by volcanic dust. Now we shall proceed to deal with the changes in the brightness of lunar eclipses which are not of volcanic origin, along the lines initiated by Danjon (1920a, b).

From the times of Tycho Brahe (end of the 16th century), when first systematic observations of lunar eclipses took place, up to the twenties of this century approximately 500 eclipses have occurred, but only about 150 have been sufficiently well observed. These observations enabled Danjon (1920a, b) to draw certain conclusions about the change in the brightness of the lunar eclipses and their connection with solar activity. As all the cases do not include measurements of the density of the shadow, the observed phenomena being only verbally described, Danjon (1920a) made use of the scale of the brightness given in Table XII.

The concept of Danjon's scale is based mostly on the color of the shadow. i.e., on the transition from the dark and colorless shadow to a bright orange shadow. In such a way the purity of the atmosphere can be characterized by setting $L = 0$ for a very dim atmosphere up to $L = 4$ for a pure atmosphere.

Danjon reduced the best observed eclipses of 1823–1920, i.e., a total number of 70 eclipses, and after him Vaucouleurs (1944), considered 47 eclipses during the years 1894–1943; they obtained a saw-toothed curve of dependence on the phase of the solar activity (Fig. 36). The brightness of the eclipse at the

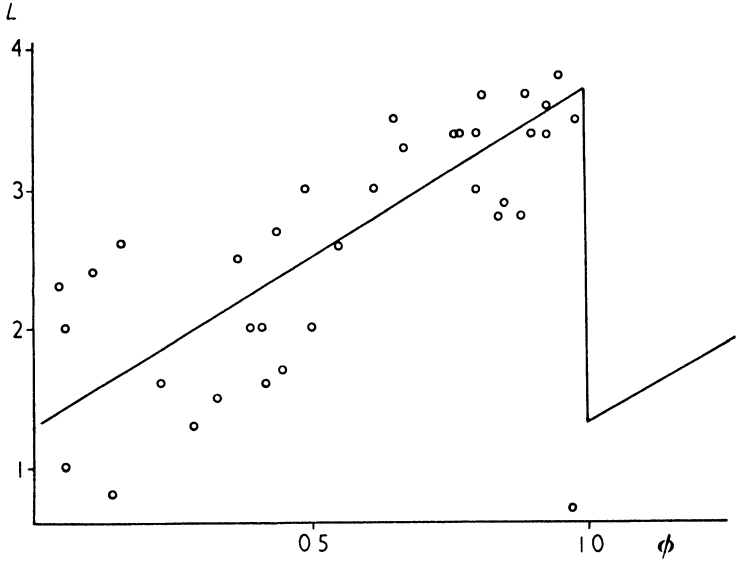

FIG. 36. Danjon's relation: Luminosity L of lunar eclipses as function of the phase ϕ within the 11-year solar cycle.

beginning of a new solar cycle will fall sharply and rise slowly up to the maximum which takes place immediately before the minimum of the next cycle. Although Danjon's relation was critized by Maunder (1921) and Fisher (1924), it seems to have satisfactorily survived all tests.

TABLE XII

DANJON'S SCALE

Degree L	Description
0	A very dark eclipse. Moon hardly visible, especially around the mid totality.
1	A dark eclipse, grey to brown colouring, details on the disk hardly discernible.
2	A dark red or rust-colored eclipse with a dark area in the center of the shadow, the edges brighter.
3	A brick-red eclipse, the shadow often bordered with a brighter yellow edge.
4	An orange or copper-colored very bright eclipse with bluish bright edge.

Certain modifications have, however, been recently suggested by work based on the measurements of the density of the shadow (Link, 1960). From the year 1921 to 1957 a total number of 18 eclipses were measured photometrically by the cat's-eye photometer (Section II, J). The brightness of the eclipse, as deduced from the density of the shadow at the distance of $\gamma' = 10'$ from its edge, does change with the solar activity (Fig. 37), but the shape of the curve is somewhat different from Danjon's sawtooth curve.

The maximum of brightness appears to take place before the minimum of the solar activity on the descending part of the curve. The color curve provided by the difference B — R in the outer parts of the shadow with $\gamma' = 10'$ and still closer to the center with $\gamma = 20'$, corresponds better to Danjon's curve. The absolute values of the densities are to be found under the value computed by Rayleigh's atmosphere with the ozone: namely, in the blue on the main part of the curve and on other parallel curves in the neighborhood of the maximum.

If we proceed to compare the differences O — C in the green with the evaluations of L on Danjon's scale (Fig. 37) there appears to be no explicit relationship between the two quantities. We may sum up by saying that Danjon's relation between the solar activity and the brightness of the eclipse expressed on the scale of L is borne out by the measurements as far as the color of the shadow is concerned. However, the course of the intensity curve is somewhat different, though fairly similar to Danjon's original relation.

The changes in the brightness of the eclipse seem to imply two influences.

The first is the absorption of light, approximately independent of wavelength, originating in the high absorbing layer or in the ozone layer. The second influence may be additional light—most probably the luminescence of the lunar surface

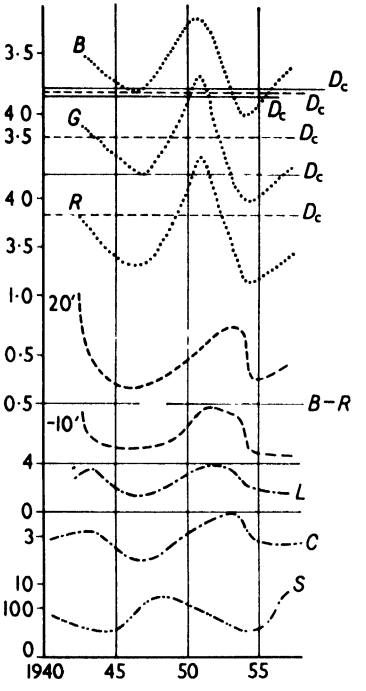

FIG. 37. Variations of the shadow during the solar cycle. *Above:* shadow density at $\gamma' = 10'$ for the blue (B), green (G), and red (R) color. D_C-density computed for Rayleigh's atmosphere (full line) or the same but with ozone (dashed line). *Center:* differences B − R (Blue − Red) at $\gamma' = 20'$ and at $\gamma' = 10'$. *Below:* L — luminosity curve, C — earthshine curve, S — sunspots curve.

(Link, 1946b). Both influences vary with solar activity, but their effects are opposite. An eclipse may be dark owing to a strong absorption in the atmosphere or to the absence of luminescence. A bright eclipse lying above the computed limit may be caused by a strong luminescence.

Dubois discovered a direct relation between the brightness of the eclipse and the earth-shine (Fig. 37), which made Vassy (1956) presume that the contents of the aerosols in the atmosphere depended on solar activity. The solar light diffused in it increases the albedo of the earth and, consequently, also the earth-shine. During an eclipse the atmosphere containing aerosols diffuses sunlight in the earth shadow, increasing the brightness of the eclipse. A closer computa-

tion shows, however, that the light diffused in this way (Section II, G) can hardly be sufficient to bring about a significant increase of the computed illumination, as it amounts to less than 10%. In the same way it is not probable that such a small contribution would bring about the variation of the density attaining 1, as it can be actually observed during eclipses.

III

ECLIPSES OF THE ARTIFICIAL AND OTHER SATELLITES

A. *Comparison with the Eclipses of the Moon*

In the same way as with the moon, the eclipse phenomena occur also with the artificial satellites at their ingress or egress from the terrestrial shadow. Their observation may, therefore, to some extent prove a substitute for the eclipse of the moon; and our present task will be to outline a theory of these phenomena (Link, 1962a).

In contrast with the eclipses of artificial satellites, the eclipses of the moon present a number of disadvantages. Because of the inclination of the lunar orbit and the distance from the earth, lunar eclipses are relatively rare (Table III). Their observations are often disturbed or made impossible by unfavorable weather. The lunar disk exhibits considerable variation in albedo, which implies that the measurements must be precisely located on its disk. With artificial satellites, for which convenient parameters as well as a shape suitable for measurement can be selected, there are no such difficulties. Their eclipses are much more frequent and their duration relatively short—all of which reduces the vagaries of the weather.

Another advantage of the eclipses of artificial satellites rests on the fact that we do not have to confine ourselves to observation from the earth alone—as for lunar eclipses—but can provide the satellites with photometers directed towards the sun. A satellite provided with an automatic photometer which would telemeter the measurements to the earth would be entirely independent of the weather existing on the ground; the measurements would be considerably more sensitive and, moreover, the shape of the satellite would be of no importance. The recent achievements of Lunik III have shown that, from the technical point of view, the orientation of the satellite towards the sun is possible; and we may anticipate that this variant of the eclipse method will prove to be very fruitful.

The duration of the eclipse will be given by two positions of the satellite, i.e., the ingress into the penumbra, whose angular radius is

$$\sigma_1 = 1.03(\pi_\odot + \pi_s) + R_\odot \tag{75}$$

and the ingress into the umbra

$$\sigma_0 = \pi_\odot + \pi_s - R_\odot - \omega_0 . \tag{76}$$

As for the penumbra, we adopt the terrestrial radius increased by 3%, so that allowance is made for the influence of the high absorbing layer. With regard to the radius of the umbra, we consider also the refraction ω_0 on the terrestrial surface. The limits of eclipse determined in this way give the difference of the angular distance from the center of the shadow

$$\Delta\sigma = \sigma_1 - \sigma_0 = 0.03(\pi_\odot + \pi_s) + 2R_\odot + \omega_0 . \tag{77}$$

If the sun were located in the plane of the satellite orbit, this angle would be measured along an arc in the orbit during the eclipse, from which the duration would follow. In any other position of the sun the arc in the orbit as well as the duration of the eclipse would be longer. For the current altitudes h of the satellite, namely, between 1000 and 2000 km, the angles $\Delta\sigma$, the time of the revolution P, the duration of the eclipse Δt, as well as the topocentric arc at the zenith $\Delta\tau$ are computed in Table XIII, the computations being based on the assumption of a circular orbit.

TABLE XIII

ECLIPSE PARAMETERS OF ARTIFICIAL SATELLITES

h(km)	1000	1200	1400	1600	1800	2000
$\Delta\sigma$ (deg)	3.25	3.18	3.11	3.05	3.00	2.94
P (min)	105	109	113	118	123	127
Δt (sec)	57	58	59	60	61	62
$\Delta\tau$ (deg)	24	20	17	15	13	12

B. *Computation of the Solar Illumination*

The computation of the solar illumination of the satellite will be effected by means of the general equations of Section I, E. In the computation of the general transmission coefficient the component t derived from molecular diffusion (8) will be the same as with the lunar eclipses. The component p derived from differential refraction (11) can be reduced to the form

$$\phi = \frac{\sin(\psi - \omega)}{\sin\psi}\left[1 - (a + h)\cos\psi\,\frac{d\omega}{dh'_0}\right] \tag{78}$$

$$\sin\psi = \frac{a + h'_0}{a + h}$$

and the expression for the angle r (10b) to

$$r = \pi_{\odot}\left(1 + \frac{h_0'}{a}\right) + \psi - \omega\,. \tag{80}$$

For the integration of the illumination with respect to the solar element di we shall make use of the developments of Section I, G, Case (d). The corresponding numerical values are given in Table II.

When performing the computations of the density of the shadow D it has not been possible to do so for all types of orbits, of which there would be too great a number. We have selected, therefore, four altitudes of the satellite, namely, $h = 1000$, 1500, 2000 km, and a stationary satellite at $h = 42{,}400$ km. For these altitudes and for three spectral regions $\lambda = 4600$, 5600, and 6200 Å the densities of the auxiliary shadow and, hence, also the densities of the actual shadow have been computed. An example of the outcome of such computations is represented in Fig. 38. For detailed tables see Link (1962a).

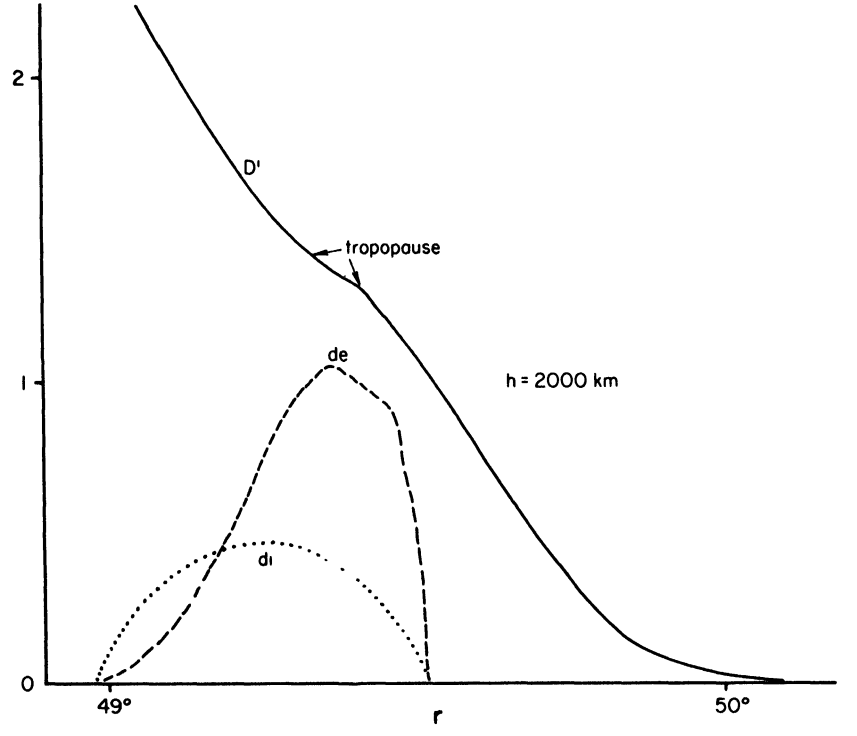

FIG. 38. Solar illumination of the artificial satellite. D′ density of the auxiliary shadow; *di*, the luminosity of the solar disk; *de* the illumination of the satellite, all as function of angle r.

C. *Photometry of Eclipses of Artificial Satellites*

In order to perform photometric measurements of the eclipses from the terrestrial surface, two methods are considered as most convenient: the photographic method and the photoelectric method. When applying both methods we shall assume that the satellite of the "Echo" type appears outside the shadow as a star of zero stellar magnitude.

Such a relatively slowly moving object can be quite well recorded photographically with an immobile camera, the method being similar to that used when photographing meteors. A filter may be employed, but spectral selection will not always be necessary. The topocentric position of the satellite during the eclipse must, of course, be known. In order to perform the photometric reduction of the photograph a photometric calibration obtained by means of a meteoric carousal (Link and Neužil, 1953), or in any other way, is necessary. With a maximum accuracy of photographic photometry around $\pm 5\%$ the method will give good semiquantitative results for the interpretation of the properties of the high atmosphere.

More accurate measurements will require the photoelectric method. Although an optical system guided along the known motion of the satellite is conceivable, a simple photoelectric photometer without optical devices can also prove successful. The modern photomultipliers easily supply a photoelectric current of 2000 amp/lumen. With a 1 cm^2 cathode surface it corresponds to a sensitivity of 0.2 amp/lux. On the edge of the shadow, in its interesting parts, the satellite can be expected to produce, on ground, an illumination of 10^{-6} lux and, hence, a photocurrent of at least 10^{-7} amp, which can easily be measured. If the visual field of the photometer is limited by a simple diaphragm with a diameter of 5° and a surface of 20°sq, the night sky will supply a photoelectric current slightly weaker than the satellite. Under these conditions, with an approximate location of the photometer, it will be possible to measure the whole interesting part of the eclipse without guiding. The light of the night sky can be eliminated by subtraction or compensation.

In the future, however, we can anticipate satellites equipped with automatic photoelectric photometers which will transmit the measurements by radio to the terrestrial surface. In this case the orientation of the photometer towards the sun will be required, which has already been obtained in astronautical technique. The direct solar illumination will be measured by means of a photometer, and so we shall hardly be limited by the sensitivity of the apparatus. The photometry of brighter stars or planets is also not excluded. In this case, instead of the densities of the shadow D, we shall consider the densities $D' = \log t \times p$.

D. *Topocentric Brightness of the Satellite*

The computed density of the shadow D will be of value for a comparison with the observation, provided that the satellite is equipped with an automatic photometer measuring the solar illumination incident on the satellite. This will not be possible, however, until the second stage; whereas at the first stage we shall measure the topocentric brightness of the satellite from the terrestrial surface. The topocentric brightness of the satellite will depend on the illumination of the satellite e, its distance from the observer x, the extinction of light between the satellite and the observer given by the air mass M_s, and on the phase angle p (Fig. 39). Furthermore, the brightness of the satellite will depend

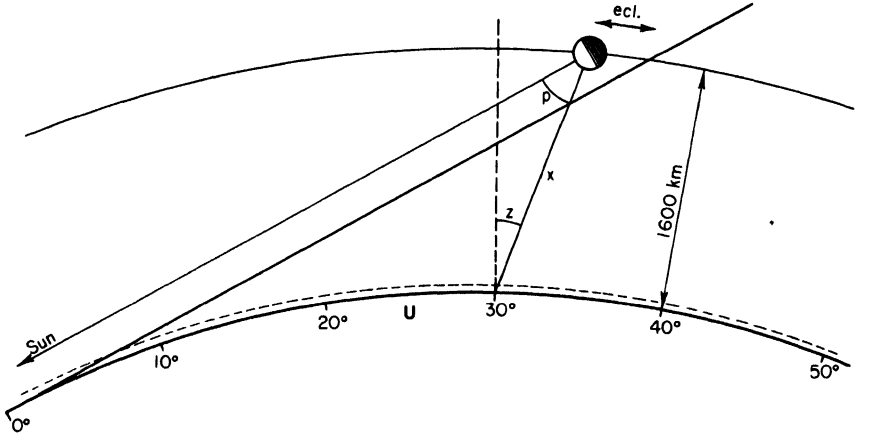

FIG. 39. Circumstances during the eclipse of an artificial satellite.

on its radius and on the parameters of the surface. Here two cases may occur. The surface of the satellite will produce either diffuse or specular reflection (like the satellite "Echo"). During one eclipse the size and the parameters of the surface will remain practically unchanged; in the course of the eclipse the other quantities will be subject to change within certain limits, which may influence the topocentric brightness. Our task will consist in determining the necessary correction.

If the topocentric brightness of the satellite was e_t at a given time of the eclipse E_t beyond the eclipse, the corresponding solar illumination at the time of the eclipse would (provide that $E = 1$) be given by the following expression for the diffusing surface

$$e = \frac{e_t}{E_t}\left(\frac{x}{X}\right)^2 10^{-A(M_s - m_s)} \frac{\varphi(P)}{\varphi(p)}. \tag{81}$$

The function φ depends on the phase angle of the satellite

$$p = 180 - z - z_{\odot} + \omega , \tag{82}$$

and on the law of diffuse reflection on the surface of the satellite. Usually the validity of the Lambert or Lommel-Seeliger law is assumed, for which the required values of the function $\varphi(p)$ (Schoenberg, 1929) have been computed.

For the case of the specular reflection we again have the equation

$$e = \frac{e_t}{E_t}\left(\frac{x}{X}\right)^2 10^{-A(M_s - m_s)} . \tag{83}$$

E. *Comparison of the Theory and Observation*

At the present time we are not yet in possession of the results of the measurements which we hope will be available soon.[1] On the basis of the results from the lunar eclipses we can anticipate, however, what a comparison would probably

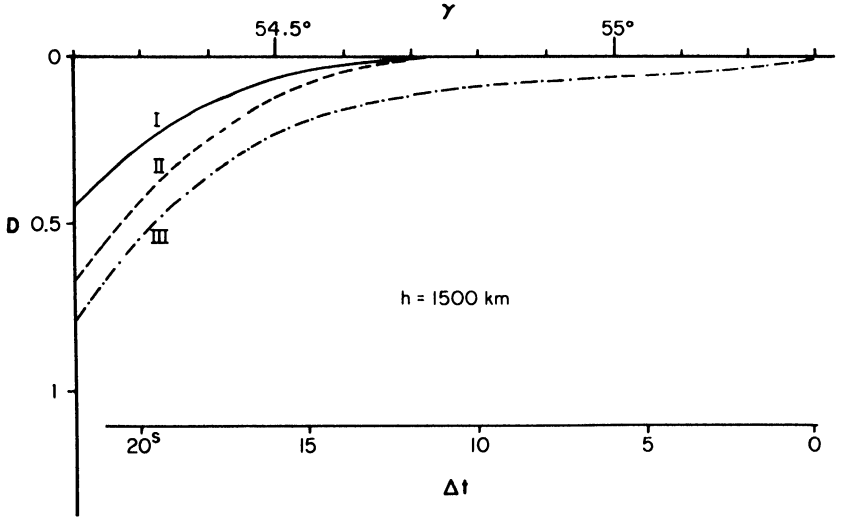

FIG. 40. Curves of shadow density during the eclipse of the artificial satellite.

look like. On the basis of the present knowledge of the structure of the high atmosphere we have computed the eclipse of the satellite at the height $h = 1500$ km, and in the green of the spectrum region. Besides the funda-

[1] Meanwhile this has been done by Venkateswaran (1961).

mental case of Rayleigh's atmosphere, as mentioned above, we have based the computation on two other cases, all of which are set forth as follows:

I. Rayleigh's atmosphere.
II. Rayleigh's atmosphere + ozone layer.
III. Rayleigh's atmosphere + ozone layer + high absorbing layer. Formula (15) with $h = 100$ km, $B = 0.006$.

According to the above-mentioned process we have begun by computing the densities of the auxiliary shadow D' and from them by integration the densities of the actual shadow D. The results are shown in Fig. 40. The structure of the high atmosphere different from Rayleigh's atmosphere will be identified here—as in the case of lunar eclipses—by two phenomena:

(a) A constant increase of the density of the shadow in its central parts, due to the ozone or to the ozone and the high absorbing layer.

(b) The increase of the density of the shadow in its border parts due to the high absorbing layer alone, which brings about the increase of the shadow. The ozone layer has practically no influence on this increase.

F. *Eclipse of the Sun Observed from the Artificial Satellites of Other Planets*

The first preliminary investigations of the planets by means of cosmic spaceships will be probably carried out at the time of a close passage, or when the spacecraft becomes a temporary satellite of the planet. On such occasions it will be possible to explore the atmospheres with methods similar to those used with the eclipse of the moon or the artificial satellites of the earth.

The advantages of such circumplanetary investigations are obvious. It means avoiding technical difficulties connected with the landing on the planet and with the takeoff for the return to the earth. It also means being independent of the living conditions existing on the planets, which in anticipation appear to be very unfavorable to our way of life. The requirements of this method are similar to those relative to the artificial satellites, i.e., the photoelectric photometry of the sun or a bright star at the time of their occultation by a planet are needed.

The photometric theory of these phenomena is closely associated with our descriptions of the eclipses of the artificial satellites and of the occultations of the stars. We shall, therefore, refrain from repeating it, and shall merely confine ourselves to demonstrating, on a few examples, the general character of the phenomena. For this purpose we have selected Venus and Mars, the planets that are certainly going to be the first targets of astronautical investigations.

We shall start off with some models of atmospheres corresponding best to the results of the observations acquired up to now, and we shall proceed to

compute the density of the shadow cast by a point source (D') on the one hand and by the sun (D) on the other. The presumed parameters of the models of the atmospheres, the partial results, as well as the final densities D' and D, are contained in Tables XIV and XV and are represented in Fig. 41.

The characteristic features of the atmosphere of Venus are assumed in accordance with the latest results acquired at the time of the occultation of the

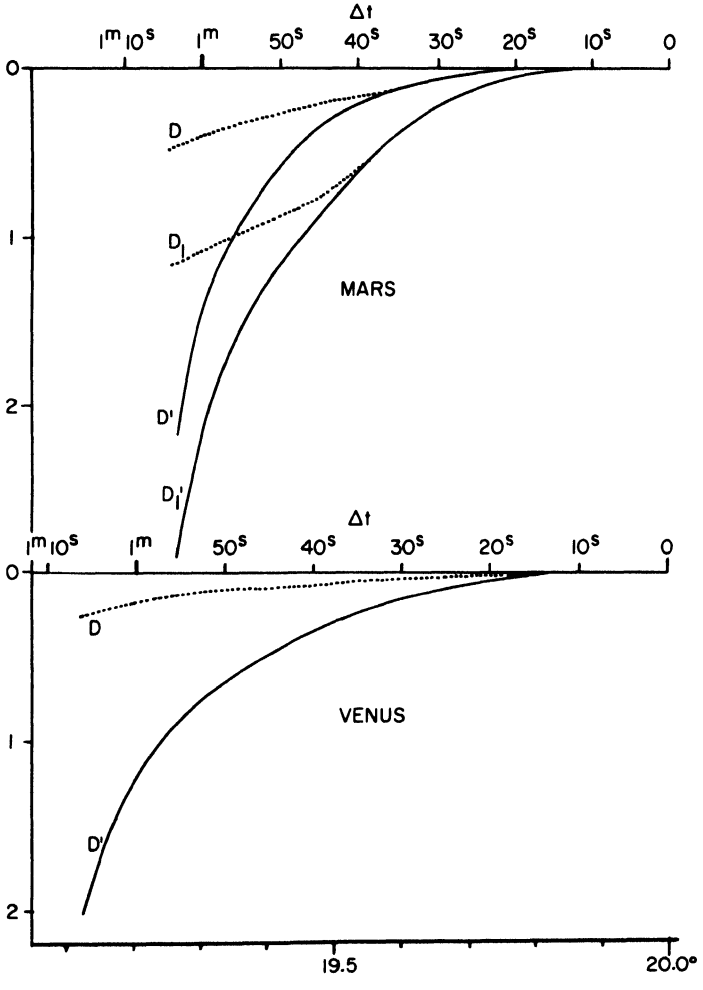

FIG. 41. Eclipse curves as observed from the artificial satellite at $h = 2a$. D—the eclipse of the sun; D'—the occultation of a star; D_1 and D_1'—the same with the dust layer in Mars.

Regulus 1959 (Menzel and Vaucouleurs, 1961). As for Mars we began by assuming an ideal atmosphere on the one hand, and the presence of a dust layer on the other (Vaucouleurs, 1961).

TABLE XIV

CIRCUMPLANETARY EXPLORATION

	Venus	Mars
$a + h = 3a$ (km)	18.300	13.200
$R_{\odot}$ (deg)	0.368	0.175
$(a + h) \cos$ (km)	17.500	12.430
$\beta = 1/H$ (km^{-1})	1/6	1/17
ω_0 (min)	1	2.76
A (km^{-1})	0.00575	0.00575
M (km)	0.97	16.85

These results (Link, 1962b) throw some light on the potentialities of circumplanetary research. In contrast with the occultations of stars by the planets as observed from the earth (Section V, B), where the rays will practically penetrate only through the highest layers of the atmosphere, the circumplanetary research will enable us to reach as far as the surface of the planet. This is of great value for astronautical needs. The different behavior is due to the difference distance between the observer and from the planet and, in consequence, to a change in the attenuation by the refraction which for the terrestrial observer attains high values even in the highest layers of the atmosphere.

In the case of Mars, the dust layer will easily lend itself to observation both through its absorption (as follows from the above-mentioned numbers) and through its diffusion producing a bright aureola round the planet, when the observer is on the limb of the shadow. The ratio of the surface brightness of the layer b to the sun $b_{\odot}$ is given by the expression (Link, 1948)

$$b = 1.2 \times 10^{-5} D b_{\odot} . \tag{68}$$

where D denotes, as before, the optical density.

In our case, for the ray at the altitude $h = 40$ km, the optical density from the diffusion is given by the equation $D = 0.02 + 0.32 = 0.34$ and the corresponding surface brightness $b = 0.5$ cd cm^{-2}, which should be clearly visible even by day. The width of the aureola will be about 12′, if the altitude of the layer is between 45 and 50 km.

TABLE XV

AUXILIARY SHADOW

Venus

h_0 (km)	ω (min)	ω (deg)	ψ (deg)	r (deg)	M (km)	AM	$\log \phi$	$-\log T$
0	1.00	0.02	19.47	19.45	5.8	0.03	0.26	0.29
5	0.73	0.01	19.48	19.47	4.2	0.02	0.21	0.23
10	0.54	0.01	19.50	19.49	3.1	0.02	0.16	0.18
15	0.39	0.01	19.52	19.51	2.2	0.01	0.14	0.15
20	0.28	0.00	19.53	19.53	1.6	0.01	0.09	0.10
25	0.21	0.00	19.55	19.55	1.2	0.01	0.07	0.08
30	0.15	0.00	19.55	19.57	0.9	0.01	0.05	0.06
40	0.08	0.00	19.60	19.60	0.5	0.00	0.03	0.03
60	0.02	0.00	19.66	19.66	0.1	0.00	0.01	0.01
80	0.01	0.00	19.72	19.72	0.0	0.00	0.00	0.00

Mars

h_0 (km)	ω (min)	ω (deg)	ψ (deg)	r (deg)	M (km)	AM	$\log \phi$	$-\log T$	$B(h_0)$[a]	$-\log T + B(h_s)$
0	2.76	0.05	19.47	19.42	46.5	0.268	0.201	0.47	0.71	1.18
5	2.06	0.03	19.49	19.46	34.2	0.200	0.158	0.36		
10	1.53	0.03	19.51	19.48	25.8	0.148	0.123	0.27	0.64	0.91
15	1.14	0.02	19.54	19.51	19.2	0.110	0.094	0.20		
20	0.85	0.01	19.56	19.55	14.4	0.083	0.073	0.15	0.55	0.70
25	0.64	0.01	19.58	19.57	10.8	0.061	0.055	0.12		
30	0.47	0.01	19.60	19.59	7.9	0.046	0.042	0.09	0.45	0.54
35	0.35	0.01	19.62	19.61	5.6	0.034	0.031	0.06		
40	0.26	0.00	19.64	19.64	4.4	0.025	0.024	0.05	0.32	0.37
45	0.20	0.00	19.66	19.66	3.4	0.019	0.018	0.04	0.22	0.26
50	0.15	0.00	19.68	19.68	2.5	0.014	0.014	0.03	0.00	0.03
60	0.08	0.00	19.73	19.73	1.3	0.008	0.008	0.02	0.00	0.02
80	0.02	0.00	19.82	19.82	0.3	0.002	0.002	0.00	0.00	0.00

[a] $B(h_0)$ is the optical density of the dust layer.

G. *Eclipses of the Jovian Satellites*

The eclipses of the Jovian satellites may be used for the investigation of Jupiter's atmosphere much in the same way as the lunar eclipses. The ratios vary here only in the angular dimensions of the geometrical shadow σ_2 and the radii of the satellites R_S and the sun $R_\odot$ as observed from Jupiter. This is shown by Table XVI.

TABLE XVI

ECLIPSE ELEMENTS OF FOUR JOVIAN SATELLITES

Satellite	$R_\odot$	π_S	R_S	σ_2
I	0.051°	9.748°	0.260°	9.697°
II	0.051	6.092	0.144	6.041
III	0.051	3.817	0.140	3.766
IV	0.051	2.172	0.077	2.121

From the earth, of course, we can measure neither the density nor the illumination at a given point of the shadow, only their average value on the whole small disk of the satellite, i.e., in the angular interval $2R_S$. However, it is possible to derive from the observed light curve a curve reduced to the point dimension of the satellite by means of a method based on successive approximations (Link, 1936),

Earlier theories, as they were summed up by Müller (1897) or applied by Sampson (1910) to numerous visual measurements of the eclipses carried out by Pickering (1900), had been based mostly on the model of bright little disk of the satellite occulted by a direct and opaque edge of the shadow, irrespective of the refraction. They intended to establish the elements of the orbits of the satellites, taking for the beginning or the end of the eclipse the moments at which the brightness of the satellite would diminish to one-half of its brightness before the eclipse.

Eropkin (1931) carried out several photographic measurements of the eclipses, commencing at a much earlier stage of the eclipse than Pickering. Their accuracy has also proved to be substantially greater. An interesting decline in brightness was shown, of the same nature for all the three observed satellites. The brightness began to decline long before the eclipse took place, then a standstill or a secondary maximum occurred to be followed by a further decline in brightness until there was complete disappearance (Fig. 42). As a rule Pickering's curves did not begin before the stationary part of Eropkin's curve, regardless of the fact that the first decline would in most of the cases have been affected by a considerable dispersion of the measured values.

This singular behavior cannot be simply attributed to the influence of the atmosphere, as Eropkin (1931) attempted to do for the rays in question pass through the altitudes of 5 to 18% of the radius of the planet. At these altitudes the density of the atmosphere and its optical manifestations are utterly negligible.

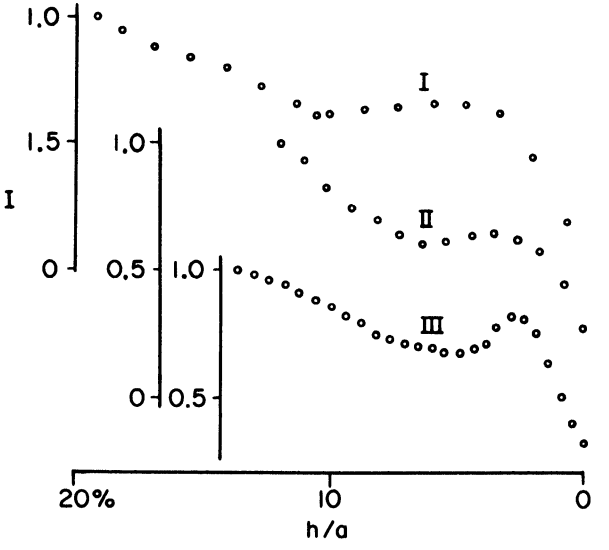

FIG. 42. Mean eclipse curves of Jovian satellites according to Eropkin, h is the minimum altitude of solar rays.

Rather, it might involve some dust layer or a rudimentary ring like the Saturn crepe ring (Link, 1936). The constants derived from Eropkin's measurements are contained in Table XVII. The optical density of the layer being small,

TABLE XVII

ABSORPTION OF LIGHT IN THE PROXIMITY OF JUPITER

Satellite	I	II	III
Altitude (% aa_4)	18	11.5	11
(max) (km)	12.800	8.200	7.900
Altitude (% aa_4)	10	6	5
(min) (km)	7.100	4.300	3.600
Width (% aa_4)	8	5.5	6
(vertical) (km)	5.700	3.900	4.300
Optical density	0.028	0.020	0.016
Jovicentric latitude	+18°	+32°	+48°

the layer would hardly be observable in the diffused light in the vicinity of the bright little disk of the planet.

In order to obtain a good explanation it will be necessary to carry out photoelectric measurements over a sufficiently long period before and after the eclipse. The existence (or, rather, the concentration) of dust in the vicinity of a planet is not so unusual; as only recently, indeed, with the help of the satellites, we have obtained direct evidence of such a dust layer surrounding our earth (Whipple, 1961; Hibbs, 1961; Glenn, 1962), not to mention indirect but conclusive evidence derived from the eclipses of the moon.

Recently Harris (1961) published some older photoelectric measurements of eclipses which do not agree with the results of Eropkin. It would be necessary to investigate the origin of this discrepancy before we conclude our problem.

IV

TRANSITS OF PLANETS

A. *Introduction*

The transits of planets across the sun hold a very significant place in astronomy, especially those of Venus. Before the telescope was invented sun-spots had been sometimes mistaken for the transits of Mercury or Venus in front of the sun. The first actual observation of the transit of Venus across the sun dates from the year 1639 XII 4 by Horrox and that of Mercury from the year 1631 XI 7 by Gassendi (Wolf, 1877).

The actual study of the transits of Venus was not, however, initiated untill the work of Gregory (1663) and, more especially, of Halley (1691, 1716), who pointed out the usefulness of the transits for the determination of the solar parallax. The transits in 1761, 1769, 1874, and 1882 were studied attentively by numerous expeditions sent out to all parts of the world. The results are known to have been rather poor and it is expected that in the future (i.e., in the years 2004 and 2012) the method will be discarded.

The transits of Venus, however, have proved very useful for the determination of the properties of the atmosphere of this planet. The very first observers of the transit in the year 1761—Chappe d'Auteroche, Strömer, Wargentin, Rumovsky, Bergmann, Lemonnier, Lomonosov, *et al.* (Link, 1959)—noticed that at the time of the ingress and egress of the dark disk of Venus the protruding part of the limb of the planet was surrounded with a radiant aureola, a phenomenon which some of the observers (especially Lomonosov and Chappe d'Auteroche) have ascribed to the presence of an atmosphere. In this way the first planetary atmosphere was discovered as far back as 200 years ago.

Similar phenomena were observed and described also at the time of subsequent transits, but only in the past few years have they been used for exploring the the atmosphere of Venus (Sharonov, 1952; Link, 1959). The aureola observed only during the transits should not be confused, however, with the extent of the cusps of Venus' crescent whenever this planet is in close conjunction with the sun (Russell, 1899; Link, 1949).

The transit of Venus across the sun presents formally the same case as the observation of the lunar eclipse from the Moon (Section II, E). The conditions in respect of the relative shape of the sun and the eclipsing body are, however, reversed. During the eclipse of the moon the sun is covered by the considerably larger earth, whereas during the transit of Venus the dark disk of the planet is obviously much smaller than the sun.

B. *Refraction in the Atmosphere of Venus*

The terrestrial observer N (Fig. 43) can see Venus V projecting itself on to the solar plane I. The luminous point M of this plane is seen by him due to refraction ω in the direction ψ, whereas without refraction it would be seen in the direction of r'. We try to determine the relation between the object angle r and the image angle ψ.

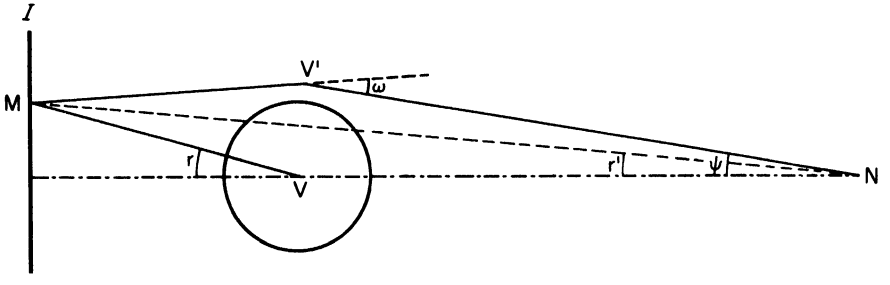

FIG. 43. Refraction in the Cytherean atmosphere.

According to Eq. (33) we can write for our case

$$r = \left(\pi_{\varphi} + r_{\varphi}\right)\left(1 + \frac{h_0'}{a}\right) - \omega\,, \tag{84}$$

$$r' = r\,\frac{r_{\varphi}}{\pi_{\varphi} + r_{\varphi}} = 0.725\,r\,, \tag{85}$$

and

$$\psi = r_{\varphi}\left(1 + \frac{h_0'}{a}\right), \tag{86}$$

where π_φ denotes the angular radius of Venus as seen from the sun (= 11.7″), r_φ denotes the angular radius of Venus as seen from the earth (= 30.9″), and for the other quantities the usual notation used in Fig. 43 has been employed. The equations (84), (86) give the desired solution in parametric form through the altitude h_0', on which the refraction ω depends.

We shall now proceed to assume an exponential atmosphere, which will be introduced in Section V, A, containing the necessary equations for the computation of the refraction, with

$$\omega = c\rho \sqrt{2\pi\beta a}\,. \tag{87}$$

The gradient of the density β is connected with the molecular weight of the gas m, its absolute temperature t, the gravitational acceleration g, and the gas constant k by means of the relation

$$\beta = \frac{mg}{kt}\,. \tag{88}$$

If we insert this value into (87) and substitute the pressure p in mm Hg for the relative density of the atmosphere, we obtain

$$\omega = c\sqrt{\frac{2\pi a g}{r}}\,\frac{273}{\sqrt{t^3}} = A\,\frac{p}{\sqrt{t^3}} \tag{89}$$

where the coefficient A for common gases assumes the values:

Gas	N_2	O_2	H_2	CO_2
A	393′	380′	49′	741′

C. *Formation of the Solar Image*

First of all we wish to establish the course of the so-called limiting curve in the solar plane. The curve is traced by the rays originating from the earth and reaching the visible surface of Venus, i.e., the cloud layer. If, at this altitude, the prevailing refraction is ω_0, the following limit angles will correspond to it

$$\begin{aligned} r_0 &= \pi_\varphi + r_\varphi - \omega_0\,, \\ r_0' &= r_\varphi - \frac{r_\varphi}{\pi_\varphi + r_\varphi}\,\omega_0\,, \end{aligned} \tag{90}$$

the second of which determines the limiting curve in the solar plane I. As long as $\pi_\varphi + r_\varphi > \omega_0$ the angles r_0, r_0' are positive, whereas for $\pi_\varphi + \pi_\varphi < \omega_0$

the angles become negative. As $\pi_{\varphi} + r_{\varphi} = 43''$ is a small angle and ω can vary along the limb of the planet, on one part of the limb we may have $r_0' > 0$ and on another $r_0' < 0$.

The side of the angle r_0' limits in the plane I a curve which, observed from the earth, represents the limb of the planet. Hence, it follows that the limiting curve can have positive ($r_0' > 0$) or negative ($r_0' < 0$) lobes.

The image of the solar plane visible from the earth arises according to the following principles:

(a) The points of the solar plane lying inside the positive lobes are invisible from the earth and vice versa.

(b) The points of the solar plane lying inside the negative lobes are visible from the earth and vice versa.

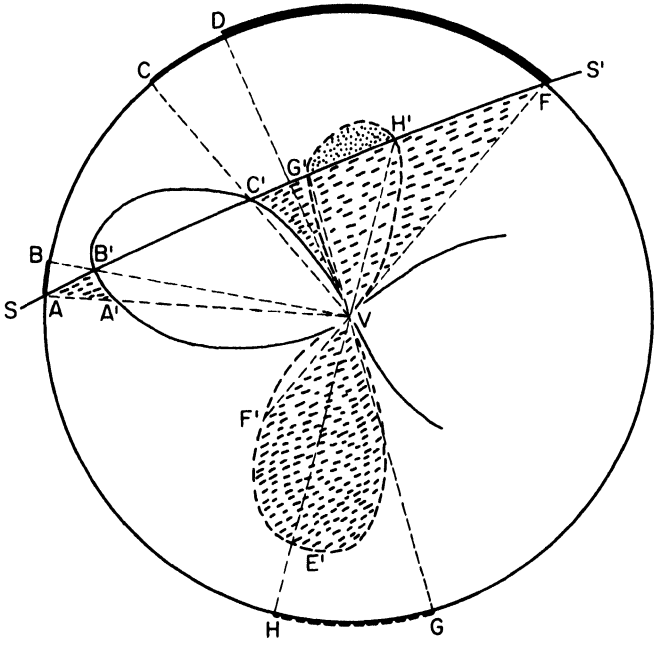

FIG. 44. Formation of the aureole on the limb of Venus during its transit.

In Fig. 44 such a case is schematically illustrated. The limb of the planet is represented by a circle with the radius VA, the immediate position of the solar limb is represented by the arc SS'; the positive lobes of the limit curve are fully drawn up and the negative lobes are dashed. The elements of the solar disk lying on the contoured surface AA'B' will be visible because of the

principle (a) and we shall spot them from the earth as an aureola on the dark limb of the planet between AB. Beyond there, the aureola is interrupted only to begin anew at the point C and to continue up to the point F. There it is composed partly of the solar elements on the dashed-line surface between C'FV and from the point D onwards also in conformity with the principle (b) of the elements on the dashed-line surface of the negative lobe VE'F'V. Finally, the dotted parts of the negative lobe between GH are not covered by the solar disk, and will appear between G and H as a slight dark protrusion of the limb of the planet.

The thickness of the aureola is given by the difference of the geocentric angles ψ for the limit curve and the border of the sun. An approximate expression for it is

$$\Delta\psi = \frac{r_\varphi}{a\beta} \log_e \frac{r_\varphi - r_0'}{r_\varphi - r_1'}, \tag{91}$$

in which the differences $r_\varphi - r_0'$ and $r_\varphi - r_1'$ can be read directly off Fig. 44. As the product $a\beta$ is of the order 10^3, the thickness of the aureola will be less than 1'' and, consequently, will be on the limit of the resolving power of the instruments. Hence, its brightness will be $b\Delta\psi$, i.e., proportional to the thicknes of the aureola and to the average surface brightness b of that part of the solar disk of which the aureola is the image.

The above general example can be simplified by reduction to two extreme cases. In the first case, when only the positive limiting curve, i.e., $\pi_\varphi + r_\varphi > \omega_0$, makes its appearance, the aureola will first be complete (Fig. 45), then at the inward contact of the limiting curve with the solar border it will split up in the direction of the point of contact into two parts adjacent to the solar border, both parts gradually getting shorter, only to disappear at the bisection of the disk of the planet by the solar limb.

In the second case, when the limiting curve is negative (Fig. 45), i.e., $\pi_\varphi + r_\varphi < \omega_0$, the aureola is complete up to point of bisection, where it begins to detach itself from the solar limb in the shape of a little cap, which shrinks gradually, disappearing at the outer contact of the limiting curve with the solar limb. This may occur even when the disk of the planet has moved away from the sun (Fig. 45, the last image).

It is important also to note the change in width as well as in brightness of the aureola with the temperature, which can of course vary along the limb of the planet. In the expression (91) the width $\Delta\psi$ depends on the temperature through (88) and r_0 (90). Differentiating with respect to t we get

$$\frac{d\Delta\psi}{dt} = \text{const.} \left(\log_e \frac{r_\varphi - r_0'}{r_\varphi - r_1'} - \frac{3}{2} \right). \tag{92}$$

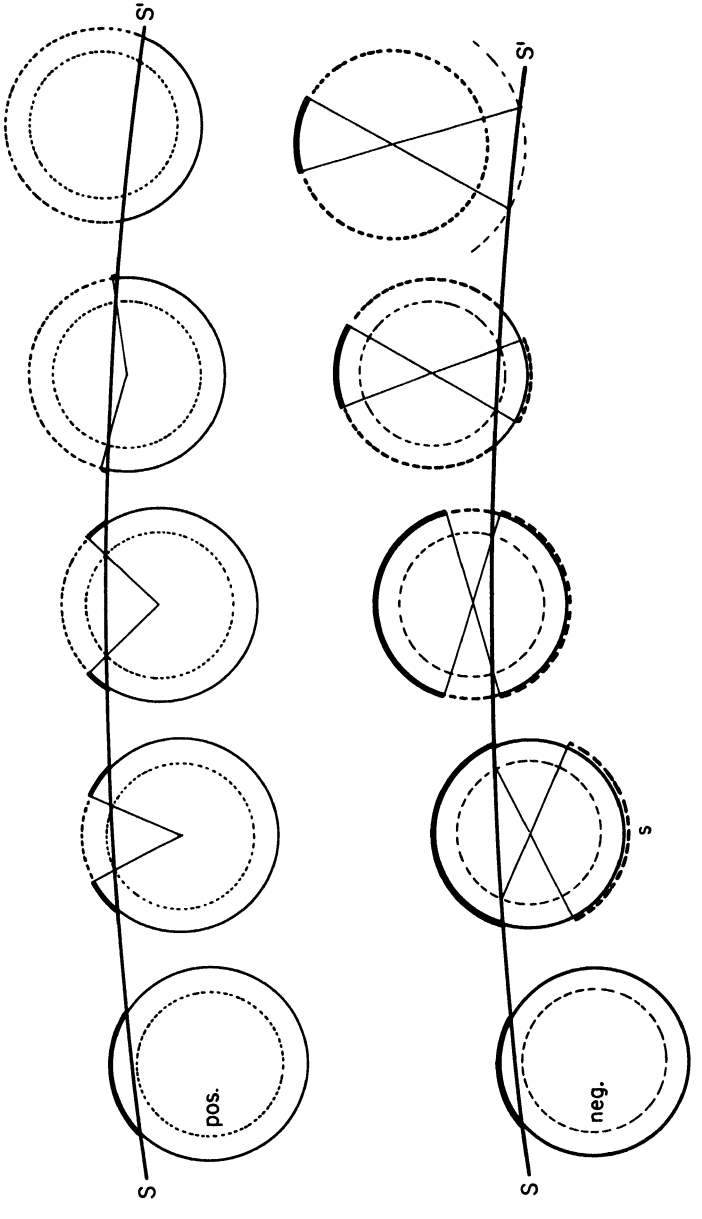

FIG. 45. Two types of Cytherean aureole. Above with the positive (p) below with the negative (n) limiting curve (circle). SS′ are solar borders. In the second case dark protrusions s are dashed.

This ratio will become negative soon after the inner contact, which means that along the limb the temperature will be declining in the direction of the increasing intensity of the aureola. Another reason for the increase in intensity of the aureola in the direction of the declining temperature is the fact that the height of the cloud layer will decrease in this direction (decrease of convection, which will bring about a rise in pressure p and, according to (87), an increase in refraction ω and, consequently, also in the width of the aureola.

From the above analysis of the formation of the refraction image of the sun the following conclusions can be drawn, of importance for the interpretation of the phenomena observed during the transits:

(a) The brightness of the aureola in general, increases along the limb in the direction of the diminishing temperature.

(b) The existence of the aureola after the bisection at the egress (before the bisection at the ingress) gives the lower limit for the refraction.

(c) At the moment of the splitting up of the aureola into two parts, or of the disappearance of the cap, the refraction in this direction is given by the expression

$$\omega_0 = \left(\pi_{\varphi} + r_{\varphi}\right)\left(1 - \frac{\Delta}{r_{\varphi}}\right), \tag{93}$$

in which Δ denotes the distance of the center of Venus from the limb of the sun ($\Delta < 0$ off the sun).

D. *Results Obtained during Earlier Transits*

The last four transits of the years 1761, 1769, 1874, and 1882 were observed for the purpose of determining the solar parallax. Some observations of the aureola as were recorded are rather casual, the observers having in their free time recorded the position and the aspect of the aureola in addition to other measurements. Nevertheless, a detailed review of the publications revealed close on one hundred observations of the aureola, which could be examined for determination of the properties of the atmosphere of Venus (Link, 1959).

To make a preliminary estimate of the conditions of observation the ephemeris based on Kuiper's rotation elements (Kuiper, 1954) was used. The latter had been deduced from ultraviolet photographs of the planet, on which parallel bands were found determining the direction of the rotation axis. The situation during the transits is illustrated in Fig. 46 and the corresponding numbers are contained also in Table XVIII. All this makes it plain that during one transit it was possible, for instance, to observe at the ingress the equatorial part of the aureola and at the egress one of the polar areas, or vice versa.

If we apply to the observations the principles set forth in Section IV, C, we should be able to derive, on the one hand, the value of the refraction ω_0 above the surface of the cloud layer on the equator or on the poles, and, on the other hand, the direction of the axis of rotation. Accordingly, from the splitting up

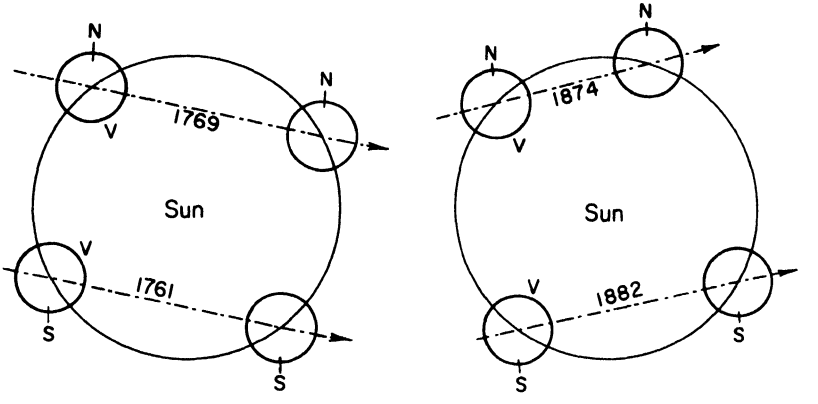

FIG. 46. Situation during the last four transits; disks of Venus are 3-times exagerated with regard to the solar disk.

of the aureola in the equatorial areas the average value of the refraction was determined to be $\omega_0 = 0.7'$.

In the polar areas of the aureola, the value of the refraction was fixed from the disappearance of the cap at $\omega_0 = 1.1'$ in summer and at $\omega_0 = 1.7'$ in winter. Furthermore, the position angle of the polar cap P was determined and found to agree satisfactorily with Kuiper's elements. All these results are summarized in Table XVIII.

TABLE XVIII

POLAR CAPS OF VENUS (Link, 1959)

Transit	Cap	$P_{obs.}$ (deg)	Number of observ-ations	Refraction (min)	Kuiper (1954) P (deg)	p (deg)	Season
1761	South	200	1	1.1?	177	120	Winter
1769	North	350	3	1.1	357	60	Summer
1874	North	20	3	1.7	3	120	Winter
1882	South	180	3	1.1	183	60	Summer

The above analysis reveals an obvious variation of the refraction from the equator to the poles, and at the poles the variation with the season as well.

These variations can be logically accounted for by the variations of temperature in accordance with the instantaneous orientation of the axis of rotation of the planet with respect to the sun. The variations of temperature along the limb of the planet also have an important bearing on the question of the axial rotation of the planet. It has often been asserted that the duration of the rotation of the planet is equal to its sideral revolution around the sun. Should it be so and should Venus thus keep turning the same face to the sun, it would follow that all the parts of the terminator of the shadow should be at the same temperature, and no differences in temperature along the limb of the planet should be observed during the transits. As this is not the case, the hypothesis of the equality of the rotation and the sideral revolution is thereby eliminated. The rotation period, therefore, has to be substantially shorter.

E. *Other Phenomena Accompanying the Transits*

During the transits of Venus other phenomena besides the aureola have been observed which have no direct bearing on the atmosphere of this planet. The phenomenon observed by Lomonosov (Suchomlinov, 1902) as a blister on the solar limb before the inner contact, when the limb of the planet has reached a distance of 1/10 of its diameter from the solar limb, would lead to an appreciable refraction at an altitude of 1200 km, which is quite out of the question. It is in all probability connected with the phenomenon of irradiation, which was also observed and described by Bigg-Wither (1883) at the time of the transit 1874.

A number of observers have seen projected around Venus a solar disk, an aureola 4–10″ wide. A similar phenomenon was observed also around the limb of Mercury or the moon under the same circumstances. We attribute it to a contrast between a bright and a dark surface.

Finally, in some isolated cases, a part of the planet's apparent disk was reported to have detached itself from the sun and become dimly visible. The phenomenon is, however, more likely to be connected with the extent of the cusps to be described in the next section.

F. *Extent of the Cusps of Venus*

This phenomenon is only in appearance connected with the phenomena occurring during the transits of Venus across the sun. Actually, it is due to the diffusion of light in the highest semitransparent layers of the cloud layer of the planet. Around the time of the inferior conjunction of Venus with the sun we can see a very narrow crescent of the planet, the cusps of which exceed

more or less the theoretical angle 180° (Fig. 47), the more so, the lesser the elongation of the planet from the sun. This phenomenon, known as far back as the end of the 18th century, was at first ascribed to refraction in the atmosphere of Venus, but this was an altogether wrong interpretation as we shall demonstrate below.

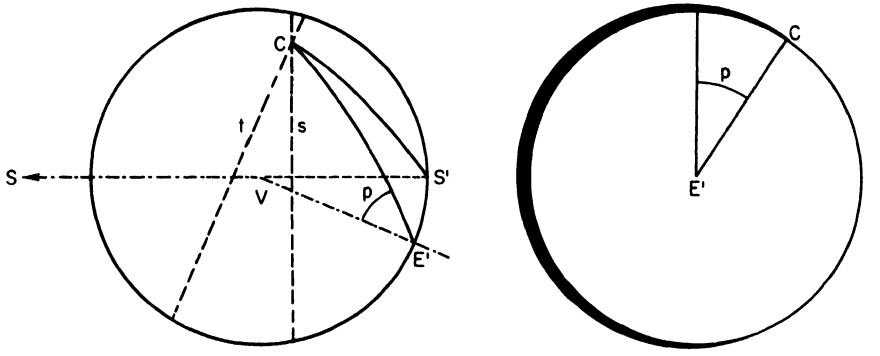

FIG. 47. Extent of the cusps of Venus.

The geometrical theory of the extension of the cusps can, however, can be laid down regardless of the actual physical cause involved. Let us assume that, for reasons not defined so far, the terminator of the shadow on the surface of the planet is in the position s (Fig. 48) and the limit of the visibility from the earth in the position t. Instead of ending in the theoretical position V the crescent will end in the position C, and the angle p will define the extent of the cusps. From the spherical triangle E'CS' it follows that

$$\sin \sigma = - \sin \tau \cos \varphi + \sin \varphi \cos \tau \sin p . \tag{94}$$

Between the elongation e and the phase angle φ there obtains the relation

$$\sin \varphi = \frac{\pi_{\varphi} + r_{\varphi}}{r_{\varphi}} \sin e . \tag{95}$$

Since the angles σ, τ, e are small we can set

$$\frac{\pi_{\varphi} + r_{\varphi}}{r_{\varphi}} e \sin p = \tau + \sigma = q \tag{96}$$

or, in the logarithmic form,

$$\log q = \log e + \log \sin p + 0.14 . \tag{96a}$$

In Fig. 49 (Link, 1949) the observations of Maedler (1849), Lyman (Russell, 1899), and Rabe (1913) have been plotted, which lead to the value

$$q = 2.63° \pm 0.05° . \tag{97}$$

According to the findings of Rabe (1948) the value of q depends also on the aperture of the telescope and on the atmospheric conditions, within the limits $1.9° < q < 3.7°$.

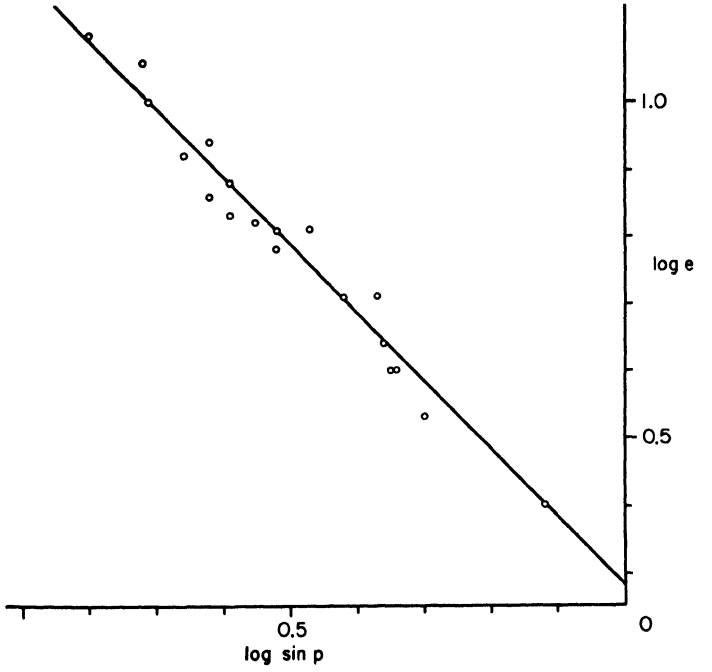

FIG. 48. Shifts of the visibility limit and of the terminator on Venus by the refraction.

G. *Explanation of the Extension of the Cusps*

The extension of the cusps was at first attributed to refraction. From Fig. 49 it is obvious that

$$\begin{aligned} \sigma &= \tfrac{1}{2}\omega - \pi_{\varphi} + r'_{\odot} , \\ \tau &= \tfrac{1}{2}\omega - r_{\varphi} , \end{aligned} \tag{98}$$

where

$$r'_{\odot} = R_{\odot} \frac{\pi_{\varphi} + r_{\varphi}}{r_{\varphi}} \tag{99}$$

represents the angular semidiameter of the sun as seen from Venus. From the sum

$$q = \sigma + \tau = \omega + r'_{\odot} - \pi_{\varphi} - r_{\varphi} \tag{100}$$

the values of the refraction can be deduced with $q = 2.63° \pm 0.05°$ and $\omega_0 = 2.25°$, which is a minimum value, the observable penumbra on the terminator of the shadow being narrower than $r'_{\odot}$.

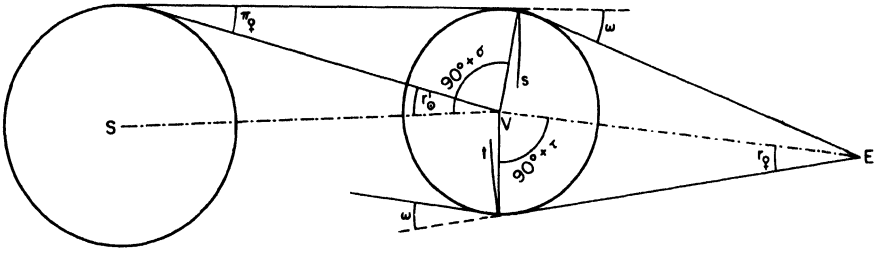

FIG. 49. Observations of the extent of the cusps.

The value of the refraction thus determined is considerably greater than that deduced from the transists of Venus across the sun, when we found a value of about $\omega_0 = 1'$. This discrepancy does not admit of the explanation that, during the conjunctions, we can penetrate the semitransparent layer of clouds into greater depths, where the refraction is greater than that obtaining from the transits across the sun. This should be just the reverse for the brightness of the sun.

Already in 1899, Russell (1899) put forward a very conclusive argument against the explanation of the conjunction phenomena by means of refraction, If we introduce the value of q (100) into Eq. (96) we shall obtain for the linking of the cusps, when $p = 90°$, the condition

$$e = \frac{r_{\varphi}}{\pi_{\varphi} + r_{\varphi}} (\omega - \pi_{\varphi} - r_{\varphi} + r'_{\odot}) = R_{\odot} - \Delta , \tag{101}$$

which, after a small adjustment, leads to the equation

$$\omega = \left(\pi_{\varphi} + r_{\varphi}\right) \left(1 - \frac{\Delta}{r_{\varphi}}\right), \tag{102}$$

which at the same time is a condition (93) for the first appearance of the refraction image. Here we encounter another very conspicuous discrepancy. If the extension of the cusps were due to refraction, the closing of the cusps would

coïncide with the appearance of the refraction image. This is not firmly established, for the linking of the cusps takes place with the elongation being 1.9°, i.e., about 1.4° from the border, whereas the first traces of the refraction image appear only after Venus has partly entered the solar disc, i.e., with an elongation of about 0.25°. This in itself proves that the extension of the cusps at the conjunction and the aureola at the transit are two distinct phenomena.

Opposing Russell's argument, based on the absence of the refraction image at the time of the closing of the cusps, Schoenberg (1949) suggested the possibility that the refraction image could disappear due to the dispersion of light on the long path between Venus and the earth. As a matter of fact this explanation does not hold good, for Schoenberg considered the dispersion of one single ray, which is physically impossible (as we have always to consider a pencil of rays). If, according to the principles mentioned above, we construct the refraction image of the sun for the violet and red rays (Fig. 50) their dimensions are but little different even for the refraction of $\omega_0 = 2.2°$, which implies that dispersion cannot bring about their disappearance (Link, 1957).

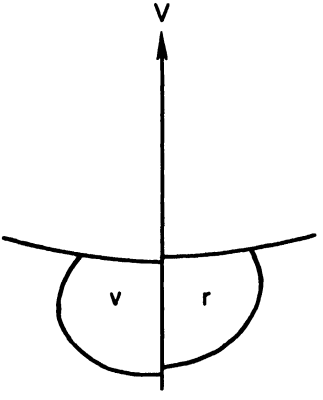

FIG. 50. Differences of violet (v) and red (r) refraction images of the sun. Distances from the planetary limb are exagerated 1000 times.

Another proof against the refraction origin of the extent of the cusps is provided by their color and brightness (Link, 1949). The refraction and the air mass traversed by the rays are in proportion, as was first shown by Laplace (Bemporad, 1908). For the current estimate the following formula can be used:

$$M = \frac{\omega'}{\beta}, \tag{103}$$

where ω' is expressed in minutes of arc. If, on Venus, we adopt a value for

β of 1/7 km^{-1}, with a refraction of $\omega' = 120'$, we shall obtain the air mass $M = 840$ km. With such a mass (which is almost treble the air mass during the sunset on the earth) the cusps of Venus should be deep red, in color which has never been observed either visually or photographically (Link, 1949).

The only solution is provided by the explanation of the extension of the cusps by means of the diffusion of light in a thin layer of dust or other layer (Russell, 1899). If the light penetrates through this layer along the path AB

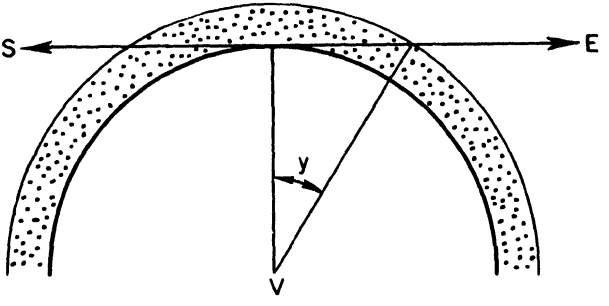

FIG. 51. Shift of the visibility limit and of the terminator by the thin diffusing layer.

(Fig. 51), the planetocentric angle $2y$ in the expression (100) stands for refraction ω. The angle y follows from

$$y = \sqrt{\frac{2h}{a}} \tag{104}$$

in which h denotes the height of the layer. With $q = 2.63°$ we shall find the height of the layer to be $h = 2.4$ km.

V

OCCULTATIONS OF STARS BY PLANETS

A. *Basic Equations*

Pannekoek (1903) was the first to draw attention to the usefulness of the occultations of stars by planets for the investigations of their atmospheres. The subject was taken up again, independently, by Fabry (1929). In principle, it means a simplification of our equations from the section on lunar eclipses to the case of a very thin atmosphere.

In the atmosphere in which the density of the air varies exponentially with the height in accordance with the equation

$$\rho = \rho_c \, e^{-\beta(h-h_c)} \tag{105a}$$

the refraction will be found from the formula

$$\omega = c\rho \sqrt{2\pi a\beta} \tag{105b}$$

and its variation with the height should be given by

$$\frac{d\omega}{dh} = -\beta c \,, \tag{106}$$

the surface h_c being represented by any surface in the atmosphere, e.g., the surface of the cloud layer (Venus) or the surface of the planet (Mars).

The air mass is denoted by the expression

$$M = \rho \sqrt{\frac{2\pi a}{\beta}} = \frac{\omega}{c\beta} \,, \tag{107}$$

and the attenuation by refraction can be expressed by the second member of Eq. (31), where we substitute the distance of the planet from the earth, l, in accordance with the equation

$$(\pi_{\mathbb{C}}) = r_p = \frac{a}{l} \tag{108}$$

and set $\pi_{\odot} = 0$, thus obtaining

$$\phi = 1 + \beta l \omega \,. \tag{109}$$

The actual angular distance will be found by

$$r = r_p \left(1 + \frac{h}{a}\right) - \omega \tag{110}$$

which can also be deduced from the ephemeris modified by the correction of the ephemeris time.

The apparent angular distance (i.e., the angular distance modified by refraction) will be

$$\psi = r_p \left(1 + \frac{h}{a}\right) . \tag{111}$$

B. *Course of the Occultation*

When observing the course of the occultation we shall consider first the time t when the attenuation by refraction attains the value 1/2, i.e., when $\phi = 2$. In accordance with Eq. (109), the following expression applies

$$\omega^* = \frac{1}{\beta l} . \tag{112}$$

As $\beta = 1/H$, however, where H is the scale height of the atmosphere, ω^* is at the same time the angular value of H visible from the earth. At that moment the minimum height of the ray is h^* and the corresponding angular radius of the planet is r_p^*. At another moment the following expressions will apply.

$$\begin{aligned} \omega &= \omega^* e^{-\beta(h-h^*)} \\ \phi &= 1 + e^{-\beta(h-h^*)} \end{aligned} \tag{113}$$

If we introduce the function

$$F(\phi) = \log_n (\phi - 1) + (\phi + 1) , \tag{114}$$

the actual and the apparent angular distance can be expressed in the following way

$$\begin{aligned} r &= r_p^* - \omega^* F(\phi) - \frac{\omega^* h^*}{a} \log (\phi - 1) \\ \psi &= r_p^* - \omega^* \log_n (\phi - 1) - \frac{\omega^* h^*}{a} \log (\phi - 1) \end{aligned} \tag{115}$$

where the last members can be neglected.

The attenuation by refraction alone will determine the brightness of the occulted star, the atenuation by extinction being negligible for any values of ϕ. The air mass for h^* is found from the expression

$$M^* = \frac{1}{\beta^2 l c} \tag{116}$$

which for the current distances l of the planets from the earth is negligible. In other words, the occulted star attenuated by refraction will disappear before extinction can influence it. This is why the occultations of stars are of no avail for the spectral analysis of planetary atmospheres, since then rays penetrate only the most tenuous parts of the atmosphere.

The course of the occultation $e = 1/\phi$ can be described by means of the dependence of the brightness of the star on the actual angular distance r, which

in the case of central occultation varies proportionally to the time. The apparent (i.e., observable) angular distance ψ will at the beginning when ϕ is slightly larger than 1, practically equal r. Later on, its decline will be slowed down due to the first member r in Eq. (115) being on the decline and the second member ω simultaneously rising. The star will ultimately reach the limb of the planet in the course of its relative motion, but its brightness will speedily decline so as to make it disappear first (Fig. 52).

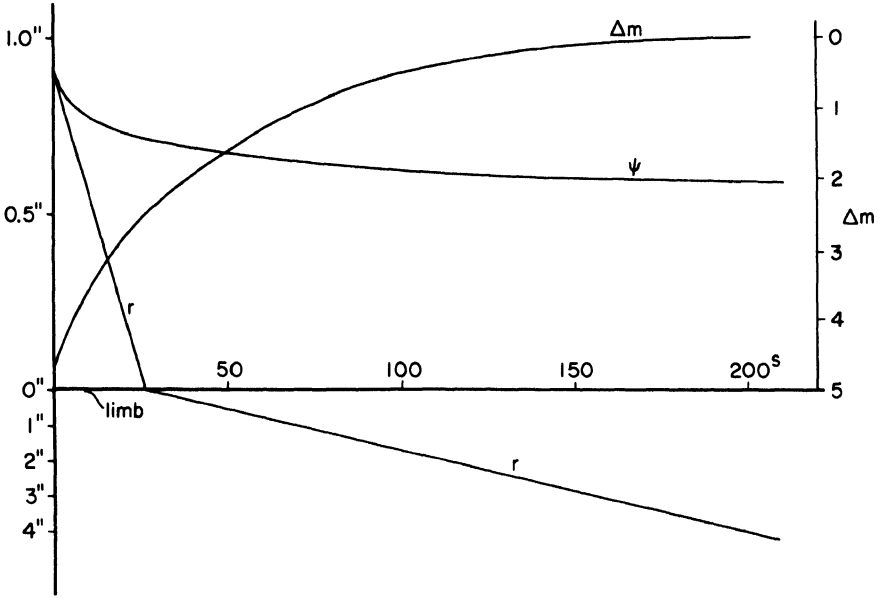

FIG. 52. Central occultation of a star by Mars with $H = 22$ km and $\dot{r} = 0.025''$/sec. Δm is the fall of brightness in magnitudes.

In what follows two different cases may theoretically occur, depending on the value of the refraction ω_c on the surface of the cloud layer or on that of the planet, i.e., whether

$$\omega_c \lessgtr r_p \left(1 + \frac{h_c}{a}\right). \tag{117}$$

In the first case the star actually disappears behind the limb of the planet. In the second case, it will remain visible throughout the occultation and its image would appear deformed as in the case of the image of the sun during the eclipses of the moon (Section II, E). In practice, of course, these phenomena will not be observable in the actual case.

Between the area of the light curve $e = f(r)$ and the height h of the rays a simple relation can be established. From the equation (110) we shall obtain by means of differentiation

$$\frac{dr}{dh} = \frac{r_p}{a} - \frac{d\omega}{dh} \tag{118}$$

and the equation (113) can be written in the form

$$\phi = 1 - l\frac{d\omega}{dh}. \tag{119}$$

By eliminating $d\omega/dh$ between these equations we obtain

$$\int_{r_1}^{r_2} e\, dr = \frac{h_2 - h_1}{l}. \tag{120}$$

In other words, the area of the light curve between the two distances r_1 and r_2 is proportional to the difference of the corresponding heights of the ray $h_2 - h_1$.

C. *Occultation of Regulus by Venus, July 7, 1959*

The light changes accompanying this occultation were measured photoelectrically by Vaucouleurs (1961). The observations were part of a major program organized by Menzel and Vaucouleurs (1961) for the purpose of a studying this rare phenomenon. The light curve is represented in Fig. 53 by single observation points on the one hand, and the theoretical curve on the other.

The actual distance r given by Eq. (115) can be expressed in its dependence on time, the equation providing also the form of the theoretical curve provided that we take as basis the given value ω^* or the value of the scale height H. The curve in Fig. 53 has been computed from the value $H = 6.8$ km. On the basis of the definition of the scale height

$$H = \frac{kt}{mg} \tag{121}$$

and assuming that the composition of the atmosphere is 90% CO_2, 9% N_2, 1% Ar and other gases, the derived mid value will be $m = 42.5$ and the temperature $t = 297°K$ for the height h.

Actually the measurements exhibit systematic deviations which can be attributed to a variation of H with the height represented by

$$\frac{dH}{dh} = H(0.010 \pm 0.002\ \text{km}^{-1}). \tag{122}$$

The variation of H with the height can be explained in two ways: it may be attributed to the temperature rising with the height $dt/dh = +3°/\text{km}$, m being constant, or (with t constant) to the diminution of the molecular weight m

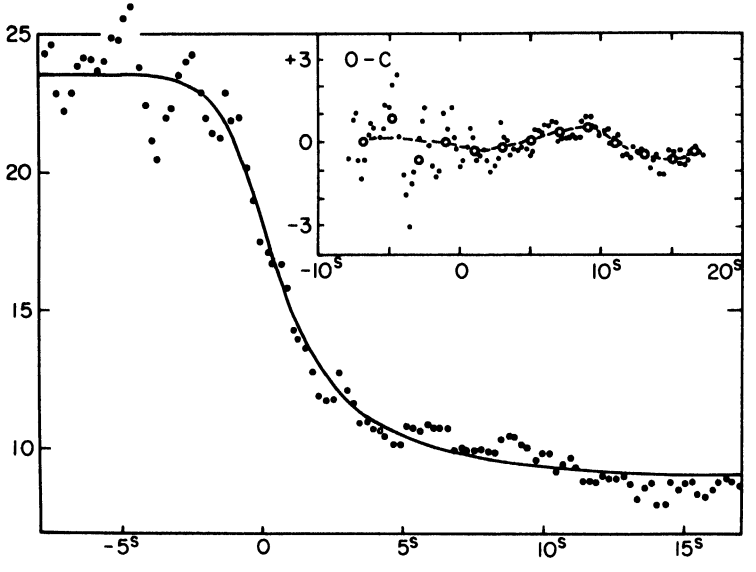

FIG. 53. Light curve of Regulus during the occulation by Venus on July 7, 1959. Points—individual measurements; curve according to the theory with $H = 6.8$ km. Inset—differences O-C.

due to the dissociation $CO_2 \rightarrow CO + O$ from the value 40–44 to the value 28–32, both variations being within the range of the 40 km height.

Additional details will be found in the papers quoted above.

D. *Influence of the Diffraction of Light*

The influence of the diffraction of light according to Fabry (1929) can be evaluated from the following consideration based on the theory of Fresnel's bands. If we introduce the length

$$x = \sqrt{\frac{l\lambda}{2}} \tag{123}$$

in the plane of the observer (II) a transition from full light to utter darkness will occur on the path whose length corresponds at the most to 5 to 6 times the

length x perpendicular to the edge of the shadow. In angular measure it will correspond to the change of the position of the planet by the angle

$$\xi < \frac{6x}{l} = 6\sqrt{\frac{\lambda}{2l}} \tag{124}$$

For instance, in the case of the occultation of Regulus by Venus as described in the last section, we have $2'' \times 10^{-3}$, i.e., the duration of the phenomenon is under 1/10 sec. With other planets too the influence of diffraction is quite negligible.

VI

ECLIPSE PHENOMENA IN RADIO ASTRONOMY

A. *General Remarks*

The radio waves can also be deflected, absorbed, or diffused in planetary atmospheres, so long as the latter are distinctly ionized. The index of refraction of such a medium, i.e., of the mixture of neutral atoms and molecules and electrically charged ions and electrons, is given by the expression

$$\mu_e^2 = 1 - \frac{Ne^2}{\pi m f^2}, \tag{125}$$

in which N is the number of electric particles per cm^3; m is their mass; e is their charge; and f is the frequency of oscillation. Of all the electrically charged particles the electrons alone will be relevant, their mass being small; and the number N will denote their concentration.

It may be of interest to point out the difference in sensitivity of the optical and the electronic refraction as it depends on the density of the medium. With the density of the air being 10^{-6} of the normal density, when the ionization of gases can take place, from the optical point of view the index of refraction will be

$$\mu_o = 1 - c\rho \tag{126}$$

which is practically equal to 1.

If we suppose that in this medium, which contains 10^{13} molecules per cm^3, only every hundred-thousandth molecule will be ionized (i.e., $N = 10^8$ electrons/cm^3) the index of refraction for the frequency $f = 100$ Mc will be

$$\mu_e = 0.45$$

i.e., clearly distinct from unity. Of course far smaller electron concentrations N are needed for a distinct electron refraction. This comparison shows the great sensitivity of the electron refraction as compared with the optical refraction.

The electron refraction is, of course, of opposite sign to that of the optical refraction, as it follows from the value $n < 1$ for the former refraction.

Below, we shall show some of the applications of radio waves to the investigation of the atmospheres during the eclipse phenomena. The following cases may be considered:

(a) Occultations of radio sources by the moon or the planets.

(b) Occultations of radio sources by the sun.

(c) Occultations of artificial satellites.

The basic theory of these phenomena is similar to that of the optical phenomena. The actual expression for the index of deflection as well as the sign of the sense of the refraction and the structure of the atmosphere (ionosphere) will vary.

B. *Occultations of Radio Sources by the Moon*

Various experiments aiming at an optical detection of the lunar atmosphere have so far led to no positive results. Lyot and Dollfus (1949) measured with a coronograph the brightness of the sky in the surroundings of the cusps of the moon in the first quarter. They found only the upper limit of the density 10^{-8} of the density of the terrestrial atmosphere at the sea level. Dollfus (1952) increased the precision of the method by measuring the polarization, and reduced the upper limit to 10^{-9}.

Radio methods are far more sensitive, taking advantage as they do of the eclipse of the sun or of the occultations of radio sources (Link, 1952a). When in the years 1955–57 a large number of occultations of the bright radio sources by the moon was due to take place (Link and Neužil, 1954), a theory of these phenomena was elaborated (Link, 1956b) which was later used by Elsmore (1957) for the interpretation of his measurements.

On the moon both basic conditions for the existence of the ionosphere can be fulfilled: namely, the presence of the diluted rarefied atmosphere and the ionization radiation. If, on the lunar surface, the density of the atmosphere was 10^{-9} of the density of the terrestrial atmosphere, it would correspond to the conditions in the terrestrial ionosphere at the altitude of about 200 km, where the electron concentration is between $N = 10^5$ and 10^6 electrons cm^{-3}. There are, accordingly, no reasons why the existence of a lunar ionosphere of similar properties should not be anticipated.

Let us depart from the model of the lunar ionosphere according to Chapman's theory (Ratcliffe and Weekes, 1960). For the electron concentration we have here

$$N = N_{\max} \exp \tfrac{1}{2}\left[1 - \frac{h - h_{\max}}{H} - \exp\left(-\frac{h - h_{\max}}{H}\right)\right], \tag{127}$$

where H is the scale height of the atmosphere. We shall assume that the ionization maximum $N_{\max}$ is not reached yet even on the surface of the moon, which implies that only the part of the curve high above the maximum of ionization can be taken into consideration. The following formula applies approximately:

$$N = N^* \exp\left(-\frac{h}{2H}\right), \tag{128}$$

where N^* is the electron concentration on the lunar surface. For the index of refraction we have, furthermore,

$$\mu^2 = 1 - 8.06 \cdot 10^{-5} f^{-2} N\,; \tag{129}$$

or, for the values μ close to 1

$$1 - \mu = 4.03\ 10^{-5} f^{-2} N. \tag{130}$$

Now for the computation of the refraction we can make use of the formula for the optical occultation of the stars (87), which leads to the expression

$$\omega = 4.03 \cdot 10^{-5} \frac{N_0}{f^2} \sqrt{\pi \frac{a_{\mathbb{C}}}{H}} = \omega^* \exp\left(-\frac{h}{2H}\right), \tag{131}$$

where N_0 is the electron concentration at the top of the trajectory and ω^* is the refraction on the surface of the moon.

Apart from the refraction we can also consider the modification of the illumination due to the influence of refraction. By modifying the general formula (11) for the opposite sign of the refraction we obtain

$$\phi = 1 - a_{\mathbb{C}} \frac{\omega}{R_{\mathbb{C}}} \left(\frac{1}{2H} - \frac{1}{a_{\mathbb{C}} + h_0}\right) - \frac{a_{\mathbb{C}}^2}{2H(a_{\mathbb{C}} + h_0)} \left(\frac{\omega}{R_{\mathbb{C}}}\right)^2, \tag{132}$$

where the second member is always negative as

$$\frac{1}{2H} > \frac{1}{a_{\mathbb{C}} + h}, \tag{133}$$

from which it follows that $\phi < 1$, and that an amplification due to refraction

always takes place. This amplification increases with the increasing refraction and approaches infinity when the critical value of refraction is

$$\omega_{cr} = 2R_{\mathbb{C}} \frac{H}{a_{\mathbb{C}}} \tag{134}$$

and the focusing of the infinitely narrow pencil takes place.

Between the actual (r) and the apparent angular distance (r') similar relations apply as with (33) and (38)

$$\begin{aligned} r &= r' + \omega \\ r' &= R_{\mathbb{C}} \frac{a_{\mathbb{C}} + h_0}{a_{\mathbb{C}}} . \end{aligned} \tag{135}$$

The beginning or the end of the occultation will take place when $h_0 = 0$, i.e., when the actual distance attains the value

$$r = R_{\mathbb{C}} + \omega_0 . \tag{136}$$

In other words, by the presence of the ionosphere the duration of the radio occultation is prolonged.

C. *A Numerical Example*

In Table XIX we find the results of the computations of the refraction and of the amplification of light caused by the refraction in the range of values H and N, which come into consideration in lunar atmosphere, and also for some frequencies used in radio astronomy.

In the terrestrial ionosphere at the altitude of 400 km the scale height equals about $H = 80$ km. On the moon, where the gravitational acceleration is $\frac{1}{6}$ of the value on the earth, the above value would ceteris paribus be about $H = 480$ km, which represents, of course, the upper limit; for on the moon we should expect to find gases heavier than on the earth. It is more reasonable, therefore, to consider the second part of our table.

In Fig. 54 the course of the radio occultation for a defined concrete case is illustrated. With the average motion of the moon of $1''$ in 2^s, and for a central occultation, the occultation would begin $4\frac{1}{2}^m$ before the geometric beginning and end the same time after the geometric end of the occultation. The duration of the occultation would thus be extended by as much as 9^m, which should indeed be easily measurable. A similar consideration will lead to the conclusion that with the complete duration of the occultation determined exactly to $\frac{1}{2}^m$ the refraction on the surface may be determined to about $0.1'$, which with

the frequency employed of 50 MHz* would, moreover, an electron concentration of $N \geqq 10^3$ electrons cm^{-3}. The photometric effect of the lunar ionosphere would, under these conditions, be negligible, the distance of the moon from the earth being too small.

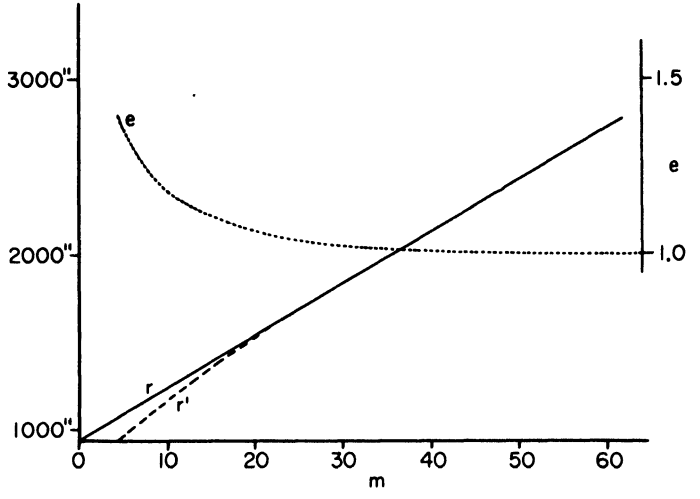

FIG. 54. Occultation of a radio source by the moon independent of the time. Lunar ionosphere: $N^* = 10^4$ electrons cm^{-3}, $H = 341$ km, $\omega^* = 137''$, $f = 50$ MHz.

In the past few years the occultations of the radio sources IC 443 of Gemini and of the Crab nebula (Elsmore, 1957, 1959) where measured in Cambridge. During the latest occultation of the Crab nebula on January 24, 1956 (Costain *et al.*, 1956) the observed duration of the occultation $59{,}6^m \pm 0.26$ was longer than the computed duration by 0.4^m. This difference leads to a refraction of $13.4'' \pm 8.7''$, if we expect ionization only on the illuminated limb of the moon. With a scale height of about 50 km it requires an electron density of 10^3 electrons cm^{-3}. If we admit, furthermore, that every thousandth molecule of the air on the moon is ionized, we obtain for the maximum density of the lunar atmosphere 2×10^{-13} of the terrestrial atmosphere (Elsmore, 1959). This implies that the radioastronomical method is over a thousand times more sensitive than the most sensitive optical method (Dollfus, 1952).

When the next favorable period 1963–64 of the occultations of the bright sources by the moon takes place, it will be essential to repeat these measurements, especially at lower frequencies $f = 38$ MHz, for the refraction is indirectly proportional to the second power of the frequency.

* MHz: a unit of frequency equivalent to Mc.

TABLE XIX

REFRACTION AND LIGHT AMPLIFICATION IN THE LUNAR IONOSPHERE

	N* (electrons/cm³)	10^5	10^4	10^3	10^2	10^1 el cm^{-3}
H = 1365 km	f = 25 MHz		4.6′	27″	2.7″	0.3″
			0.95	0.99	1.00	1.00
ω_{cr} = 24.4′	50 MHz	11.4′	1.1′	6.9″	0.7″	0.1″
		1.08	0.97	1.00	1.00	1.00
	100 MHz	2.9′	17″	1.7″	0.2″	0.0″
		0.96	0.99	1.00	1.00	1.00
	200 MHz	23″	2.3″	0.2″	0.0″	0.0″
		0.99	1.00	1.00	1.00	1.00
	400 MHz	11″	1.1″	0.1″	0.0″	0.0″
		1.00	1.00	1.00	1.00	1.00
H = 341 km	f = 25 MHz		9.1′	55″	5.5′	0.6″
			1.02	1.17	1.00	1.00
ω_{cr} = 6.1′	50 MHz		2.3′	14″	1.4″	0.1″
			1.39	1.02	1.00	1.00
	100 MHz	5.7′	34″	3.4″	0.3″	0.0″
		11.6	1.10	1.01	1.00	1.00
	200 MHz	1.4′	8.6″	0.9″	0.1″	0.0″
		1.17	1.01	1.00	1.00	1.00
	400 MHz	21″	2.1″	0.2″	0.0″	0.0″
		1.04	1.00	1.00	1.00	1.00
H = 152 km	f = 25 MHz			1.4′	8.2″	0.8″
				1.86	1.04	1.00
ω_{cr} = 2.7′	50 MHz		3.4′	21″	2.1″	0.2″
			3.1	1.12	1.01	1.00
	100 MHz	8.6′	51″	5.1″	0.5″	0.1″
		0.56	1.27	1.03	1.00	1.00
	200 MHz	1.8′	10.8″	1.1″	0.1″	0.0″
		2.7	1.05	1.00	1.00	1.00
	400 MHz	32″	3.2″	0.3″	0.0″	0.0″
		1.15	1.00	1.00	1.00	1.00

D. *Occultations of Radio Sources by the Solar Corona*

The solar corona radiates in the optical range mainly by the sunlight scattered on the free electrons. From the decline in brightness with the distance the structure of the corona may be derived, i.e., the function indicating the diminution in electron density with the distance. In conformity with Van de Hulst (1950) we shall set forth the following characteristic cases:

$$N = 1.74 \times 10^7 \left(\frac{t_\odot + h}{a_\odot}\right)^{-6}$$ polar region during the minimum

$$N = 3.10 \times 10^7 \left(\frac{a_\odot + h}{a_\odot}\right)^{-4} \text{ equatorial region during the maximum}$$

$$N = 1.55 \times 10^8 \left(\frac{a_\odot + h}{a_\odot}\right)^{-6} \text{ middle regions (Allen, 1947).} \tag{137}$$

Machin and Smith (1951) proposed the use of the occultations of radio sources by the corona for the determination of the electron density of the corona, and the mathematical theory of these phenomena was established by Link (1952b). This theory is, so to speak, a transfer of our general relations to the electron refraction.

We shall take as out starting point the general formula for the structure of the corona in the shape of

$$N = \alpha \left(\frac{a_\odot + h}{a_\odot}\right)^{-n}. \tag{138}$$

The index of refraction is accordingly given by the expression

$$\mu^2 = 1 - 8.06 \times 10^{-5} f^{-2} N \tag{139}$$

where f is the frequency in MHz, or also by

$$\mu^2 = 1 - 8.06 \times 10^{-5} f^{-2} \alpha \left(\frac{a_\odot + h}{a_\odot}\right)^{-n}, \tag{140}$$

Furthermore, the classical theory of refraction leads to the expression

$$\omega = B f^{-2} \alpha \left(\frac{a_\odot + h_0}{a_\odot}\right)^{-n}, \tag{141}$$

where h_0 denotes the altitude of the summit of the trajectory and the constant B depends on the exponent n in the formula (141) in conformity with Table XX.

TABLE XX

n	1	2	3	4	5	6
10^5 (rad)	8.06	12.66	16.12	18.99	21.49	23.74

During the occultation of the radio source at infinity by the solar corona two phenomena will occur: namely, the deviation of the rays, and the change in brightness (i.e., in the illumination in the terrestrial plane II). Between the

geometrical distance of the source r and the apparent distance r' modified by refraction an analogy with Eqs. (33) and (38) will apply:

$$r = r' + \omega, \qquad r' = R_\odot \frac{a_\odot + h_0}{a_\odot}; \tag{142}$$

and for the modification of brightness an analogy with Eq. (31), which in our case gives

$$\phi = 1 - (n-1)\frac{\omega}{R_\odot}\frac{a_\odot}{a + h_\odot} - n\left(\frac{\omega}{R_\odot}\frac{a_\odot}{(a + h_0)}\right)^2. \tag{143}$$

E. *Course of the Occultation*

Figure 55 illustrates the dependence of the geometrical and the apparent distance for the state of the corona given by the last formula (137). We can see

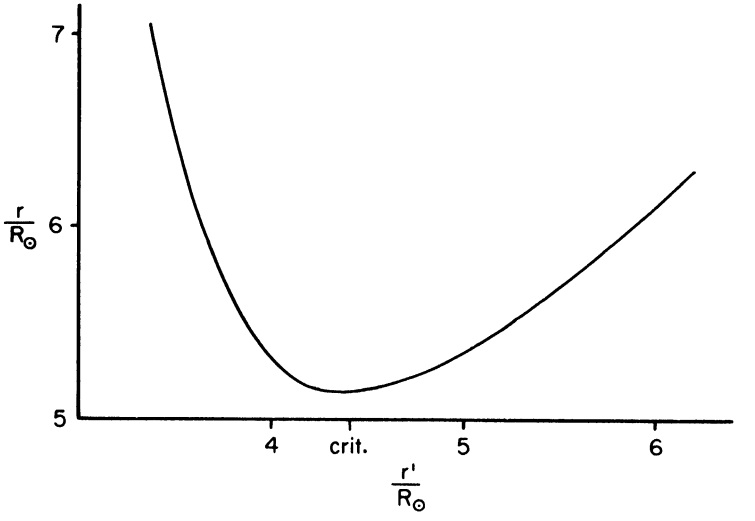

FIG. 55. Geometric and apparent distances during the eclipse by the solar corona.

that a certain point N of the terrestrial plane II is generally reached by two rays: one higher and the other lower than the critical distance r_{cr}, which can be deduced from the condition for the minimum r, i.e.,

$$\begin{aligned} \frac{dr}{dh_0} &= R_\odot - n\alpha B f^{-2}\left(\frac{a_\odot + h_0}{a_\odot}\right)^{-n-1} = 0 \\ \frac{d^2r}{dh_0^2} &= n(n+1)\alpha B f^{-2}\left(\frac{a_\odot + h_0}{a_\odot}\right)^{-n-2} > 0 \end{aligned} \tag{144}$$

which for the critical distance of the rays gives

$$\left(\frac{a_\odot + h_0}{a_\odot}\right)_{cr} = \left(\frac{\alpha B n}{R_\odot f^2}\right)^{1/(1+n)} \tag{145}$$

for the critical refraction

$$\omega_{cr} = \alpha B f^{-2} \left(\frac{\alpha B n}{R_\odot f^2}\right)^{-n/(1+n)} \tag{146}$$

and the critical geometric distance

$$r_{cr} = \frac{n+1}{n} R_\odot \left(\frac{\alpha B n}{R_\odot f^2}\right)^{1/(1+n)} \tag{147}$$

Both critical distances (145) and (147) define the instant when the radio source will disappear behing the "radio limb" of the sun, which is much farther than the photospheric limb, as is shown by Table XXI.

TABLE XXI

CRITICAL VALUES OF THE SOLAR CORONA

	38 MHz		81.5 MHz		210 MHz	
	ρ_{cr}[a]	r_{cr}[b]	ρ_{cr}	r_{cr}	ρ_{cr}	r_{cr}
Polar region minimum	3.23	3.77	2.60	3.03		
Equatorial region maximum	3.19	3.99	2.57	3.21		
Middle conditions	4.42	5.15	3.54	4.13	2.70	3.15

[a] $\rho_{cr} = [(a_\odot + h_0)/a_\odot]_{cr}$.
[b] r_{cr} in solar radii.

The deviation of the rays is accompanied by a change in the brightness of the source, i.e., the amplification, as $\phi < 1$. For the distant rays $\phi \approx 1$ and only a very slight amplification takes place. As soon as r approaches the critical distance, r_{cr} quickly falls to zero, i.e., the brightness of the source approaches infinity. With a very narrow pencil of rays close on r_{cr} the actual focusing of the rays takes place. With rays lower than r_{cr} the brightness of the source declines again (Fig. 56) to be followed by even an attenuation of brightness. The actual illumination at the position of the observer is, of course, a sum of the illuminations originating from two rays $r_1 \geqslant r_{cr}$ and $r_2 < r_{cr}$.

In Fig. 56 the progress of the brightness of the source in its dependence on

$r'/R_\odot$ is represented. The reciprocally corresponding rays 1 and 2 are linked by segments. A similar curve of progress would also mark, of course, the total intensity of the covered radio source.

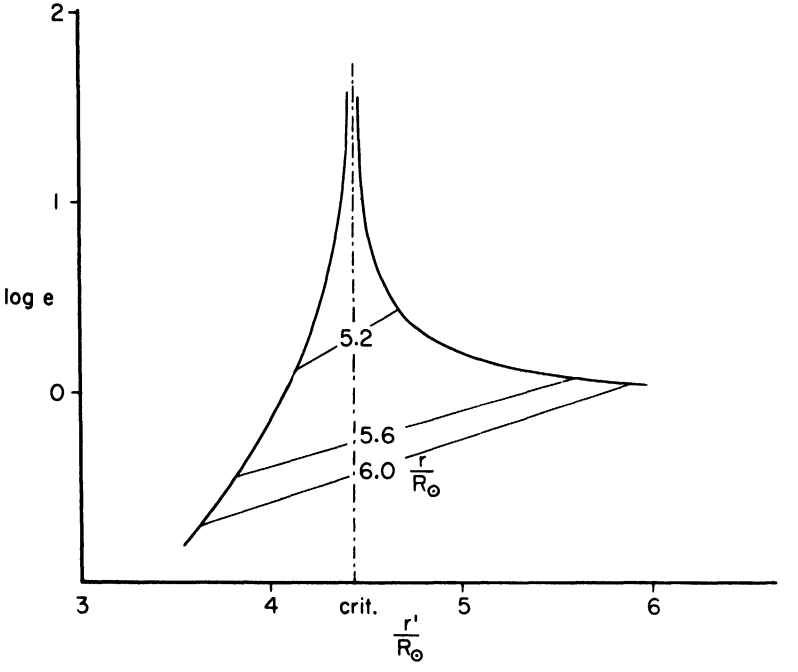

FIG. 56. Illumination by a point source during the radio eclipse by the solar corona.

F. *Results of Observations*

Every year, by the middle of June, a close approach of Crab nebula to the sun at a minimum distance of 4.6 $R_\odot$ will take place. Under these circumstances illustrated in Table XXI a certain increase in intensity might take place, as in fact for a frequency of 38 MHz, the minimum distance 4.6 $R_\odot$ is near the critical distance r_{cr} or is even smaller in accordance with the adopted structure of the corona (Table XXI).

As a matter of fact the first successful observations (Machin and Smith, 1952) showed a decline in brightness beginning at a distance of 15 $R_\odot$ and most of the later observations effected in the years 1953-1958 confirmed the decline (Hewish, 1959). Only the observations of Blum and Boischot (1959) in the years 1957 and 1958 showed an increase in brightness of about 60%. The decline in brightness was, according to Hewish (1955), due to a scattering

mechanism arising from the presence of irregular variations of electron density in the corona. He suggested that the irregular structure represented an extension of the visible coronal rays.

Refraction cannot explain these phenomena, partly because of the opposite influence on the intensity of the source (i.e., an attenuation instead of an amplification) and partly because no dependence on frequency, which as a rule conspicuously accompanies refraction, has been observed. The amplification observed by Blum and Boischot would lead to a relatively considerable refraction of 12′ at the distance of 7 $R_{\odot}$, all this depending on the limit of the accuracy of their findings. These authors further ascertained a threefold increase of the apparent diameter, which with refraction would lead to a much greater amplification of the intensity of the source. It is not impossible that two phenomena of refraction and diffusion should have combined here. A more detailed study of the problem is, however, beyond the scope of the present chapter.

References

Abbot, C. G. (1922). *Ann. ap. Obs. Smithson Instn.* **4**, 220.
Allen, C. W. (1947). *M. N. R. A. S.* **107**, 426.
Arend, S. (1942). *Ciel et Terre* **58**, No. 11-12.
Barbier, D., and Chalonge, D. (1942). *Ann. Ap.* **9**, 227.
Bauer, E., and Danjon, A. (1923). *C. R. Acad. Sci., Paris* **176**, 761.
Bemporad, A. (1908). *Enc. Math. Wissensch.* **VI.2**, No. 2, 329.
Bigg, E. K. (1957). *J. Met.* **14**, 524.
Bigg-Wither, A. C. (1883). *Mem. R. A. S.* **47**, 97.
Blum, E. J., and Boischot, A. (1959). *I. A. U. Symp.* (*Radio Astr.*), *Paris*, p. 282.
Bouška, J. (1948). *B. A. C.* **1**, 37.
Bouška, J. (1949). *B. A. C.* **1**, 75.
Bouška, J. (1950). *B. A. C.* **2**, 28.
Bouška, J. (1956). *B. A. C.* **7**, 85.
Bouška, J. (1958). *B. A. C.* **9**, 245.
Bouška, J. (1960). *B. A. C.* **11**, 145.
Bouška, J., and Link, F. (1947). *C. R. Acad. Sci., Paris* **224**, 1483.
Bouška, J., and Růžičková, B. (1953). *B. A. C.* **4**, 14.
Bouška, J., and Švestka, Z. (1950). *B. A. C.* **2**, 6.
Bowen, E. G. (1953). *Aust. J. Phys.* **6**, 490.
Bowen, E. G. (1956a). *J. Met.* **13**, 142.
Bowen, E. G. (1956b). *Tellus* **8**, 394.
Brossinsky, A. (1889). "Über die Vergrösserung des Erdschattens," Göttingen.
Brunner, H. (1935). *Publ. Sternw. Zürich* **6**, 81.
Cabannes, J. (1929). "Sur la diffusion moléculaire de la lumière," p. 167, Paris.
Cabannes, J., and Dufay, J. (1927). *J. Phys., Paris* **8**, 125.
Cassini, J. D. (1740). "Tables astronomiques," p. 34. Paris.
Cimino, M., and Fresa A. (1958). *R. C. Accad. Lincei* 25, 58.
Costain, C. H., Elsmore, B., and Whitfield, G. R. (1956). *M. N. R. A. S.* **116**, 380.

Danjon, A. (1920a). *C. R. Acad. Sci., Paris* **171**, 127.
Danjon, A. (1920b). *C. R. Acad. Sci., Paris* **171**, 1207.
Danjon, A. (1928). *Ann. Obs. Strasbourg* **2**, 1.
Dmitrijev, A. A., and Czili, A. B. (1958). *Trudy morskogo geof. Inst. Akad. Nauk S.S.R.S.* **12**, 181.
Dobson, G. M. B. (1929). *Gerl. Beitr. Geoph.* **24**, 8.
Dollfus, A. (1952). *C. R. Acad. Sci., Paris* **234**, 2046.
Donitsch, N. (1900). *A. N.* **151**, 3.
Dufour, Ch. (1899). *L'Astronomie* **13**, 115.
Elsmore, B. (1957).*I. A. U. Symp.* (*Radio Astr.*) No. 4.
Elsmore, B. (1959). *I. A. U. Symp. Paris* (*Radio Astr.*), No. 9, 47.
Eropkin, D. J. (1931). *Z. Ap.* **3**, 163.
Fabry, Ch. (1929). *J. d'Obs.* **12**, 1.
Fesenkov, V. (1932). *Bull. Acad. Sci. U.R.S.S.* No. 1.
Fesenkov, V. (1937). *A. Zh.* **14**, No. 5.
Flammarion, C. (1884). *L'Astronomie* **3**, 401.
Fisher, W. (1924). *Smithson. misc. Coll.* **76**, No. 9.
Frisch, Chr. (1858). *Joh. Kepleri opera omnia* **2**, 297.
Glenn, J. H. (1962). *Science* **136**, 1093.
Greenstein, J. L. (1937). *Harv. Circ.* No. 422.
Gregory, J. (1663). "Optica promota," London.
Guth, Vl., and Link, F. (1936). *J. d'Obs.* **19**, 1929.
Guth, Vl., and Link, F. (1939). *Z. Ap.* **18**, 207.
Guth, Vl., and Link, F. (1941). *Z. Ap.* **20**, 1.
Halley, E. (1691). *Phil. Trans.* p. 511.
Halley, E. (1716). *Phil. Trans.* p. 454.
Hansa, M., and Zacharov, I. (1958). *B. A. C.* **9**, 236.
Harris, D. L. (1961). *In* "Planets and Sattelites," Vol. III of "The Solar System" (G. Kuiper and B. M. Middlehurst, eds.). Univ. of Chicago Press, Chicago, Illinois.
Hartmann, J. (1891). *Abh. sachs. Ges. Wiss., Math.-Phys. Kl.* **17**, 365.
Hausdorff, F. (1895). *Ber. Verh. sachs. Akad. Wiss.* p. 401.
Hefferman, K. J., and Bracewell, R. N. (1959). *J. Met.* **16**, 337.
Hepperger, J. (1895). *Sitzber. Akad. Wiss. Wien, Math.-Phys. Kl.* **54** (II).
Hewish, A. (1955). *Proc. roy. Soc.* **A228**, 238.
Hewish, A. (1959). *I. A. U. Symp. Paris* (*Radio Astr.*), No. 9, 268.
Heyden, *et al.* (1954). *Ap. J.* **118**, 412.
Hibbs, A. R. (1961). *J. geoph. Res.* **66**, 371.
Koebcke, F. (1951). *Bull. Soc. Amis Sci. Poznan* **XI**(B).
Koebcke, F. (1954). *Bull. Soc. Amis Sci. Poznan* **XIII**, 385.
Kosik, S. M. (1940). *Bull. Tashkent astr. Obs.* **2**, 79.
Kosik, S. M. (1955). *Dokl. Akad. Nauk S.S.S.R.* **104**, 828.
Kühl, A. (1928). *Phys. Z.* **29**, 1.
Kuiper, G. (1954). *Ap. J.* **120**, 603.
Lahire, P. (1707). "Tabulae astronomicae," Paris.
Lalande, J. F. (1782). "Astronomie," Vol. 2, p. 337.
Lemonnier, P. C. (1746). "Institutions astronomiques," p. 251. Paris.
Letfus, V. (1953). *B. A. C.* **4**, 36.
Link, F. (1929). *Bull. Obs. Lyon* **11**, 229.
Link, F. (1933). *Bull. astr., Paris* **8**, 77.

Link, F. (1936). *Bull. astr., Paris* **9**, 227.
Link, F. (1943). *Gerl. Beitr. Geoph.* **60**, 139.
Link, F. (1946a). *C. R. Acad. Sci., Paris* **222**, 333.
Link, F. (1946b). *C. R. Acad. Sci., Paris* **223**, 976.
Link, F. (1946c). *B. A. C.* **1**, 13.
Link, F. (1946d). *Ann. d'Ap.* **9**, 227.
Link, F. (1948). *Ann. Geoph.* **4**, 211.
Link, F. (1949). *B. A. C.* **1**, 77.
Link, F. (1950a). *Bull. astr., Paris* **15**, 143.
Link, F. (1950b). *B. A. C.* **2**, 1.
Link, F. (1952a). *B. A. C.* **3**, 82.
Link, F. (1952b). *B. A. C.* **3**, 6.
Link, F. (1956a). *Publ. Obs. Prague* No. 29.
Link, F. (1956b). *B. A. C.* **7**, 1.
Link, F. (1957). *Mém. Soc. Sci. Liège* **18**, 148.
Link, F. (1958). *B. A. C.* **9**, 169.
Link, F. (1959). *B. A. C.* **10**, 105.
Link, F. (1960). *B. A. C.* **11**, 13.
Link, F. (1961). *Stud. Geoph. Geodet.* **5**, 64.
Link, F. (1962a). *B. A. C.* **13**, 1.
Link, F. (1962b). *Space Research* **3**, in press.
Link, F. (1963). *Stud. Geoph. Geodet* **7**, in press.
Link, F., and Linková, Z. (1954a). *Publ. Obs. Prague* No. **25**.
Link, F., and Linková, Z. (1954b). *B. A. C.* **5**, 82.
Link, F., and Neužil, L. (1953). *B. A. C.* **4**, 85.
Link, F., and Neužil, L. (1954). *B. A. C.* **5**, 112.
Lyot, B., and Dollfus, A. (1949). *C. R. Acad. Sci. Paris* **229**, 1277.
Machin, K. E., and Smith, F. G. (1951). *Nature* **168**, 599.
Machin, K. E., and Smith, F. G., (1952). *Nature* **170**, 319.
Maedler, J. H. (1838). *A. N.* **15**, 1.
Maedler, J. H. (1849). *A. N.* **29**, 107.
Malsch, W. (1923). *A. N.* **218**, 19.
Maunder, E. W. (1921). *J. Brit. astr. Ass.* **31**, 346.
Menzel, D., and Vaucouleurs, G. de (1961). Air Force Cambridge Research Lab. Report **227**, Cambridge, Massachusetts.
Müller, G. (1883). *Publ. astroph. Obs. Potsdam* **13**, 285.
Müller, G. (1897). "Photometrie der Gestirne," Leipzig.
Neužil, L. (1961). *Stud. Geoph. Geodet.* **5**, 252.
Oppolzer, Th. V. (1887). *Denkschr. Akad. Wiss. Wien, Math.-Phys. Kl.* **52**.
Paetzold, H. K. (1950). *Z. Naturforsch.* **5a**, 661.
Paetzold, H. K. (1951). *Z. Naturforsch.* **6a**, 339.
Paetzold, H. K. (1952). *Z. Naturforsch.* **7a**, 325.
Paetzold, H. K. (1953). *Z. Ap.* **32**, 303.
Pannekoek, A. (1903). *A. N.* **164**, No. 3913.
Pickering, E. C. (1900). *Harv. Ann.* **52**(2).
Proctor, R. A., and Raynard, A. G. (1892). "Old and New Astronomy," p. 503-509. London.
Rabe, W. (1913). *A. N.* **196**, 405.
Rabe, W. (1948). *A. N.* **276**, 111.

Ratcliffe, J. A., and Weekes, K. (1960). *In* "Physics of the Upper Atmosphere" (J. A. Ratcliffe, ed.), p. 387. Academic Press, New York.
Regener, E., and Regener, V. H. (1934). *Phys. Z.* **35**, 788.
Rocket Panel (1952). *Phys. Rev.* **88**, 1027.
Rougier, G., and Dubois, J. (1944). *Ciel et Terre* **60**, No. 5.
Russell, H. N. (1899). *Ap. J.* **9**, 284.
Sampson, R. A. (1910). Tables of Four Great Satellites of Jupiter." London.
Saussure, M. de (1931). *Verh. naturforsch. Ges. Basel* **42**.
Schoenberg, E. (1929). *Handb. Ap.* **2**/1, 255.
Schoenberg, E. (1949). *A. N.* **277**, 123.
Seeliger, H. (1896). *Abh. bayr. Akad. Wiss., II. Kl.* **19** (2).
Sharonov, V. V. (1952). *Dokl. Akad. Nauk S. S. S. R.* **82**, 351.
Suchomlinov (1902). *M. V. Lomonosov Works* **5**, 113.
Symons, G. L. (1888). "Report on Krakatoa Committee." London.
Švestka, Z. (1948). *B. A. C.* **1**, 48.
Švestka, Z. (1950). *B. A. C.* **2**, 41.
Van de Hulst, H. C. (1950). *B. A. N.* **11**, 135, 150.
Vassy, E. (1956). *La Mét.* **8**, 1.
Vaucouleurs, G. de (1944). *C. R. Acad. Sci., Paris* **218**, 655, 805.
Vaucouleurs, G. de (1961). *Ann. Obs. Houga* **III**.
Venkateswaran, S. V. Moore, J. G., and Krueger, A. J. (1961). *J. geophys. Res.* **66**, 1751.
Vigroux, E. (1954). *Ann. d'Ap.* **17**, 399.
Walker, M. F., and Reaves, G. (1957). *P. A. S. P.* **69**, 153.
Whipple, F. L. (1961). *Nature* **189**, 127.
Wirtz, C. W. (1906). *A. N.* **171**, 97.
Wirtz, C. W. (1917). *A. N.* **205**, 135.
Wolf, R. (1877). "Geschichte der Astronomie." München.
Zacharov, I. (1952). *B. A. C.* **3**, 82.
Zacharov, I. (1961). Thesis, Prague.

White Dwarfs

W. J. LUYTEN
University of Minnesota, Minneapolis, Minnesota

I. Introduction 199
II. Historical 200
III. Discovery 201
IV. Magnitudes, Colors, Spectra 203
V. Spectra 206
VI. Motions 208
VII. Luminosities 209
VIII. Masses 210
IX. Red Shift 213
X. Frequency in Space 214
XI. White Dwarfs in Clusters 215
XII. Individually Interesting Stars 216
XIII. Conclusions and Suggestions for Future Work 217
References 217

I

INTRODUCTION

White Dwarfs are among the most remarkable of known stars. With their planetlike diameters and sunlike masses, their densities are of the order of 10,000 or more. As such they represent a state of matter totally unknown and possibly wholly unapproachable on earth.

White Dwarfs are relatively easy to discover but, because of their faintness, they are among the most difficult objects to observe. They are now generally believed to represent one of the last stages of stellar evolution—if not for all stars then at least for a considerable fraction. This stage, in the course of which the white dwarfs change their physical features extremely slowly, in all probability immediately precedes their ultimate extinction as self-luminous objects.

Because of their unusual features, white dwarfs have formed the subject of an enormous amount of theoretical research, romantic speculation, and hopeful divination, but observationally speaking these stars have been badly neglected. Consequently, many of the fundamental astrophysical data about them are known only poorly, if at all.

II

HISTORICAL

The story of the discovery of the first two white dwarfs has been told so often that a very brief sketch will suffice here.

Since the beginning of the nineteenth century it was known that Sirius, the brightest star in the sky, did not move along an arc of a great circle but followed an oscillating curve. This implied acceleration and hence a force; to the astronomer the obvious force is that of gravitation and so it was concluded that Sirius was revolving around the common center of mass with an unseen companion. In 1862 the companion was discovered by Alvan Clark, and by 1910 the orbit of the binary became well determined; a period of over 50 years and a mean separation of 19 astronomical units, masses of 2.5 and 0.96 were derived for Sirius and its companion. Measures of the brightness and of the parallax and distance indicated that the luminosities of the two components in terms of that of the sun are 25 and 1/400, respectively. Taken by themselves these data are not unusual but when in 1915 Adams found the spectral class of the companion to be *F*, indicating a surface temperature of over 8000°K, a glaring discrepancy appeared. Assuming that stars radiate roughly as black bodies, we calculate from this that its surface brightness is three times that of the sun; hence its total surface must be 1200 times smaller, indicating a radius of 1/35 of that of the sun—about equal to that of Uranus—and a volume 1/40,000 of that of the sun. With a mass of 0.96 this leads to a mean density of 5×10^4 cgs.

At about the same time Mrs. Fleming at Harvard determined the spectral class of o_2 Eridani B and found it to be A0, indicating a surface temperature of 10000°K. But this star being a component of a binary was known to have a mass of 0.44 and a luminosity 1/400 of that of the sun, again indicating a density of the order of 5×10^4 cgs.

Almost immediately Eddington provided the explanation: at the high temperatures which must prevail throughout the interior of these stars, virtually all atoms are completely ionized; hence under the concomitant terrific pressures it should be possible to reach densities of 10^6 cgs and higher. Following Eddington, Fowler and Chandrasekhar developed the fundamental theory of the structure and behavior of matter under these extreme conditions. Since the present summary deals mainly with the observational aspects of white dwarfs, let it suffice here to state that in these stars matter no longer follows the classical gas laws, that relativistic troubles occur arising from the excessively high speeds of the electrons and that a "gas" under these conditions is generally described as degenerate.

Owing to their small size, low luminosity, and generally high surface tempe-

rature the name White Dwarf was suggested for these stars. Although we now know many similar stars with temperatures equal to and even lower than that of the sun, this appellation has been generally retained, although perhaps the term Degenerate Stars would be more appropriate.

III

DISCOVERY

Shortly after the discovery of the first two white dwarfs a third was found by Van Maanen, Wolf, and Seares. Although not a component of a binary, but a single star, this faint object of apparent magnitude $12^{m}.5$, with the very large proper motion of 3″ annually—indicating a very low luminosity—and a surface temperature almost equal to that of the sun, must obviously belong to the same category as the companion to Sirius. The manner of its discovery set the pattern for future searches; since white dwarfs are objects of low luminosity and relatively high surface temperature, we must look for stars that are near, appear faint, and are relatively white. The dispersion in stellar velocities being much smaller than that in distance, stars that are near reveal themselves most easily by their large angular motion across the sky.

In 1922 the present writer began observing spectra for a number of faint stars with large proper motion, but out of one hundred stars observed only one proved to be a white dwarf and it became clearly indicated: (a) that the majority of white dwarfs were too faint for the then existing spectroscopic equipment, and (b) that more faint stars with large motions needed to be found first. The latter helped to decide the writer to undertake the Bruce Proper Motion Survey (1931-1961) for stars of large proper motion.

The plate material used consisted of the unique collection of the Harvard Observatory, where, on 1000 plates taken with the 24-in. Bruce telescope, around 1900, an almost complete coverage of the southern hemisphere down to photographic magnitude 16 existed. Repetition of these plates was begun by the writer in 1929, and the taking of the new plates was continued by the Harvard Observatory and completed by 1935. Subsequently, pairs of plates for another 300 scattered regions in the northern hemisphere were added to the program. 100,000 stars with appreciable motion out of the 60 million odd stars shown on the plates were marked. All motions have been measured, reduced, and published in seven catalogues which give data for 94,000 different stars (due to many objects having been found twice on overlapping plates). Yellow plates were taken with the same Bruce telescope and all proper motion stars in the entire area south of declination −45° have been examined for color. North of that limit some ten thousand stars have been observed individually for color on

plates taken at the Cordoba and Steward Observatories. From these observations, more than four hundred white dwarfs—certain, probable and possible—have been found by the writer, constituting more than eighty per cent of the total now known.

A very similar proper motion program is now in progress at the Lowell Observatory under Giclas (1959, 1961), mainly for the northern hemisphere, and to date 48 additional stars have been designated as probable white dwarfs. Luyten (1961b) has furthermore blinked five pairs of plates taken with the Palomar 48-in. Schmidt telescope, with intervals of about 8 years, and found another twenty probable white dwarfs. Among these is one star near the North Galactic Pole with $m = 20.8$ pg, $\mu = 0''.53$, $B - V = +0.8$, probably the least luminous and smallest white dwarf now known. In addition to these, other white dwarfs have been identified by spectroscopic observers, mainly Kuiper (1941), who determined spectra for faint stars of known proper motion largely found by Wolf and Ross. It is curious to note that usually the sole credit for the discovery is claimed by the spectroscopic observer—although it was the preceding proper motion survey which "screened out" and enriched the original material by a factor of more than three hundred to one.

In all programs described above proper motions were determined first, colors and spectra later. While this constitutes a straightforward and relatively simple technique, the first phase of it—the discovery of the proper motion stars—is tedious, slow, and lengthy. An entirely different and novel technique was introduced by Zwicky and Humason in 1947: they searched for faint blue stars in regions of the sky where distant stars are expected to be absent, such as (a) heavily obscured galactic regions, and (b) areas of high galactic latitude. Their original publication listed 48 stars, 15 near the Hyades and 33 near the north galactic pole. Upon more detailed subsequent observation, the former did, indeed, prove to be largely white dwarfs, but among the latter only 2 appear to be "ordinary" white dwarfs, most of the others being the first representatives of a new type of stellar object: the coronal blue stars, mainly Population II objects lying well to the left of the main sequence in the HR diagram, possibly related to and precursors of the ordinary white dwarfs but probably having absolute magnitudes around +3 or so, and hence much more luminous than the "classical" white dwarf such as o_2 Eridani B. Following Zwicky and Humason, Luyten (1953-1962) has made extensive searches and to date has found more than 7000 such faint blue stars, 5000 of which have been published. Similarly, using Haro's three-image method, Haro, Iriarte, and Chavira at Tonantzintla have published data (see Chavira and Iriarte, 1957, 1958, 1959) for more than 2000 faint blue stars, while Feige (1958) has added another 115 from Palomar Survey plates. Finally, Haro and Luyten (1962) together have examined some

2000 square degrees near the south galactic pole and published data for 8700 faint blue stars found.

While among this colossal number of blue stars there must be many white dwarfs, the original optimistic guess that white dwarfs could be uniquely identified from accurately determined B — V and U — B colors alone has not been substantiated and it now appears that colors, spectra, and especially proper motions will all be needed. Among 100 of the brighter blue stars found by Feige there is only one bona fide dwarf (L 726-7); on the other hand it is entirely possible that among blue stars of the 18th magnitude and fainter the fraction of white dwarfs is substantial. However, a detailed discussion of these faint blue stars is outside the scope of the present treatise and reference may be made to an article by the present writer for the Handbook (1962). Data for 25 representative white dwarfs are given in Table I, where the different columns give, in order, a current serial number for easy reference, the original designation of the star, the position for 1950, the apparent, visual magnitude, the B — V and U — B colors, if known, the spectral class, total proper motion and its direction, and the parallax if known. The last four columns give the astrophysically important quantities calculated—or estimated as best we can—from the observational data, viz., the visual absolute magnitude, the luminosity and diameter in terms of that of the sun, and finally the density in cgs units, estimated on the assumption that the mass of a white dwarf is equal to $0.40\odot$ (except for those two stars where the mass is known).

IV

MAGNITUDES, COLORS, SPECTRA

Since most white dwarfs have been found in the course of extensive proper motion programs the magnitudes and colors originally published usually represent rather crude, routinely made estimates. The writer has tried to determine more accurate magnitudes—referred to the Mount Wilson Selected Area standards—by using 103aO and 103aG + No. 12 filter plates taken with aluminized reflectors—and has published data (Luyten, 1950, 1951) for some 74 white dwarfs. While the photovisual magnitudes obtained in this way appear to be reasonably close to the Johnson-Morgan V system, the photographic magnitudes are generally brighter than the Johnson-Morgan B values, due to the strong ultraviolet excess of white dwarfs. Thus the pg-pv colors obtained by the writer are probably a combination of the usual B-V and U-B. Unfortunately, however, accurate photoelectric data on magnitudes and colors are still woefully lacking, only some stars having been observed by Harris, Iriarte,

TABLE I

Note no.	Name	R.A. 1950	Dec.	m_v	B-V	U-B	Sp	μ	θ	p	M_v	$10^2 L$ (⊙ = 1)	$10^2 D$ (⊙ = 1)	$10^4 \rho$ (gm/cm³)
1.	VMa 2	00ʰ46ᵐ5	+ 5°09′	12.36	+0.56	+0.04	DG	2.98	155°	0.236	14.2	1.6	1.3	26.
2.	LP 468-176	1 40. 2	+ 12 16	18.8	+0.2			0.10	101		13.6	2.8	0.9	26.
3.	LB 210	1 53. 1	+ 0 13	16.8	−0.1			0.07	62		10.:	80.	3.3	1.6
4.	LB 3303	3 10. 0	− 68 47	11.3	−0.1		DA	0.09	147		10.:	80.	3.3	1.6
5.	W 219	3 41. 7	− 18 16	15.20	+0.30	−0.52	Dp	1.25	158	0.068	14.3	3.5	0.8	110.
6.	o_2 Eri B	4 13. 1	− 7 44	9.50	+0.03	−0.69	DA	4.08	213	0.200	11.0	28.	2.2	5.2
7.	L 879-14	4 35. 4	− 8 53	13.4	+0.5		Dp	1.49	171		13.:	4.	1.8	10.
8.	LB 3532	5 41. 7	− 2 31	19.51	−0.22	−1.22					11.:	100.	2.7	2.8
9.	HL 4	5 52. 7	− 4 09	15.0	+0.7			2.38	167		16.5	0.2	0.45	600.
10.	α CMa B	6 43. 0	− 16 39	8.5			DF	1.32	204	0.376	11.3	25.	2.8	6.0
11.	L 886-6	6 59. 6	− 6 23	15.95	−0.15		DA	0.82	185	(140)	16.:	0.3	0.3	2000.
12.	L 745-46A	7 38. 1	− 17 17	13.04	−0.32	−0.63	DF	1.26	117	0.140	13.7	2.5	1.0	56.
13.	L 97-12	7 52. 8	− 67 38	14.5	+0.5			2.05	135	0.170	15.7	0.4	0.65	200.
14.	L 532-81	8 39. 6	− 32 48	11.9	−0.02		DA	1.69	321	0.102	12.0	12	1.6	14.
15.	LDS 275 AB	9 35. 0	− 37 07	14.3	−0.10		DC	0.37	295		12.:	6.	1.0	56.
16.	LP 321-98	12 39. 8	− 30 14	19.5	+0.8			0.60	234		18.0	0.05	0.3	2000.
17.	HZ 43 A	13 14. 0	+ 29 22	12.86	−0.10	−1.14	DA	0.18	240		9.:	200.	6.5	0.2
18.	W 489	13 34. 4	+ 3 58	14.68	+0.96	+0.37	DK	3.87	253	0.131	15.3	0.6	1.4	20.
19.	L 770-3	16 15. 0	− 15 29	13.4	−0.23	−1.06	DA	0.25	223		10.:	80.	3.7	1.1
20.	LB 3553	16 24. 3	− 23 59	17.8	+0.8						15.:	0.7	1.3	26.
21.	Grw + 70°8247	19 00. 7	− 70 34	13.19	+0.05	−0.85	DCp	0.52	12	0.066	12.3	9.0	1.6	14.
22.	WZ Sge	20 05. 7	+ 17 33	15.2	+0.09	−0.71	DAp	0.08	101	0.012	10.6	45.	3.7	1.1
23.	LP 234-4	20 52. 3	+ 44 22	10.0	+0.2						10.:	80.	3.5	1.3
24.	L 1363-3	21 40. 5	− 20 45	13.3	+0.2		DC	0.66	201		12.:	12.	2.0	7.
25.	L 930-80	21 44. 9	+ 7 58	14.91	−0.14	−0.99	DB	0.39	114		12.5	7.	1.3	26.

Notes to Table I

1. Van Maanen's star; spectrum shows mainly lines of Ca II and iron.

2. One of the faintest white dwarfs for which a proper motion is known.

3. Possibly variable—perhaps eclipsing?

4. The spectrum shows broad, shallow hydrogen lines, and little else; if this is a classical white dwarf it must have one of the smallest tangential velocities known.

5. Peculiar spectrum, showing mainly the broad band at 4670 A which is probably due to C_2.

6. The prototype of classical white dwarfs.

7. Spectrum very similar to that of W 219 (No. 5).

8. Although no motion is known it seems very probable that this is a white dwarf since it appears projected against the Horsehead Nebula.

9. Unquestionably a degenerate star of low luminosity, though little more is known.

10. The companion to Sirius.

11. Although the provisional parallax is probably too large there can be little doubt that this is a star of very high density.

12. Has a 17^m red companion, and a well-determined parallax. Orbital motion should soon be measurable.

13. A yellow degenerate star, possibly similar to Nos. 5 and 7.

14. An almost normal classical white dwarf with rather sharp hydrogen lines.

15. The only double white dwarf now known; orbital motion becoming noticeable.

16. Probably the lowest luminosity and smallest degenerate star now known.

17. Probably rather more luminous than a classical white dwarf; has a 15^m red companion.

18. The yellowest degenerate star known.

19. An extremely blue star, possibly more luminous than a classical white dwarf.

20. No motion or accurate colors are known but star is seen against darkest portion of the ρ Ophiuchi cloud.

21. The spectrum of this star shows the as yet unidentified Minkowski band at 4135 A.

22. An old recurrent nova, possibly more luminous than a classical white dwarf.

23. No motion or accurate colors are known but star appears against a dark portion of the North America Nebula.

24. Classified as DC by Greenstein; has the color of an F star.

25. The first white dwarf to show only helium and no hydrogen lines.

or Johnson in the U, B, V system (see Harris, 1956). Determination of these data for as large a number of stars as possible by a single observatory—preferably in low latitude—on a unified system is an urgent necessity.

From the rather meager data now available it appears that typical white dwarfs have values of B-V and U-B running from −0.3, −1.4 for the bluest stars of absolute magnitude around +7 perhaps, through 0.0 or +0.1, −0.7 for the classical type with M around +11 to +1.0, +0.4 for the yellowest degenerate stars now known with M around +15. There are indications that white dwarfs have slightly more positive values of B-V than main-sequence stars of the same temperature and it might well be therefore that, ironically, the writer's color indices, which of course have been largely ignored, are as good an indication of the surface temperature for a white dwarf as the photoelectric value of B-V (Greenstein, 1958a).

V

SPECTRA

The first white dwarf spectra obtained were of small dispersion and could reasonably well be classified on the Henry Draper system. As more such stars became known and larger dispersions were employed pronounced differences between the spectra of some white dwarfs and those of "normal" stars revealed themselves. One of the reasons for these differences is due to the very large Stark effects on the lines, due to the powerful, electrostatic fields resulting from the high densities and degeneracy. The first attempt at a differentiation in classification was made by Kuiper (1941); the symbols proposed by him proved, however, to be both inadequate and illogical (and probably because of these features his system has been widely followed by astronomers outside the field). Thus to classify the spectrum of o_2 Eridani B as wA is redundant since it is unnecessary to add that a star whose general spectral features resemble that of a star of class A is *white*, and to classify a star whose color index is +0.7 as wG5 is incorrect since such a star is obviously not white.

A provisional classification for these stars using the letter D (indicating *d*warfs, high *d*ensity, and *d*egeneracy) followed by the usual Draper capital letter and a further number was proposed by the writer (Luyten, 1945). It should be emphasized, however, that, except for those classified as DA, there is little or no similarity among the features of white dwarf spectra to those of ordinary stars, and the letters F, G, and K if added to the classification letter D indicate solely that these stars are judged to have surface temperatures similar to those of ordinary stars of these spectral classes. For the time being this

appears to be adequate and the various types of white dwarf spectra may be described as follows:

DA indicates the type of spectrum that shows mainly or only hydrogen lines—by far the most frequently observed to date; numbers from 0 to 7 and beyond may perhaps be used to indicate the sharpness or the intensity or perhaps even the maximum number of H lines observed. Probably at least a two-dimensional classification will have to be used ultimately since some stars, such as o_2 Eridani B, show wide extremely shallow hydrogen lines (sometimes with a very sharp core) as those in main sequence stars.

DB would classify those spectra showing only helium lines (L 930-80, L 1573-31, LDS 749 B, etc.), with again numbers for further subdivision if and when needed.

DO might perhaps be reserved for extremely high temperature white dwarfs but none have as yet been observed that would fit this classification.

DC is assigned to those spectra which appear wholly continuous and show no lines at all. However, it would seem quite possible that when greater accuracy is obtained many if not most white dwarfs now classified as DC will be assigned to other classes. One star, e.g., Grw + 70°8247, quite blue in color, shows the as yet unidentified "Minkowski" band at λ 4135 but is provisionally classified as DCp by Greenstein (1958b).

DF may be used for van Maanen's star and similar objects which show strong H and K lines but very little else and thus do not really resemble ordinary F stars, although their B-V are about the same as those for ordinary F dwarfs.

DG and DK perhaps may be reserved for future spectra of stars of still lower temperatures though the few stars observed thus far (W 489, L 879-14) possess spectra that do not show the remotest resemblance to ordinary G or K spectra. Some of them show unusual bands at λ 4670 provisionally identified as due to C_2.

It seems of the utmost importance to the writer that our system of classification be kept provisional and fluid. After all we do not yet know how white dwarfs originate: if indeed a typical white dwarf does not contain any hydrogen (less than 0.0001 by mass seems to be the present estimate) and if that hydrogen is obtained mainly through accretion from clouds in space, then only the rather rare DB classification would indicate a real uncontaminated white dwarf spectrum, whereas the now much more common DA would show features of an extraneous atmosphere acquired later. Furthermore, if white dwarfs originate out of the sudden inward collapse of a star, accompanied by an enormous, explosive loss of mass from the surface, it would seem quite possible that if this collapse-cum-explosion takes place not quite isotropically, the ultimate white dwarf remnant acquires a large space—as well as a large rotational velocity—which might be expected to show in the profiles of the absorption lines.

VI

MOTIONS

There are two principal difficulties with any analysis of the motions of white dwarfs. First, since the large majority of known white dwarfs were found from proper motion surveys, there is strong observational selection in favor of large tangential velocities among them. Secondly, the determination of radial velocities is observationally difficult because so many white dwarfs show only wide and diffuse lines—or no lines at all—while, moreover, the actual value obtained for the radial velocity is always contaminated by the red shift (see Section IX). Such preliminary analyses of the (proper) motions as have been made indicate, as expected, that the white dwarfs form a fairly flat subsystem and appear to be mainly Population II stars. While for some white dwarfs found in blue star surveys proper motions have been subsequently determined by the writer, their total number is still small and their distribution over the sky sufficiently non-uniform to prevent the calculation of solar motion, etc. Moreover it is fairly evident that blue star surveys will favor the discovery of the bluer white dwarfs including perhaps, stars of the SS Cygni group or linkages between these and the RR Lyrae stars, many of which should perhaps not properly be called white dwarfs. The yellower and perhaps older white dwarfs are generally missed and it is not at all certain that all white dwarfs regardless of color, luminosity, age, etc., possess the same kinematic properties.

At the Berkeley meeting of the International Astronomical Union, Greenstein stated that out of 70 blue stars (B-V < -0.05) observed—probably mainly brighter than $m = 14$—47 were normal main sequence stars or subdwarfs while 23 were white dwarfs, and predicted that down to $m = 18$ near the Galactic Pole about half the blue stars would be white dwarfs of M around $+9$ and half subluminous O or B stars with M between $+2$ and $+5$. My own data do not indicate such a conclusion. For about 200 blue stars—most of them fainter than $m = +14$, and some as faint as 17.5—whose proper motions have been determined, only 10 out of these 200 appear to be definitely classical white dwarfs. The remainder have proper motions suggesting that their absolute magnitudes may lie anywhere between 0 and $+7$. Since the group measured for proper motion were generally fainter and included many with B-V $= 0.0$ or even $+0.1$, one would expect the percentage of classical white dwarfs to be larger here than among the brighter and bluer stars used by Greenstein. Several of the stars claimed by Greenstein to be white dwarfs have motions so small that, if they are to be of absolute magnitude fainter than $+9$, they must have extraordinarily small tangential velocities. While this may, and should occasionally, happen it does not seem probable to the present writer that it would

happen in so many instances. Moreover, if indeed there is such a large number of white dwarfs with small tangential velocities one would expect to find, even among white dwarfs found through proper motion surveys, an occasional star with very low tangential velocity; yet among the 20 odd white dwarfs found in this manner, for which parallaxes are available, there are none with $T < 40$ km/sec.

Again, the argument may well hinge on the definition of what constitutes a white dwarf. The only conclusion that can be drawn safely at the present time appears to be that both Population I and II are represented among white dwarfs but that a great deal more observational material must be obtained before more detailed results concerning the motions and kinematic properties of white dwarfs can be arrived at.

VII

LUMINOSITIES

At the time of writing (September 1961) trigonometric parallaxes for only some 15 white dwarfs have been published. To these may be added the data for 7 white dwarfs belonging to the Hyades cluster and 2 members of Praesepe. For a further 10 objects which belong to binaries of which the other component appears to be a normal main sequence, yellow or red dwarf parallaxes may be fairly reliably estimated from the spectra or colors of these other components. Luminosities have been determined spectroscopically for a number of white dwarfs, degenerate and semidegenerate stars, but here it should be borne in mind that the spectra of these stars are very unlike those of any others, and hence that the calibration of the spectroscopic criteria must remain uncertain for some time to come. Here one may also cite the remark made by G. Münch at the Mexico meeting of the American Astronomical Society to the effect that he had classified as a supergiant a star which Greenstein had called a subdwarf.

In order to fit the white dwarfs into their proper place in the HR diagram their spectra and/or colors must be known as well as their luminosities. Unfortunately there are still many white dwarfs—even those with reasonably well determined luminosities—for which no spectra and only very crude colors are known. This writer combined all reasonably reliable data known in 1951 into a diagram which is reproduced here (Fig. 1) with the incorporation of all additions and changes to date. The main conclusions to be drawn are still the same as those from 1951, viz.:

1. The white dwarfs seem to occupy a fairly well defined locus in the HR diagram covering a range from about $m = +8$ to $m = +19$ and lying some 8-10 magnitudes below the main sequence.

2. While the data are still somewhat uncertain there appears to be definite evidence for a dispersion in luminosity for a given color rather than for the existence of several, almost parallel loci.

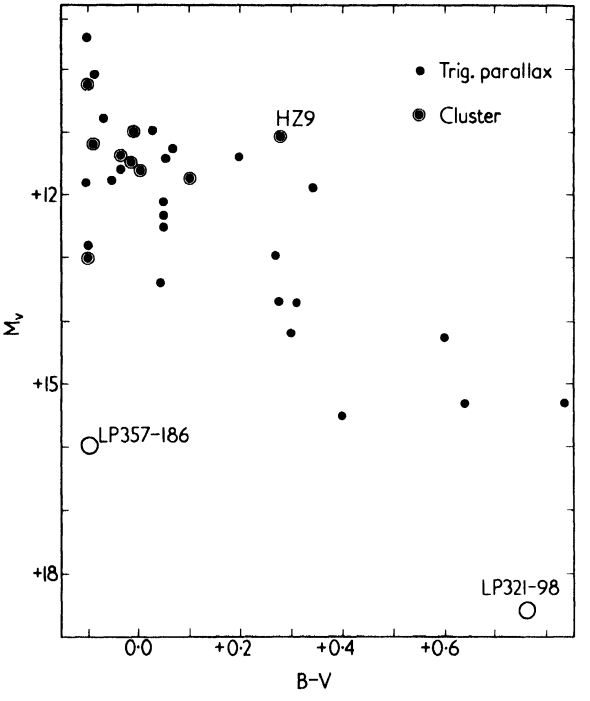

FIG. 1. Plot of the relationship between luminosity and color for white dwarfs. Black dots represent white dwarfs with reliable trigonometric parallaxes, circled dots those contained in open clusters—Hyades, Pleiades, and Praesepe. Large open circles represent the two extreme stars, LP 357-186 and LP 321-98, for which the luminosity has been estimated statistically from the proper motion. Abscissae are B-V colors; ordinates, visual absolute magnitudes. The star HZ 9 has a red companion, and therefore appears much redder than an ordinary white dwarf of the same luminosity.

VIII

MASSES

The first two white dwarfs discovered—the companions to Sirius and o_2 Eridani —belong to binary systems with known orbits and masses. The companion to Procyon was found shortly thereafter to possess a mass much larger than appears appropriate for its luminosity and is therefore generally considered to

be a white dwarf. These are the only three for which masses are now known; the salient data for all three are given below:

	m	M	S	Mass
o_2 Eridani B	9.7	11.2	DA	0.44⊙
α CMa B	8.	11.	DF	0.96⊙
α CMi B	12.	14.	—	0.61⊙

Due to the proximity of the primaries the magnitudes and spectra of the last two stars are not too reliably determined. Moreover, the companion to Sirius has even been suspected to be double itself, although this is now generally disbelieved. The upshot of it all is, therefore, that we have only one star for which the mass as well as all other astrophysical data are reasonably well determined. Yet on this has been erected an imposing structure of theories of white dwarf constitution—one theoretician going so far even as to calculate masses for seven more white dwarfs from pure theory, subsequently to declare these as known, then to proceed to use them to prove his theories.

Although this situation has existed for several decades nothing has been done to improve it, even though a remedy is near at hand: viz. a statistical determination by means of orbital motions. Among the white dwarfs found by this author a number are components of wide binaries. At the time of this writing some thirty such pairs are known, including two in which both components are white dwarfs (Luyten, 1956). (It may be mentioned that, in addition to these, Haro and Luyten (1962) have published data on 72 faint wide pairs containing one white and one red star and on 31 faint white doubles and that probably many of these are white dwarfs.) Data for some representative samples are given in Table II where the different columns give in order the star's designation, the position for 1950, the magnitudes and colors of the components, the total proper motion, the position angle and separation of the pairs, and the expected order of magnitude of the orbital motion. While for most of these pairs the orbital motion is exceedingly slow and must wait many decades for accurate determination, there are several cases, notably L 587-77, L 879-2/3, L 1046-18, −37:10050, and especially LDS 275, where the motion should be rapid enough to be accurately measurable in a short time. Using a miscellany of plates taken with seven different refractors and reflectors situated in widely different latitudes—a setup not conducive to high accuracy—the present author made a preliminary solution of the problem (Luyten, 1961) and found, very provisionally, that indeed the masses of white dwarfs are larger, perhaps by a factor of 2, than those of main sequence stars of the same luminosity. It is to be hoped that this kind of investigation be taken in hand without delay with

TABLE II

	RA (1950) Dec.	m_1	B-V_1	m_2	B-V_2	μ	θ	s	w
L 170-14AB	$0^h27^m.5 - 54°58'$	15.7	−0.1	15.8	+1.3	0″.36	327°	3″.4	0″.0053
L 587-77AB	3 26. 7 − 27 32	13.8	−0.1	15.2	+1.1	0.84	227	7.3	0.012:
L 879-2/3	4 34. 0 − 6 17	16.0	+1.4	17.1	+0.3	0.54	312	7.8	0.0046
L DS 275	9 35. 0 − 37 07	14.7	−0.1	15.1	−0.1	0.37	337	3.8	0.0064
L 1046-18AB	12 14. 3 + 3 14	14.7	+1.5	14.9	0.0	0.72	178	3.1	0.014:
HZ 43AB	13 14. 0 + 29 22	12.5	−0.4	14.7	+1.3:	0.17	280	3 :	0.005:
L 619-49/50	13 48. 1 − 27 18	13.9	+1.6	15.0	−0.1	0.22	233	8.9	0.0029
L 151-81AB	14 54. 0 − 63 05	16.5	0.0	17.0	+0.1	0.05	74	2.4	0.0007
−37:10500	15 44. 2 − 37 46	6.8	+0.7	13.2	0.0	0.49	131	14.6	0.023:
W 672AB	17 16. 2 + 2 00	14.2	0.0	15.6	+1.5	0.49	137	13.0	0.0024
LDS 749	21 29. 6 0 00	11.0	+1.0	14.2	−0.1	0.42	29	132.5	0.0025
LDS 826	23 51. 5 − 33 33	14.5	0.0	15.0	+1.2	0.59	0	7.2	0.0066

the aid of long-focus refractors or large reflectors, since obviously this is now the only observational material from which even a statistical evaluation of the masses of white dwarfs can be obtained.

IX

RED SHIFT

It follows from Einstein's relativity theory that the wavelength of a ray of light leaving a strong gravitational field must be lengthened by an amount proportional to the gravitational potential M/R. For the sun this amounts to a "red shift" equal to a Doppler velocity of only 0.6 km/sec and as such it was extremely difficult to measure it with sufficient accuracy. As soon as the first white dwarfs were discovered it was recognized that these constitute the only class of stars where M/R can reach large values which could be easily observed. As early as 1918 Adams observed its amount for the Sirius companion as $+19$ km/sec (see Adams, 1925) and the close agreement with the then calculated theoretical values of $+20$ constituted one of the important early experimental proofs for Einstein's relativity. In 1954 Popper obtained a similar value of $+21 \pm 4$ km/sec for o_2 Eridani B which again agrees well with Greenstein's calculated $+16$ km/sec (see Popper, 1954).

Although determination of the precise values of these red shifts constitutes one of the most direct proofs of the extraordinarily high densities and concomitant degeneracy of white dwarfs, very little observational material has been obtained in addition to that mentioned above. This is partly due to the fact that actual, direct verification is possible only in the case of components of binaries where the theoretical "unreddened" velocity of the white dwarf can be calculated from that observed for the other component. Part of it stems from the still existing uncertainty in the spectral class and magnitude of Sirius B and the resultant uncertainty in the predicted value of the red shift, as well as from the fact that the Sirius companion has been inobservably close to its primary for more than 25 years. During the next decade the companion will be in its optimum position for observing and it is to be hoped that many of the remaining uncertainties about this star will then be settled.

Finally, the theoretical prediction of the exact amount of the red shift has become somewhat confused with the other effects resulting from the high density gradient in the atmospheres of white dwarfs. Until the entire theory covering the sum total of these effects has reached a satisfactory state it will be difficult to use the observed red shifts in the verification of masses and high densities.

X

FREQUENCY IN SPACE

The question of the over-all frequency of white dwarfs in space is still difficult to answer at the present time. Using data from the Bruce Proper Motion Survey, the writer arrived at a value of 1.9 expressed as a percentage of all stars in space in the neighborhood of the sun (Luyten, 1946). Using a survey of wide double stars this was later raised to 2.1%. More recently, from an analysis of the nearly 10,000 stars with $\mu > 0''.2$ in the southern hemisphere the writer obtained $2.3 \pm 0.3\%$. Theoreticians working from theories of stellar evolution have generally obtained much higher values, some running as high as 10%. This is partly a matter of definition: What is a white dwarf? This writer feels that the only realistic definition of a white dwarf is that of a star with a luminosity between, say, +8 and +16, lying some 8-10 magnitudes below the main sequence. To be sure, if blue stars with absolute magnitudes down to +3, and also lying some 8 magnitudes below the main sequence are included, the value of 2.3% given above could be raised somewhat. However the increase would probably be very slight as it is now fairly apparent that stars above the blue end of the white dwarf sequence are very rare in space. At the other—faint—end of the white dwarf sequence degenerate stars may well be very numerous, but such objects with, say $M = +18$, $B - V = +1^m.0$ are almost discovery-proof and at present the main arguments for their existence in large numbers come from pure theory. Another criticism which may be leveled at the writer's estimate of 2.3% is that this was derived from stars of large proper motion only and that it may well be that large numbers of Population I white dwarfs with low velocities exist. However, if anything like the current theories on the catastrophic formation of white dwarfs is accepted it would seem likely (see Section V) that white dwarfs are more likely to be high velocity objects, hence the increase in the value 2.3% due to undiscovered low velocity white dwarfs is probably small.

The writer has attempted to obtain still further information on this point by following up Humason and Zwicky's ingenious method of searching for faint blue stars in heavily obscured areas such as the ρ Ophiuchi region, where no distant objects occur. Here one can be reasonably sure that any faint blue stars found must be nearby white dwarfs. This investigation is still in progress and final results will not be known for some time, but preliminary indications are that the space density of white dwarfs in these regions of low galactic latitude is not high.

XI

WHITE DWARFS IN CLUSTERS

Two white dwarfs were found in the Hyades by Ramberg, van Rhyn and Raimond (see van Rhyn and Raimond, 1934). Several more were added by Humason and Zwicky (1947) in the research referred to before and 2 more by the present writer (Luyten, 1960). In searching pairs of blue and yellow plates of Praesepe the author found a number of blue stars of about the expected magnitude (Luyten, 1954), and after measuring the proper motions of two of them could prove that these are white dwarf cluster members. Luyten and Herbig (1960) have published data on a faint star which may be a white dwarf member of the Pleiades. Luyten and Miller (1956) have searched the region of the Ursa Major cluster without finding any likely prospects, and the companion to Sirius—if indeed the primary belongs to the cluster—appears to be the only white dwarf now known to be in it. Luyten (1953) has made several searches in the Coma Cluster, and while several blue stars of about the right magnitude were found none of these seem to belong to the cluster, which conclusion is supported by a further spectroscope search by Stephenson (1960). A further systematic search in galactic clusters not more distant than about 1000 parsecs and without much reddening was undertaken by the author (Luyten, 1961b). Blue and red duplicate negatives from the Palomar Survey were blinked, in the cluster area as well as in one or two control areas of about the same size. Within the areas of the clusters M 36, M 38, M 39, M 41, NGC 129, and NGC 6885 actually fewer faint blue stars were found than in the corresponding control areas. Within IC 4665 and M 34 a slight excess of blue stars was found, while in NGC 752 a very large number of blue stars was found—but a statistically equally large number in the control area. The cluster M 67 presents a special case; it has been rumoured that Baade found a large number of white dwarfs here though Baade himself never published anything on it. With $m - M = 9.6$ and negligible reddening, an o_2 Eridani B type of white dwarf should appear with $m = 20.8$, close to the limit of the blue Palomar Survey plates, and one would therefore expect to find only the bluer and more luminous white dwarfs on these plates. Actually only 2 or 3 stars of approximately the right magnitude and color were found and obviously this is a case where only the very large reflectors can give decisive information.

For all the other clusters a great many follow-up observations on accurate colors, spectra, and proper motions will be required before definite conclusions can be drawn as to how many white dwarfs occur in them. Until such observations are available it would be meaningless to compare and discuss the present preliminary data in the light of theoretical calculations and predictions, important

as such a comparison may be for our knowledge of stellar and cluster ages and stellar evolution.

XII

INDIVIDUALLY INTERESTING STARS

LB 210, 1:53.1 + 0:13 (1950) 16.7. This object was first noticed by Luyten and Carpenter in S.A. 93 and, by using the old Mt. Wilson plate, the large motion of +0".095, +0".032 was derived. Since the star appeared much fainter on the Mt. Wilson plate it was assumed that it was an ordinary red dwarf which happened to have flared when the Tucson blue plate was taken. However, in the South Galactic Pole survey by Haro and Luyten the star was again found as an unquestionably very blue object of about the same apparent magnitude as on the Tucson plates. Remeasurement reduced the proper motion somewhat, to +0".058, +0".040, indicating that the star is a white dwarf. The Mt. Wilson magnitude of nearly 18 pg, if not due to a flaw, then suggests the possibility that the star is variable—perhaps even an eclipsing binary.

HZ 9, 4:29.4 + 17:38 (1950) 14.0 DA. This star whose proper motion indicates it to be a member of the Hyades cluster has the unusually large B-V of +0.33. Greenstein has found emission lines of Ca II in its spectrum, which give a radial velocity varying by as much as 250 km/sec. It seems possible, therefore, that we again have here a binary, composed of a white dwarf and a late Me dwarf, because of the large radial velocity change, possibly eclipsing.

LDS 275, 9:35.0 — 37:07 (1950), 14.6-15.0 DC. The relative position of the components of this binary has changed from 36°0 3".36 (1942.34) to 37°5 3".76 (1959.22) and hence an orbit of high inclination is indicated, the period being perhaps of the order of 700 years. Since the proper motion is 0".37 in 298° the star may have a larger parallax than normal. If only the parallax could be determined, it should be possible to make a rough guess as to the masses of the components from further measures of orbital motion.

Finally, among the most intriguing degenerate stars are those of yellow color, and, presumably, very low luminosity—such as W 129, LP 414-106, L 879-14, HL 4, L 97-12, LP 321-98, W 489, and L 40-109, and many others —which are now beginning to be found in larger numbers. Spectroscopically, these should be rewarding objects and accurate determination of their spectral features should give us a great deal of further information on the probable constitution and chemical composition of these, by far the densest objects known.

XIII

CONCLUSIONS AND SUGGESTIONS FOR FUTURE WORK

While white dwarfs have been known for nearly 50 years, comparatively little observational work was done on them—except by this writer—until about ten years ago. It would be merely trite, therefore, to say that more observations of all kinds especially with very large telescopes are urgently needed before the problems of their origin, mass, composition, structure, age, evolution, and kinematic properties can be properly tackled.

Determination of beginning orbital motions for the fifteen or so most promising wider binaries, of parallaxes, and B-V, U-B colors for at least representative objects from the bluest to the yellowest—and faintest—spectra, radial velocities and red shifts for at least another dozen carefully selected white dwarfs, and perhaps even rotational velocities for some helium white dwarfs seem to be among the most important observational data now needed.

References

Adams, W. S. (1925). *Proc. nat. Acad. Sci. Wash.* **11**, 382.

Bruce Proper Motion Survey (1941-1961). General Catalogue, Parts A-G.

Chavira, E., and Iriarte, B. (1957). *Bol. Obs. Ton. y Tac.* **16**.

Chavira, E., and Iriarte, B. (1958). *Bol. Obs. Ton. y Tac.* **17**.

Chavira, E., and Iriarte, B. (1959). *Bol. Obs. Ton. y Tac.* **18**.

Feige, J. (1958). *Ap. J.* **128**, 267.

Giclas, H. L. Slaughter, C. D., and Burnham, J. (1959). *Lowell Obs. Bull.* **102**.

Giclas, H. L. Burnham, J., and Thomas, H. (1961). *Lowell Obs. Bull.* **112**.

Greenstein, J. L. (1958a). *In* "Handbuch der Physik" (S. Flügge, ed.), Vol. 50, p. 176. Springer, Berlin.

Greenstein, J. L. (1958b). *In* "Handbuch der Physik" (S. Flügge, ed.), Vol. 50, p. 170 ff. Springer, Berlin.

Handbook (1962). G. P. (Kuiper's Handbooks: this particular volume edited by M. Schmidt (in preparation).

Haro, G., and Luyten, W. J. (1962). *Bol. Obs. Ton. y Tac.* **22**.

Harris, D. L. (1956). *Ap. J.* **124**, 665.

Humason, M. L., and Zwicky, F. (1947). *Ap. J.* **105**, 85.

Kuiper, G. P. (1941). *P. A. S. P.* **53**, 248.

Luyten, W. J. (1945). *Ap. J.* **101**, 131.

Luyten, W. J. (1946). *A. J.* **52**, 36.

Luyten, W. J. (1950). *Ap. J.* **112**, 212.

Luyten, W. J. (1951). *Ap. J.* **113**, 701.

Luyten, W. J. (1953). "A Search for Faint Blue Stars", Vol. I.

Luyten, W. J. (1954). *H. A. C.* **1244**.

Luyten, W. J. (1956). Binaries with white dwarf components. *In* "A Search for Faint Blue Stars," Vol. VIII.

Luyten, W. J. (1958). On the frequency of white dwarfs in space. *In* "A Search for Faint Blue Stars," Vol. XVI.
Luyten, W. J. (1960). *H. A. C.* **1496.**
Luyten, W. J. (1961). *Pub. Obs. Minn.* **III**, No. 9.
Luyten, W. J. (1961a). *Pub. Obs. Minn.* **III**, No. 10.
Luyten, W. J. (1961b). "A Search for Faint Blue Stars," Vols. XXIII-XXV, XXVII.
Luyten, W. J. (1953-1962). "A Search For Faint Blue Stars," Vols. I-XXX, 1953-1962.
Luyten, W. J., and Herbig, G. H. (1960). *H. A. C.* **1474.**
Luyten, W. J., and Miller, F. D. (1956). "A Search for Faint Blue Stars," Vol. V.
Popper, D. M. (1954). *Ap. J.* **120**, 316.
Stephenson, C. B. (1960). *P. A. S. P.* **72**, 42.
van Rhyn, P. J., and Raimond, J. J. (1934). *M. N. R. A. S.* **94**, 508.

For a general bibliography, see:

G. P. Kuiper, "Colloquium on Novae and White Dwarfs." Hermann, Paris, 1941.
W. J. Luyten, The spectra and luminosities of White Dwarfs. *Ap. J.* **116**, 283 (1952).
W. J. Luyten, White dwarfs and degenerate stars. *In* "Vistas in Astronomy" (A. Beer, ed.), Vol. II, p. 1048. Pergamon, New York, 1956.
J. L. Greenstein, The spectra of white dwarfs. *In* "Handbuch der Physik" (S. Flügge, ed.), Vol. 50, p. 161. Springer, Berlin, 1958.

For announcements of discovery of white dwarfs, see:

Harvard Announcement Cards, beginning with No. 515 (1939); four lists by W. J. Luyten in *Proc. nat. Acad. Sci. Wash.* Vols. 37-40 (1951-1954).

The Stray Bodies in the Solar System. Part I. Survival of Cometary Nuclei and the Asteroids*

ERNST J. ÖPIK†
Department of Physics, University of Maryland, College Park, Maryland

I. Introduction 220
II. Survival in Encounters 221
A. The Statistical Setting 221
B. Probability of Close Passage and Collision 222
C. Probability of Angular Deflection 224
D. Partial Crossings 226
E. Auxiliary Tables 227
III. Dynamical Probabilities of Elimination for Comets and Related Objects 230
A. Multiple Crossings 230
B. Dynamical Probabilities of Survival for Selected Lists of Objects . 231
C. Dynamical Survival of Comets in Incomplete or Near Crossing with Jupiter 236
D. Asteroids in Close Appulses to Jupiter 238
IV. Genetic Relationships of Comets and Asteroids 240
A. Origin of Comets and Structure of Nuclei 240
B. Types and Physical Survival of Comet Nuclei. 243
C. Dead Comet Nuclei and the Origin of the Apollo Group 244
V. Capture of Comets into Terrestrial Space and Statistical Balance with Apollo Group 250
A. Definition 250
B. Statistical Equilibrium of Disintegration and Dynamical Elimination 250
C. Injection from General Field of Comets 251
D. Comet Diameters and Magnitudes 253
E. Gravitational Capture from Jupiter's Family of Comets 257
F. Capture from Jupiter's Family of Dead Nuclei 259
G. Evolution through Jet Deceleration 259
H. Conclusion 261
References 261

* Supported by a grant from the National Aeronautics and Space Administration Grant NsG-58-60. Paper presented at the Comet Symposium of the American Astronomical Society at Nantucket, June 20, 1961.

† Present Address: Armagh Observatory, Northern Ireland.

Formulas for the probability of collision and orbital change in close encounters with the planets are further developed, auxiliary tables calculated, and the theory applied to comets and asteroidal populations. Probabilities and lifetimes for collision and ultimate orbital change are calculated for selected objects, or groups of objects, crossing the orbits of the principal planets.

Objects crossing Jupiter's orbit are chiefly eliminated by orbital change and ejection to infinity, and have a relatively short lifetime of the order of 10^6 years. Those confined to the region of the terrestrial planets are chiefly removed by physical collisions and are more longlived, with a lifetime of the order of 10^8 years for the Apollo group, and 6×10^9 years for those crossing the orbit of Mars alone, so that about 50% of their original population may have survived from the beginnings of the solar system. On the contrary, the Apollo group objects cannot have survived over such long intervals of time; their present number must depend upon the balance between elimination and supply from other sources.

The origin, structure, and dimensions of comet nuclei are reviewed. Oort's hypothesis of their origin as asteroids ejected from the inner portions of the solar system is considered as most plausible. Their recapture by Jupiter, and by the terrestrial planets as a second stage, feeds comets into "terrestrial" space, or that inside Jupiter's orbit. However, the chief process in decreasing their aphelion distances appears to be Whipple's "rocket effect" for nuclei in retrograde rotation.

Statistical grounds are pointing to Apollo group asteroids chiefly originating from residual nuclei of comets, the supply from the asteroidal belt by Mars perturbations being inadequate though not negligible.

A formula for estimating the diameters of comet nuclei from photometric data is proposed and statistically checked as to order of magnitude. The average diameter of the nucleus of a comet of the sixth absolute magnitude (specially defined) is estimated to be 10 km, an order of magnitude smaller than suggested by former estimates. The new estimates are also supported by the apparent decrease of the gravitational constant, caused by the jet of gases ejected sunward.

I

INTRODUCTION

Comets represent the most conspicuous group of changing objects in the solar system. Their orbits, affected by stellar perturbations at great distances, and by planetary perturbations when near the sun, are intrinsically unstable and, by shedding off matter, they are undergoing a process of disintegration which may end either in complete or in partial destruction. The changes in

comets are directly observable, involving processes which may have been instrumental in the formation of the members of the solar system. With the cosmogonic implications in mind, this article considers in particular the dynamical survival of comets and other stray bodies in encounters with the planets; hence also a clue to a possible genetic link between comets and asteroids is indicated statistically.

II

SURVIVAL IN ENCOUNTERS

A. *The Statistical Setting*

Two intersecting orbits may result in large perturbations at close encounters, or even in a physical collision. The same holds for *crossing* orbits which do not intersect but which cover a common range in heliocentric distance; this follows from the general character of the secular perturbations, usually a precession of the node and advance of the perihelion which, after intervals of the order of 10^4-10^5 years in the inner portions of the solar system, lead repeatedly to intersection. An orbit of a small body crossing that of a principal planet is therefore intrinsically unstable, unless a particular mechanism of commensurability (e.g., in the case of Pluto with respect to Neptune, see Öpik, 1961a) prevents the two objects from coming close together. For comets and most other bodies no such commensurability exists, so that their survival is a matter of statistical expectation.

The expectation of orbital change of objects crossing the orbits of planets can be treated according to the theory of probabilities. The fate of individual bodies may be virtually unpredictable by the methods of celestial mechanics, but statistical predictions may still hold as averages for an entire population.

Only interactions at close encounters are considered here; these lead to the major changes. Orbital change from perturbations at great distances is less drastic and, in comparison, can be disregarded.

The probabilities depend on the orbital elements and, as these are changed in an unpredictable manner, the problem becomes highly involved when individual objects are considered. However, if a steady or slowly changing orbital population of the stray bodies (comets) is assumed, calculations based on any existing sets of orbital elements will yield correct average results.

For a similar reason, mathematical simplifications can be introduced without essentially affecting the calculated probabilities. The mass of the stray body is assumed to be infinitesimal, the orbit of the planet a circle as a first approximation (its eccentricity being allowed for as a second step), and the motion of a

stray body inside D, a conventionally defined radius of the sphere of action, is assumed to be governed only by the gravitational field of the planet, and outside D only by the solar field. D is defined by the condition that the solar perturbation on the body when in conjunction with the sun be equal to the planet's attraction (Öpik, 1951) and, in units of the planet's orbital radius, equals

$$D = (\tfrac{1}{2}\mu)^{1/3} \tag{1}$$

where μ is the mass of the planet in solar units, assumed to be small. Tisserand's definition is somewhat different, but not essentially, and less suitable for our purposes.

In such a manner the problem of encounter is reduced to a combination of two-body problems.

B. *Probability of Close Passage and Collision*

The relevant formulas for physical collision and cumulative angular deflection in repeated encounters have been given by the author (1951, 1961a). With the planet's mean heliocentric distance as unit of length, and setting equal to unity the sun's mass, the planet's mean orbital velocity, and mean motion (unit of time $= 1/2\pi$ of the period of revolution; gravitational constant $= 1$), in a frame of cartesian coordinates rotating with the "mean planet," near the point of intersection of the two orbits but outside the sphere of action of the planet, the components of the unperturbed velocity of the stray body (further also called "the particle") relative to the mean planet are

$$U_x^2 = 2 - A(1 - e^2) - A^{-1} \tag{2}$$

(x-axis in the radial direction toward the sun),

$$U_y = \pm [A(1 - e^2)]^{1/2} \cos i - 1 \tag{3}$$

(y-axis tangential in the direction of the planet's orbital motion), and

$$U_z^2 = A(1 - e^2) \sin^2 i. \tag{4}$$

The total relative velocity U, an invariant in repeated encounters within the frame of our mathematical simplifications, is then

$$U^2 = 3 - 2[A(1 - e^2)]^{1/2} \cos i - A^{-1} \tag{5}$$

where A, e, and i are the semimajor axis, eccentricity, and inclination (relative to the planet) of the heliocentric orbit of the particle. The "mean planet" is

defined as one moving in a circular orbit at the mean distance of the real planet.

Unless perturbed by a planet, in purely Keplerian motion around the sun the U-components remain unchanged. In close encounters with the planets, the components may change and the U-vector change direction, its absolute value remaining constant.

Let s denote the target radius at encounter ("impact parameter") or the distance of the asymptote of the hyperbolic relative orbit of the particle from the planet, in the conventionally assumed two-body interaction during the passage of the particle through the sphere of action of the planet. The mathematical expectation, p (to be further called "probability") of a passage within target radius s from the planet is

$$p = \frac{fs^2}{\pi \sin i} \left(\frac{U^2 + 0.44\, e_0^2}{U_x^2 + 0.44\, e_0^2} \right)^{1/2} \tag{6}$$

per heliocentric revolution of the particle. Here e_0 is the eccentricity of the planet's orbit (averaged over secular perturbations) and f the "overlapping fraction" or the fraction of the planet's orbit over which crossing is possible. Usually the crossing is complete and $f = 1$. For a single passage the actual inclination is to be taken, but the fromula does not apply when i is very small ($< 0.^\circ 4$). Over long intervals of time and when $\sin i$ is small, the statistical average defined through

$$\sin^2 i = \sin^2 i_c + \sin^2 i_0 \tag{7}$$

can be used; here i_c and i_0 are the average inclinations, relative to the invariable plane, of the orbits of particle and planet, respectively.

The relation of periastron (perigee) distance, r, to the target radius, s, in the two-body encounter of particle with planet is

$$s = r(1 + 2\mu/r\, U^2)^{1/2}. \tag{8}$$

Substituting this into Eq. (6), an expression for the probability of a planetocentric passage, at a distance closer or equal to r, can be obtained.

For nearly parabolic, nonperiodic orbits, p is the average probability per apparition for objects with similar orbital elements if the longitudes of their nodes and perihelia are distributed at random; the parameter, $A(1 - e^2)$, is then to be set equal to $2Q$, the double perihelion distance.

For a periodic orbit, of a period $(a_0 A)^{1.5}$ in years, where a_0 is the mean heliocentric distance of the planet in astronomical units, the probability P per year, corresponding to a reciprocal of the lifetime τ, is

$$1/\tau = P = p(a_0 A)^{-1.5}(\mathrm{yr}^{-1}). \tag{9}$$

When $r = R$, the radius of the planet, Eqs. (6), (9), and (8) define the probability of physical collision and its target radius $s = S$.

C. *Probability of Angular Deflection*

In the conventionally assumed two-body free encounter, when $r > R$, the U-vector remains constant and only changes direction by an angle γ, given by

$$\sin \tfrac{1}{2}\gamma = (1 + rU^2/\mu)^{-1} \tag{10}$$

or

$$\tan (45^\circ + \tfrac{1}{4}\gamma) = (1 + 2\mu/rU^2)^{1/2} = s/r. \tag{11}$$

The direction of the U-vector determines the elements of the heliocentric orbit of the particle in a trivial manner (Öpik, 1951), by way of Eqs. (2)-(5). The angle α of the U-vector with the y-axis, defined by

$$\cos \alpha = U_y/U \tag{12}$$

plays an important role in determining the heliocentric orbit of the particle.

For $U < \sqrt{2} - 1$, the largest aphelion distance attainable through encounters with one planet corresponds to $\alpha = 0^\circ$ and is

$$Q'_{\max} = [A(1 + e)]_{\max} = (1 + U)^2/(1 - 2U - U^2). \tag{13}$$

For U equal or exceeding the limit, parabolic and hyperbolic orbits become possible.

For $U < 1$, the smallest possible perihelion distance is different from zero; it corresponds to $\alpha = 180^\circ$ and is

$$Q_{\min} = [A(1 - e)]_{\min} = (1 - U)^2/(1 + 2U - U^2). \tag{14}$$

For U equal or exceeding unity the case $Q = 0$ (falling into the sun) is allowed, although its probability is small (cf. Table IV).

By using these formulas, the probabilities of angular deflection and orbital change in a single encounter can be calculated from Eqs (6) and (8).

The largest deflection, $\gamma_{\max}$, corresponds to grazing passage, $r = R$. Table I contains some sample values for this case.

For comets the U-values are usually between 1 and 2. It can be seen from the table that the terrestrial planets can but slightly change the orbit of a passing comet in a single encounter.

However, for objects in short-period orbits such as periodic comets, the angular deflections accumulate according to the rule of random walk, i.e., they

are summing up quadratically for successive encounters. An accumulated average deflection of 90°, or a "full deflection" can be assumed to be equivalent to the establishment of a random orientation of the U vector, without "memory"

TABLE I

MAXIMUM SINGLE ANGULAR DEFLECTION

Planet	R	$2\mu/R$	U = 0.1	U = 0.2	U = 0.5	U = 1.0	U = 2.0
			γ_{max} (deg)				
Earth	4.26×10^{-5}	0.1423	122.5	79.6	25.6	7.6	2.0
Mars	1.48×10^{-5}	0.0438	86.7	41.5	9.3	2.5	0.6
Jupiter	8.90×10^{-5}	21.5	175.1	170.1	155.5	132.4	95.6

of its former direction so that the probability θ of its being directed into solid angle ω is then

$$\theta = \omega/4\pi. \tag{15}$$

For repeated passages within the limits of from R to D the target radius σ for full deflection, to be used with Eq. (6) by setting $s = \sigma$, is then defined (Öpik, 1961a) by

$$\sigma^2 = B \ln [(D^2 + B)/(S^2 + B)] \tag{16}$$

where

$$B = \left(\frac{4\mu}{\pi U^2}\right)^2. \tag{17}$$

The probability $p\theta$ (per revolution) or $P\theta$ (per year) of a given orbital change can then be calculated, when the solid angle ω for the changed group of orbits is given. This can be computed by numerical integration in a somewhat involved manner, except in the case of ejection from the solar system, when the parabolic limit $A \to \infty$ yields directly

$$\theta_\infty = \tfrac{1}{2}(1 - \cos \alpha_\infty) = (U^2 + 2U - 1)/4U. \tag{18}$$

This follows from the expression for the heliocentric velocity

$$W^2 = 1 + U^2 + 2U \cos \alpha \tag{19}$$

which defines α_∞ when $W^2 = 2$ is set as for escape.

In the general case of orbital change resulting in perihelion distances less

than $q = Q < 1$, or aphelion distances greater than $q = Q' > 1$, an approximate procedure is sufficient for most purposes. Defining

$$\theta_q = \tfrac{1}{2}(1 \mp \cos \alpha_q) \tag{20}$$

where the upper $(-)$ sign corresponds to $q > 1$ (large aphelion), the lower sign to $q < 1$ (small perihelion), the effective value of $\cos \alpha_q$ can be assumed approximately equal to

$$\cos \alpha_q = \tfrac{1}{2}(\cos \alpha_1 + \cos \alpha_2). \tag{21}$$

Here α_1 is the limiting angle which leads to an orbit with the prescribed value of q when the U-vector is in the tangential plane ($U_x = 0$), and α_2 when the U-vector is in the radial plane ($U_z = 0$). These angles are given by

$$\cos \alpha_1 = [(q - 1)/(q + 1) - U^2]/2U \tag{22}$$

for $q \gtrless 1$, and

$$\cos \alpha_2 = \{(q^2 - 1) \mp [(q^2 - 1)^2 - (q - 1)^2 + q^2U^2]^{1/2}\}/U \tag{23}$$

with the sign rule as in Eq. (20).

Special cases, when the procedure as described above does not apply, are as follows:

1. For $q > 1$ and large U, when $\cos \alpha_1 < -1$, $\cos \alpha_2 > -1$, set in Eq. (21) $\cos \alpha_1 = -1$; when also $\cos \alpha_2 < -1$, set $\theta_q = 1$.

2. For $q > 1$ and small U (q near 1), when $\cos \alpha_1 > 1$, set $\theta_q = 0$; when $\cos \alpha_1 < 1$, $\cos \alpha_2 > 1$, set in Eq. (21) $\cos \alpha_2 = 1$.

3. For $q < 1$ when $\cos \alpha_1 < -1$ and both solutions α' and α'' of Eq. (23) are real,

$$\theta_q = 1 - \cos \tfrac{1}{2}(\alpha' - \alpha'') \tag{20a}$$

can be assumed.

D. *Partial Crossings*

When the perihelion or aphelion of the particle is placed between the perihelion and aphelion of the planet, the crossing is partial. The overlapping fraction, to be used with Eq. (6), is then (Öpik, 1951)

$$f = (\text{arc cos } E)/\pi \tag{24}$$

where

$$E = [A(1 - e) - (1 - e_0^2)]/[e_0A(1 - e)] \tag{25}$$

for crossings near perihelion of the particle, and

$$E = [(1 - e_0^2) - A(1 + e)]/[e_0 A(1 + e)] \tag{26}$$

for crossings near aphelion of the particle.

All formulas apply without modification for $1 > f > 0.5$. However, when $f < 0.5$, U_x becomes imaginary and further adaptation of the formulas is required. Evidently, the probabilities of encounter will not vary much with small variations in the orbital dimensions of the planet. Hence, for

$$0.5 > f > 0 \tag{27}$$

in Eqs. (2)-(5) it is proper to use $A/(1 + e_0)$ instead of A for perihelion crossings, and $A/(1 - e_0)$ for aphelion crossings.

When $A(1 - e) > 1 + e_0$, or $A(1 + e) < 1 - e_0$, $|\cos E| > 1$, f is imaginary and crossing is formally not possible. Collisions are then not allowed. However, especially with the giant planets, close encounters may still be efficient in producing angular deflection. In such a case it is advisable to use Eqs. (2)-(5) with $A/(1 + e_0 + D)$ instead of A for perihelion appulses (no longer crossings), and with $A/(1 - e_0 - D)$ for aphelion appulses, to substitute $A(1 - e) - (1 + e_0)$ or $(1 - e_0) - A(1 + e)$ for S in Eq. (16), and subtract D from the numerators of Eqs. (25) and (26).

Angular deflection makes ultimately real crossing and collisions possible whose second-stage probabilities can be treated by the standard formulae.

The procedure which is here described, although not precise, will yield approximations which are close enough for practical use.

E. *Auxiliary Tables*

Table II contains cross section data calculated for the principal planets, to be used for assessing the probabilities of collision and orbital change. The radius and mass of the particle are assumed to be zero, and the calculations have been made according to Eqs. (8) and (15)-(18). With Eqs. (6) and (9), the interpolated value of $s^2 = S^2$ from the table yields then the probability of physical collision, and with $s^2 = \sigma^2 = S^2 \times (\sigma^2/S^2)$ the same equations yield the probability of a full deflection in angle. The table contains also the relative probabilities (θ) of ejection and deflection to crossings with other planets.

Deflection to a close passage by the sun is also of special interest, from the standpoint of survival of the particle. The limiting condition for such a deflection is summarized in the second line of Table III. The table lists the extreme limits of heliocentric distance attainable through repeated encounters with a single planet as calculated from Eqs. (13) and (14).

TABLE II

COLLISION AND ANGULAR DEFLECTION PARAMETERS FOR CLOSE ENCOUNTERS[a, b]

	Mercury $R = 4.18 \times 10^{-5}$; $D = 4.38 \times 10^{-3}$; $\mu = 1.67 \times 10^{-7}$			Venus $R = 5.63 \times 10^{-5}$; $D = 0.0107$; $\mu = 2.45 \times 10^{-6}$			Earth $R = 4.26 \times 10^{-5}$; $D = 0.01148$; $\mu = 3.03 \times 10^{-6}$		
U	S^2 (10^{-9})	σ^2/S^2	$\theta\rightarrow$ (Jupiter)	S^2 (10^{-9})	σ^2/S^2	$\theta\rightarrow$ (Jupiter)	S^2 (10^{-9})	σ^2/S^2	$\theta\rightarrow$ (Jupiter)
0.10	3.15	12.2	—	30.7	21.4	—	27.7	35.3	—
0.15	2.37	3.32	—	15.3	10.1	—	13.3	17.6	—
0.20	2.10	1.21	—	10.1	5.32	—	8.28	9.87	—
0.25	1.98	0.534	—	7.56	3.05	—	5.96	6.07	—
0.30	1.90	0.269	—	6.22	1.85	—	4.68	3.90	0.019
0.35	1.87	0.148	—	5.40	1.17	0.056	3.92	2.57	0.111
0.40	1.84	0.089	0.065	4.87	0.771	0.135	3.48	1.76	0.183
0.4142	1.83	0.077	0.086	4.78	0.696	0.155	3.32	1.59	0.200
0.50	1.80	0.037	0.197	4.27	0.368	0.254	2.85	0.889	0.292
0.60	1.78	0.018	0.294	3.82	0.195	0.340	2.54	0.489	0.372
0.80	1.77	0.006	0.433	3.60	0.067	0.468	2.22	0.179	0.491
1.00	1.77	0.0024	0.536	3.45	0.029	0.564	2.07	0.079	0.666
1.50	1.75	0.0005	0.733	3.29	0.006	0.751	1.92	0.017	0.764
2.00	1.75	0.0002	0.893	3.23	0.002	0.907	1.89	0.005	0.916
2.4142	1.75	0.0001	1.000	3.22	0.001	1.000	1.86	0.003	1.000

	Mars $R = 1.48 \times 10^{-5}$; $D = 5.46 \times 10^{-3}$ $\mu = 3.24 \times 10^{-7}$				Jupiter $R = 8.90 \times 10^{-5}$; $D = 0.0782$; $\mu = 9.55 \times 10^{-4}$				
U	S^2 (10^{-10})	σ^2/S^2	$\theta\rightarrow$ (Jupiter)	$\theta\rightarrow$ (Earth)	S^2 (10^{-8})	σ^2/S^2	$\theta\rightarrow$ (∞)	$\theta\rightarrow$ (Earth)	$\theta\rightarrow$ (Saturn)
0.10	11.8	13.3	—	—	1700	298	—	—	—
0.15	6.43	5.38	—	0.135	757	432	—	—	0.077
0.20	4.57	2.52	—	0.225	425	438	—	—	0.224
0.25	3.72	1.30	0.033	0.279	273	391	—	—	0.308
0.30	3.26	0.730	0.134	0.314	189	340	—	—	0.369
0.35	2.98	0.432	0.209	0.340	140	290	—	—	0.418
0.40	2.78	0.276	0.269	0.357	107	250	—	—	0.458
0.4142	2.75	0.245	0.283	0.361	100	241	0.000	—	0.467
0.50	2.58	0.122	0.360	0.381	69.0	189	0.125	0.052	0.522
0.60	2.47	0.061	0.429	0.395	48.0	148	0.233	0.106	0.574
0.80	2.34	0.021	0.534	0.408	27.4	96.2	0.388	0.164	0.658
1.00	2.28	0.009	0.618	0.406	17.8	67.7	0.500	0.189	0.727
1.50	2.23	0.0015	0.786	0.381	8.36	33.6	0.708	0.195	0.864
2.00	2.21	0.0006	0.934	...	5.06	19.4	0.875	...	0.974
2.4142	2.21	0.0003	1.000	...	3.71	13.1	1.000	...	1.000

TABLE II (Continued)

	Saturn $R = 4.07 \times 10^{-5}$; $D = 0.0522$; $\mu = 2.86 \times 10^{-4}$				Uranus $R = 8.66 \times 10^{-5}$; $D = 0.0279$; $\mu = 4.37 \times 10^{-5}$					
U	S^2 (10^{-8})	σ^2/S^2	$\theta\rightarrow$ (∞)	$\theta\rightarrow$ (Jupiter)	S^2 (10^{-9})	σ^2/S^2	$\theta\rightarrow$ (∞)	$\theta\rightarrow$ (Saturn)	$\theta\rightarrow$ (Jupiter)	$\theta\rightarrow$ (Neptune)
0.10	234	675	—	—	75.8	1330	—	—	—	—
0.15	104	652	—	...	34.7	878	—	—	—	0.172
0.20	58.8	530	—	0.129	19.0	608	—	0.040	—	0.285
0.25	37.7	423	—	0.199	12.2	446	—	0.124	—	0.360
0.30	26.2	340	—	0.244	8.47	343	—	0.180	—	0.415
0.35	19.3	278	—	0.276	6.25	270	—	0.220	0.016	0.458
0.40	14.8	233	—	0.300	4.81	219	—	0.248	0.065	0.495
0.4142	13.9	222	0.000	0.306	4.48	208	0.000	0.255	0.077	0.504
0.50	9.53	169	0.125	0.330	3.10	153	0.125	0.285	0.132	0.562
0.60	6.67	128	0.233	0.348	2.18	113	0.233	0.307	0.174	0.605
0.80	3.83	80.2	0.388	0.364	1.26	68.3	0.388	0.328	0.217	0.684
1.00	2.51	55.2	0.500	0.366	0.833	45.3	0.500	0.333	0.234	0.749
1.50	1.20	23.2	0.708	0.346	0.411	20.0	0.708	0.316	0.231	0.878
2.00	0.750	14.2	0.875	...	0.264	10.5	0.875	...	...	0.980
2.4142	0.568	9.2	1.000	...	0.204	6.55	1.000	...	...	1.000

	Neptune $R = 5.89 \times 10^{-5}$; $D = 0.0294$; $\mu = 5.08 \times 10^{-5}$					
U	S^2 (10^{-9})	σ^2/S^2	$\theta\rightarrow$ (∞)	$\theta\rightarrow$ (Uranus)	$\theta\rightarrow$ (Saturn)	$\theta\rightarrow$ (Jupiter)
0.10	59.7	2160	—	—	—	—
0.15	26.6	1450	—	0.100	—	—
0.20	15.0	1010	—	0.204	—	—
0.25	9.57	745	—	0.262	—	—
0.30	6.66	577	—	0.300	0.000	—
0.35	4.89	457	—	0.326	0.058	—
0.40	3.78	369	—	0.346	0.102	—
0.4142	3.50	352	0.000	0.350	0.114	—
0.50	2.42	260	0.125	0.371	0.164	0.041
0.60	1.69	193	0.233	0.386	0.200	0.095
0.80	0.964	119	0.388	0.398	0.239	0.156
1.00	0.631	80.0	0.500	0.398	0.253	0.182
1.50	0.300	37.2	0.708	0.407	0.384	0.190
2.00	0.184	20.6	0.875	...	...	...
2.4142	0.137	13.4	1.000	...	...	...

[a] R = radius of planet, S = target radius for physical collision, σ = target radius for full deflection, D = radius of sphere of action, all in units of the planet's mean heliocentric distance; μ = mass of the planet, in solar units; θ = relative probability of orbital change ($\rightarrow\infty$, escape to infinity; $\rightarrow$ planet, to crossing with another planet)

[b] Symbols: —, combination nonexistent; ..., combination not calculated.

TABLE III

MINIMUM AND MAXIMUM ATTAINABLE HELIOCENTRIC DISTANCES FROM CLOSE ENCOUNTERS WITH ONE PLANET

U:	0.00	0.05	0.10	0.15	0.20	0.25	0.30	0.35	0.40	0.4142	0.50	0.60	0.80	$\geqslant 1.00$
$Q_{\min}$:	1.000	0.822	0.681	0.566	0.471	0.382	0.325	0.268	0.220	0.207	0.143	0.087	0.020	0.000
$Q'_{\max}$:	1.000	1.228	1.531	1.952	2.571	3.572	5.452	10.27	49.00	∞	∞	∞	∞	∞

For small values of Q, instead of Eq. (14), the approximation

$$Q_{\min} = \tfrac{1}{2}(1 - U)^2 \tag{28}$$

holds closely.

Table IV contains the probability factors as defined by Eq. (15) and calculated from Eq. (20a) for deflection to a perihelion distance of $Q_{\min} \leqslant 0.0054$. With respect to Jupiter, this corresponds to a distance of 0.028 A.U. or six solar radii, where the equilibrium black-body temperature of a sphere is 1670°K, likely to lead to rapid destruction of small solid bodies.

TABLE IV

RELATIVE PROBABILITY OF DEFLECTION TO PERIHELION DISTANCE 0.0054 AND OF EJECTION TO INFINITY

U:	$\leqslant 0.896$	0.9	1.0	1.2	1.5	>1.8
$\theta(0.0054)$:	0	0.0012	0.0270	0.0134	0.0042	Hyperbolic only
$\theta(\infty)$:	$\leqslant 0.445$	0.447	0.500	0.592	0.708	...

According to Table IV, the probabilities of ejection, and their range of U (> 0.4142), are so very much greater than those of deflection to a small heliocentric distance that few objects in an existing population can be expected to have undergone excessive heating in close approaches to the sun. This has an important bearing on the interpretation of the life history of meteorites.

III

DYNAMICAL PROBABILITIES OF ELIMINATION FOR COMETS AND RELATED OBJECTS

A. *Multiple Crossings*

The total probability of an event, depending on crossings with several planets, is conventionally assumed to be equal to the sum of the probabilities for each separate crossing. The interaction of the crossings, in making possible orbital

changes which are not allowed by single crossings, is provisionally not taken into account for reasons put forward in Section II, A. This interaction, or "playing ball" with the crossing particle, can be considered as a second step (Öpik, 1951, 1961a). Deflection to a crossing with a much larger planet (Jupiter) is practically equivalent to elimination of the particle from the original population, because of the much greater probability of encounter and shorter lifetime relative to the large planet.

If P_k [Eq. (9)] is the probability for one crossing of an event leading to the termination of existence of the particle (either destruction or elimination from the original environment), the total probability or inverse lifetime is given by

$$1/\tau = P_0 = \sum P_k \tag{29}$$

and the partial probability of one particular event (collision with a planet, ejection to infinity, deflection to a crossing with a larger planet) is defined as

$$j_k = P_k/P_0. \tag{30}$$

This is a true probability, conforming to its mathematical definition, whereas the P-values as used here are actually mathematical expectations.

B. *Dynamical Probabilities of Survival for Selected Lists of Objects*

Tables V-VII contain the results of calculations for typical comets and some groups of asteroids which (Apollo group) may be partly related to comets (cf. next section). In the tables, U is the relative velocity in a crossing, in units of the mean orbital velocity of the planet, calculated according to Eq. (5). j_c is the relative probability of collision, j_∞ (Table V) the probability of ejection to infinity, j_J (Table VI) of deflection to Jupiter's crossing (equivalent to elimination from the terrestrial group), J_E (Table VII) of deflection to Earth's crossing (equivalent to elimination from Mars group and transfer to terrestrial group), all as defined by Eqs. (30) and (29). τ is the lifetime, defining the fraction χ_t of the original population surviving after an interval t as

$$\chi_t = \exp(-t/\tau). \tag{31}$$

The survival probabilities for all crossings combined are

$$J_c = \sum j_c, \qquad J_\infty = \sum j_\infty, \qquad J_J = \sum j_J \tag{32}$$

denoting the total probabilities of collision, of ejection to infinity, and of deflection to Jupiter's crossing, respectively. In table VII, only j_E is given; the relative probability of physical collision with Mars is then

$$j_c = 1 - j_E. \tag{33}$$

TABLE V

DYNAMICAL PROBABILITIES OF ELIMINATION FOR SELECTED OBJECTS IN CROSSINGS WITH JUPITER

Object	944 Hidalgo	Comet 1939 IV Väisälä	Comet 1942 II Väisälä	Comet Giacobini-Zinner (Giacobinids)	Comet 1866 I Tempel (Leonids)	Comet 1862 III Tuttle (Perseids)	Comet Halley (η Aquarids, Orionids)
Diam. nucleus (km)	45.	...	...	1.1 c	...	13. c	11. c
Period (yr)	13.9	10.52	85.5	6.59	32.2	119.6	76.0
$a(1-e)$ (A.U.)	1.995	1.752	1.287	0.995	0.977	0.963	0.587
$a(1+e)$ (A.U.)	9.59	7.85	37.53	6.02	19.67	47.60	35.31
i (deg)	41.0	11.3	38.0	30.8	162.7	113.6	162.2
			Venus crossing				
U	—	—	—	—	—	—	2.32
j_c	—	—	—	—	—	—	0.006
j_∞	—	—	—	—	—	—	0.0000
			Earth crossing				
U	—	—	—	0.694	2.35	2.01	2.23
j_c	—	—	—	0.001	0.009	0.007	0.003
j_∞	—	—	—	0.0003	0.0000	0.0000	0.0000
			Jupiter crossing				
U	0.966	0.677	1.281	0.729	1.91	1.81	1.90
j_c	0.021	0.026	0.031	0.027	0.044	0.043	0.044
j_∞	0.711	0.974	0.893	0.972	0.805	0.844	0.816
			Saturn crossing				
U	0.747	—	1.305	—	1.71	1.72	1.77
j_c	0.008	—	0.005	—	0.008	0.006	0.007
j_∞	0.260	—	0.060	—	0.119	0.091	0.104
			Uranus crossing				
U	—	—	1.201	—	1.32	1.57	1.55
j_c	—	—	0.0002	—	0.001	0.0003	0.0006
j_∞	—	—	0.004	—	0.015	0.003	0.006
			Neptune crossing				
U	—	—	1.073	—	—	1.40	1.30
j_c	—	—	0.0002	—	—	0.0003	0.0006
j_∞	—	—	0.008	—	—	0.006	0.012
			All crossings				
J_c	0.029	0.026	0.036	0.028	0.062	0.057	0.061
J_∞	0.971	0.974	0.964	0.972	0.938	0.943	0.939
τ (10^6 yr)	2.27	0.340	37.	0.504	14.0	162	38.

TABLE VI

DYNAMICAL PROBABILITIES OF ELIMINATION FOR OBJECTS IN MULTIPLE CROSSINGS WITH TERRESTRIAL PLANETS (COMPLETE LIST)

Object	Encke's Comet (Taurids)	Comet 1949 III Wilson Harrington	Geminids	Apollo	Adonis	Hermes
d (km)	1.7 c	5.9	—	1.0	1.3	0.4
a (A.U.)	2.22	1.746	1.38	1.49	1.97	1.29
$a(1-e)$	0.338	1.0276	0.140	0.65	0.44	0.68
$a(1+e)$	4.10	2.47	2.62	2.34	3.51	1.90
i (deg)	12	2.2	24	6	1.5	5
			Mercury crossing			
U	0.581	—	1.10	—	0.459	—
j_C	0.27	—	0.23	—	0.02	—
j_J	0.002	—	0.000	—	0.0001	—
			Venus crossing			
U	0.924	—	1.17	0.400	0.754	0.319
j_C	0.42	—	0.44	0.58	0.40	0.61
j_J	0.009	—	0.007	0.060	0.017	0.000
			Earth crossing			
U	1.000	0.219	1.16	0.574	0.856	0.485
j_C	0.25	0.772	0.28	0.26	0.48	0.29
j_J	0.013	0.000	0.011	0.052	0.040	0.072
			Mars crossing			
U	1.029	0.430	1.07	0.597	0.896	0.455
j_C	0.03	0.214	0.04	0.04	0.04	0.03
j_J	0.000	0.014	0.000	0.001	0.0003	0.002
			All crossings			
J_C	0.975	0.986	0.983	0.884	0.943	0.926
J_J	0.025	0.014	0.017	0.116	0.057	0.074
τ (10^6 yr)	265.	330.	245.	64.	68.	39.

TABLE VI (*continued*)

Object	Icarus	1950 DA	Geographos 1951 RA	1948 OA	1948 EA
d (km)	1.4	1.3	2.8	4.8	6.3
a (A.U.)	1.08	1.65	1.24	1.38	2.26
$a(1-e)$	0.19	0.84	0.83	0.77	0.89
$a(1+e)$	1.98	2.46	1.65	1.98	3.63
i (deg)	23	12	13	10	18
			Mercury crossing		
U	0.979	—	—	—	—
j_C	0.22	—	—	—	—
j_J	0.0003	—	—	—	—
			Venus crossing		
U	1.040	—	—	—	—
j_C	0.44	—	—	—	—
j_J	0.009	—	—	—	—
			Earth crossing		
U	1.004	0.449	0.382	0.443	0.696
j_C	0.28	0.73	0.71	0.72	0.81
j_J	0.014	0.21	0.22	0.22	0.11
			Mars crossing		
U	0.827	0.556	0.342	0.462	0.809
j_C	0.04	0.06	0.07	0.06	0.08
j_J	0.0004	0.002	0.006	0.004	0.0008
			All crossings		
J_C	0.976	0.787	0.781	0.784	0.890
J_J	0.024	0.213	0.219	0.216	0.110
τ (10^6 yr)	165.	272.	152.	185.	1010.

The diameters of asteroids and of the nucleus of Comet 1949 III (where the magnitude of the nucleus was observed) are calculated on the assumption of a lunar albedo (Öpik, 1951), according to Eq. (40). For a few comets which have their integrated magnitude derived by a standard procedure, the few diameters of the nuclei are tentatively derived from Eq. (50) with $C = 2.18$; these diameters are marked with the letter c.

TABLE VII

DYNAMICAL PROBABILITIES OF ELIMINATION FOR OBJECTS IN SINGLE CROSSINGS WITH MARS (COMPLETE LIST)

Object	d (km)	$a(1+e)$	U	τ (10^9 yr)	j_E
132 Aethra	89	3.61	0.512	24.5	0.042
323 Brucia	54	3.10	0.470	22.0	0.058
391 Ingeborg	30	3.03	0.447	15.4	0.068
433 Eros	20	1.78	0.289	1.84	0.205
475 Ocllo	35	3.58	0.444	20.5	0.071
699 Hela	23	3.68	0.392	17.9	0.097
719 Albert	5.2	3.98	0.502	7.56	0.045
887 Alinda	6.2	3.89	0.510	6.62	0.043
985 Rosina	14	2.98	0.210	3.68	0.353
1009 Sirene	5.2	3.82	0.437	10.8	0.074
1011 Laodamia	10	3.23	0.266	4.48	0.242
1036 Ganymed	59	4.10	0.661	16.4	0.019
1131 Porzia	8.7	2.93	0.200	2.87	0.362
1134 Kepler	6.6	3.94	0.442	11.1	0.068
1139 Atami	12	2.44	0.298	4.03	0.190
1170 Siva	22	3.02	0.479	18.8	0.055
1198 Atlantis	5.2	3.00	0.228	1.84	0.316
1204 Renzia	13	2.93	0.205	3.17	0.353
1221 Amor	1.8	2.76	0.483	5.31	0.053
1235 Schorria	6.8	2.21	0.486	10.5	0.054
1293 Sonja	12	2.83	0.190	3.24	0.374
1310 Villigeria	28	3.24	0.487	17.5	0.051
1316 Kasan	11	3.18	0.460	17.3	0.064
1374 Isora	11	2.87	0.221	4.83	0.333
1468 Zomba	11	2.86	0.281	8.52	0.214
1474 Beira	26	4.07	0.619	15.8	0.022
1508 1938 UO	10	3.93	0.609	29.8	0.022
1580 Betulia	4.4	3.44	1.006	17.8	0.003
... 1950 LA	3.5	2.28	0.578	7.55	0.028
... 1951 SA	40	4.02	0.415	10.7	0.083
... 1953 EA	0.6	3.85	0.666	14.2	0.019
... 1953 RA	8	3.26	0.452	6.85	0.067
... 1951 QZ	11	3.08	0.232	2.14	0.326
... 1957 NA	5.5	2.59	0.421	4.02	0.078
1929 SH		Identical with 1957 NA			

The tables are grouped according to the type of orbital elements and crossings, as these alone determine the dynamical survival without regard to the physical properties of the bodies (except when they are very small and influenced by radiation pressure and drag).

Table V contains only objects crossing Jupiter's orbit. The condition turns out to be equivalent to a selection of comets, and of meteor streams related to comets. The majority of periodic comets could have been incorporated in the table but for a few cases, completely listed in Tables VI and IX. The only apparently noncometary object of this qualification is the asteroid Hidalgo; however, there are no reliable indications as to its physical nature; it could well be an inactive cometary nucleus, rather than a runaway asteroid. As compared with a former publication where only physical collisions were considered (Öpik, 1951), the total probabilities of elimination of the objects of Table V are much greater and the lifetimes shorter, as a consequence of elimination by angular deflection in Jupiter's gravitational field.

On the other hand, for the objects of Table VI crossing only the orbits of the terrestrial planets the angular deflection is relatively insignificant, especially at high velocities, so that physical collisions dominate the process of elimination. This is even more true of the objects of Table VII in single crossings with Mars.

It is significant that the condition of selection by Jupiter crossing in Table V yields numerous comets but only one doubtful asteroid Hidalgo. This is explained by the short lifetime of asteroidal objects (i.e., those of moderate inclination and eccentricity) in Jupiter crossings (cf. the second and fourth entires of Table V), so that they are eliminated much faster than their rate of injection into the Jupiter group. On the other hand, the rate of injection into the group of comets by capture from the nonperiodic complex (Oort, 1950) is very much higher than from the asteroidal population, so that many of the captured comets are still observable and prevail in the list, despite their rapid disappearance.

C. *Dynamical Survival of Comets in Incomplete or Near Crossing with Jupiter*

Tables VIII-X contain data for objects in partial crossing or in near appulses to Jupiter, calculated with the aid of the rules and equations of Section II, D. In the case of Jupiter, the two-body approximation of close encounters is no longer satisfactory; it is even less so for imperfect crossings. Nevertheless, the calculated lifetimes for a given set of orbital elements still may be reliable to within 30-50%. The objects of these tables are especially important in evaluating possible relationships between comets and asteroids; for this purpose the knowledge of the survival time scales to a close order of magnitude is quite sufficient.

For the objects of Table IX, collisions with Jupiter are not allowed immediately, but become possible as a consequence of orbital change through angular deflection; the probabilities of collision were calculated therefore as a second step. In view of orbital change, these objects are only temporarily inside Jupiter's

TABLE VIII

DYNAMICAL PROBABILITIES OF ELIMINATION OF COMETS IN PARTIAL CROSSINGS WITH JUPITER, $0 < f < 0.5$, $4.94 \leq a(1+e) \leq 5.20$ (COMPLETE LIST)[a]

Object	Period (yr)	$a(1+e)$	$a(1-e)$	i (deg)	U	τ (10^6 yr)	τ_σ (10^3 yr)	J_c	J_∞
De Vico-Swift	5.86	5.11	1.39	3.0	0.386	0.93	3.4	1.00	0.00
Holmes	6.86	5.10	2.12	20.8	0.408	5.5	22.	1.00	0.00
Whipple	7.41	5.15	2.45	10.2	0.272	1.5	4.1	1.00	0.00

[a] τ = total lifetime; τ_σ = time of 90° deflection in angle.

perihelion; for about 70% of their lifetime they are expected to be crossing with Jupiter. From this standpoint, there is little difference between the objects of Table VIII and Table IX. However, Comets De Vico-Swift and Tempel (1) have periods in near commensurability of $\frac{1}{2}$ with Jupiter's and may be relatively stable, as are 525 Adelaide and other asteroids discussed in the following Section III, D. In such a case the calculated lifetimes and probabilities do not apply to these two objects.

The elements of Comet Oterma (Table IX) are changing in a very peculiar manner during close approaches to Jupiter (Oterma, 1958); of the three calculated orbits, only one (1965) is a close appulse according to our conventional definition; only for this was a calculation made and the probability divided by 3, to obtain a kind of average for all three calculated orbits. The case is on the borderline of application of our schematically defined probabilities.

TABLE IX

DYNAMICAL PROBABILITIES OF ELIMINATION OF COMETS IN CLOSE APPULSES TO JUPITER'S PERIHELION, $4.94 \geqslant a(1+e) \gtrsim 4.54$ (COMPLETE LIST)[a]

Object	Period (yr)	$a(1+e)$	$a(1-e)$	i (deg)	U	τ (10^6 yr)	τ_σ (10^3 yr)	J_c	J_∞
Grigg-Skjellerup[b]	4.90	4.92	0.85	17.6	0.587	0.21	50.	0.02	0.98
Tempel (2)	5.31	4.70	1.39	12.4	0.404	4.4	80.	1.00	0.00
Neujmin (2)	5.43	4.84	1.34	10.6	0.442	0.63	30.	0.11	0.89
Tempel (1)	5.98	4.82	1.77	9.8	0.367	3.5	16.	1.00	0.00
Schwassmann-Wachmann	6.53	4.83	2.15	3.7	0.318	1.2	3.6	1.00	0.00
Oterma (1934)	18.0	8.07	5.65	2.9	0.148				
Oterma (1950)	7.9	4.54	3.40	4.0	0.100	1.6[c]	0.8[c]	1.00	0.00
Oterma (1965)	19.21	8.99	5.35	1.9	0.145				

[a] Cf. Table VIII for notations.

[b] Diameter of nucleus = 0.4 km, from Eq. (50).

[c] Averaged over the three orbits.

TABLE X

WOULD-BE[a] DYNAMICAL PROBABILITIES OF ELIMINATION OF ASTEROIDS IN CLOSE APPULSES TO JUPITER'S PERIHELION, 4.94, $> a(1 + e) >$ 4.54. REPRESENTATIVE SAMPLES[b]

Object	$a(1 + e)$	i	U	τ (10^6 yr)	τ_σ (10^3 yr)	J_c	J_∞
153 Hilda	4.59	8.7	0.179	0.68	1.5	1.00	0.00
499 Venusia	4.84	3.9	0.195	0.92	2.2	1.00	0.00
525 Adelaide	4.58	2.1	0.221	0.22	0.6	1.00	0.00
1038 Tuckia	4.88	8.4	0.249	2.7	10.	1.00	0.00

[a] The close appulses, however, apparently cannot take place, on account of near commensurability of the periods of planet and Jupiter and ensuing preventive perturbations, as in the case of Pluto with respect to Neptune (Öpik, 1961a), so that the lifetimes are extended indefinitely.

[b] Cf. Table VIII for notations.

D. *Asteroids in Close Appulses to Jupiter*

These are selected on the basis of their aphelia being potentially within the sphere-of-action distance from Jupiter's perihelion; a complete list is given in Table XI, with the omission of Hidalgo which belongs to a different group (Table V).

Fourteen out of fifteen entries of Table XI belong to the Hilda family of asteroids, with the periods of revolution in a near commensurability ratio of 2/3 to that of Jupiter (cf. fifth column of the table); the only exception is 525 Adelaide, with a period ratio close to 1/2.

The lifetimes of representative objects of this group, calculated by the conventional methods, are given in Table X. Although at present none of these objects trespasses over Jupiter's perihelion of 4.94, it is conceivable that but a slight deflection in angle of the U-vector would bring them into real crossing with Jupiter, when physical collision becomes possible. The probability of collision, p_c, is then calculated as a second step from the probability of angular deflection, p_σ, from

$$p_c = f\theta_J p_\sigma S^2/\sigma^2$$

in former notations, with $\theta_J = 0.70$ very closely and $f = 0.5$ as for half-crossing.

The lifetimes (fifth column of Table X), of the order of one million years, are surprisingly short as compared with the time scale of the solar system. The objects would have been eliminated in the very beginning of the solar system if the calculated probabilities were valid.

TABLE XI

COMPLETE LIST OF ASTEROIDS IN WOULD-BE APPULSES TO JUPITER'S PERIHELION
$a(1+e) \geq 4.54$[a]

Object	d (km)	a	$a(1+e)$	n/n_J	n'/n'_J	$L_a-12°$ (deg)	$L_c-12°$ (deg)	ΔL_c (deg)	T_{ac} A.D.
153 Hilda	150	3.975	4.59	1.497	1.018	−143	−70	+4	1520
190 Ismene	200	3.947	4.61	1.513	1.004	89	74	−18	1930
361 Bononia	110	3.936	4.77	1.519	0.959	−19	106	−26	2070
499 Venusia	125	3.963	4.84	1.503	0.915	−11	18	−4	2110
525 Adelaide	58	3.340	4.58	1.944	0.936	90	−63	+21	1990
748 Simeisa	98	3.934	4.65	1.520	0.990	−7	132	−28	2070
958 Asplinda	68	3.934	4.66	1.520	0.960	−32	60	−28	2030
1038 Tuckia	49	3.917	4.88	1.530	0.891	115	−12	−41	1870
1180 Rita	74	3.988	4.69	1.486	0.910	24	−124	+21	2110
1202 Marina	59	3.930	4.74	1.522	0.948	123	−46	−30	1820
1212 Francette	55	3.965	4.68	1.502	0.978	162	170	−3	2020
1345 Potomac	76	3.968	4.66	1.501	0.984	47	96	−1	3100
1512 1939 FE	38	3.955	4.63	1.508	1.000	55	−112	−10	1550
1529 1938 BC	32	3.996	4.76	1.485	0.945	111	−7	+22	2060
1578 Kirkwood	17	3.959	4.84	1.506	0.915	174	50	−9	1610

[a] n/n_J = ratio of mean motion to Jupiter's; n'/n'_J = ratio of angular motion in aphelion to that of Jupiter in perihelion; L_a = longitude of aphelion; L_c = longitude of conjunction nearest to epoch; 12° = longitude of Jupiter's perihelion; ΔL_c = displacement in longitude per conjunction; T_{ac} = nearest epoch of conjunctions in aphelion.

In addition, within time intervals of the order of τ_σ (sixth column of Table X), or a few thousand years, the exclusive distribution of the aphelia would be upset completely, about 70% being expected to reach beyond 5.20 A.U., Jupiter's mean distance. This certainly is not the case, and the absence of larger aphelia can in no way be ascribed to observational selection. Eighty per cent of the objects of Table XI exceed in diameter (actually brightness) the lone exception, Hidalgo (Table V); if the latter were an escaped asteroid, larger and more easily observable objects in similar orbits should exist, which apparently is not the case. Besides, the lifetime of Hidalgo as an object in twofold crossing with Jupiter and Saturn is definitely short and cannot refer to a case of "long storage," whatever the commensurability ratio of the present period with Jupiter's (Öpik, 1961a).

We conclude that, by some interplay of perturbations in nearly commensurable periods, the asteroids of Table XI are not only virtually stable, but even their aphelia are somehow made to comply with the limit of Jupiter's perihelion. The mechanism preventing close approaches of these objects to Jupiter may be similar to that of Pluto with respect to Neptune (Öpik, 1961a), more com-

plicated owing to the greater relative extent of the sphere of action of Jupiter, as compared with Neptune's. The mechanism is directly related to close commensurability of the periods (Öpik, 1961a).

Orthodox methods of celestial mechanics seem to fail in the case of these objects. Thus, if Chebotarev's calculations (1953; Chebotarev and Boshkova, 1954) of secular perturbations of the asteroids of the Hilda family are taken at their face value, we would be made to believe that the present statistical picture of their orbital elements, including near commensurabilities of the mean motions and the limitation of the aphelia to less than 4.94 A.U., is a rare coincidence, valid only for our time ± 100 years. A few hundred years before or after, the mean motions and aphelia, according to Chebotarev, would have been spreading over a wide range of values, without any trace left of the present statistical regularity. The probability of the present peculiar distribution to have taken place accidentally is less than $(\frac{1}{3})^{15}$ for the mean motions, less than $(\frac{1}{2})^{15}$ for the aphelia, or a total probability of less than 10^{-12}. It is not reasonable to accept such an improbable coincidence. Clearly, Chebotarev's calculations of secular perturbations of the planets of the Hilda family, made by expanding into exponential and trigonometric series of time as the only variable, cannot be valid over time intervals exceeding 100 years (Öpik, 1961a).

A method of calculation which would give realistic results consists in numerical integrations of the space motion of these objects, and not of abstractions such as orbital elements. The relative accuracy of the integrations need not be excessively high; a nominal accuracy of 10^{-6} would suffice. If automatic regulation of the orbits and close approaches exists, it will reveal itself in the calculations despite errors. In other words, the mechanism of regulation will respond equally to true imperfections in the orbital elements, as well as to spurious imperfections caused by the method of calculation. A spurious divergence of mean longitude and other rotating elements with time may result, but the (a, e, i) set of elements must keep within definite limits in spite of errors of calculation.

IV

GENETIC RELATIONSHIPS OF COMETS AND ASTEROIDS

A. *Origin of Comets and Structure of Nuclei*

It is almost impossible to conceive how the cloud of comets, situated at 5×10^4 to 1.5×10^5 A.U. from the sun (Oort, 1950), could have come there into being by condensation of diffuse matter; under any reasonable assumptions as to the original mass (1 solar mass) and density of the solar nebula (less than 10^{-22} gm/cm^3), and with the low molecular velocities at these distances and

low temperatures, of the order of 10^4 cm/sec for the component normal to the accreting surface (the relative orbital velocity (10^3 cm/sec) being negligible), the maximum size of solid particles accreted in four billion years could have been of the order of 0.1 cm, and much less during the first few hundred million years of the formation of the solar system. The formation of comet nuclei 1-100 km in diameter is out of the question under these circumstances. They must have originated in much denser regions of space, closer to the sun.

From this standpoint, a suggestion by Oort (1950) that the comets are "minor planets escaped, at an early stage of the planetary system, from the ring of asteroids, and brought into large, stable orbits through the perturbing actions of Jupiter and the stars," deserves particular attention as the only consistent hypothesis of the origin of comets. In addition to Jupiter, it may be that primordial rings of asteroids from the vicinity of other planets may also have contributed to the cloud of comets. The formulas and tables of the two preceding sections can be used to describe quantitatively this process of escape, as well as the subsequent capture of these objects by Jupiter and the other planets into periodic orbits, when the mixing action of stellar perturbations (Oort, 1950; Öpik, 1932) happens to bring them back into the inner portions of the solar system. This, however, is not the purpose of the present investigation.

The common origin would imply some common properties in the physical structure of comets and asteroids. We do not know much about the physical structure of these bodies, except that asteroids must contain compact solid substance similar to that of meteorites, whereas comets must carry on their surfaces a mixture of ices and dust (Whipple's mixture, see 1950, 1951) which is not obviously present in the asteroids. If Oort's concept is correct, it is likely that the asteroidal fragments have acquired a coating of the icy conglomerate in the very beginning, when the temperature in their region was very low—the sun's radiation being screened off by intervening dust. Those fragments which were sent away to the distant regions of the solar system have retained their icy coating; they appear thus as comet nuclei, although their cores may be similar to the asteroids. The latter have lost their ices by evaporation, at least from near the surface, after the dust had cleared out of the inner portions of the solar system and solar radiation became effective.

The mechanical structure of comet nuclei still remains a mystery. In all probability, very different types of structure may exist. The old theory of a cluster of particles bound together by mutual gravitation and easily disrupted by tidal action near the sun is still upheld in some recent papers, although the role of collisions in leading to condensation of the cluster is not overlooked (Schatzman, 1953). Undoubtedly, small particles cannot account for the persistence of the gaseous emissions from comets over a great number of revolutions. These emissions must originate in bulky objects. Also, well-known cases of

comets splitting up into two or more components of a similar order of magnitude indicate that the number of components is small, and their sizes comparable. It is inadmissible to assume that the comets have split into several independent clusters. The centers of these division products must be bulky objects, not clusters which would have completely dispersed in the process of fission.

It appears to be plausible to assume that comets are not composed of clusters of small particles crossing each other's orbits; these must have been eliminated very soon in mutual collisions. What has survived of the original structure may be single or multiple bulky nuclei, orbiting in a regular manner without crossing, similar to the principal planets of the solar system, or to multiple star systems built on the hierarchical principle, i.e., with the orbital dimensions of successive members increasing by orders of magnitude (a close binary with a distant companion, etc.). Loss of mass by evaporation and tidal action may then lead to the observed fission.

Evaporation of the ices from a bulk nucleus may leave behind a giant dustball structure which, at a density of $\delta = 0.6$ gm/cm^3 and a minimum strength of the order of $s = 10^4$ dynes/cm^2, assumed equal to that observed in cometary dustball meteors (Öpik, 1956, 1958a), will withstand compression at the center from its own gravity (central pressure equals $\frac{1}{6}\pi G\delta d^2$, where G = gravitational constant) up to a diameter of $d = 7$ km.

With a conductivity as low as that of lunar dust, it can be shown that an icy conglomerate sphere of 2 km diameter may take 3×10^8 years to lose all its ices by evaporation if the dust is not removed from the surface. Exhausted or "dead" comet nuclei may thus exist as dustballs up to this limit of size, comparable to the members of the Apollo group (Table VI); beyond this size they may still possess an icy core surrounded by uncompacted dust layers.

The dustball structure of dead comet nuclei and, perhaps, of some asteroids may account also for a peculiar object, Comet Wilson-Harrington 1949 III (see Table VI), which entirely belongs to the Mars-earth space and is well separated from Jupiter's perihelion. The gravitational field of Mars is too weak to have achieved its caputre from the outside field with some probability; the relative velocity, $U = 0.430$, is high enough to permit an origin from Jupiter's crossing, but the time scale for capture from the Jupiter field, $\tau/j_J = 2.4 \times 10^{10}$ years, is rather long as compared with the total lifetime. On the other hand, interaction with the earth has a short enough time scale, but, on account of the low relative velocity, $U = 0.219$, encounters with earth cannot send this object to Jupiter's crossing (cf. Table III), nor could an object captured by the earth from Jupiter's field have a velocity less than $U = 0.29$. The object is thus almost completely isolated in terrestrial space.

As to the calculation of lifetime, Comet 1949 III does not cross the present orbit of the earth. The approach is, however, so close that variations in the

orbital eccentricity of the earth would make crossing possible even if the orbit of the object itself did not change. From calculated eccentricities over $\pm 400{,}000$ years (Matukuma, 1949) it follows that during 32% of the time the eccentricity of the earth's orbit exceeded $e_0 > 0.0276$ and had then a mean value of 0.0346. This gives $f = 0.32f'$, with $f' = 0.21$ according to Eqs. (24) and (25). The probability of collision with earth was then calculated according to Eq. (6).

It is thus improbable that Comet Wilson-Harrington was evern captured into terrestrial space from outside; this object may be an asteroid of the icy conglomerate type, with ices in the interior preserved and insulated by an outer dust layer. The impact of another asteroid or meteorite may have thrown open the interior, exposing the ices to direct heating and evaporation, with the ensuing cometary appearance.

A dustball structure of 2.2 km diameter can resist tidal disruption at grazing passage by the earth (Jeffreys, 1947; Öpik, 1950) by virtue of its cohesion; for compact ice the limit of diameter is 50-70 km; beyond a distance of four earth radii from the earth, or 2.5 solar radii from the sun (Roche's limit), dustball structures of any size will be held together by their own gravitation. Hence it is clear that even loosely bound compact nuclei can exist indefinitely, and that the observed breakup of some comets into separate nuclei only can be explained by these nuclei being separated beforehand, orbiting around the common center of gravity at distances which are much greater (100 times, to name a figure) than the diameters of the nuclei themselves. Some comet nuclei, at least, must consist of multiple gravitating systems with a small number of principal members; others may be single bulk bodies.

B. *Types and Physical Survival of Comet Nuclei*

In Table VI, there are listed eight known objects of the Apollo group, coexistent with and of similar orbital properties and dynamical age as the three cometary entries of the table (Encke's comet, the Germinids, and Comet 1949 III). There is some reason to suspect that their physical origin may also be similar, partly at least.

A cometary nucleus, or a proto-asteroid which, according to Oort's concepts, has become a comet, may have a structure of one of the following two basic types: type I, consisting entirely of Whipple's (1950, 1951) icy-dust conglomerate; and type II, consisting partly of solid meteorite chunks or even one solid nucleus, surrounded by the icy conglomerate. When becoming a periodic comet, the icy conglomerate partly evaporates in the sunlight, partly scatters as dust and dustball meteors, a process usually called disintegration. Type I may either disintegrate completely, leaving only meteoric matter dispersed in space

behind, or may survive as a giant dustball. Type II, after losing its volatile and dust coating, will become almost unobservable, but its solid meteoritic portion will continue in the orbit. In both cases the residual nuclei will appear as asteroids similar to the objects of the Apollo group, being only observable under favorable circumstances.

Whether the Apollo group is likely to contain such nuclei of dead or "disintegrated" comets can be decided statistically with the aid of the probabilities of elimination. The answer turns out to be in the positive. The apparent disintegration time of periodic comets is estimated to run into about 70 revolutions (Oort, 1950) or 10^3 years; although the figure is rather uncertain, it is sufficient to show that the rate of disintegration is certainly very much faster than that of dynamical elimination (time scale 10^6-10^8 years). Therefore, the number of dead nuclei of comets must exceed the number of live periodic comets of type II by many orders of magnitude. If all were of type II, the number of asteroids in cometary orbits would probably greatly exceed the actual number, as can be judged from the lists in Tables VI and V (Apollo group and Hidalgo). Although a definite estimate cannot be made, from the relative scarcity of Apollo type objects we have to conclude that most comet nuclei are of type I which disintegrate completely and that only a few are of type II, or of type I leading to a residual giant dustball.

The simultaneous existence of cometary nuclei of both types may be understood on the following working hypothesis. At an early stage in the inner portions of the solar nebula the temperature must have remained at a low level, on account of absorption by dust along the ecliptical plane; there the first objects to condense were planetesimals of the icy conglomerate type I. Some of them were ejected into the present cometary cloud. Others agglomerated further, forming sizable planets in which the conglomerate was ultimately differentiated into gas and solid rock. Before the nebula cleared, collisions were breaking up some of the planets, releasing asteroidal and meteoritic compact fragments which, after covering up with the hoar-frost of the icy mixture, were also partly ejected to the cometary cloud, thus forming nuclei of type II. Being of later origin, these may be expected to be less numerous than the nuclei of type I, and the composition of their conglomerates may also be different; the diversity of comet spectra and tails may be understood on these lines as a difference in early age.

C. *Dead Comet Nuclei and the Origin of the Apollo Group*

Excluding the three cometary objects of Table VI, comet Encke, the Germinids, as well as Comet Wilson-Harrington, the harmonic mean lifetime of the eight apparently asteroidal members of the Apollo group is found to equal

$$\bar{\tau}_A = [(1/\tau)_{av}]^{-1} = 1.02 \times 10^8 \text{ years.} \qquad (34)$$

If these were the remnants of a population *in situ* which has decreased exponentially according to Eq. (31), the original number 4500 million years ago would have been 2.5×10^{19} times greater and, allowing for the considerable incompleteness of the list due to observational limitations, would correspond to a total of 100 times the sun's mass. The absurdness of such an assumption is obvious. In any case, the survival since the beginning of the solar system of the three short-lived objects, Apollo, Adonis, and Hermes, would be as probable as a miracle.

We have to conclude therefore that the asteroids of the Apollo group are not permanent members of the space occupied by the terrestrial planets where they are now but, while they are eliminated chiefly by collisions on a time scale of 10^8 years, they are currently supplied from some source or sources, so that the balance of the population is maintained. Two sources can be thought of: the asteroidal belt and comets.

None of the aphelia of the regular asteroids reaches Jupiter's perihelion (Table XI), so that there is no crossing with the giant planet; this is readily explained by rapid elimination of crossing objects (Öpik, 1951). And, as has been pointed out in Section III, D, the present asteroids of the Hilda family must be virtually stable, otherwise they would have disappeared long ago. Also, none of the aphelia [$a(1 + e)$, Table VI] of the eight members of the Apollo group comes anywhere near Jupiter's orbit, the largest values being 3.51 and 3.63 A.U., well below those of the outer asteroids of Table XI. An origin from the asteroidal belt by way of Jupiter's perturbations thus seems to be excluded.

Next come the asteroids crossing Mars, an almost complete up-to-date list of which is given in Table VII. As can be seen from the τ-values, these are long-lived objects which could well have been present there since the origin of the solar system. The harmonic mean lifetime for the 34 asteroids listed is

$$\bar{\tau}_M = 6.02 \times 10^9 \text{ years} \tag{35}$$

and longer than the age of the solar system. According to Eq. (31), in 4500 million years their numbers must have decreased by 50%, so that about one-half of the original population may have survived in Mars crossings. Unlike the other terrestrial planets, the interaction cross section of Mars is small enough to make reasonably probable a prolonged coexistence with crossing asteroids.

Although collisions with Mars are the chief source of removal of these objects, a not negligible fraction (J_E, Table VII) is diverted to earth crossings and is thus injected into the Apollo group. From Table VII, the average value of j_E weighted by $1/\tau$ is

$$(j_E)_{av} = 0.211 \tag{36}$$

and the annual injection rate from the Mars asteroids (Table VII) into the Apollo group (Table VI) becomes

$$I_{ME} = 0.211\ N_M/\tau_M = 3.50 \times 10^{-11}\ N_M \tag{37}$$

where the numerical value of τ_M is substituted from Eq. (35); here N_M is the population of the Mars group. The annual loss from the Apollo group, corresponding to the lifetime defined by Eq. (34), is

$$L_A = 9.8 \times 10^{-9}\ N_A \tag{38}$$

where N_A is the population of the Apollo group.

Let L_{AM}, N_{AM} in Eq. (38) refer to that part of the population of the Apollo group which derives from the Mars group. If the limits of selection (e.g., by diameter) are the same and statistical equilibrium holds

$$L_{AM} = I_{ME}$$

whence, from Eqs. (38) and (37),

$$N_{AM} = 0.0036\ N_M. \tag{39}$$

Now, the selection limits of the two lists are not comparable and are strongly dependent on diameter. The Apollo group list goes down to a diameter of about 1.0 km, whereas the Mars group is equally complete (or incomplete) at about 5 km. We may attempt an evaluation of the selection effects.

For the Mars group we may use statistical data on apparent magnitudes of asteroids in general. It has been found concordantly by different authors (Stroobant, Baade, Putilin, Öpik) that the increment in cumulative numbers (i.e., total sum down to a certain diameter) of asteroids in the observed range of size proceeds nearly with the 1.6 power of the limiting diameter (population index = 1.6) (Öpik, 1960). By extrapolation of the numbers with the aid of this index (which requires a trebling of the number for a decrease to one-half of the diameter) and basing on the number of large diameters assumed to be listed completely, the data of Table XII are obtained.

Taking $N_M = 1215$ for $d \geqslant 1.05$ km, according to the last line of Table XII, Eq. (39) yields an equilibrium population of the Apollo group, $N_{AM} = 4.4$, as maintained by injection from the Mars asteroids.

The number listed in Table VI with $d \geqslant 1.0$ km is 7 which would seem to be close enough to the expectation. Actually, however, the list of the Apollo group cannot be complete; there are undoubtedly many more undiscovered objects in the group. The selection effects are difficult to allow for, but their order of magnitude may be estimated as follows. The present list of the Apollo

TABLE XII

SELECTION BY SIZE IN MARS GROUP OF ASTEROIDS

Limits of diameter (km):	>68	34-68	17-34	8.5-17.0	4.2-8.5	2.1-4.2	1.05-2.1	0.52-1.05
Number in list, first half:	1	3	4	4	5	0	0	0
Number in list, second half:	0	1	2	7	4	1	1	1
Total number in list:	1	4	6	11	9	1	1	1
Observed cumulative number:	1	5	11	22	31	32	33	34
Extrapolated true cumulative number	1	5	15	45	135	405	1215	(3645)

group is mainly due to charting with the 48-in. Mount Palomar Schmidt. For the sake of simplicity we assume that the sky has been efficiently covered twice with this instrument to a limiting magnitude 18.5 for a moving object at 2.0 A.U. geocentric distance. This probably exaggerates the completeness of coverage. With lunar albedo, the conventional diameter (d in km) of an object of apparent magnitude m in mean opposition is

$$\log d = 3.63 + \log r\Delta - 0.2\, m \tag{40}$$

where r and Δ are heliocentric and geocentric distance in A.U., respectively (Öpik, 1951). Allowing for the effect of motion on the photographic plate, the photographic image intensity varies as Δ^{-1}, not as Δ^{-2}, with geocentric distance, and the limiting minimum diameter of an asteroid, observable with a given instrumental set, thus varies with the two distances as

$$d_{\min} \sim r\Delta^{1/2}. \tag{41}$$

Setting $r = 1$, $\Delta = 1$, $m = 18.5$ in Eq. (41), $d_{\min} = 0.8$ km obtains at the unit distances for opposition; under an average phase angle of 30° this reduces somewhat to perhaps $d_{\min} = 1.2$ km as an effective limit. Hence, according to Eq. (41),

$$d_{\min} = 1.2\, r\Delta^{1/2} \tag{41a}$$

in km, for r and Δ in A.U.

On account of phase effects, the discovery of the fainter asteroids can take place mainly when they are outside the earth's orbit, $r > 1$, $\bar{r} = 1 + 0.5\Delta$, whence

$$d_{\min} = 1.2(1 + 0.5\Delta)\Delta^{1/2}. \tag{42}$$

If V_0 is the total volume of space effectively occupied by the asteroids, and V is the volume covered by observation, the "coefficient of perception" or the relative completeness of the resulting list of discoveries is

$$\eta = 1 - \exp(-V/V_0). \tag{43}$$

For asteroids of the Apollo group moving between effective distances of $q = 0.7$ and $q' = 2.0$ A.U., the volume occupied is approximately

$$V_0 = \tfrac{4}{3}\pi[(q')^3 - q^3] = 32(A.U.)^3. \tag{44}$$

For an observing distance Δ and double coverage of the sky

$$V = \tfrac{8}{3}\pi\Delta^3 \doteq 8\Delta^3. \tag{45}$$

Hence

$$\eta = 1 - \exp(-\tfrac{1}{4}\Delta^3) \tag{46}$$

and this is linked to the minimum diameter by way of Eq. (42). Hence follows the coefficient of perception of the Apollo list depending on diameter as given in Table XIII.

TABLE XIII

COEFFICIENT OF OBSERVATIONAL SELECTION, η, FOR APOLLO ASTEROIDS

Δ (A.U.):	0.1	0.2	0.3	0.4	0.6	0.8	1.0	1.5	2.0
η:	2.5×10^{-4}	0.0020	0.0068	0.016	0.054	0.13	0.22	0.57	0.86
d_{min} (km):	0.40	0.59	0.76	0.91	1.15	1.50	1.80	2.57	3.39

Statistics of the small number of Apollo asteroids cannot be very significant; nevertheless, with population indices of $s = 2.7$ (probable value, see Öpik, 1960) and 1.6 (asteroidal), the idealized distribution of the objects is found to be as in Table XIV. Here n is the idealized true relative number of objects (to an arbitrary factor of proportionality), η the average coefficient of perception according to Table XIII, and $\eta\ n$ the expected number of observed objects.

For a population index of $s = 2.7$, $d \geqslant 1.0$ km, the probable ratio of the true number to the number of discovered objects is $27.5/4.63 = 6.1$; for $s = 1.6$, it is $16.52/4.79 = 3.5$. The case $s = 2.7$ is in better agreement with the observed distribution of diameters. It means that the 7 objects of the Apollo group with $d > 1.0$ km represent a true population of about $N_A = 7 \times 6.1 = 43$. The estimate probably errs on the lower side. The fact that each of the asteroids of the Apollo group has been observed only once, by mere chance at discovery, and then hopelessly lost, would indicate that only a very small fraction of them is presently known.

TABLE XIV

SELECTIVITY OF THE LIST OF APOLLO ASTEROIDS

Limits of d (km):	1.00-1.19	1.19-1.41	1.41-1.68	1.68-2.00	2.00-2.38	2.38-2.83	>2.83	All >1.00
η:	0.04	0.08	0.15	0.25	0.35	0.60	0.80	
				Population index $s = 2.7$				
n:	10.2	6.4	4.1	2.6	1.6	1.0	1.6	27.5
ηn:	0.41	0.51	0.62	0.65	0.56	0.60	1.28	4.63
				Population index $s = 1.6$				
n:	4.00	3.00	2.28	1.72	1.32	1.00	3.20	16.52
ηn:	0.16	0.24	0.34	0.43	0.46	0.60	2.56	4.79
ηn observed:	1	3	0	0	0	1	2	7

In any case, the probable number N_A as estimated here is ten times the number N_{AM} expected from the injection of Mars asteroids; the injection is apparently inadequate.

Hence it appears that the majority of the Apollo asteroids cannot have originated from the asteroidal belt. They may indeed be dead comet nuclei, or other objects infiltrating from the region of the cloud of comets, such as true asteroidal bodies not covered with the hoar-frost coating and thus unobservable except at close distance.

Asteroidal collisions as a source of Apollo type fragments might be considered next. Leaving aside the infrequency of such collisions, and the circumstance that the aphelia of the Apollo group are not crowded toward the densest portion of the asteroidal belt, but are spreading definitely inwards of it, there is one argument which makes the suggestion unacceptable. To reach the earth after collision from a distance of 2.7-3.1 A.U., the fragments must acquire a relative velocity in our notation of $U \cong 0.3$ or 5 km/sec. The average velocity of collision of two asteroids is of the order of

$$U = (2 \sin^2 i + 2e^2)^{1/2} \cong 0.28$$

or barely equal to the required velocity of ejection of the fragments. This is definitely inadequate, considering that most of the kinetic energy of the collision is released inelastically. The fragments can attain only a fraction of the velocity of collision. Moreover, from the theory of meteorite crater formation (Öpik, 1958b 1961b) it appears that in a collision with cosmic velocity, large fragments cannot survive the accelerations required to eject them with large velocities. Only small meteoritic fragments can arrive on earth from the asteroidal region

as the result of collisions, not bodies measuring kilometers or hundreds of meters in diameter, even when consisting of a material as hard as compact nickel iron. The idea must be abandoned with respect to the Apollo group.

V

CAPTURE OF COMETS INTO TERRESTRIAL SPACE AND STATISTICAL BALANCE WITH APOLLO GROUP

A. *Definition*

Terrestrial space is here defined as that inside Jupiter's orbit. The orbital characteristics of objects belonging to this space are defined by the absence of Jupiter crossings, or by the aphelia being less than 4.94 A.U. However, the range from 4.54 to 4.94 A.U. remains within the sphere of action of Jupiter as a transition region. The objects of Tables VI and VII belong to this space, although Table VII represents a more narrow selection of Mars space. In particular, the Apollo group is characteristic of terrestrial space.

B. *Statistical Equilibrium of Disintegration and Dynamical Elimination*

Let N_c be the number of comets in terrestrial space, τ_c the lifetime of their "disintegration," i.e., evaporation of the volatile substances with all its consequences, and k_2 the fraction of type II or other surviving nuclei among them; and let N_{AC} be the number of objects in the Apollo group derived from the "disintegration" of the comets, τ_A their dynamical lifetime. Equilibrium conditions require

$$k_2 N_c/\tau_c = N_{AC}/\tau_A$$

or

$$k_2 N_c = N_{AC}\tau_c/\tau_A. \tag{47}$$

Assuming $N_{AC} = N_A - N_{MC} = 43 - 4 = 39$ for $d \geqslant 1.0$ km, according to Section IV, C, $\tau_A = 10^8$ years, $\tau_c = 10^4$ years which is more than usually ascribed to comets, we obtain $k_2 N_c = 0.004$ as the required time-average number of "live" comets in the terrestrial space, capable of yielding residual nuclei exceeding 1.0 km in diameter. In Table VI, there is one bona fide comet of $d = 1.7$ km[1] and a meteor stream (Geminids) which must have recently (on a time scale of 10^8 years) been formed from a disintegrated comet. In addition, periodic comet Grigg-Skjellerup has its aphelion exactly at the limit

[1] As suggested in Section IV, A, Comet Wilson-Harrington is more properly counted with the bona fide asteroids deriving from the Mars region.

of 4.94 A.U. (Table IX). Only objects with Apollo group characteristics, i.e., crossing the orbit of the earth and potentially capable of reaching Jupiter are thus included. The observed number may thus be set at $N_c = 1.5$ ($d > 1.0$ km); this is satisfied by a very low margin of efficiency, $k_2 = 0.003$. The estimate is extremely uncertain, but sufficient to show that the hypothesis of some members of the Apollo group having been derived from disintegration of comets does not require many live comets to be present in the terrestrial space.

C. *Injection from General Field of Comets*

From the "new" comets temporarily entering terrestrial space from outer regions, the terrestrial planets may partly eliminate some by collisions, and may partly perturb their motions in close encounters, capturing them into terrestrial space. If the outer planets were not there, the probabilities of collision and capture could be calculated from Eq. (6), with the encounter target radii being given by Eqs. (8) and (17) and the relative probability of a certain orbital change being defined by Eq. (15). In such a case the relative probability for the changed orbit to be entirely inside Jupiter's orbit is evidently

$$\theta_i = 1 - [\theta \rightarrow (\text{Jupiter})] \tag{48}$$

with θ — (Jupiter) being given in Table II.

In the presence of the outer planets, the collision probabilities will not be affected. However, orbital change of crossing orbits is so efficiently caused by Jupiter that the angular deflections induced by the terrestrial planets cannot accumulate in random walk and Eq. (17) does not apply. Only deflections in single encounters are effective. These impose severe limitations on the possibility of orbital change.

The calculation of probabilities of orbital capture in single encounters is rather complicated, except for parabolic objects. For them, the writer estimated by numerical integrations [using Eq. (11)] that, from an isotropically distributed population of parabolic objects [$W^2 = 2$, Eq. (19)], captures by the earth can take place only in the velocity range of $U = 0.48$-0.72, and the total probability of capture into terrestrial space per crossing and perihelion passage of a parabolic comet ($\sqrt{2} - 1 \leqslant U \leqslant \sqrt{2} + 1$) is then

$$P_A = 1.0 \times 10^{-11}.$$

The captures take place in a close range of perigee passages between 1.00 and 1.09 earth radii.

Application of the cumulative random walk procedure with Eqs. (17) and (15) to 25 nearly parabolic or long-period ($\geqslant 90$ years) objects which have been

observed crossing the earth's orbit during 1936-1949 (Bouška, 1953) yielded an average of

$$P_A' = 2.9 \times 10^{-11}.$$

The average is sensitive to individual values of p which flutuate considerably. Thus, excluding Comet 1941 II, which has the largest value of the probability, the average becomes

$$P_A' = 0.6 \times 10^{-11}.$$

One can see that, although theoretically the cumulative procedure is not justified, in practice it yields a numerical result sufficiently close to the correct one for deflection in single encounters.

It can be assumed that the cumulative procedure yields an acceptable approximation also in the case of the periodic orbits, where the exact calculation is complicated, but which chiefly contribute to the probability of being more easily captured than the parabolic objects.

From a complete list of comets over 14 years (Bouška, 1953), for 30 observed apparitions of objects crossing the orbits of earth and Jupiter (repeated apparitions of periodic comets being counted individually), the average probabilities per apparition of collision (P_c) and of capture (P_A) into Apollo-type orbits of terrestrial space, were found as listed in Table XV. In the notations of Table II, in each individual case

$$P_A = P_c(\sigma^2/S^2)\,[1 - \theta \rightarrow (\text{Jupiter})].$$

TABLE XV

	By earth	By Venus	Total per apparition
Probability of collision, P_c:	45.9×10^{-10}	13.8×10^{-10}	59.7×10^{-10}
Probability of capture, P_A:	2.65×10^{-10}	0.27×10^{-10}	2.92×10^{-10}

If ν_c is the true number of apparitions per year of comets whose nuclei are of the right size, to become ultimately members of a population N_{AC} of the Apollo group with an efficiency factor k_2, for statistical equilibrium

$$P_A k_2 \nu_C = N_{AC}/\tau_A \tag{49}$$

or, with $\tau_A = 10^8, P_A = 2.9 \times 10^{-10}, N_{AC} = 39\,(d > 1.0\text{ km}), k_2\nu_C = 1.3 \times 10^3$; for $1 \geqslant k_2 \geqslant 0.003$, this is equivalent to from 10^3 to 4×10^5 comets per year with nuclei exceeding 1 km in diameter crossing the orbit of the earth; such a number is absolutely out of the question.

This statistical puzzle can also be treated in a more direct way. If the observational selectivity of comets in general and those in terrestrial space is the same, instead of guessing the very uncertain selection factors, the adequacy of injection can be tested directly from the number of recorded objects. In the preceding subsection it has been shown that one or two live comets, actually known to be present in terrestrial space, are amply sufficient for maintaining the population of the Apollo group at its present level, even with an efficiency as low as 0.003 for the fraction of surviving residual nuclei. It thus remains to account for the origin of the observed number of live comets in terrestrial space, $N_C = 1.5$. In the notations of this and the preceding subsections, we have then

$$N_C = \nu_0 P_A \tau_C \tag{47a}$$

where ν_0 is the annual number of all observed apparations without selection effects. With $\nu_0 = 30/14 = 2.1$, $P_A = 2.9 \times 10^{-10}$, $\tau_C = 10^4$ years, $N_C = 6 \times 10^{-6}$ obtained, which is insignificant as compared with an observed effective number of 1.5. According to this criterion too, direct capture of field comets by the earth cannot account for adequate injection into terrestrial space, the rate being short by a factor of 10^5.

D. *Comet Diameters and Magnitudes*

If the evaporation intensity per unit surface of the nucleus, and thus the total brightness of a comet, is a unique function of heliocentric distance, the diameter of a comet nucleus must be given by a formula of the type

$$\log d = C - 0.2\, m_0 \tag{50}$$

where m_0 is the Bobrovnikoff-Schmidt "absolute" or standard magnitude reduced to unit heliocentric and geocentric distances and to standard instrument (Bobrovnikoff, 1942; Schmidt, 1950). The equation may involve considerable deviations in individual cases, but should apply as an average.

For the period 1853-1948, of almost a century, for which photometric data are available, the absolute magnitude distribution and number of apparitions of bright comets, with perihelion distances less than 1.02 A.U., is given in section (a) of Table XVI, according to Vanýsek (1952); in section (b) the statistics of all apparitions is presented according to the catalogue of Baldet and Obaldia (1952).

The first line in section (a) of the table gives the relative diameter in units of that of the $m_0 = 5.0$-5.9 group, according to Eq. (50). The population index of diameters (Öpik, 1960) defined here as

$$s = 5d(\log N)/dm_0 \tag{51}$$

TABLE XVI

ABSOLUTE MAGNITUDES AND APPARITIONS OF BRIGHT COMETS ($q < 1.02$ A.U.)

(*a*)

Relative diameter:	>6.3	4.0	2.5	1.6	1	0.62	0.40
m_0, mag.:	<1.9	2.0-2.9	3.0-3.9	4.0-4.9	5.0-5.9	6.0-6.9	7.0-7.9
Number, 1853-1948:	1	0	2	5	13	17	5
Cumulative number, N:	1	1	3	8	21	38	43
Population index, s:		—	2.4	2.1	2.1	(1.3)	—

(*b*)

Period of observation:	1853-1899	1900-1935	1936-1948
(I) Total apparitions, $q < 1.02$:	121	72	33
(II) Number with $m_0 < 5.9$:	11	7	3
Selection ratio (I) to (II):	11.0	10.3	11.0
Apparitions per year:	2.58	2.00	2.35

is given in the fifth line of the table. Its decrease beyond $m_0 = 5.9$ and the statistical comparison with section (b) of the table indicates that down to $m_0 = 5.9$ there is no relative selection in the photometric data of these bright comets whence, down to this limit, the average population index of diameters is $\bar{s} = 2.1$. With this, the cumulative numbers increase in a ratio of 4.3 for a ratio of limiting diameters of one-half, or in a ratio of 2.63 per magnitude interval of m_0.

Allowing for unfavorable perihelion passages, we may estimate that, despite their relative completeness as compared with the total number of apparitions, probably only one-quarter of all comets with $m_0 \leqslant 5.9$ have been recorded, so that the true annual number of comets brighter than the sixth magnitude crossing the orbit of the earth may be estimated at

$$\nu_6 = 21 \times 4/96 = 0.88.$$

With $s = 2.1$ the true number of apparitions down to a magnitude limit $m = m_0 > 6$ can be extrapolated with the aid of the formula

$$\nu_m = 0.88 \times 2.63^{(m-6)}.$$

For lunar albedo, Eq. (40) yields for the magnitude m_C of the nucleus at unit distances ($r = 1$, $\Delta = 1$, or the same for which the integrated magnitude m_0 of the comet is calculated) and full phase

$$m_C = 18.15 - 5 \log d_C \qquad (52)$$

whence from Eq. (50)

$$m_C - m_0 = 18.15 - 5C. \tag{53}$$

The virtual invisibility of the true nuclei of most comets would imply $m_C - m_0 > 5$ or $C < 2.6$ as an over-all upper limit for the average value of the parameter.

A direct determination of the constant C is possible only on rare occasions. From two cases when the true nucleus was observed, the writer made a reduction of the photometric observations to the conventional 3-in. telescope standard and unit heliocentric distance using an exponent $\bar{n} = 3.3$ for the heliocentric reduction (Bobrovnikoff-Schmidt reduction, see Bobrovnikoff, 1942; Schmidt, 1950). Assuming lunar albedo, the results for the constant in Eq. (50) were: $C = 2.25$ for periodic Comet Harrington-Abell 1955a; $C = 2.15$ for Comet 1946a Timmers. An average of $C = 2.18$ was actually adopted and used (Öpik, 1958b, 1960). If the albedo of the nuclei is as low as that of zodiacal dust, which is not improbable for the dust-covered radiation-damaged surface, $C = 2.6$ would be indicated. Undoubtedly, individual comets may differ widely in this respect, according to the surface rate of evaporation of the ices, but the average may be used for statistical purposes.

As shown in Table XVII, the "minimum" diameters of comet nuclei proposed by Richter (1948) are by almost an order of magnitude greater than our larger set of values ($C = 2.6$).

TABLE XVII

DIAMETERS OF COMET NUCLEI BY DIFFERENT METHODS

Comet:	1903 IV	1904 I	1907 IV	1932 V	1932 VI	1936 II	1937 IV
m_0:	6.5	3.4	4.3	7.4	5.1	6.8	6.2
d(Eq. (50), C = 2.6) (km):	20	83	55	13	38	17	23
d (Eq. (50), C = 2.18) (km):	7.6	32	21	5.0	13	6.6	8.7
d_{min} (Richter) (km):	307	232	194	73	200	106	77
m_C (Richter diameter, lunar albedo):	5.7	6.3	6.7	8.8	6.6	8.0	8.7

The values of m_C, calculated from Richter's diameters, require the nuclei to yield from 7 to 200% of the total light of the comet at unit heliocentric distance. From the observational standpoint this is an unacceptably high, partly impossible ratio. There can be little doubt that Richter's diameters are too large for compact nuclei, and that most of the light he attributed to the nucleus must have come from the "false nucleus," the concentration of gas and dust leaving the nucleus in all directions.

Even the values calculated with $C = 2.6$ appear to be too high. The number of craters in the lunar Mare Imbrium, depending essentially on the frequency

and size distribution of comet nuclei, and calculated with $C = 2.18$ for the comets, agrees with the observed number (Öpik, 1960). The agreement disappears when $C = 2.6$ is assumed, increasing the volume and mass of each projectile 18 times. The calculated number of craters for given size limits would then increase about 5 times and exceed in this ratio the observed number. Whatever the uncertainties in the estimate of the frequency of lunar craters, it would be quite difficult to bridge this gap.

For working purposes, and with a tentative probable error, we can thus assume for the parameter of Eq. (50)

$$C = 2.18 \pm 0.2$$

or values between 2.0 and 2.4 as the extreme range.

There exists an independent check on this figure which carries more weight than any estimates of the diameters of comet nuclei ever made. It is based on the apparent decrease in the gravitational constant k_2, caused by the inertial reaction of the sunward jet of vapors from the nucleus (rocket effect). Hamid and Whipple (1953) have published relevant data for 64 comets with definitive orbits which yielded a significant weighted mean value of $\Delta k/k = -0.53 \times 10^{-5}$ in the expected direction. From their few most accurate entries it can be judged that the real spread in $\Delta k/k$ is of the order of $\pm 0.6 \times 10^{-5}$. Therefore, using only the very best data for which the observational mean error in $\Delta k/k$ is less than spread, there remain six comets (1861 I, 1853 III, 1886 II, 1882 I, 1858 VI and 1896 III) for which the standard magnitude m_0 on the Bobrovnikoff-Schmidt scale has also been determined. With a correcting factor of 0.89, assumed to represent the fraction of solar heat used up in the sublimation of the ices (lunar albedo and surface radiation loss at —100°C being assumed), and with $\Delta k/k = -0.67$ (± 0.18 p.e.) $\times 10^{-5}$, Eq. (1) by Hamid and Whipple (1953) yields the harmonic mean diameter for these six comets as

$$d_k = 3.2 \pm 0.8 \text{ (p.e.) } km$$

based on the jet effect.

For the same six comets Eq. (50) with $C = 2.18$ yields a harmonic mean of $d_m = 5.8$ km (extreme range from 3.6 to 9) based on the observed standard magnitudes.

The agreement is better than ever in estimates of comet diameters; it seems that here at last a reliable basis has been found for assessing the true dimensions of comet nuclei.

The estimate from $\Delta k/k$ gives the mass per unit surface of the nucleus; that based on m_0 yields the total surface of the nucleus. If both estimates are taken at their face value, they could be reconciled by assuming an average

comet nucleus to consist of three spherical components, each of an average diameter of 3.2 km, so that their total reflecting surface would equal that of a sphere of 5.8 km diameter. In view of what was said about the multiple structure of comet nuclei, this model and the absolute dimensions of the nuclei may be close to the truth despite the uncertainties of the estimates. The occurrence of multiple meteor craters on earth (Kaalijärv in Estonia, Henbury in Australia, and others) adds further weight to this concept.

E. *Gravitational Capture from Jupiter's Family of Comets*

This is a two-stage process, Jupiter capturing comets from the general field, and the terrestrial planets, chiefly the earth, capturing into terrestrial space comets with aphelia near Jupiter's orbit. The probability of capture by the earth from Jupiter's family is some three orders of magnitude greater than directly from the long-period or parabolic field whence, despite the smaller number of objects, the expectation of capture is very much greater than from the general field.

The population of the Jupiter family we consider as given, without inquiring how it got there. Capture into terrestrial space is then the net balance between incoming and outgoing objects, a problem of diffusion inwards. The capture is noncumulative, achieved by individual deflections according to Eq. (11). There is a minimum value of γ which can produce the required orbital change, and this sets an upper limit to the perigee distance r and the target radius σ_{max}. For a small change in the desired direction, the probability of the change per encounter varies from nearly one-half (0.45-0.48) at grazing passage to zero at σ_{max}; an average value of the probability per target cross section $\pi\sigma_{max}^2$ is obtained by integration.

For an original set of elements with $a = 3.00$ A.U., $a(1 - e) = 0.8$, $a(1 + e) = 5.2$, a change to typical elements of a "captured" orbit, $a = 2.8$, $a(1 - e) = 0.8$, $a(1 + e) \leqslant 4.8$ can be achieved by earth encounters at conditions set forth in Table XVIII.

TABLE XVIII

CONDITIONS FOR EARTH ENCOUNTERS TO DECREASE PARTICLE'S APHELION BY 0.4 A.U. FROM 5.2 TO 4.8 A.U. OR LESS ($U > 0.29$)

U:	0.30	0.35	0.40	0.5	0.6	0.8	1.0	1.5	2.0
Probability of desired change at grazing passage:	0.45	0.48	0.48	0.48	0.47	0.47	0.46	0.43	0.35
σ_{max} (earth radii):	10.8	21.4	23.0	21.6	19.3	14.9	11.6	6.8	3.3

For the range of U from 0.3 to 0.6, as is actually covered by the relevant objects of Tables VIII and IX, the probabilities and target radii in Table XVIII vary but moderately, leading to an almost constant probability of "capture" (or an almost equal probability of a change in opposite direction) of

$$p_t = 7.3 \times 10^{-8}$$

per orbital revolution; with an average period of revolution of 5 years, this defines the probability of capture per annum as

$$P_t = 1.5 \times 10^{-8}.$$

"Capture" is here identified as a decrease of the aphelion distance by 0.4 A.U. or more.

From a population of N_j comets in the Jupiter family, capable of reaching earth's crossing ($U > 0.44$ with respect to Jupiter is the condition, cf. Tables II and III), a fraction P_t is injected annually into a population N_C of live comets in terrestrial space. Of the latter, the same fraction P_t is returned to the Jupiter family (when $U > 0.30$ with respect to earth), and a fraction $1/\tau_C$ decays or disintegrates. The statistical equilibrium condition can then be written as

$$P_t N_j = P_t N_C + N_C/\tau_C$$

or

$$N_C = N_j/(1 + 1/P_t\tau_C). \tag{54}$$

With $P_t = 1.5 \times 10^{-8}$ yr^{-1}, $\tau_C = 10^4$ yr, this becomes

$$N_C = 1.4 \times 10^{-4} N_j. \tag{55}$$

From Tables VIII and IX, $N_j = 2$ is the observed value, as only two objects (Grigg-Skjellerup and Neujmin 2) satisfy the condition $U > 0.44$. Hence

$$N_C = 3 \times 10^{-4} \tag{56}$$

is the *observed* equivalent value of live comets in terrestrial space, in equilibrium with the injection rate. This is very much less than the actual observed number, $N_C = 1.5$. Thus, although the equilibrium value of N_C is now 40 times that which can be sustained by injection from the general field (cf. Section V, C), it is still unable to account for the actual number of live comets present in terrestrial space.

Of course, the statistics in this case is based on a single object (Comet Encke) and the conclusion that "there are too many objects" need not be significant (however, the sampling error for one observed event may lie within the limits of -50 to $+100\%$ and the result still carries definite weight).

Disregarding the single event and assuming that the average observable number of live comets in terrestrial space equals the value of Eq. (55) calculated from injection, in former notations the observable number (without selection being allowed for) of residual nuclei in the Apollo group becomes

$$N_A' = N_C \tau_A / \tau_C = 3,$$

or of the right order of magnitude if the efficiency, k_2, is assumed equal to unity.

Thus, the two-stage injection by capture from the Jupiter family can almost account for the population of the Apollo group except that the improbable assumption of $k_2 = 1$ must then be made. In such a case comet Encke would represent a freak whose probability to be present in a random sampling by time (over intervals of $\tau_C = 10^4$ years) is 3×10^{-4}.

F. *Capture from Jupiter's Family of Dead Nuclei*

In addition to live comets in terrestrial space, the Apollo group could be supplied by injection of extinct nuclei still crossing Jupiter's orbit. The probable ratio of the number n_j of dead nuclei to that of live comets in Jupiter crossings is

$$n_j / N_j = k_2 \tau / \tau_C \tag{57}$$

in former notations, with τ = dynamical lifetime in Jupiter crossings. The harmonic mean lifetime of the nine objects of Tables VIII and IX is $\bar{\tau} = 8.5 \times 10^5$ years; with $\tau_C = 10^4$,

$$n_j / N_j = 85\, k_2$$

For $k_2 < 1$, $N_j = 2$ as for objects which can cross the orbit of the earth,

$$n_j < 170$$

and from Eq. (55) the observable number of dead nuclei diverted to the Apollo group from Jupiter crossings becomes

$$n_C < 0.024$$

which again is negligible. Although the dead nuclei of comets in Jupiter's family may be numerous, Hidalgo possibly being an outstanding example, they hardly can help in understanding the origin of the Apollo population through gravitational capture.

G. *Evolution through Jet Deceleration*

Whipple's ideas (1950, 1951) about jet accelerations or decelerations of comets, by way of a lag in evaporation from the surface of a rotating comet nucleus,

may be considered next as a possible cause of bringing members of the Jupiter family into terrestrial space. Nuclei in retrograde rotation in which a tangential jet force operates in a direction opposite to the orbital motion may lead to loss of angular momentum, chiefly near the perihelion, and to a decrease in the aphelion distance and semimajor axis. The apparent acceleration of Comet Encke may be attributed to this cause (Whipple, 1950, 1951).

As a rough estimate, we may assume that 25% of all nuclei have retrograde rotation in the plane of the orbit, with a lag of maximum evaporation of 30° in longitude (corresponding to an hour angle of 2 p.m.]. With a velocity of the escaping gases equal to 0.56 km/sec, or a component $0.56 \times \pi/4 = 0.44$ km/sec in the equatorial plane, the tangential component opposing orbital motion is $0.44 \sin 30° = 0.22$ km/sec. At unit distance from the sun (1 A.U.) this equals 0.0073 in the U-units. Hence, for a loss of mass in the ratio of M_2/M_1, the loss in the perihelion velocity becomes

$$\Delta U = -0.0073 \ln (M_1/M_2). \tag{58}$$

The identity of the comet may still remain preserved for a mass loss ratio of $M_1/M_2 = 8$, whence

$$\Delta U = -0.015 \tag{59}$$

appears to be the order of magnitude of the maximum attainable loss of angular momentum per unit mass. Equation (13) then yields the following variation in the aphelion distance for a perihelion at 1 A.U.:

$a(1 + e)$, initial:	5.7	4.95	4.00
$a(1 + e)$, final ($\Delta U = -0.015$):	4.9	4.4	3.54

The orbital change is sufficient to lead to practical injection of all comets with $a(1 + e) < 5.2$ into terrestrial space. The time scale of the process if τ_C, equal to that of apparent disintegration. In notations of the preceding sections we have then (with 25% of the comets subject to the effect)

$$N_C/\tau_C = \tfrac{1}{4} N_j/\tau_C$$

or

$$N_C = \tfrac{1}{4} N_j = 0.5$$

The present value of N_C is 1.5, of the same order of magnitude as that calculated.

The "rocket effect" in retrograde rotation is thus quantitatively adequate in supplying live comets to terrestrial space. Comet Encke appears to be still drifting inwards.

H. *Conclusion*

The supply of live comets, suspected parent bodies of the majority of the Apollo group asteroids, is efficiently achieved by an inward drift of some of the comets of the Jupiter family, caused by the jet deceleration of nuclei in retrograde rotation. Only a small fraction of the Apollo group, of the order of 20% or less, can be regarded as bona fide asteroids, diverted to earth crossing through accumulated perturbations by Mars.

The loss in U, the Jacobian relative velocity, as due to the rocket effect is comparatively small, of the order of -0.015. Hence the objects which have filtered into terrestrial space must have retained almost their original U values. This may be used as a means of guessing their possible origin in individual cases.

To have originated from the Jupiter family, $U \geqslant 0.29$ is required with respect to the earth, $U \geqslant 0.18$ with respect to Mars. Hence all objects of Table VI, with the exception of Comet Wilson-Harrington, may well have originated from the Jupiter family. The average U-value with respect to Mars of all 11 objects in this table is $\bar{U} = 0.679$, with a range from 0.382 to 1.07. For the 34 Mars asteroids of Table VII the corresponding figures are $\bar{U} = 0.429$, range 0.190-1.006. There is indeed a marked difference between the two groups, suggestive of different origin; the smaller U-value for the Mars asteroids is in harmony with the hypothesis that they are indigenous to the Mars space, whereas the higher relative velocity of the Apollo group objects and related comets would indicate a more extraneous origin. As to the relatively small aphelion distances of the objects of Table VI (except its most recent member, Comet Encke), they may have been brought about by the accumulated effect of close approaches to the terrestrial planets. The probabilities are not too favorable for this assumption, but it is difficult to find a more plausible explanation.

References

Baldet, F., and Obaldia, G. de (1952). "Catalogue général des orbites de comètes." C.N.R.S., Paris.

Bobrovnikoff, N. T. (1942). *Contr. Perkins Obs.* No. 16.

Bouška, J. (1953). *Acta Astr., Sér. C* **5**, 33.

Chebotarev, G. A. (1953). *Bull. Inst. Theor. Astr., Leningrad* **5**, 393.

Chebotarev, G. A., and Boshkova, A. I. (1954). *Bull. Inst. Theor. Astr., Leningrad* **5**, 571.

Hamid, S. E., and Whipple, F. L. (1953). *A. J.* **58**, 100.

Jeffreys, H. (1947). *M. N. R. A. S.* **107**, 260.

Matukuma, T. (1949). *Sendai astr. Rap.* **2**, 115.

Öpik, E. J. (1932). *Proc. Amer. Acad. Arts Sci.* **67**, 169; *Harv. Reprint* No. 79.

Öpik, E. J. (1950). *Irish astr. J.* **1**, 25.

Öpik, E. J. (1951). *Proc. roy. Irish Acad.* **54A**, 165; *Armagh Obs. Contr.* No. 6.

Öpik, E. J. (1956). *Irish astr. J.* **4**, 84.
Öpik, E. J. (1958a). "Physics of Meteor Flight in the Atmosphere." Interscience, New York.
Öpik, E. J. (1958b). *Irish astr. J.* **5**, 14; *Armagh Obs. Contr.* No. 24.
Öpik, E. J. (1960). *M. N. R. A. S.* **120**, 404.
Öpik, E. J. (1961a). *Ann. Acad. Sci. Fenn.* **A3**, 185.
Öpik, E. J. (1961b). Notes on the theory of meteor craters. *Proc. Cratering Symp., Washington, D. C.*, 1961 (to be published).
Oort, J. H. (1950). *B. A. N.* **11**, 91.
Oterma, L. (1958). *Astr.-Opt. Inst. Turku, Informo* No. 17.
Richter, N. (1948). *A. N.* **172**, 41.
Schatzman, E. (1953). *Mém. Soc. Sci. Liège* **13**, 313.
Schmidt, M. (1950). *B. A. N.* **11**, 258.
Vanýsek, V. (1952). *Contr. astr. Inst. Masaryk Univ.* 1(9), 1.
Whipple, F. L. (1950). *Ap. J.* **111**, 375.
Whipple, F. L. (1951). *Ap. J.* **113**, 464.

Recent Developments in Studies of the Magellanic Clouds

A. D. THACKERAY

Radcliffe Observatory, Pretoria, South Africa

I. Introduction 264
II. Form, Brightness, and Distance of the Clouds 265
A. Optical Structure 265
B. Charts of the Clouds and Coordinate Systems 268
C. Radio Structure 269
D. Integrated Magnitudes and Colors 270
E. Interstellar Absorption in the Clouds 271
F. Polarization 273
G. Distance of the Clouds 274
III. Nebulae and Clusters 275
A. Emission Nebulae 275
B. Open Clusters 276
C. Globular Clusters 278
IV. Variable Stars 280
A. Classical Cepheids and the P-L Relation 281
B. RR Lyrae Variables 284
C. Novae 286
D. Eclipsing Binaries 287
E. Long-Period and Irregular Variables 287
V. General Stellar Content 288
A. Brightest Stars 288
B. Red Stars 291
C. C.M. Arrays of the General Field 292
D. General Luminosity Function and Foreground Stars 294
VI. Dynamics of the Clouds 296
A. Motions within the Large Cloud 296
B. Motions within the Small Cloud 299
C. Relative Motions of the Clouds 299
VII. Conclusions 301
References 302

I
INTRODUCTION

The two Magellanic Clouds occupy a strategic position in cosmology and indeed in most problems of astrophysics. At a distance of probably less than one tenth that of the Andromeda nebula they can be studied in very great detail, and yet they are sufficiently removed from us that, as in a galactic or globular cluster, all objects contained within each Cloud can be treated as effectively at the same distance. While a galactic cluster contains only a very limited range of astrophysical objects for intercomparison, the Clouds are known to contain representatives of Baade's Populations I and II; with little absorption present to confuse the issue, straight comparison of apparent magnitudes becomes a direct comparison of luminosities. Such a direct and comprehensive comparison of diverse objects within our own Galaxy is impossible. Accurate photometry can of course be achieved for the most luminous objects in the Clouds, down to say $M_V = -4$, just where the calibration of luminosities is most uncertain in the Galaxy; with increasing uncertainty Cloud photometry can be extended to $M_V = +1$ into the range where galactic luminosities are well determined. The secure bridging of this gap remains perhaps the most important problem posed by the Magellanic Clouds.

The Magellanic Clouds have the great disadvantage of being situated deep in the southern sky, below $-65°$ declination. Consequently they were inaccessible to all the great reflectors erected in the early part of this century. The great developments in astrophysics which were brought about by those reflectors would no doubt have been profoundly affected had even one of them been directed to the study of the Clouds. Until work was started with the 74-in. telescopes of the Radcliffe and Mt. Stromlo Observatories, our knowledge of the Clouds depended very heavily on the work of the Harvard Boyden Station at Bloemfontein (previously at Arequipa, Peru) and on the temporary work of the Lick Southern Station.

The situation is very different now. In addition to the two 74-in. telescopes and the Cordoba 60-in. reflector, Schmidt telescopes equipped with objective prisms are in operation at Bloemfontein and Canberra; the Leiden 36-in. reflector is being used with remarkable efficiency for multicolor photometry; and very recently Fehrenbach has applied his objective prism technique with a 40-cm telescope to detection of bright Cloud members. Moreover, the Sydney team of radio astronomers have been discovering exciting new facts about the Clouds from studies at 21 cm and other wavelengths. This work will become all the more vital with the operation of the great 210-ft Sydney telescope.

Apart from the developments in radio astronomy, these modern programs represent, in many respects, refinements of earlier pioneering discoveries made

with Harvard equipment. The period-luminosity relation discovered by Miss Leavitt a half-century ago in the Magellanic Clouds is perhaps the most important tool in the hands of the observational cosmologist. Quantitatively, our knowledge of the relation is only beginning to be put on a sound basis.

An exhaustive review of work on the Clouds up to 1954 was published by de Vaucouleurs, Buscombe, and Gascoigne (1954). A supplementary review was more recently published by Gascoigne (1961). The bibliography attached to the present article is not intended to be as exhaustive as those given in the foregoing reviews to which the reader is referred. Many problems concerned with the Clouds are in a very fluid state so that discoveries emerging from current programs may change the picture fundamentally. Nevertheless, it is hoped that the current brief review may be of some interest to those new to the topic as well as to those already familiar with the problems.

II

FORM, BRIGHTNESS, AND DISTANCE OF THE CLOUDS

A. *Optical Structure*

The Magellanic Clouds are classified as Irregular Galaxies and as such are referred to as standards. Both are clearly visible to the naked eye in a dark sky appearing like isolated off-shoots of the Milky Way with apparent diameters of about 6° (LMC) and 3° (SMC).

The Large Cloud has an "axial bar" with very high concentration of faint stars, as one of its principal features (see Fig. 1). North of its following end lies the 30 Doradus Complex, a stupendous association of hot stars and nebulosity. Further north is Constellation III (Shapley and Nail, 1953b), rich in luminous stars scattered roughly in the shape of the Greek letter χ, but relatively deficient in nebulosity.

The irregular distribution of clusters and diffuse nebulae in the Large Cloud contrasts with a more uniform stellar distribution in the Small Cloud. In the latter there is again the suggestion of a main "axial bar," broader at its southern end (see Fig. 2). A faint extension towards the Large Cloud, called the "wing" (or "bulge") showed prominently on some small-scale Harvard photographs (Shapley, 1940); it appears to have been noticed visually by Sir John Herschel (1847) in one of his sweeps as, "here after a region of utter barrenness, commences a somewhat brighter region."[1] The wing has proved to be a particularly powerful source of 21-cm radiation.

[1] I am indebted to Dr. E. M. Lindsay for drawing my attention to this quotation.

Short-focus photographs by de Vaucouleurs (1954, 1960a) showed that both Clouds could be traced optically to as great angular distances as 10° (LMC) and $4\frac{1}{2}°$ (SMC). In addition, de Vaucouleurs traced faint "spiral loops" up to

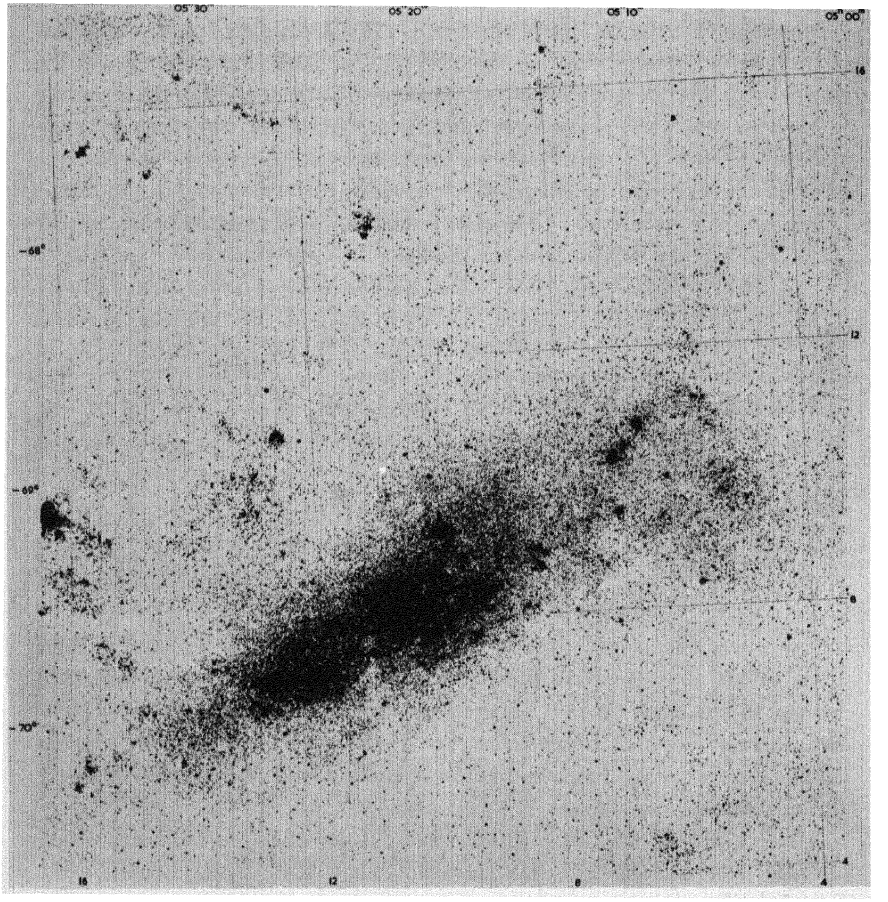

FIG. 1. Axial bar of the Large Magellanic Cloud. Part of 30 Doradus appears on left hand edge, Constellation III in top left corner. (Uppsala Atlas.)

about 20° from the LMC. Some of these at least appear to be associated with foreground nebulosity rather than with the Magellanic Clouds (H. M. Johnson, 1959b). The surface brightness of these outer extensions is exceedingly faint, representing only a small increase over the night-sky brightness. Even extra-terrestrial observations would be faced with the difficulty of distinguishing

between extensions belonging to the Clouds and to our own Galaxy, whether consisting of gaseous filaments or faint stars. The distinction of gaseous filaments might conceivably be achieved through the use of narrow-band filters passing Hα, making use of the Doppler shift of 6 Å which corresponds to the mean velocity of the LMC. De Vaucouleurs (1954) has also claimed the existence of a bridge connecting the Galaxy with the Large Cloud, as suspected originally from naked eye observations by Herschel (1847). Photoelectric measures of the Milky Way by Elsasser and Haug (1960) have given some support to the claim,

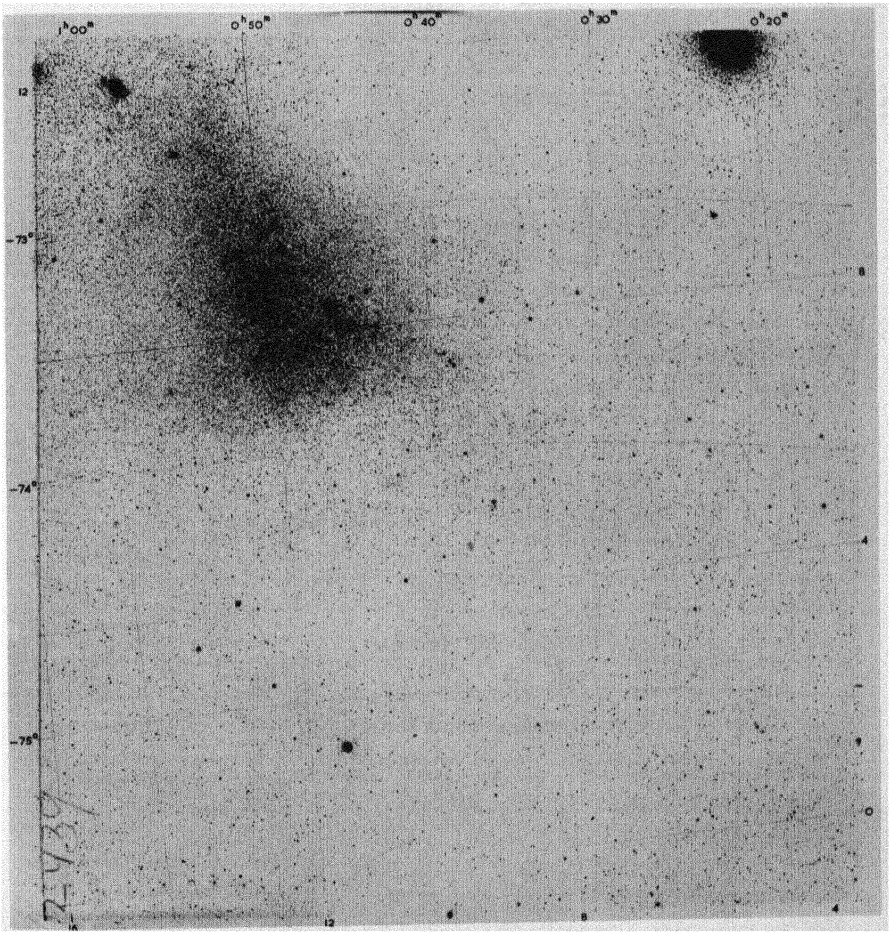

FIG. 2. Part of Small Magellanic Cloud. Part of 47 Tucanae appears in top right corner. (Uppsala Atlas.)

but whether the slightly increased width of the Milky Way in longitude 240° is directly associated with the Large Cloud in any way remains to be proved.

De Vaucouleurs has suggested, on the basis of star counts, that both Clouds are flattened systems with small inclinations to the plane of the sky (de Vaucouleurs *et al.*, 1954). He draws analogies with certain other irregular galaxies (e.g., NGC 55 seen edge-on). He classifies such systems as SBm; an axial bar together with faint outer spiral structure shows a relationship to the barred spirals, and "m" is used to underline the irregularity characteristic of Magellanic-type systems. This classification of the LMC has some support from dynamical considerations (Section VI), but the actual value of the inclination (about 25° according to de Vaucouleurs) is most uncertain. H. M. Johnson (1959a) has a far more complicated model, for which the evidence is hardly convincing, consisting of a "Sc galaxy, seen nearly pole-on and with its nucleus at 30 Doradus, in front of another 'population' which is part of the 'bar.' " Johnson also finds an elliptical distribution of infrared light of the LMC suggesting an E5 galaxy.

Conflicting models have been proposed for the SMC. Kron (1956b) proposes a spiral distribution of clusters and emission patches. Lindsay (1958) finds a larger number of nonglobular clusters than Kron and places 63% of them within an ellipse, without noting any sign of spiral distribution; the ratio of major/minor axes of Lindsay's ellipse is 2.4 instead of 1.4 (Kron). Rodgers (1959) strings the H II regions of the SMC along a single curved line along the main axis, curving out to the "wing" and eventually towards the LMC.

It is easy enough in work of classification of galaxies to have a wastepaper basket into which to cast all "Irregulars," and it is perhaps surprising that not more than $2\frac{1}{2}\%$ were so classed by Hubble. On the other hand, efforts to find some order in the detailed structure of the Magellanic Clouds have not been very rewarding. The fundamental fact remains that neither of them, optically, has a dominant *nucleus*, although the most obvious feature in each is a *bar* whose orientation is visible to the naked eye. It is of pressing importance to devise tests for de Vaucouleurs' inclined plane models.

B. *Charts of the Clouds and Coordinate Systems*

Recently published (1961) charts of both Clouds consist of enlargements of yellow photographs taken with the Uppsala Schmidt at Mt. Stromlo, and serve as an indispensable guide to all who plan detailed programs. Examples appear in Figs. 1 and 2. Each chart covers $4° \times 4°$ at a scale of 3 in. per degree. A total area of $10° \times 10°$ of the LMC is covered by nine charts, and $7° \times 7°$ of the SMC by four charts. The photographs reach a limit of about visual magnitude 18.

In the crowded fields of both Clouds the identification of individual stars poses considerable problems and puts considerable responsibility on anyone wishing

to publish lists of objects for identification by others. Clusters and nebulae can normally be identified easily enough with accurately determined equatorial coordinates. But attention is drawn to Henize's (1956) photographs with outlined (and catalogued) areas of widespread nebulosity. Individual stars and other objects have been commonly specified by means of the Harvard X, Y system (Leavitt, 1907) originally applied to the numerous Harvard variables in both Clouds. Wesselink (1959) has raised objections to the X, Y system and proposes a new system of standard coordinates ξ, η defined rigorously by CPD stars, with centers near the center of each Cloud. He gives formulas for converting α, δ (1875) into ξ, η and X, Y and vice versa. Tables of all three coordinates for Harvard variables, CPD stars in the SMC, and HDE stars in the LMC, based on computations in H. M. Nautical Almanac Office, have been published by the Radcliffe Observatory (1961).

Wesselink's system has the great virtue that it can be extended readily beyond the limits of the original Harvard photographs into regions that were originally hardly visualized as forming parts of the Clouds. The system was formally recommended by the I.A.U. Sub-Commission on the Magellanic Clouds at its 1960 Conference at Cordoba. ξ, η coordinates, as well as α, δ, appear on the Uppsala-Mt. Stromlo charts. The general adoption of this system would seem to be highly desirable.

C. *Radio Structure*

Observations with radio telescopes of both Clouds have proved most informative, particularly at 21 cm, and very important results are to be expected with the new Sydney 210-ft telescope, with which fine details of the Clouds are to be expected to appear. This instrument may well revolutionize some of our concepts of the Clouds before the publication of this review.

In the meantime, the latest 21-cm isophotes obtained in 1960 by the Australian group (Hindman *et al.*, 1961) are reproduced here in Fig. 3. Two new and very striking results of this survey were (1) the bridge of weak 21-cm radiation connecting the two Clouds, and (2) the steepness of the gradient of radiation on the preceding side of the SMC and following side of the LMC.

There is no suggestion here of a bridge connecting our Galaxy and the Clouds and little to confirm de Vaucouleurs' longest external loop of the LMC. It is noteworthy that the tonguelike extension towards $\alpha = 6h$, $\delta = -80°$ found in the earlier 21-cm survey is not confirmed.

The relative strength of the SMC in 21 cm radiation has been known for some years. In these 1960 isophotes the peak brightness of the SMC is in fact larger than that of the LMC. The "wing" on the following side of the SMC, pointing towards the LMC, is very well marked in the 21-cm isophotes.

A bridge connecting the two Clouds at $\delta = -72°$ had already been suspected by Mills (1955, 1959) in his 3.5-meter survey of continuum radiation. Other radio surveys of the Clouds have been made at 50 cm (Piddington and Trent,

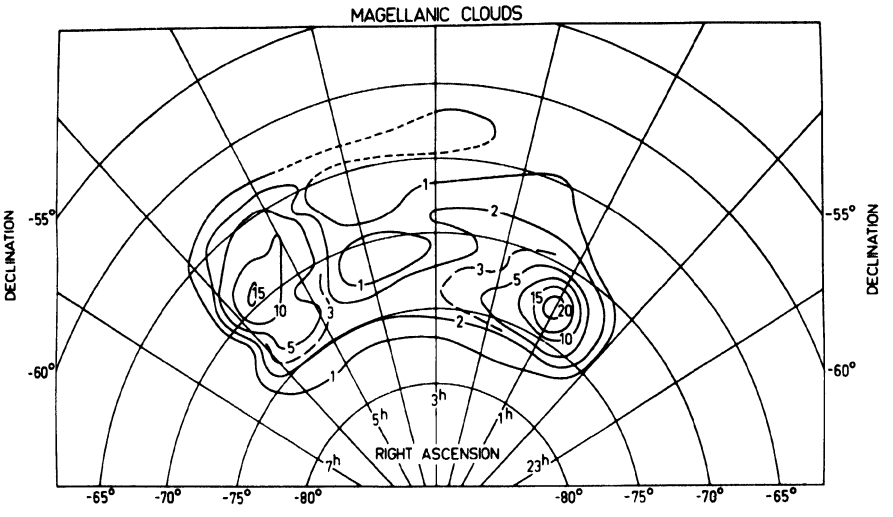

FIG. 3. 21-cm isophotes of the Magellanic Clouds. (Courtesy, F. J. Kerr.)

1956), 3 meters (Mills, 1954), and 15 meters (Shain, 1958). The general spectrum in this wavelength region of the continuum appears to be similar to that of the disk of our Galaxy and to M 31, believed to be due to synchrotron radiation.

The important results of 21-cm radial velocities are discussed later (Section VI).

D. *Integrated Magnitudes and Colors*

Four independent measures of integrated magnitudes and colors of the Clouds have been discussed in a useful compilation by de Vaucouleurs (1960b). All but one of the four original determinations were based on photoelectric photometry. The interagreement is good, and becomes still better in de Vaucouleurs' coordinated reduction to standard systems of magnitudes and colors, and to the same areas.

The final mean values of magnitude B and color B − V are given in Table I for specified areas, and extrapolated to infinity. The probable errors of these

figures (which have mostly been rounded off to 0.1 mag.) run from 0.03 to 0.09 according to de Vaucouleurs.

TABLE I

	LMC		SMC	
Area	100□°	∞	12□°	∞
B	0.9	0.6	2.9	2.8
B — V	0.5	0.55	0.4	0.6

The calculations within the limited areas of 100□° (LMC) and 12□° (SMC) refer to a level of brightness 25.3 mag./sec² (*B*), i.e., only about 6% above the mean sky brightness (22.3 mag./sec²). The small extrapolation to infinity for integrated magnitudes (difficult enough for any extragalactic system, but worse for such a system as the LMC) must be subject to considerable uncertainty.

The surface brightness and colors of the central regions of the Clouds are found to be as follows:

	LMC	SMC
B (mag./sec²)	21.2	21.4
B — V	+0.46	+0.25

It seems well established that the central regions of SMC are considerably bluer than the outer regions, and that the increase in color index proceeds fairly smoothly; it is reasonable that the color of the axial bar implies a concentration of early-type stars within the bar. According to Elsasser (1959) 60% of the total light of the SMC comes from stars brighter than 20th magnitude.

The color of the LMC shows a very much smaller gradient outwards; in fact, de Vaucouleurs' curve shows that from 2° to 3° from the center the color is bluer than in the center, while further out it rapidly becomes as red as the general sky background. This is no doubt a consequence of the patchy concentrations of blue stars (e.g., in Constellation III).

E. *Interstellar Absorption in the Clouds*

The frequent appearance of emission nebulae in both Clouds points to a strong gaseous component of the interstellar medium of the Clouds, and this is strongly confirmed by the 21-cm observations. The first observation of an interstellar absorption line due to extragalactic gas was by Feast (1953) in the

nucleus of the 30 Dor nebula. Other cases have been noted in both Clouds by the Radcliffe observers (Feast *et al.*, 1960); in some stars absorption by foreground galactic calcium is also found despite the high galactic latitude.

Reddening and absorption by dust (whether in the galactic foreground or within the Clouds) is sometimes ignored altogether. However, some absorption lanes are certainly present within the LMC (see the bottom left corner and the center of the southern edge of the bar in Fig. 1). Some smaller lanes and patches also seem to be present in the main body of the SMC (Fig. 2).

Shapley (1951) wrote of the SMC as essentially transparent, but later workers have tended to ignore his supplementary remarks that absorption by a few tenths of a magnitude could be present in the crowded center. Wesselink (1961a) has made a very careful survey of external galaxies on Radcliffe plates covering fields in and around the SMC and finds much too large a drop in numbers on the central plates to be explained away in terms of crowding. At more than 4° from the SMC he found a "reduced count" of 16.7 galaxies per plate, of which he estimates about half could be lost in the crowded center. In 14 fields within 2° of the SMC center the mean reduced count is as low as 1.7 per plate. In a further paper Wesselink (1961b) discusses the frequency distribution of color excesses in a system containing dust, and shows that the fact that bright stars in both Clouds are exceptionally blue, by galactic standards, need not necessarily indicate the absence of dust. A normal mean ratio of dust/gas in either Cloud can still be regarded as consistent with observation, although one must be prepared to find the usual patchiness of distribution.

Cloud cepheids which have been proved to be very blue are presumably suffering very little absorption. Even if all cepheids in a certain area and covering a wide range of magnitudes have been studied, Wesselink's arguments regarding the mean color excesses should still apply, but some reddened cepheids might be expected to appear. It is not clear to what extent selection of apparently absorption-free areas for extensive programs of photometry of cepheids may have played a part in failing to reveal reddened cepheids. It is further possible that statistically cepheids are less associated with regions of dust than early-type stars.

Further evidence of some small absorption in front of and within the Clouds is provided by Radcliffe spectroscopy and photometry of proved Cloud members (of early type) and foreground stars. The data in Table II are extracted from Table IV of Feast *et al.* (1960).

Some reddening appears to be present in both Clouds and to be occurring both within the Clouds and in the galactic foreground. It is important to note that Cloud stars within nebulosity are significantly more reddened than those outside nebulosity; in fact the reddening of stars outside nebulosity can be attributed entirely to the foreground.

The reddening properties of the Cloud dust appear to be identical with those of galactic dust, so far as the evidence goes (Feast *et al.*, 1960; Wesselink, 1962).

TABLE II

MEAN ABSORPTIONS ($A_V = 3E_{B-V}$) FOR STARS EARLIER THAN A2 (PECULIAR STARS OMITTED)

	LMC			SMC		
	A_V (mag.)	s.e. (mag.)	(n)	A_V (mag.)	s.e. (mag.)	(n)
All stars	0.33 ±	0.03	(48)	0.34 ±	0.03	(15)
Stars within nebulosity	0.40	0.04	(30)			
Stars not in nebulosity	0.21	0.04	(18)			
Greatest value	0.96			0.60		
Foreground absorption	0.21	0.12	(5)	0.21	0.03	(8)

Arp (1960) finds a mean color excess (E_{B-V}) for supergiants and cepheids in his SMC field of 0.05 to 0.06. This corresponds to only about half the absorption tabulated above, probably due to selection of stars. It is possible that the reddening of Arp's stars occurs mainly in the Galaxy rather than in the Cloud.

Walker (1962) has searched for 4430 A absorption through narrow-band photometry in Cloud stars; there seems to be some evidence for this interstellar band occurring in some SMC stars, but the meager results available for LMC stars are less conclusive.

F. *Polarization*

Polarization of the Large Cloud in blue light was reported by H. M. Johnson (1959a) but its amount could not be estimated. Recently Wolstencroft (1962) has measured photoelectrically large degrees of polarization in both Clouds. He finds polarization of 25% in blue light in p.a. 126° for a 3½° field centered on the LMC; the direction is closely that of the axial bar. However, curiously enough, yellow light from a 4½° field gives polarization of 33 ± 7% in the very different direction of 88°. The polarization of the SMC is given as 24% in p.a. 177°.

It is of interest that Vashakidze (1955) has found large degrees of polarization for two irregular galaxies NGC 3077 (15%) and NGC 4449 (21%). These are considerably larger values than those found for spirals and ellipticals in Ohman's pioneer observations.

Clearly more detailed work on polarization in the Magellanic Clouds is highly desirable.

G. *Distance of the Clouds*

The brittleness of all methods of measuring large astronomical distances is well illustrated by the successive attempts to estimate more accurately the distance of the Clouds since the 1952 revision of the cepheid zero point.

The zero point itself of the P — L relation is believed to be more securely determined now through the use of a few cepheids within galactic clusters, but doubts whether the P — L relation is unique are strengthened by the recent Herstmonceux finding that the P — L relation is apparently different for the Large and Small Clouds. Population II cepheids and RR Lyrae variables are subject to similar uncertainties.

The method of "zero-age fitting," commonly applied to galactic clusters, has an error of order 0.4 mag.; but the error must be larger in the Clouds since the fit has to be made at very faint magnitudes where photometry in crowded fields is difficult.

Spectroscopic parallaxes are suspect when applied to "evolved stars" and in any case at present can only refer to the brightest Cloud stars whose galactic counterparts, if recognized, are at unknown distances. Conceivably the equivalent width of Hγ could be measured for 14th-15th magnitude A stars in the Clouds with sufficient accuracy for an improved modulus. The Walravens' (1960) five-color photometry, applied to stars of this brightness or fainter, may provide a very accurate calibration in due course.

Integrated magnitudes, apparent diameters, and magnitudes of brightest stars of clusters are all recognized as most unreliable criteria of distance.

Maximal magnitudes of novae at maximum could give an improved distance if the Cloud statistics were more numerous and the light curves better observed.

The apparent diameters of Hα emission rings or spheres also offers an approach of some promise, although statistics again are small. The method is of interest in being essentially independent of measures of apparent brightness. The method could be improved by observations of electron density through the [O II] 3727 doublet ratio supplemented by spectral classification of the exciting stars.

The brightest stars in the Clouds as a whole cannot be trusted any more than the brightest stars in clusters. This criterion would give a distance modulus for the SMC 1 magnitude larger than for the Large Cloud, presumably because the latter is a richer system. The other criteria put both Clouds at about the same distance, but it is possible that the SMC has the larger modulus by a few tenths of a magnitude.

Perhaps the dominant influence in instilling doubts whether any criterion at present will give a distance modulus better than 0.3 mag. is the recognition of probably widespread differences in chemical abundances in individual stars and

possibly in whole systems (see Arp, 1961). Such differences must undermine the reliability of almost all the usual astrophysical criteria of distance.

The time is not ripe for a detailed evaluation of the distance of the Clouds by the various methods, but for purposes of discussion in this article an apparent (visual) distance modulus of 19.0 will be used.[2] Allowing 0^m3 for absorption, the corrected distance modulus is

$$(m_0 - M) = 18.7$$

corresponding to a distance of 55 kpc. At this distance it is interesting to note that the corresponding scale in the sky is

$$1^\circ = 1.0 \text{ kpc},$$

while a tangential motion of 10 km/sec would yield a proper motion of 37 sec of arc per million years. It is clear that on this scale the brightest stars in the Clouds (a) can be used as a convenient astrometric framework for proper motions of the galactic foreground, and (b) must be seen within a few minutes of arc of their birthplace in the Clouds.

III

NEBULAE AND CLUSTERS

The profusion of clusters and nebulae at galactic latitudes 33° (LMC) and 45° (SMC) is one of the most distinctive features of the Magellanic Clouds. John Herschel (1847) recorded visually the positions of 919 star clusters and nebulae in the Large Cloud and 214 in the Small Cloud, with individual notes which occasionally still provide interesting reading. A more recent visual survey by Innes and van den Bos (1924) with the Johannesburg 26-in. refractor is also of value.

A. *Emission Nebulae*

An admirable survey of 532 nebulae and 236 stars with bright Hα in both Clouds has been published by Henize (1956). Photometric measures of the LMC nebulae have been published by Doherty, Henize, and Aller (1956). Henize includes lists of stars believed to be the source of excitation of the nebulae. Lindsay (1961) lists 593 point-source emission-line objects in the SMC, mostly showing bright Hα. Thirty of these objects are regarded as planetary nebulae,

[2] For a recent discussion see Sersic (1962) who gives apparent moduli of 18.8 ± 0.2 (LMC) and 18.9 ± 0.2 (SMC). For general problems of distance scale see Sandage (1958).

and a further 19 objects may belong to this class. While Lindsay's identification of planetaries depends on objective prism spectra, Koelbloed (1956) has identified 16 faint objects by photographic technique with the Radcliffe reflector using filters that essentially isolate the nebulium lines. Koelbloed's objects range from -1 to -5.5 in M_{pg} but only four are brighter than -3.5; Lindsay's list of 30 "certain" planetaries average -3.0 in M_{pg}. Unfortunately neither survey goes deep enough to derive a meaningful average luminosity for a planetary or a range in luminosities.

Feast (1961) has published a very detailed study of the great 30 Doradus nebula, based on slit spectra of various portions of the nebula and involved stars. From intensity ratios of the [O II] 3727 doublet, which is completely resolved on his spectra, he derives electron densities ranging from 200 to 2000 per cm^3; the highest density found is actually in the central "star"—a diffuse object about 2 sec of arc across—outwards from which the density falls sharply. The densities are comparable with those found in the outer parts of the Orion nebula and Feast emphasises that in linear dimensions the central "star" must correspond to the central 4 minutes of arc in the Orion nebula. The variations in brightness in the nebula are probably caused by real variations in density; for example one of the brightest looped wisps shows a diminishing density with brightness along its length. The profusion of *W* stars in this region was already known, but Feast has discovered more and has shown that all in this region belong to the WN sequence.

The H/He ratio appears to be normal in the 30 Dor region, and in other Cloud nebulosities according to spectroscopic observations (Feast *et al.*, 1960) and also from spectral scans by Aller and Faulkner (1961).

Emission nebulae in the Clouds are statistically related to supergiants of type B2 and earlier (Feast *et al.*, 1960) just as in the Galaxy (as established many years ago by Hubble).

B. *Open Clusters*

Catalogs of open clusters have been given for the LMC by Shapley (1931) and for the SMC by Kron (1956a) and Lindsay (1958). Lindsay has a list of about 1000 LMC clusters in preparation.

There is some danger of confusion in terminology when comparing Cloud clusters with the familiar open clusters of the Galaxy. At 55 kpc, the Pleiades, for instance, would appear as only 20 sec of arc across. Shapley's (1931b) discussion, based on the old distance scale, shows full awareness of the incompleteness of his survey. With the revised distance scale most of the clusters currently being studied for color-magnitude arrays are large enough to qualify for the term "associations" rather than galactic clusters. As an example of a

cluster of ordinary galactic dimensions, one may quote the compact group (about 25 sec of arc across) dominated by the famous variable S Dor lying within the much larger association NGC 1910. The compact group contains some 8 stars besides S Dor, all blue, with absolute magnitudes probably exceeding −2.5. Not much can be said about the extension to fainter magnitudes within this group and the cluster I 2602, dominated by the O star θ Car would perhaps be a better comparison than the Pleiades.

Hodge (1961a) has given the name "young populous cluster" to objects resembling NGC 1866. This cluster, which on ordinary photographs appears very like a globular cluster in shape and richness, is rich in blue stars (as well as red giants) which are responsible for Miss Cannon's spectral classification as "A." NGC 1866 also claimed attention on account of its containing cepheid variables (see Section IV). Hodge (1961a) lists 23 LMC clusters which he places in this "young populous" group. He recognizes them as generally larger and more populated than "any open cluster in our Galaxy."

Woolley (1960) has published c.m. arrays of the LMC clusters NGC 2004, 1810, and 1818 (of which the last appears in Hodge's list). NGC 2004 and 1818 both show a marked vertical sequence of some four magnitudes range at B − V = 0 or bluer, together with a considerable number of red stars, some as bright as $V = 13$. Woolley makes an interesting contribution to the question of terminology by suggesting that NGC 2004 and 1818, at present blue, will evolve into red globular clusters. He prefers a dynamical definition of clusters—globulars being those from which most stars cannot escape, while the open ones or moving associations are those which are disintegrating in the course of time.

Arp (1959a,b) in his very extensive program of photometry in the SMC has discussed color-magnitude arrays of the clusters NGC 458 and 330. Both clusters contain vertical branches of very blue stars together with some red supergiants. The brightest stars are 15 to 16 (V) in NGC 458 and 12 to 13 (V) in NGC 330; and while the red stars in the former are around B − V = +0.8, those in NGC 330 are much redder (B − V = +1.4 to +1.6). Both clusters show well-defined Hertzsprung gaps, but Arp stresses the narrowness of this gap in NGC 458. The ages are believed to be similar to that of the Pleiades. Arp holds that there are differences between the c.m. arrays of these clusters and those in the Galaxy which must stem from differences in chemical composition, but this conclusion has been questioned by Feast (1960). If a cluster is sufficiently populous, then red stars may be expected to appear, as has indeed been found to be the case in the rich galactic clusters M 11 (H. L. Johnson *et al.*, 1956) and NGC 6067 (Thackeray *et al.*, 1962); in both these latter cases red stars form some 15 to 20% of the total number of bright stars. The proportion is probably higher than this in Arp's clusters, but it is not clear how complete the selection of cluster members in the SMC has been.

Hodge (1961c) has found four supergiants in the compact cluster NGC 1844 (LMC) with colors all near +1.0 but a range of 2 mag. in luminosity.

Westerlund (1961b) has studied c.m. arrays of the three clusters NGC 456, 460, 465 in the SMC "wing" down to $V \sim 19$. The usual strong vertical branch of very blue stars is present, but fewer red stars are found than in Arp's fields. Westerlund regards his region as almost pure Population I (with emission nebulosity present), while Arp's field probably also contains older Population I and Population II stars. There is nothing in such a regional variation to indicate a general dissimilarity of SMC and the Galaxy.

Westerlund (1961a) has also discussed similarly c.m. arrays of 26 associations, clusters, and fields in the Large Cloud down to $V \sim 16$. The vertical blue branches are always present, but a few red stars appear, whose Cloud membership should be checked when possible. A point of particular interest is that whenever a Wolf-Rayet star is found it lies near the upper end of Westerlund's main sequence. A similar phenomenon appears in Houck's c.m. array for the galactic cluster NGC 6231. Westerlund gives ages of 3×10^6 to 10×10^6 years for the ages of these LMC clusters and about 10×10^6 years for his SMC clusters.

In such work on Cloud clusters interest is concentrated on determination of ages and possible spread of ages in different clusters: this is a difficult enough task since it involves carrying accurate photometry to a faint limit in crowded fields. A second point of interest concerns the red stars whose evolution is still obscure. At this bright level the photometry presents no serious problem, but spectroscopy is urgently required both to check Cloud membership and for purposes of spectral classification. The faintest red star belonging to the LMC yet studied with slit spectroscope is R 108 of Feast *et al.* (1960), with $B = 14.1$, a member of NGC 2004. It shows [Fe II] emission, and Henize has also observed Hα bright. Thus the red colors may not always imply low surface temperature.

Finally, it may be pointed out that inspection of any large scale photograph of the Clouds will reveal the bewildering complexity of the clusters, in richness, diameters, and magnitudes of brightest stars. Shapley has used variety in the last two criteria to point out that they are "not sharp enough tools" for measuring distances within the Galaxy. Current programs have naturally selected some of the brightest and largest clusters in the two Clouds. The smaller clusters, particularly if they are poor enough to be well resolved for photometry, also deserve attention.

C. *Globular Clusters*

In this section we restrict ourselves only to those clusters whose brightest stars are definitely red, as in the familiar globular clusters of our Galaxy. NGC

121 (SMC) and 1978 (LMC) were the first proved examples of this group (Thackeray, 1951). The strong contrast in integrated colors of such globulars with the "young populous" variety is shown by the photoelectric measures of Gascoigne and Kron (1952).

Hodge (1960) has listed 35 LMC clusters which he places in the category of true globular clusters on the basis of yellow-blue comparisons of ADH photographs. The area searched excluded NGC 2257 which is also known to belong to this category.

In the SMC NGC 419 and 361, studied by Arp (1958a,b), NGC 121 and (Gascoigne, private communication) Lindsay 5 and NGC 339 all appear to be true red globulars. Arp's c.m. arrays for the first two clusters extend to nearly 20 mag. and show the usual red-giant branch characteristic of these objects (together with a blue main sequence, presumably belonging to the general field of the Cloud). The horizontal branch, if it exists in these clusters, is too near the limit and too weak to show up conspicuously in this work. Arp points out a peculiar break in the giant branch of NGC 419 and also finds a few stars redder than $B - V = +1.6$ (where the giant branches of most globulars in the Galaxy cut off).

The extension of the red branch is particularly well marked in the very rich globular cluster NGC 1783 (Sandage and Eggen, 1960) in the LMC. Sandage and Eggen compare NGC 1783 with M3, M92 and NGC 6356, and deduce that "no cluster in our own Galaxy is known to be similar to NGC 1783 in all its features." However, Wildey's c.m. array of 47 Tuc (which does not include some of the reddest stars in the crowded center) differs from others in the Galaxy more than does NGC 1783. It thus seems premature to draw conclusions about general differences between globular clusters in the Clouds and the Galaxy.[3]

Judging by variable star content of NGC 121, 2257, and 1466 no outstanding differences have been found from variables in globulars within our own Galaxy (see Section IV).

The c.m. array of NGC 121 has been studied by Tifft (1962) down to fainter than 20 mag. More than 1000 stars belonging to NGC 121, the SMC halo or the galactic foreground (including outliers of 47 Tuc) are included in Tifft's study. The c.m. array for the innermost zone (about 0'.5 to 1'.0 of arc from the cluster center) is shown in Fig. 4. The red giant branch is very well shown extending to $B - V = +1.6$ (with Thackeray's two red variables lying still further to the right). A well populated "horizontal" branch is also seen with the mean position of the RR Lyrae variables lying at the left end. This c.m. array is quite similar

[3] *Added in proof:* Gascoigne (1962; *M.N.R.A.S.* **124**, 201) has recently published a c.m. array of NGC 1783 differing from Eggen and Sandage's in some important respects, but very similar to Arp's c.m. arrays of NGC 361, 419.

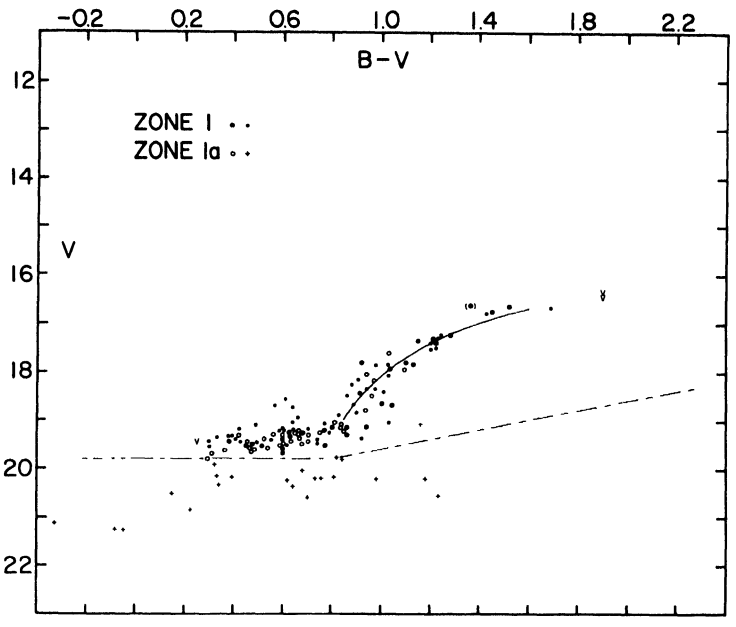

FIG. 4. C.M. array of NGC 121 (SMC globular). (Courtesy, W. G. Tifft, from M.N.R.A.S.)

to those studied in the Galaxy. It seems probable that nearly all stars in the diagram really belong to the cluster. NGC 121 (like all the conspicuous Cloud globulars) is a large cluster with a radius of about 50 parsecs according to Tifft. Unfortunately the c.m. arrays of the truly central portions of Cloud globulars are essentially unobservable, but it is satisfactory that such a clear array is shown by the outer parts of NGC 121. Tifft comments on the oblateness of Cloud globulars which may perhaps indicate more rapid rotation than in globulars of our Galaxy.

Information regarding spectra of red globulars in the Clouds is extremely scanty. Kinman has classified NGC 1835 (LMC) as F6 from H lines, F3 from Fe lines, and intermediate from CH/H a situation that is very similar to that in normal globulars (Thackeray, 1959).

IV

VARIABLE STARS

As an introduction to the subject of variables in the Magellanic Clouds, Table III summarizes the position regarding the known existence of various types of variables in the Clouds.

TABLE III

VARIABLES REPRESENTED IN THE CLOUDS

	LMC	SMC	Reference
Cepheids	Numerous	Numerous	
RR Lyr (clusters)	Yes	Yes	
RR Lyr (general field)	?	Yes	
Novae	6[a]	4[a]	
Eclipsing binaries	23	27	(Shapley and Nail, 1953a)
LPV (clusters)	?2	3	
(general field)	?	?2	(Dessy, 1959)

[a] Only 3 novae are quoted by Payne Gaposchkin (1954) for each Cloud.

A. *Classical Cepheids and the P-L Relation*

The richness of both Clouds in Cepheid variables at essentially the same distance and to a large extent free from serious reddening is perhaps the most important aspect of the Magellanic Clouds at the present time, as it has been since Miss Leavitt's discovery of the Period-Luminosity relation. Shapley and Nail (1955) have given a useful bibliography of the extensive Harvard work on periods of individual Cepheids.

Current efforts are of course being directed towards establishing the period-luminosity relation on a firm photometric basis. Two-color light-curves were derived photographically by Arp (1960) for 69 SMC cepheids based on a photoelectric sequence down to $V = 19.0$. The general character of the old Harvard light curves were confirmed by Arp, but secondary "bumps" are not mutually confirmed, as though they represented transient features. It is instructive to compare Shapley's (1940) old P — L relation (photographic)

$$m = 17.04 - 1.74 \log P$$

with Arp's

$$B = 17.70 - 2.23 \log P$$

The changes are a direct consequence of the old Harvard sequence being too bright, and increasingly so towards fainter magnitudes. Arp finds a standard deviation of ± 0.24 mag. about his mean relation. There is a marked correlation between individual deviations from the mean P — L relation (ΔB) and deviations in color from the mean color-magnitude relation. Arp holds these to be intrinsic deviations, although it could be due in part, if not largely, to reddening of the cepheids within the SMC, or in the galactic foreground (Section II). Theoretically, the intrinsic deviations in ΔB correlate with color deviations in very much the same way as deviations due to reddening.

Woolley (1962) has reported on the results of the Herstmonceux LMC program which, like Arp's work, depended on photographs taken at the Cape Observatory and a photoelectric sequence set up with the Radcliffe reflector. For 48 LMC variables periods were derived for 31 cepheids (of which 19 were known Harvard variables). The material for deriving the P — L relation was restricted to cepheids with the largest amplitudes ($\Delta B > 1.4$), as in Arp's work. The resulting P — L relation is

$$B = 17.86 - 2.85 \log P$$

It is clear that these results agree with Arp's for the Small Cloud at the faint end (where there are numerous variables) but that the rarer long-period cepheids in the LMC are some 0.7 to 0.8 mag. brighter than those in the SMC. Whether the discrepancy is a general one characteristic of the whole Clouds will therefore depend on further investigations of bright cepheids in the two Clouds. Gascoigne, Hodge, and Tifft are all working on this problem. Gascoigne's (1960) results imply little difference between the two Clouds.

For comparison with the galactic cepheids Kraft (1961) has compiled accurate data for the few variables apparently associated with galactic clusters and found slopes of the P — L relation highly dependent on whether the pulsation parameter Q is constant (Case I) or increasing linearly with P (Case II); the corresponding slopes are 3.05 and 2.15, respectively.

It has long been known from the Harvard work that a considerable scatter exists in the P — L relation of both Clouds. While the accuracy of modern photometry will undoubtedly reduce the scatter, it seems certain that an intrinsic scatter will persist. Mrs. Gaposchkin (1961) lists the following factors contributing to the scatter, nearly all of which have been previously mentioned by Shapley:

1. Internal absorption in the Clouds.
2. Thickness of the systems ($\pm 0^m2$).[4]
3. Undetected companions.
4. Errors in the magnitude systems.
5. Intrinsic dispersion.
6. Possible errors in periods.

Mrs. Gaposchkin has plotted *minimal* magnitudes (rather than the customary mean magnitudes) against $\log P$, and distinguished light curves of various classes by different symbols. In this presentation, variables of a given class of light curve seem to follow different P — L relations from that suggested when all variables are lumped together indiscriminately.

[4] For a local investigation, like Arp's, this figure should be smaller if the cepheids, as Population I, are confined to a plane as in de Vaucouleurs' model.

As is well-known from Shapley's work, the frequency distribution of periods in the SMC seems to differ significantly from that of galactic cepheids, in the sense that periods less than 2 days are extraordinarily common in the SMC. The question of the thoroughness of search in the Galaxy for the (fainter) variables with periods less than 2 days deserves examination, although it is perhaps unlikely to be responsible for the whole difference. Shapley has also found that in the dense inner regions of the SMC the frequency distribution is more normal. The suspected correlation of frequency distribution of periods with star density does not seem to be confirmed in the Large Cloud (Shapley, 1961).

Arp and Kraft (1961) found that Arp's SMC cepheids differ from galactic cepheids near the sun in their period-frequency distribution, their period-amplitude relations, and to a much less extent in their period-color relations. They also point out that the space density of their cepheids in the SMC is approximately three times that of galactic cepheids near the sun. Perhaps the most striking difference lies in the large amplitudes of the numerous 2-day cepheids in the SMC; the relatively few 2-day cepheids near the sun have small amplitudes. The scarcity of comparable variables in the Galaxy can hardly be attributed to selection, but the possibility remains that it is a scarcity characteristic of the sun's galactocentric distance.

In the LMC the frequency-distribution of periods appears to be intermediate between the SMC and the Galaxy.

Feast (1956) has made important spectroscopic observations at 86 A/mm of some of the brightest cepheids in the Cloud, which not only prove Cloud membership through radial velocity but fail to reveal significant differences from galactic cepheids (see also Feast *et al.*, 1960).

It is of interest to note that the intensive search for cepheids in galactic clusters since about 1955 was stimulated at least in part by the discovery of some 13 cepheids in the LMC cluster NGC 1866 by Shapley and Nail (1951a) and independently at the Radcliffe Observatory (quoted by Baade, 1951). Two-color light-curves of these variables based on Radcliffe plates are being worked up by Sandage. Hodge (1961a) has discovered a few more such variables in NGC 1856 and in other blue LMC clusters. The periods of the variables in NGC 1866 are very strongly concentrated near 3 days, but this is not the case with Hodge's additional variables.

In concluding this section, it is obvious that our knowledge of the cepheid phenomenon and of the intrinsic width of the period-luminosity relation will be enormously deepened by current programs of photometry of Cloud cepheids. In no other field of astronomy has the concentration of astronomical equipment and manpower in the north been more unfortunate.

B. *RR Lyrae Variables*

The first definite examples of this important class of variable in the Clouds were discovered at the 19th magnitude in the globular cluster NGC 121 (Thackeray, 1951), originally considered as possibly lying beyond the SMC. However, further examples were discovered in the LMC clusters NGC 1978, 1466 (Thackeray and Wesselink, 1953, 1955) and later in NGC 2257 (Alexander, 1960). Since the character of the Cloud globulars was considered to be somewhat different from that of the globulars in our own Galaxy, these discoveries constituted the first definite proof of a Population II component in both Clouds.

Periods and light curves have been derived for 3 RR Lyr variables in NGC 121 (Thackeray, 1958) and the periods confirmed by Tifft (1962), who however finds these variables considerably fainter than Thackeray and Wesselink (1955). Alexander (1960) has detected 28 variables in NGC 2257 (LMC outskirts) and derived periods between 0.51 and 0.69 days for 6. Characteristics of the Bailey a- and b-types are well shown in all the known light-curves. Moreover, it seems certain that some of Alexander's variables in NGC 2257 are of Bailey c-type, with sinusoidal light curves of small amplitude; the period of one of these variables appears to be either 0.2497 or 0.3329 day. Wesselink has found 44 short-period variables in the cluster NGC 1466 lying roughly midway between the Clouds, and derived periods for 7 of them; one of them at least appears to be a Bailey c-type, with varying amplitude.

The small amount of data to hand on such variables suggests properties very similar to those in well studied globular clusters in the Galaxy.

Since all these three clusters containing known variables lie in the outskirts of the Clouds it might be held that the properties of clusters depend on how far they lie from the centers of the Clouds. However, it must be stressed that the detection of faint variables in Cloud clusters, and still more the derivation of periods, is not an easy matter even when one is dealing with an outlying cluster freed from the interference of the general background of Cloud stars. A few variables have been detected in the LMC globular NGC 1978 situated in a rich region, but such clusters lying within the general body of the Clouds have certainly not been searched so intensively and cannot be searched so efficiently as those lying in the outskirts.

Outside of globular clusters, a few short-period variables are known in the general field of the SMC. Six are known near NGC 121 (Thackeray, 1958; Tifft, 1962) with $V = 19.6$ according to Tifft. At Cordoba, variables with periods less than 1 day were found at about magnitude 17 by Dartayet and Dessy (1952) and Dessy (1959). Dessy (1959) reports 14 stars with periods less than 1 day, 7 with periods between 0.8 and 0.9 day. These stars are bluish-white in color. Four of them are classed as eclipsing binaries, and 8 of the remaining

10 are classed as certainly cepheids. These 8 stars have a mean apparent magnitude 17.0 ± 0.2 and are thus much brighter than the RR Lyr variables in NGC 121 (and the surrounding field). One may reasonably enquire whether some of them belong to the galactic halo rather than to the SMC. Not much is known about the frequency of faint RR Lyr variables in the galactic halo, but Baade found 5 of about 17th magnitude in a field of 8.5□°. Dessy's field was only 0.6□°. On this count therefore one can hardly attribute more than one at most of Dessy's 8 cepheids to the galactic halo. It is possible that Dessy's field has been more intensively searched for variables and it is also possible that his stars are somewhat fainter than 17.0 mag., but there can be little doubt that most of these stars are true Cloud members. Dessy regards them as Population I variables, as opposed to the fainter cluster variables. Dessy (private communication) is similarly investigating a field centred on CoD −70°330 (LMC) and has found several hundred variables, not yet classified.

Arp (1960) had one SMC Harvard variable (11197) with period 1.07 day in his field of about 1° which he considered to be like Dessy's variables, although with $B = 16.7$ it is somewhat bright. Arp regards this variable as a Cloud member pulsating in a higher mode. The possibility of its being a foreground star does not seem to have been excluded.

Wesselink (1962 private communication) has discovered 5 stars (of about 18th apparent magnitude) in a rich field of the SMC with periods less than 1 day, which may belong to the same group as Dessy's variables.

A 1.43-day cepheid near NGC 121 discovered by Tifft (1962) and independently at the Radcliffe Observatory is regarded by Tifft as the first known case of a Population II cepheid in the SMC. This classification is based on Tifft's observations of magnitude and color ($V = 18.05$, $B - V = +0.35$).

The fragmentary information to hand suggests that there may be a spread of at least 1.0 mag. in the apparent magnitudes of RR Lyr variables in the SMC at a given period. As with the classical cepheids there is little reason to suppose that this can be attributed to varying absorption. Intrinsic scatter in the P — L relation seems to be indicated for both RR Lyr and classical cepheid variables.

The space density corresponding to Dessy's 10 variables, considered all as RR Lyr variables belonging to the SMC, is about 7 variables per kpc^3, which is considerably less than the space density of at least 20 near the sun in the galactic plane (Oort and van Woerkom, 1941) and of course far less than the space density of RR Lyr variables near the galactic nucleus. The space density of the fainter RR Lyr variables near NGC 121 is probably higher, but until a much more exhaustive survey of these difficult objects has been made no fair comparison with the Galaxy can be made. As has been mentioned above, Arp and Kraft find the space density of *classical* cepheids to be higher in the SMC than near the sun.

C. *Novae*

The total of novae recorded in the Clouds remains at the low figure of 10, and relevant data for this short list are quoted in Table IV from Henize *et al.* (1954), with N Hyi 1935 added although this may have been a supernova in the outskirts of NGC 1511. In many cases the light-curves are very fragmentary, and the maximal magnitudes are often quite uncertain. The column headed a_{pg} is an estimate (by the writer) of the amount of photographic absorption (whether foreground or in the Cloud) taking into account the distance from the center of each Cloud. The absolute magnitudes are derived taking account of this absorption and with $m_0 - M = 18.7$. It is remarkable that 4 of these novae were discovered between 1948 and 1952. An intensive patrol of the Clouds for novae, such as that carried out by Arp in M 31, would probably not be very rewarding, but nevertheless with many suitable telescopes now operating in the south it is to be hoped that we may gain a more accurate idea of the true frequency of occurrence of Cloud novae.

TABLE IV

NOVAE IN THE MAGELLANIC CLOUDS

SMC	m_{pg} (Max:)	a_{pg}	M_{pg}	Type	Reference	Distance from core
N Tuc 1897	11.0:	0.2	− 7.9	Fast	H.B., 920	1°.8
N Tuc 1927	11.4:	0.3	7.6	Slow	H.B., 898	0.7
N Tuc 1951	11.5	0.3	− 7.5	Fast	H.A.C., 1143	0.7
N Tuc 1952	11.0	0.4	− 8.1	Fast		0
LMC						from bar
RY Dor 1926	12.0:	0.3	− 7.0	Slow	H.B., 847	1°.8
N Hyi 1935	11.0	0.2	- 7.9	Fast	H.B., 917	°.5
N Dor 1936	10.5:	0.3	− 8.5	Fast	H.B., 912	1.8
N Dor 1937	13.0:	0.4	− 6.1	Slow		0
N Men 1951	11.9	0.4	− 7.2	Very fast		0.1

It is interesting to compare the frequency of occurrence in the Clouds with that in M 31 for which Arp (1956) gives an accurate figure of 26 ± 4 per annum. The combined masses of the Clouds may be taken as very roughly 15% of M 31 (Section VI), so that if the frequency of novae in M 31 is diminished in proportion to the masses one might expect about 2 per annum (or 1 per observing season) in the Clouds. There is nothing to suggest that the Cloud novae are

unduly rare. Henize *et al.* (1954) point out that the frequency *per mass* is probably higher in the SMC than the LMC.

Few of the ten novae listed occurred within the main body of either Cloud. It seems probable that many may have been missed owing to crowded images. It is worth recalling here that several Cloud members bear some resemblance in their spectra to Eta Carinae in its present stage of development. If these are old "slow supernovae" which passed through a maximum of similar luminosity to that of Eta Car in 1841, they would have reached the level of naked eye visibility.

The rates of decline, whether fast or slow, are quoted in the table, and it should be pointed out that the two slowest (RY Dor 1926 and N Dor 1948) are also the faintest, thus confirming the correlation of luminosity and rate of decline found by McLaughlin and Arp. Schmidt (1957) has used this correlation to derive a distance modulus of 19.2 for the Clouds.

D. *Eclipsing Binaries*

Shapley and Nail (1953a) have discussed 49 eclipsing variables which appear to belong to the two Clouds. The earliest cases known were presumed to be foreground, but a concentration of four 15th magnitude binaries near 30 Doradus was the first indication of Cloud membership, and then too many cases appeared elsewhere in the Clouds to be attributed to the foreground.

Russell (1956) has analyzed the light-curves of four well observed binaries (3 SMC, 1 LMC) and finds them essentially similar to β Lyr variables in the Galaxy, with partial eclipses of moderate depth. The one suggestion of a difference lies in the relatively low density found for the Cloud stars, but Russell suggests that this may be due to selection of long periods. One of Russell's four stars (HV 2241) has been proved spectroscopically to be a B type member of the LMC (Thackeray, 1962).

The famous variable S Dor is no longer to be regarded an eclipsing binary (Wesselink, 1956). A minimum was observed disagreeing with Gaposchkin's ephemeris, during which [Fe II] emission developed. The variations may perhaps be as unpredictable as those of Eta Carinae. Wesselink draws a very reasonable parallel between S Dor and the Hubble-Sandage variables in M 31.

E. *Long-Period and Irregular Variables*

Irregular variability must be very common among the brightest stars in the Clouds, more particularly among the red stars.

True "long-period variables" comparable with the Mira-type variables in the Galaxy may not yet have been detected in the Clouds. Shapley and Nail (1951b) have listed 11 red variables with periods ranging from 254 to 741 days which are

probably SMC members; but in photographic absolute magnitude at maximum they range from −2.7 to −4.5, and they are thus considerably brighter than the typical Me variables; moreover, they suggest a P — L relation quite different from that for galactic Me variables. The survey should be carried down to 20th magnitude, more particularly as the relationship of the Me variables to Baade's Populations I and II remains somewhat obscure.

In the SMC globular cluster NGC 121 Thackeray (1958) found two of the brightest stars to be long-period variables with periods of 140 and 112 days. Tifft (1962) in confirming photometry gives them ranges in V of 15.4 to 17.3, and 16.3 to 16.55, respectively, and colors B — V of +1.9. Tifft has also found signs of irregular variability in several red stars of similar brightness in the surrounding field. Gascoigne (private communication) has found one red variable (V = 15.4 to 16.4) in NGC 1783, presumably of long period.

V

GENERAL STELLAR CONTENT

A. *Brightest Stars*

Just as visual surveys and direct photography had shown clusters and nebulae in both Clouds which are normally found only in the galactic plane, so the spectral classifications contained in the HD Catalogue (and particularly in the HD Extension Catalogue covering the Large Cloud) showed the presence of numerous examples of extreme Population I—stars of type B, emission O, and P Cygni.

Our knowledge of these extremely luminous objects has been considerably refined by means of slit spectroscopy undertaken for some years at the Radcliffe Observatory. Feast *et al.* (1960) have published spectral classifications for over 150 objects, and a few more have recently been added to the list (Thackeray, 1962). In most cases a single slit spectrum gives convincing proof whether or not a particular star is a true member of the Magellanic Clouds; the two criteria—(a) large radial velocity (about +275 or +170 km/sec for Large and Small Cloud, respectively) and (b) characteristics of high luminosity—can usually be recognized through examination under a hand eyepiece. Rare instances of residual doubt occur. The high velocities of each Cloud largely reflect the component of galactic rotation of the solar neighborhood; thus one must expect some galactic foreground stars belonging to Population II to have velocities similar to the Clouds. However, the spectral characteristics should clearly distinguish such objects.

Slit spectroscopy tends of course to be an inefficient approach to the problem of

distinguishing between Cloud members and foreground stars (unless one has already some safe guide like a Harvard classification of "B"). A far more rapid approach is through Fehrenbach's objective prism technique; the first successful application of this technique to the LMC was recently announced (Fehrenbach and Duflot, 1962) in which a double exposure (2 + 2 hr) with a 40-cm objective prism yielded some 250 spectra of which more than 30 could be quickly recognized as Cloud members. The objective prism technique will be of special importance in two directions: (a) in the Small Cloud where there are no HDE classifications and only 11 Cloud members included in the HD Catalogue; (b) in the recognition of the red super-supergiants, five of which were discovered by Feast and Thackeray (1956) (see following section). The foreground abounds in stars with the same colors as these important stars.

The two brightest stars in the LMC are HD 33579 and the variable star S Dor, both with V near 9.2 and consequently $M_V \sim -10$. These "stars" radiate approximately a million times as much as the sun. Their masses are probably of the order 100 $\odot$ and they must be regarded as at the limit of stellar stability. Both stars are of type A, and in fact the HR diagram yielded by the Radcliffe observations shows a band sloping down to the left from these A supergiants to absorption O stars which are not found brighter than $V = 12.0$. *Bolometrically* the stars in this band are comparable, and this upper bolometric limit corresponds reasonably well with the predictions of Schwarzschild and Härm (1958). These workers predict that the most luminous stars near this limit should show signs of instability, possibly fluctuating in light with periods of a few hours. Spectroscopically the brightest Cloud stars *do* show some signs of instability in the appearance of P Cyg type emission. The photoelectric observations also show some evidence of *small* variability (of order 0.15 mag. for the red stars); periods as yet have not been derived and may not exist.

It is of interest that at a slightly lower luminosity ($M_V \sim -7.5$) some objects are found with [Fe II] emission, thus having some affinity to Eta Car (currently $M_V \sim -6$). S Dor itself showed [Fe II] emission during a minimum phase (Wesselink, 1956). The [Fe II] emission probably originates in a vast low-excitation corona, perhaps with a diameter like that of the solar system; rare supermassive objects like these may be producing clusters or expanding associations of stable stars as Eta Carinae appears to be doing. H. Smith (1957) has described spectra of 11 emission objects in the LMC with [Fe II] or He I bright. Photometrically he finds ultraviolet excess compared with B stars, which in some cases seems to be due to continuous radiation.

Wolf Rayet stars appear in the LMC in considerable numbers and at least one is known in the SMC. The spread in magnitude is large; in the HDE examples (classed as "O") are known extending from 11 to 16 mag. and fainter ones may still be found. The region of the great 30 Dor nebula shows a regional

concentration of these stars; Feast (1961) has added some new examples to the HDE list and finds that every one in the 30 Dor region is of WN type; however, two WC objects (HD 32228 and R 90) are known elsewhere in the LMC.

Detailed comparison of the spectra of O, B, and A type members of both Clouds with MK standards has so far failed to reveal any outstanding differences which one would attribute to a *general* difference in composition of the Clouds and Galaxy. The few peculiarities noted probably arise from the extraordinary luminosity of the Cloud supergiants and the difficulty of finding exact galactic counterparts, particularly among the cooler stars. It is possible that the spectra of some or most Cloud supergiants are complicated by the presence of circumstellar shells.

A list of 23 elements certainly and 3 doubtfully identified in Cloud spectra has been compiled by the Radcliffe observers; lanthanum is certainly the heaviest found.

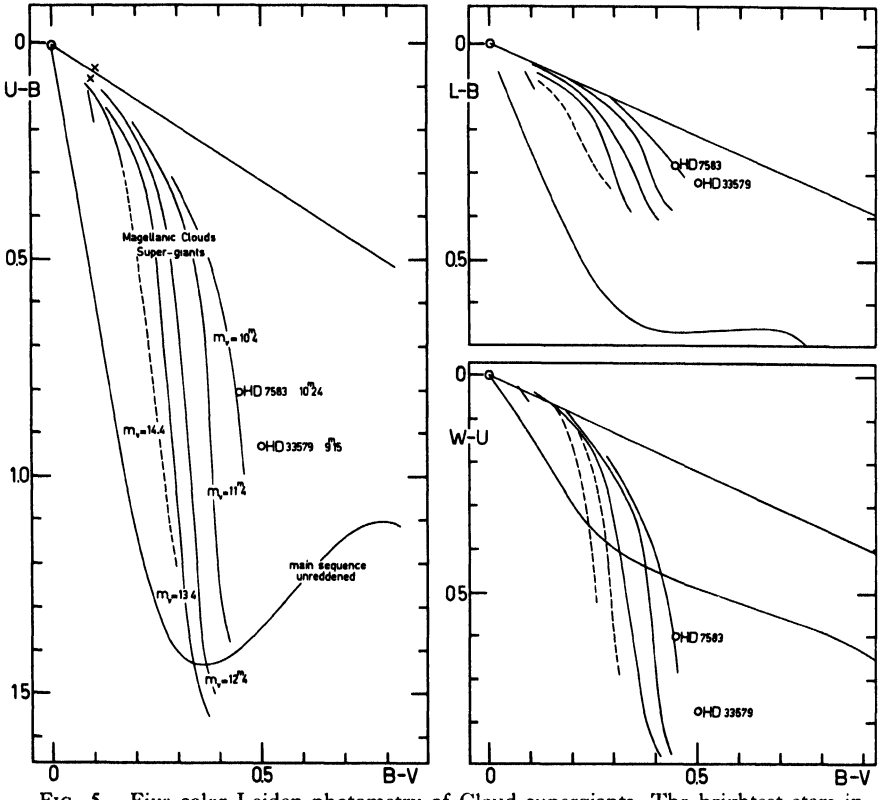

FIG. 5. Five-color Leiden photometry of Cloud supergiants. The brightest stars in each Cloud are shown—H. D. 33579 (LMC) and 7583 (SMC). (Courtesy, T. and J. Walraven.)

The Walravens reported important results of their 5-color photometry (T. and J. Walraven, 1960) of bright Cloud supergiants at the 1962 IAU Congress. Figure 5 shows UBV, LBV, and (W − U) − (B − V) plots. Among the blue supergiants it appears that there is a family of curves in the UBV diagram with luminosity as a definitive parameter. A similar situation occurs in the other plots. Here there seems to be scope for an accurate comparison with galactic stars at a lower limit of luminosity than can be comfortably reached in Cloud spectroscopy. It is at the level of 15 mag. or fainter that the comparison of Cloud and galactic stars offers the best hope for determining the distance modulus with an accuracy of 0.1 mag.

Wesselink (1962) has also published a UBV plot of bright Cloud supergiants in which there is no essential difference between SMC and LMC stars. He has set up bright standards distributed over both Clouds in the Johnson U, B, V system, and the reader will find useful references in the paper to standard photoelectric sequences used by other workers in the Clouds. Wesselink has also plotted the Johnson-Morgan parameter Q (independent of reddening) against spectral type. Here there is some indication that the A supergiants differ in the two Clouds as if the Balmer jump were stronger in the SMC than the LMC; the B stars remain similar. The few A type spectra that are available have sometimes been suspected as showing somewhat stronger H absorption in the SMC, but this has been attributed to lower luminosity of the stars concerned.

When the UBV plot is extended to include the red super-supergiants Radcliffe photometry has shown a smooth curve with essentially no "hydrogen dip" (Thackeray, 1957). This is not surprising in view of the extreme narrowness of the H lines in these supergiants.

B. *Red Stars*

While the evolution of massive and luminous OB stars seems to be well understood from studies of galactic clusters, the picture of how supergiants come to occupy and pass through the top right corner of the HR diagram is still obscure. Luminous red stars, some of them *very* red ($B - V > 2$), are present in considerable numbers in the Clouds. Shapley and Nail (1953b) deduced the probable existence of such objects from star counts and statistical allowance for foreground. They are sometimes referred to as M-type supergiants, on account of red color, but the first actual observation of TiO bands in 13th magnitude stars which probably belong to the Cloud was by Westerlund (1960) working at 2200 A/mm. The red super-supergiants (F to G) discovered by Feast and Thackeray are very red for their spectral types, but this can be understood in terms of an extension of the normally increasing redness of giants compared with dwarfs at the same ionization temperature. Fehrenbach and

Duflot (1962) have discovered HDE 269788 to be a LMC member with spectral type K5, later than any in the Radcliffe list; Radcliffe spectra in the green region of this star have failed to show any sign of the strong TiO bands that might be detected with higher dispersion.

Westerlund (1960) has cataloged 303 very red stars in various regions of the LMC based on an infrared survey with the Uppsala Schmidt telescope at Canberra. Of these, 225 are classed as MO by Westerlund, and 9 of them appear to be carbon stars. His stars are much redder than HDE 269788, mentioned above. Radcliffe spectra of a few of Westerlund's brightest stars have failed so far to find any true Cloud members. However, at a fainter limit so many red stars are present that their Cloud membership cannot be doubted. Very red stars in or near clusters have already been noted (Section III). Arp (1958a) has recorded half a dozen stars with B − V about +3 to +4, all with M_V about −2 on the assumption that they are Cloud members. It seems highly probable that these are N stars.

C. *C.M. Arrays of the General Field*

A start has been made in the study of the color-magnitude characteristics of the general field in both Clouds, particularly in regions close to clusters. It is to be expected that c.m. arrays will vary from one part of the Clouds to another, and this has indeed been found to be the case.

Arp's (1958a) c.m. array for the SMC field near NGC 419 is reproduced in Fig. 6. The blue limit, nearly vertical in the diagram, closely corresponds to the "zero-age main sequence." The sloping boundary on the right-hand side seems to indicate a real deficiency of faint red stars (*not* defined by the limit of the blue plates). The rich scattering of supergiants above $V = 17$ is found right across a very shallow Hertzsprung gap in much the same way as the super-supergiants cross the top of the HR diagram of the brightest stars. Near the top of the Hertzsprung gap there lie three cepheids (shown by crosses in the figure) and there are possibly more undetected cepheids in the diagram.

In contrast with this figure for a field close to the main body of the SMC, the c.m. array for a region far out from the SMC by Tifft (1962) is shown in Fig. 7. This field is complex in that it combines numerous members of the globular cluster NGC 121 (cf. Fig. 4), and a galactic foreground which is partly composed of outlying members of 47 Tuc.

The outlying field near NGC 121 is obviously deficient in the blue main sequence which dominates the more central region near NGC 419. Moreover, Tifft draws attention to the spread in luminosities of the red giants compared with the red giant branch of NGC 121 itself (Fig. 4). Finally there are some very faint red stars which (provided that they belong to the SMC rather than

to the galactic foreground) Tifft regards as older than the members of NGC 121 and of the galactic cluster M 67. Tifft reports that preliminary results on another SMC field not so far out as NGC 121 indicate a population intermediate in age between the fields of Figs. 7 and 4. Clearly such regional surveys in the Clouds are of utmost importance to theories of stellar evolution.

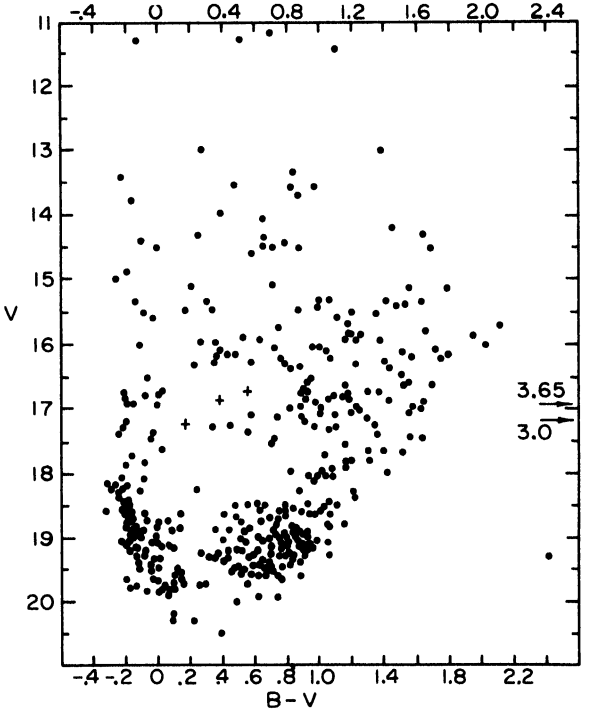

FIG. 6. C.M. array of the SMC field near NGC 419. (Courtesy, H. C. Arp, from A.J.)

Hodge (1961b) has published c.m. arrays of two relatively open LMC areas. These are based on complete sampling of all measurable stars to $V = 17$ and extending to $V = 18$. His area I (miscalled II in his Fig. 1) includes a moderately well-populated part of the Cloud and shows a nearly vertical blue branch, together with some very red stars out to $B - V = +2.1$. There are many stars filling what would normally be the Hertzsprung gap at colors $B - V = +0.6$ to $+1.2$. In Hodge's area II, which is poorly populated, there is no sign of a vertical blue branch. In other words, the contrast between the two areas is similar to that between Figs. 7 and 4 referring to the SMC. However, Hodge appears to have made inadequate allowance for foreground stars, especially in Area II (see following section).

It should be borne in mind when examining such c.m. arrays going to faint limits that not only some foreground stars must be expected, but also that the arrays have been drawn up under the assumption of no reddening. Foreground stars will be troublesome in sparse areas like Hodge's, and reddening, varying across the field, may be present in the richer areas.

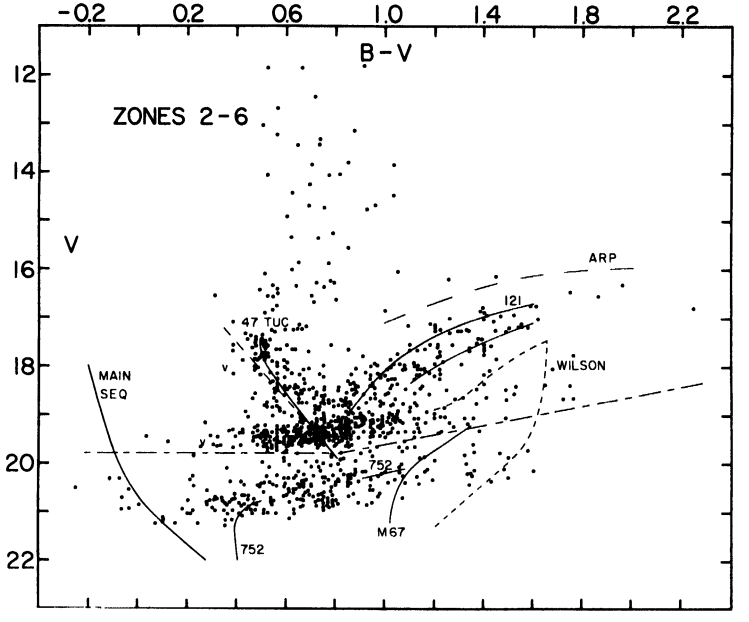

FIG. 7. C.M. array of the SMC field near NGC 121 (Courtesy, W. G. Tifft, from M.N.R.A.S.)

D. *General Luminosity Function and Foreground Stars*

In view of current interest in the general field of both Clouds, Shapley's (1931a, 1932) early work on the LMC luminosity function becomes of renewed interest, despite the necessity to revise magnitude scales. Within the area of Cloud clusters one may be reasonably sure that one is dealing almost entirely with Cloud members, but in the general field it is far more difficult to eliminate the contribution of foreground stars.

In Fig. 8 Shapley's general luminosity function for the LMC appears as the right-hand part of the solid curve, while in the lower left-hand corner open circles correspond to the luminosity function defined by known bright members of the Cloud. Down to 10.7 (B) our knowledge of Cloud members is probably nearly complete; fainter than this, the counts include all O, B, Con stars in the

HDE Catalogue of the LMC (with magnitudes corrected by 0.3 as appears to be required). Shapley's luminosity function must have greatly overestimated the number of bright stars (M brighter than -7). The solid curve represents a rough attempt to interpolate between the revised bright end and Shapley's faint end.

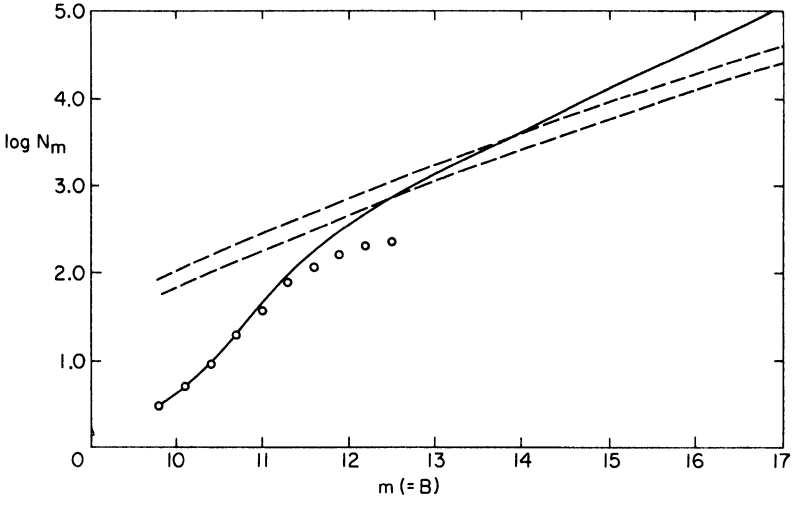

FIG. 8. Approximate general luminosity function for the LMC (continuous curve). Open circles represent counts of known bright members. Dashed curves represent foreground stars (Seares, v. Rhijn) within circles of radius 3°3 (upper) and 2°6 (lower).

The two dashed lines give log N_m for the foreground stars taken from van Rhijn and Seares for an area centered on the LMC; the upper curve corresponds to a circle radius 3°3 (which contains all bright Cloud members), the lower to a circle radius 2°6. Taken at its face value, the figure suggests that in a random choice of stars within the LMC one does not have more than a 50% chance of picking a Cloud member until below $m_{pg} = 14.0$. Since the old photographic magnitudes (for both Cloud and foreground stars) are increasingly too bright at the faint end, the 50% level probably lies even fainter than $m_{pg} = 14.0$.

Of course, the general luminosity function for the whole Cloud carries little meaning, as Shapley stressed, in view of the very strong tendency towards clustering in certain areas, and it is these areas which have attracted most attention so far. De Vaucouleurs *et al.* (1954) have published luminosity functions for various areas which emphasize Shapley's conclusions regarding strong regional variations.

Westerlund (1961a,b) has derived luminosity functions for clustered regions

in both Clouds. The slope of his function ($\Delta \log N_m/\Delta m$) is flatter than that of the solid line in Fig. 8 presumably because his regions are concentrated on young bright stars. Westerlund finds that his function for both Clouds compares well with Sandage's (1957) initial luminosity function $\psi(M_V)$ and still better with Sandage's "evolved luminosity function" $\psi(M_V + 1.5)$. In the SMC, Westerlund's region includes clusters which appear to form "part of the youngest arm of the Galaxy."

VI

DYNAMICS OF THE CLOUDS

For nearly 40 years our knowledge of the motions of the Clouds was confined to 17 radial velocities of emission nebulae somewhat concentrated in a few regions of the LMC, together with one SMC nebula, all observed by the Lick Southern Expedition. Nevertheless, these observations had two important results. One was that the large mean velocities of +275 km/sec (LMC) and +168 km/sec (SMC) suggested that the Clouds probably lay outside the main body of the Galaxy. It is now recognized that these velocities mainly reflect the component of the sun's galactic rotation. The second result of the Lick observations was a rather vague suggestion of a gradient of velocities across the body of the LMC which could be due to either rotation (Wilson, 1917) or translation (Hertzsprung, 1920) with a very high velocity.

A. *Motions within the Large Cloud*

The first results of 21-cm velocities in the LMC, due to the Sydney observers (Kerr *et al.*, 1954) put the gradient of velocities beyond doubt and were particularly important in that the direction of maximum gradient lay along de Vaucouleurs' major axis defined by faint outer isophotes. This in itself gave some support to de Vaucouleurs' model of an inclined plane for the LMC. However, the gradient of 21-cm velocities was smaller than that from optical velocities [14.2 km/sec/deg according to the latest optical results (Feast *et al.*, 1961)]. The contrast between optical and radio results is especially marked if median 21-cm velocities instead of peak velocities are used. The H I profiles are considerably asymmetrical in different senses on opposite sides of the LMC.

While the gradient of velocities is nearly linear out to 3° from the center of the LMC, the 21-cm results gave the first indications that the velocity-curve bends over beyond 3° as if the system were subject to differential rotation like the Galaxy. Thus we have proof that the LMC is rotating and that the gradient of velocities is not *primarily* due to translation. However, since the proper motions

of the Clouds cannot be measured, we can say nothing about their translational velocities, except that they are unlikely to exceed 100 km/sec. If the LMC should in fact be moving at 100 km/sec in the plane of the sky along the direction of maximum gradient of radial velocities (p.a. 171°), then this would account for 12% of the observed velocity gradient. Any derivation of mass from the observed gradient must be subject to this limiting accuracy (Feast *et al.*, 1961). However, the masses that have in fact been derived are subject to considerably greater uncertainties.

The greatest uncertainty arises from the assumed inclination i of the system (considered either as a thin disc, or ellipsoid, or a combination of ellipsoids) to the plane of the sky. The mass derived is proportional to $\csc^2 i$. De Vaucouleurs considers values of i in the range 27° to 15° (with the former regarded as the best) and the consequent range of masses is about 3 : 1. Clearly, the Clouds can only be considered as thin discs or ellipsoids to a very rough approximation.

Secondly, the mass of the Cloud must increase directly with the assumed distance, and must therefore remain in considerable doubt until this fundamental measure has been improved.

Finally, the outer part of the rotation curve is poorly determined, and the mass determination is subject to the usual doubts of extrapolation to "infinity" for whole galaxies.

In the first determination of mass of the LMC (with $i = 25°$) Kerr and de Vaucouleurs (1956) gave 3.0×10^9 ⊙ as their best estimate, chiefly from 21-cm velocities. Later, de Vaucouleurs (1960a) increased the estimate nearly tenfold to 2.5×10^{10} ⊙ in a rediscussion using a few new nebular velocities by himself from Mt. Stromlo data. The increase was chiefly due to the larger angular velocities suggested by optical data (Feast *et al.*, 1955). In a later revision, de Vaucouleurs (1962) reduces the mass to $(1.4 \pm 0.3) \times 10^{10}$ ⊙, partly as a result of using a smaller distance.

Feast *et al.* (1961) used Radcliffe radial velocities of 61 LMC stars (extending further along the major axis than de Vaucouleurs' material) combined with the Lick nebular velocities in a new discussion. The best estimate of the mass of the LMC within 4°.5 of the center is considered to be 1.0×10^{10} ⊙. H I is found to contribute about 6% of the total mass (with 8% as a maximum).

One of the puzzling features of these results is that both radio and optical velocities define rotation curves which are symmetrical about a center displaced by about 1° to the north of the main axial bar. However, the centroid defined by the 21-cm isophotes does appear to coincide roughly with this center of rotation.

The asymmetry of the H I profiles is a further interesting feature which may become better understood when observations with the 210-ft telescope become available. Kerr and de Vaucouleurs were inclined to attribute the low-velocity

wings of the profiles to a smaller angular velocity at a considerable height above the central plane. However, it seems simpler to attribute it to the slower rotation to be expected in the outer parts of a roughly spherical gaseous system; while the high-velocity peaks arise within the main plane, closer to the center. The nebulae and luminous stars responsible for the optical rotation curve should be visualized as confined to the main plane.

The stellar radial velocities are particularly important in that they provide for the first time a direct idea of the velocity dispersion of stars in an external system, and we can also study to some extent how this velocity dispersion varies across the system. After correction for rotation, the directly observed dispersion for 61 supergiant stars (excluding P Cyg and other peculiar objects) is 17.5 km/sec (Feast *et al.*, 1961); allowance for observational errors reduced this to 15.1 ± 1.9 km/sec or less.

This is a relatively small value, comparable with that found for galactic B stars, and considerably smaller than that suggested for the H I gas by the early 21-cm profiles. It is no longer true that the energy of random motions in the LMC is comparable with the energy of rotation as first maintained by Kerr and de Vaucouleurs (1956), at least for the region occupied by the supergiants. The smallness of the velocity dispersion compared with the rotational velocities does in fact offer rather strong support to de Vaucouleurs' inclined-plane model. It is of course reasonable that the velocity-dispersion should increase out of the plane, as in the galactic halo, and that a higher velocity-dispersion should show up in the 21-cm results than in the optical results, providing the H I gas extends well out of the plane.

The random velocities of emission nebulae measured optically is claimed by de Vaucouleurs (1960a) to be as low as 7 km/sec, while Feast (1961) has found 11.3 ± 3.2 km/sec for parts of the 30 Dor nebula from slit spectra. Within the same nebula Feast finds that the spectrum of turbulence does not obey Kolmogoroff's law.

The Radcliffe stellar velocities are sufficiently numerous to be subdivided according to position within the Clouds or according to physical properties. There is a definite tendency for the random velocities to be greater in the *center* of the LMC than in the outer regions, and a less certain indication that the brightest Cloud members show greater random velocities than the fainter stars studied (which are still to be regarded as very luminous supergiants).

A larger velocity dispersion is to be expected in the center for a number of models, e.g., a spherical system held together gravitationally (neglecting stellar encounters), or an expanding spherical system, or in de Vaucouleurs' flattened system. It is tempting to draw an analogy with the larger velocity dispersion which must be associated with the nuclear bulge of spirals. However, the LMC stars observed for velocity are all young Population I stars.

With regard to the vaguer suggestion that the brightest Cloud stars have greater random velocities than those slightly fainter, we may draw an analogy with the surprising number of galactic O stars with high velocities. The Zwicky-Blaauw mechanism, in which one component of a massive binary system disintegrates rapidly and frees the other component with its orbital velocity, provides a possible origin for such high-velocity supergiants. The brightest star in the LMC (HD 33579) has a residual velocity from the mean rotation curve of −38 km/sec. (A still more striking case is HD 7099, one of the brightest stars in the SMC, with a residual of +81 km/sec). The random signs of the large residuals exclude the possibility of some *systematic* P Cyg effect in the spectra. However, it is conceivable that some of these high "velocities" may prove to arise in orbital motions or in circumstellar shells.

Despite the considerable effort that has gone into such matters, more observations are of course required. The objective prism technique will help enormously in this direction.

B. *Motions within the Small Cloud*

The 21-cm data suggest that the SMC is also rotating, the gradient of velocities being very roughly 6 km/sec/deg (Kerr and de Vaucouleurs, 1955). The optical data are at present too few (and of lower quality than in the LMC) and cover too small a part of the Cloud to confirm this, but suggest a smaller gradient of about 2 km/sec/deg, i.e., about one-seventh the gradient observed in the LMC. According to de Vaucouleurs, the plane of the SMC is seen less openly (with $i = 60°$) than the LMC; conditions ought therefore to be more favorable to measures of a rotational gradient of velocities.

The analysis is complicated by the presence of the wing pointing towards the LMC which is prominent in 21-cm radiation. The position of the H I centroid outside the main bar of the SMC recalls the similar situation in the LMC.

Kerr (1961) reported an extraordinary doubling of 21-cm profiles in the SMC, which he was at that time inclined to attribute to gas moving inwards from either side of the central plane.

The velocity dispersion derived from Radcliffe data (40 stars) is 15.4 km/sec (corrected for observational scatter), and is thus closely similar to the value for the LMC.

The mass of the SMC is even more uncertain than that of the LMC. According to Kerr and de Vaucouleurs (1956) the ratio of masses SMC/LMC is 0.2 to 0.5.

C. *Relative Motions of the Clouds*

The earlier determinations suggested that the masses of the Clouds were too small to keep them moving together. The larger masses that have been demanded

by the new optical velocities show that they might be moving in a closed orbit. However, a new uncertainty enters into this question, quite independently of the formidable difficulty of accurately measuring masses: we must know the sun's galactic rotation much better than at present before we can speak with confidence of the relative galactocentric velocities of the Clouds (along the directions to the sun). The situation is summarized in Table V. The radial velocities quoted are taken from the formulas of Feast *et al.* (1961) corresponding to the rotational centers. The components of solar motion plus galactic rotation ($S + G$) is given for the two values of galactic rotation 216 and 300 km/sec toward $l^I = 57$, $b^I = 0$, and finally the corresponding residual radial velocities. The differences in these residual velocities change from 59 to 40 km/sec for the two cases.

TABLE V

RADIAL VELOCITIES OF THE CLOUDS, CORRECTED FOR SOLAR MOTION AND GALACTIC ROTATION (216 OR 300 KM/SEC)

	LMC	SMC
Rotational center (1950)	$05^h20^m - 68°.8$	$00^h51^m - 73°.1$
Radial velocity	+275 km/sec	+163 km/sec
$S + G$ (216 km/sec)	+194	+141
$S + G$ (300 km/sec)	+264	+192
Residual velocity		
($G = 216$)	+ 81	+ 22
($G = 300$)	+ 11	− 29

Clearly the question of orbital motions of the Clouds cannot be solved without a much more precise knowledge of their masses, distances, and of the component of galactic rotation; and even then we are still left in complete ignorance of their cross-motions.

Finally, as pointed out by Kerr and de Vaucouleurs (1956) the problem is essentially a three-body one in that with the LMC having about one-twentieth the mass of the Galaxy and the SMC being even less massive the field due to the Galaxy at the Clouds is about the same as that of either Cloud at the other.

It is of interest to note that if the LMC is describing a circular orbit around the Galaxy, the orbital period would be about 10^9 years—longer than the ages of the conspicuous supergiants that we observe. Further, if we assume (following de Vaucouleurs) a value of $i = 27°$ for the LMC the rotational period for its central parts must be about 2×10^8 years. There has been a suggestion of tidal disturbances in the Galaxy by the Clouds. Is it possible that for the LMC at

least its orbital period is equal to its rotational period? Such a situation would only have physical significance if the rotational axis of the LMC were at least roughly perpendicular to the plane of the presumed orbit around the Galaxy. However, the rotational axis appears to point roughly toward the center of the Galaxy (with de Vaucouleurs' sign for the tilt of the LMC) and the approximate equality of orbital and rotational periods must be regarded as coincidental.

VII

CONCLUSIONS

There has been an extraordinary awakening of interest in the Magellanic Clouds in the past decade. We can expect many questions, at present in a confused state, to be more precisely answerable after a further 10 years' of photometric and spectroscopic effort; and perhaps the most hopeful line of progress lies in the detailed study of 21-cm radiation from the Clouds with the higher resolving power of the new radio telescopes. Will this prove the existence of interstellar magnetic fields more clearly than has been possible in the Galaxy?

At the 1957 Stockholm Conference on Coordination of Galactic Research (Blaauw *et al.*, 1959), the following seven heads were listed as deserving special attention:

(a) Accurate photometry of classical cepheids and RR Lyrae variables.

(b) Spectral classification and radial velocities of the brightest stars.

(c) Color-magnitude arrays of associations and globular clusters (including radial velocities where possible).

(d) Searches for long-period, RV Tau, and RR Lyr variables in the general field.

(e) Objective prism surveys for classification and radial velocities, especially in the Small Cloud.

(f) Searches for bright variables (brighter than 13th magnitude).

(g) Identification charts.

Progress has been made in many of these fields, but is only just beginning in some. The recent Herstmonceux results on the period-luminosity law raise doubts not only as to the reliability of this criterion of distance, but also as to our understanding of the whole cepheid phenomenon. We need to know far more about the Dessy-Wesselink variables of short period. We have nearly no knowledge of Me variables in the Clouds. It is possible that undetected novae have appeared in both Clouds during the past decade. We are still lacking an objective prism survey of the Small Cloud analagous to the HDE covering the Large Cloud.

Various problems, not included in the above list but which now deserve attention, have been mentioned in the course of this review—especially, studies of polarization, color-magnitude arrays of the smaller clusters, and a more accurate knowledge of the color-magnitude array of the galactic foreground in each Cloud. The list could be extended almost indefinitely, but the researches themselves will suggest the most promising lines of attack.

References

Alexander, J. B. (1960). *M.N.R.A.S.* **121**, 99.
Aller, L. H., and Faulkner, D. (1961). *A. J.* **66**, 37.
Arp, H. C. (1956). *A. J.* **61**, 15.
Arp, H. C. (1958a). *A. J.* **63**, 273.
Arp, H. C. (1958b). *A. J.* **63**, 489.
Arp, H. C. (1959a). *A. J.* **64**, 175.
Arp, H. C. (1959b). *A. J.* **64**, 254.
Arp, H. C. (1960). *A. J.* **65**, 404.
Arp, H. C. (1961). *Science* **134**, 810.
Arp, H. C., and Kraft, R. P. (1961). *Ap. J.* **133**, 420.
Baade, W. (1951). *Mich. Obs. Publ.* **10**, 14.
Blaauw, A., Larsson-Leander, G., Roman, N. G., Sandage, A. R., Weaver, H. F., and Thackeray, A. D. (1959). *I.A.U. Symp.* No. 7, 82.
Dartayet, M., and Dessy, J. L. (1952). *Ap. J.* **115**, 279.
Dessy, J. L. (1959). *P.A.S.P.* **71**, 435.
de Vaucouleurs, G. (1954). *Observatory* **74**, 158.
de Vaucouleurs, G. (1960a). *Ap. J.* **131**, 265.
de Vaucouleurs, G. (1960b). *Ap. J.* **131**, 574.
de Vaucouleurs, G. (1962). *Ap. J.* **136**, 118.
de Vaucouleurs, G., Buscombe, W., and Gascoigne, S. C. B. (1954). *Aust. J. Sci.* Suppl. to **17**, No. 3.
Doherty, L., Henize, K. G., and Aller, L. H. (1956). *Ap. J.* Suppl. 2, 345.
Elsasser, H. (1959). *Mém. Soc. Sci. Liège*, [5] **3**, 122.
Elsasser, H., and Haug, U. (1960). *Z. Ap.* **50**, 128.
Feast, M. W. (1953). *Observatory* **73**, 255.
Feast, M. W. (1956). *M.N.R.A.S.* **116**, 583.
Feast, M. W. (1960). *Observatory* **80**, 104.
Feast, M. W. (1961). *M.N.R.A.S.* **122**, 1.
Feast, M. W., and Thackeray, A. D. (1956). *M.N.R.A.S.* **116**, 587.
Feast, M. W., Thackeray, A. D., and Wesselink, A. J. (1955). *Observatory* **77**, 216.
Feast, M. W., Thackeray, A. D., and Wesselink, A. J. (1960). *M.N.R.A.S.* **121**, 337.
Feast, M. W., Thackeray, A. D., and Wesselink, A. J. (1961). *M.N.R.A.S.* **122**, 433.
Fehrenbach, C., and Duflot, M. (1962). *C. R.* **254**, 1382; *E. S. O. Comm.* 1.
Gascoigne, S. C. B. (1961). *Trans. I.A.U. XIA*, 292.
Gascoigne, S. C. B., and Kron, C. E. (1952). *P.A.S.P.* **64**, 196.
Gascoigne, S. C. B. (1960). *Trans. I.A.U. X*, 687, Fig. 5.
Henize, K. G. (1956). *Ap. J.* Suppl. 2, 315.

Henize, K. G., Hoffleit, D., and Nail, V. McK. (1954). *P. N. A. S.* **40**, 365; *Harv. Repr.* No. 387.
Herschel, Sir John (1847). Observations at the Cape of Good Hope.
Hertzsprung, E. (1920). *M.N.R.A.S.* **80**, 782.
Hindman, J. H., McGee, R. X., Caren, A. W. L., (1961). *A. J.* **66**, 45.
Hodge, P. W. (1960). *Ap. J.* **131**, 351.
Hodge, P. W. (1961a). *Ap. J.* **133**, 413.
Hodge, P. W. (1961b). *Ap. J.* Suppl. 57.
Hodge, P. W. (1961c). *Ap. J.* **134**, 226.
Innes, R., and van den Bos, W. H. (1924). *U.O.C.* **61**, 243.
Innes, R., and van den Bos, W. H. (1927). *U.O.C.* **73**, 415.
Johnson, H. L., Sandage, A. R., and Wahlquist, H. D. (1956). *Ap. J.* **124**, 81.
Johnson, H. M. (1959a). *P.A.S.P.* **71**, 301:
Johnson, H. M. (1959b). *P.A.S.P.* **71**, 342.
Kerr, F. J. (1961). *I.A.U. Symp.* No. 15.
Kerr, F. J., *et al.* (1954). *Aust. J. Phys.* **7**, 297.
Kerr, F. J., and de Vaucouleurs, G. (1955). *Aust. J. Phys.* **8**, 508.
Kerr, F. J., and de Vaucouleurs, G. (1956). *Aust. J. Phys.* **9**, 90.
Koelbloed, D. (1956). *Observatory* **76**, 894.
Kraft, R. P. (1961). *Ap. J.* **133**, 39; **134**, 616.
Kron, G. E. (1956a). *P.A.S.P.* **68**, 125.
Kron, G. E. (1956b). *P.A.S.P.* **68**, 326.
Leavitt, H. S. (1907). *Harv. Ann.*, **60**, 87.
Lindsay, E. M. (1958). *M.N.R.A.S.* **118**, 172: Unit of Table III is 0.1 of arc, see de Vaucouleurs, G. (1959). *P.A.S.P.* **71**, 202.
Lindsay, E. M. (1961). *A.J.* **66**, 169.
Mills, B. Y. (1954). *U.R.S.I., Spec. Rept.* No. 3.
Mills, B. Y. (1955). *Aust. J. Phys.* **8**, 368.
Mills, B. Y. (1959). *In* "Handbuch der Physik" (S. Flügge, ed.), Vol. 53, p. 239.
Oort, J. H., and van Woerkom, A. J. (1941). *B.A.N.* No. 338.
Payne Gaposchkin, C. H. (1954). "Variable Stars and Galactic Structure," p. 61. Oxford Univ. Press, London and New York.
Payne Gaposchkin, C. H. (1961). *In* "Vistas in Astronomy" (A. Beer, ed.), Vol. 4. Pergamon, New York.
Piddington, J. H., and Trent, G. H. (1956). *Aust. J. Phys.* **9**, 74.
Radcliffe Observatory (1961). Memorandum 1.
Rodgers, A. W. (1959). *Observatory* **79**, 49.
Russell, H. N. (1956). *In* "Vistas in Astronomy" (A. Beer, ed.), Vol. 2, p. 1177. Pergamon, New York.
Sandage, A. R. (1957). *Ap. J.* **125**, 422.
Sandage, A. R. (1958). *Ap. J.* **127**, 513.
Sandage, A. R., and Eggen, O. J. (1960). *M.N.R.A.S.* **121**, 232.
Schmidt, T. (1957). *Z. Ap.* **41**, 182.
Schwarzschild, M., and Härm, R. (1958). *Ap. J.* **128**, 348.
Sersic, J. L. (1962). *Ann. d'Ap.* **25**, 211.
Shain, C. A. (1958). *I.A.U. Symp.* No. 9, 328.
Shapley, H. (1931a). *Harv. Bull.* No. 881.
Shapley, H. (1931b). *Harv. Bull.* No. 884.
Shapley, H. (1932). *Harv. Bull.* No. 886.

Shapley, H. (1940). *Harv. Bull.* No. 914.
Shapley, H. (1940). *P.N.A.S.* **26**, 541; *Harv. Repr.* No. 207.
Shapley, H. (1951). *P.N.A.S.* **37**, 136; *Harv. Repr.* No. 345.
Shapley, H., ed. (1961). "Galaxies," rev. ed., p. 63. Harvard Univ. Press, Cambridge, Massachusetts.
Shapley, H., and Nail, V. McK. (1951a). *A.J.* **55**, 249.
Shapley, H., and Nail, V. McK. (1951b). *P.N.A.S.* **37**, 15; *Harv. Repr.* No. 344.
Shapley, H., and Nail, V. McK. (1953a). *P.N.A.S.* **39**, 1; *Harv. Repr.* No. 368.
Shapley, H., and Nail, V. McK. (1953b). *P.N.A.S.* **39**, 358; *Harv. Repr.* No. 373.
Shapley, H., and Nail, V. McK. (1955). *P.N.A.S.* **41**, 685; *Harv. Repr.* No. 426.
Smith, H. (1957). *P.A.S.P.* **69**, 137.
Thackeray, A. D. (1951). *Observatory* **71**, 219.
Thackeray, A. D. (1957). Stellar populations. *Spec. Vaticana, Ric. astr.* **5**, 195.
Thackeray, A. D. (1958). *M.N.R.A.S.* **118**, 117.
Thackeray, A. D. (1959). *A.J.* **64**, 437.
Thackeray, A. D. (1962). *M. N. astr. Soc. S. Afr. XXI*, 47, 74.
Thackeray, A. D., and Wesselink, A. J. (1953). *Nature* **171**, 693.
Thackeray, A. D., and Wesselink, A. J. (1955). *Observatory* **75**, 33.
Thackeray, A. D., Wesselink, A. J., and Harding, G. A. (1962). *M.N.R.A.S.* **124**, 445.
Tifft, W. G. (1962). *M.N.R.A.S.* in press.
Vashakidze, M. A. (1955). *Bull. Abastumani Obs.* **18**, 15.
Walker, G. (1962). Cambridge Thesis.
Walraven, T., and Walraven, J. (1960). *B.A.N.* No. 496; also Report to I.A.U., 1961.
Wesselink, A. J. (1956). *M.N.R.A.S.* **116**, 3.
Wesselink, A. J. (1959). *M.N.R.A.S.* **119**, 576.
Wesselink, A. J. (1961a). *M.N.R.A.S.* **122**, 503.
Wesselink, A. J. (1961b). *M.N.R.A.S.* **122**, 509.
Wesselink, A. J. (1962). *M.N.R.A.S.* **124**, 179.
Westerlund, B. (1960). *Uppsala Ann. IV*/**7**.
Westerlund, B. (1961a). *Uppsala Ann. V*/**1**.
Westerlund, B. (1961b). *Uppsala Ann. V*/**2**.
Wilson, R. E. (1917). *Lick Publ.* **13**, 187.
Wolstencroft, R. D. (1962). *Nature* **194**, 1066.
Woolley, R. v.d.R. (1960). *M.N.R.A.S.* **120**, 214.
Woolley, R. v.d.R. (1962). *Roy. Obs. Bull.* No. 58; *Observatory* **82**, 42.

Author Index

Abbot, C. G., *195*
Adams, W. S., 213, *217*
Alden, H. L., 78, *84*
Alexander, J. B., 284, *302*
Allen, C. W., 191, *195*
Aller, L. H., 275, 276, *302*
Arend, S., 137, *195*
Arp, H. C., 44, 65, 74, *84*, 273, 275, 277, 281, 283, 285, 286, 292, *302*

Baade, W., 44, 51, *84*, 283, *302*
Babcock, H. W., 59, 65, *84*
Baldet, F., 253, *261*
Barbier, D., 127, *195*
Barnard, E. E., 4, 21, *40*
Bartlett, *40*
Bauer, E., 133, *195*
Baum, R. M., *40*
Becker, W., 64, *85*
Bemporad, A., 178, *195*
Bigg, E. K., 143, *195*
Bigg-Wither, A. C., 174, *195*
Blaauw, A., 44, *84*, 301, *302*
Blum, E. J., 194, *195*
Bobrovnikoff, N. T., 253, 255, *261*
Boischot, A., 194, *195*
Boshkova, A. I., 240, *261*
Bouška, J., 137, 142, 150, *195*, 252, *261*
Bowen, E. G., 143, *195*
Bracewell, R. N., 143, *196*
Brashear, J. A., *40*
Brossinsky, A., 137, *195*
Brunner, H., 135, *195*
Burnham, J., *217*
Buscombe, W., 265, 268, 295, *302*

Cabannes, J., 94, 129, *195*
Campbell, W. W., 5, *40*
Canright, 7, 10, 12, 13, 16, 18, *40*
Caren, A. W. L., 269, *303*
Cassini, J. D., 135, *195*
Chalonge, D., 127, *195*
Chandrasekhar, S., 52, 64, 74, *84*
Chavira, E., 202, *217*
Chebotarev, G. A., 240, *261*
Cimino, M., 127, *195*
Costain, C. H., 189, *195*
Cowling, T. G., 75, *84*
Cox, J. P., 77, *84*
Crawford, J. A., 76, 83, *84*
Czili, A. B., 143, *196*

Danjon, A., *40*, 125, 133, 151, *195*, *196*
Dartayet, M., 284, *302*
Denning, W. F., *40*
Dessy, J. L., 281, 284, *302*
Deutsch, A. J., 75, *84*
de Vaucouleurs, G., *41*, 151, 162, 183, *197*, *198*, 265, 266, 267, 268, 270, 295, 297, 298, 299, 300, *302*, *303*
Dmitrijev, A. A., 143, *196*
Dobson, G. M. B., 129, *196*
Doherty, L., 275, *302*
Dollfus, A., 186, 189, *196*
Donitsch, N., 137, *196*
Dubois, J., 120, *198*
Dufay, J., 129, *195*
Duflot, M., 289, 292, *302*
Dufour, Ch., 147, *196*

Edjuk, *41*
Edson, J. B., 7, 10, 12, 13, 16, 18, *41*
Eggen, O. J., 67, *84*, 279, *303*
Elsasser, H., 267, 271, *302*
Elsmore, B., 186, 189, *195*, *196*
Elvey, C. T., 59, 65, *84*
Eropkin, D. J., 164, 165, *196*

Fabry, Ch., 179, 184, *196*
Faulkner, D., 276, *302*
Feast, M. W., 271, 272, 273, 276, 277, 278, 283, 288, 289, 290, 296, 297, 298, 300, *302*
Fehrenbach, C., 289, 291, *302*
Feige, J., 202, *217*
Fesenkov, V., 123, *196*
Fisher, W., 152, *196*
Flammarion, C., 147, *196*
Fresa, A., 127, *195*
Frisch, Chr., 104, *196*

Gaposchkin, C. P., 43, *84*
Gascoigne, S. C. B., 265, 268, 279, 282, 295, *302*

Giclas, H. L., 202, *217*
Giuli, R. T., 77, *84*
Glenn, J. H., 135, 166, *196*
Graff, K., 5, *40*
Grant, G., 45, 63, *84*
Greenstein, J. L., 48, 52, 68, 70, 74, *84*, 143, *196*, 206, 207, *217*
Gregory, J., 166, *196*
Guth, Vl., 126, 130, 148, *196*
Guthrie, 3, *40*

Härm, R., 289, *303*
Haffner, H., 67, *84*
Halley, E., 166, *196*
Hamada, T., 64, *84*
Hamid, S. E., 256, *261*
Hansa, M., 142, 144, *196*
Harding, G. A., 277, *304*
Haro, G., 202, 211, *217*
Harris, D. L., 166, *196*, 206, *217*
Hartmann, J., 136, 137, *196*
Hastings, C. S., *40*
Haug, U., 267, *302*
Hausdorff, F., 133, *196*
Heath, M. B. B., *40*
Hefferman, K. J., 143, *196*
Henize, K. G., 269, 275, 286, 287, *302*, *303*
Hepperger, J., 122, 139, *196*
Herbig, G. H., 65, 78, 80, 82, 83, *84*, 215, *218*
Herschel, Sir John, 265, 267, 275, *303*
Herschel, W., 3, *40*
Hertzsprung, E., 296, *303*
Hewish, A., 194, *196*
Heyden, F., 98, *196*
Hibbs, A. R., 166, *196*
Hiltner, W. A., 82, *84*
Hindman, J. H., 269, *303*
Hodge, P. W., 277, 278, 279, 283, 293, *303*
Hoffleit, D., 286, 287, *303*
Huang, S.-S., 66, 77, *84*
Humason, M. L., 202, 215, *217*

Innes, R., 275, *303*
Iriarte, B., 202, *217*

Jeffreys, H., 243, *261*
Johnson, H. L., 82, *84*
Johnson, H. L., 277, *303*
Johnson, H. M., 266, 268, 273, *303*
Joy, A. H., 45, 62, 83, *84*

Kerr, F. J., 296, 297, 298, 299, 300, *303*
Kitamura, M., 65, 66, 67, 68, *84*
Koebcke, F., 137, *196*
Koelbloed, D., 276, *303*
Kosik, S. M., 137, *196*
Kraft, R. P., 44, 46, 48, 52, 56, 59, 65, 66, 74, 76, 83, *84*, *85*, 282, 283, *302*, *303*
Kron, C. E., 279, *302*
Kron, G. E., 268, 276, *303*
Krueger, A. J., *198*
Krzeminski, W., 55, 72, *85*
Kühl, 140, *196*
Kuiper, G. P., *40*, 55, *85*, 172, 173, *196*, 202, 206, *217*

Lahire, P., 135, *196*
Lalande, J. F., 135, *196*
Larsson-Leander, G., 301, *302*
Lemonnier, P. C., 135, *196*
Letfus, V., 150, *196*
Lindsay, E. M., 268, 275, 276, *303*
Link, F., *40*, 105, 120, 123, 126, 128, 129, 130, 132, 133, 134, 135, 137, 139, 141, 142, 143, 147, 148, 150, 152, 153, 154, 156, 157, 162, 164, 165, 166, 167, 172, 173, 176, 178, 179, 186, 191, *195*, *196*, *197*
Linková, Z., 137, 141, 142, *197*
Linnell, A. P., 82, 83, *85*
Luyten, W. J., 202, 203, 206, 211, 214, 215, *217*, *218*
Lyman, Th., 4, 21, *40*
Lyot, B., 186, *197*

McGee, R. X., 269, *303*
Machin, K. E., 191, 194, *197*
McLaughlin, D. B., 43, 70, *85*
Maedler, J. H., 3, *40*, 136, 176, *197*
Malsch, W., 137, *197*
Mannino, G., 64, *85*
Matukuma, T., 243, *261*
Maunder, E. W., 152, *197*
Menzel, D. H., 162, 183, *197*
Mestel, L., 76, *85*
Miczaika, G., 64, *85*
Miller, F. D., 215, *218*

Mills, B. Y., 270, *303*
Mintz, Y., 29, *41*
Moore, P., *40*
Moore, J. G., *198*
Morton, D. C., 67, *85*
Müller, G., 133, 164, 197

Naef, R. A., 8, *41*
Nail, V. McK., 265, 281, 283, 286, 287, 291, *303*, *304*
Neužil, L., 135, 157, 186, *197*

Obaldia, G. de, 253, *261*
Öpik, E. J., 221, 222, 224, 225, 226, 231, 234, 236, 238, 239, 240, 241, 242, 243, 245, 246, 247, 248, 249, 253, 256, *261*, *262*
Oort, J. H., 236, 240, 241, 244, *262*, 285, *303*
Oppolzer, Th. v., 103, 104, *197*
Oterma, L., 237, *262*

Paetzold, H. K., 127, 129, 140, *197*
Pannekoek, A., 179, *197*
Payne Gaposchkin, C. H. (*also* Gaposchkin, C. F.), *43*, *84*, 281, 282, *303*
Perkins, B., 82, *84*
Pickering, E. C., 164, *197*
Piddington, J. H., 270, *303*
Popowkina, *41*
Popper, D. M., 213, *218*
Prendergast, K. H., 55, *85*
Proctor, R. A., 113, *197*

Rabe, W., 5, 6, *41*, 176, *197*
Raimond, J. J., 215, *218*
Ratcliffe, J. A., 187, *198*
Raynard, A. G., 113, *197*
Reaves, G., 127, *198*
Regener, E., 129, *198*
Regener, V. H., 129, *198*
Richter, N., 5, *41*, 255, *262*
Rodgers, A. W., 268, *303*
Roman, N. G., 301, *302*
Rosino, K., 64, *85*
Rougier, G., 120, *198*
Ruddy, H. E., *41*
Russell, H. N., 4, 5, 21, *41*, 167, 176, 177, 179, *198*, 287, *303*
Růžičková, B., 137, *195*

Sahade, J., 65, *85*
Salpeter, E., 64, 74, 77, *84*, *85*
Sampson, R. A., 164, *198*
Sandage, A. R., *303*
Sandner, W., *41*
Sandage, A. R., 67, 83, *85*, 275, 279, 296, 301, *302*, *303*
Sanford, R. F., 46, *85*
Saussure, M. de, 123, 140, *198*
Sauvenier-Goffin, E., 52, *85*
Schatzman, E., 52, 75, *85*, 241, *262*
Schmidt, M., 253, 255, *262*
Schmidt, T., 287, *303*
Schoenberg, E., *40*, 159, 178, *198*
Schroeter, J. H., 3, 29, *41*
Schwarzschild, M., 63, 83, *85*, 289, *303*
Seeliger, H., 122, 139, *198*
Sersic, J. L., 275, *303*
Shain, C. A., 270, *303*
Shapley, H., 265, 272, 276, 281, 283, 287, 291, 294, *303*, *304*
Sharonov, V. V., *41*, 167, *198*
Sinton, W. M., *41*
Slaughter, C. D., *217*
Slipher, E. C., 7, *41*
Smart, W. M., 64, *85*
Smith, F. G., 191, 194, *197*
Smith, H., 289, *304*
Sotkin, I. T., *41*
Stephenson, C. B., 215, *218*
Strand, K. A., 64, *85*
Strong, J., *41*
Struve, G., *41*
Suchomlinov, 174, *198*
Švestka, Z., 121, 142, 150, *198*
Symons, G. L., 147, *198*

Thackeray, A. D., 272, 273, 276, 277, 278, 279, 280, 283, 284, 287, 288, 289, 291, 296, 297, 298, 300, 301, *302*, *304*
Thomas, H., *217*
Tifft, W. G., 279, 284, 295, 288, 292, *304*
Tombaugh, C. W., 8, *41*
Trent, G. H., 270, *303*
Trouvelot, E., *41*

Van de Hulst, H. C., 190, *198*
van den Bos, W. H., 275, *303*
Van Gent, H., 80, *85*

van Rhyn, P. J., 215, *218*
van Woerkom, A. J., 285, *303*
Vanýsek, V., 253, *262*
Vashakidze, M. A., 273, *304*
Vassy, E., 153, *198*
Vaucouleurs, G. de, *see* de Vaucouleurs, G.
Venkateswaran, S. V., 159, *198*
Ventosa, V., *41*
Vigroux, E., 127, 131, *198*

Wahlquist, H. D., *303*
Walker, G., 273, *304*
Walker, M. F., 46, 47, 48, 51, 52, 56, 70, 82, 83, *85*, 127, *198*
Wallerstein, G., 65, *84*, 85
Walraven, J., 274, 291, *304*
Walraven, T., 274, 291, *304*
Weaver, H. F., 301, *302*
Weekes, K., 187, *198*
Wesselink, A. J., 269, 272, 273, 276, 277, 278, 283, 284, 285, 287, 288, 289, 291, 296, 297, 298, 300, *302*, *304*
Westerlund, B., 278, 291, 292, 295, *304*
Whipple, F. L., 166, *198*, 241, 243, 256, 259, 260, *261*
Whitfield, G. R., 189, *195*
Wilson, R. E., 296, *304*
Winget, 7, 10, 12, 13, 16, 18, *40*
Wirtz, C. W., 137, *198*
Wolf, R., 166, *198*
Wolkow, W. W., *41*
Wolstencroft, R. D., 273, *304*
Woolley, R. v. d. R., 277, 282, *304*
Wright, 7, 10, 12, 13, 16, 18, *40*

Young, C. A., *42*

Zacharov, I., 142, 144, *198*
Zwicky, F., 202, 215, *217*

Subject Index

A

Adonis, 233, 245
AE Aqr, 54, 76, 83
Albedo, lunar, 234
Algol-type variables, 82
α CMa B, 211
α CMi B, 211
Angular deflection, probability of, 224
Apollo, 233, 245
  asteroids, 249
  group, 220, 231, 242, 244, 245, 246, 250, 251, 253, 259, 261
    origin of, 244
  -type orbits, 252
Artificial satellites, 161
  eclipses of, 154, 158, 159
    photometry of, 157
  (of other planets) eclipse of the Sun observed from, 160
  solar illumination of, 156
  topocentric brightness of, 158
Asteroids, 219, 231, 236, 237, 238, 241
  Adelaide, 237, 238, 239
  Aethra, 235
  Albert, 235
  Alinda, 235
  Amor, 235
  Asplinda, 239
  Atami, 235
  Atlantis, 235
  Beira, 235
  Betulia, 235
  Bononia, 239
  Brucia, 235
  Eros, 235
  Francette, 239
  Ganymed, 235
  Hela, 235
  Hermes, 233, 245
  Hidalgo, 232, 238, 239, 244
  Hilda family, 238, 239, 240, 245
  Icarus, 234
  Ingeborg, 235
  Ismene, 239
  Isora, 235
  Kasan, 235
  Kepler, 235
  Kirkwood, 239
  Marina, 239
  Ocllo, 235
  Porzia, 235
  Potomac, 239
  Renzia, 235
  Rita, 239
  Rosina, 235
  Schorria, 235
  Simeisa, 239
  Sirene, 235
  Siva, 235
  Sonja, 235
  Tuckia, 238, 239
  Venusia, 238, 239
  Zomba, 235
  1929 SH, 235
  1938 BC, 239
  1938 UO, 235
  1939 FE, 239
  1950 LA, 235
  1951 QZ, 235
  1951 SA, 235
  1953 EA, 235
  1953 RA, 235
  1957 NA, 235
  of Mars, 246, 261

B

β Lyr variables, 287
Bruce proper motion survey, 201, 214

C

Cataclysmic double stars, 77
Cataclysmic variables, 43, 56
Cat's-eye photometer, 125, 152
Cepheids, 281
  classical, 285, 301
Close binary systems, "non-explosive", 77
Close passage and collision, probability of, 222
Coma cluster, 215
Cometary nuclei, 219, 220, 241, 256
Comets, 220, 221, 230, 231, 236, 241
  De Vico Swift, 237
  Encke, 233, 243, 244, 258, 259, 260, 261
  Giacobini-Zinner, 237
  Grigg-Skjellerup, 237, 250, 258
  Halley, 232
  Harrington-Abell, 255
  Neujmin (2), 237, 238
  Oterma, 237
  Oterma (1934), 237
  Oterma (1950), 237
  Oterma (1965), 237
Schwassmann-Wachmann, 237
  Tempel (1), 237
  Tempel (2), 237
  Tempel 1866 I, 232
Timmers 1946a, 255
Tuttle 1862 III, 232
  Vaisälä 1939 IV, 232
  Vaisälä 1942 II, 232
  Wilson Harrington 1949 III, 233, 242, 243, 244, 250, 261
  1949 II, 252
  1949 III, 242, 243
  diameters of, 253
  magnitudes of, 253
  nuclei, diameters of, 255
  origin of, 241
  periodic, 236
Coriolis forces, 55
Crab nebula, 189, 194

D

Danjon's sawtooth curve, 152
Danjon's scale, 152
Degenerate stars, 201
Differential refraction, 95
DI Lac, 68, 69, 83
30 Doradus complex, 265, 266, 268
30 Doradus nebula, 276, 287, 289
DQ Herculis, 47, 48, 49, 50, 51, 53, 54, 55, 68, 69, 70, 74, 75, 76, 77, 80, 81, 82, 83
Dwarf novae, 43, 44, 45

E

Earth, 225, 228, 232, 233, 234, 242
Echo satellite, 158
Elipses,
  occultation, 89
  phenomena, 88, 89
    in radio astronomy, 185
  transit, 89
Eclipsing binaries, 281, 287
Einstein's relativity theory, 213
Encounters, interactions at, 221
Encounters, survival in, 221
ϵ Aurigae, 47
Eridani B, 200, 202, 206, 207, 210, 211, 213, 215
η Aquarids, 232
η Car, 57, 287, 289
EX Hya, 57, 62
EY Cyg, 57, 62, 64

F

Fermi threshold, 52
Fresnel's bands, 184

G

Geminids, 233, 243, 244, 250
Giacobinids, 232
GK Per, 68, 69, 70
GRW + 70°8247, 207

H

HD 7099, 299
HD 7583, 290
HD 33579, 289, 290, 299
HDE 269788, 292
Hermes, asteroid, 233, 245

Hertzsprung gap, 277
Hidalgo, asteroid, 232, 238, 239, 244
High absorbing layers, 96, 97, 130, 133, 140, 141, 143, 144
HL 4, 216
HV 2241, 287
Hyades cluster, 210, 215
HZ 9, 210, 216

I

IC 443, 189
IC 4665, 215
Icarus, asteroid, 234
Impact parameters, 223
Irregular galaxies, 265
Irregular variables, 287

J

Jacobi's integral, 55
Jovian satellites, 165
  eclipse elements of, 164
  eclipses of, 164
Jupiter, 164, 165, 225. 228, 231, 236, 237, 238, 239, 241, 250, 257, 258, 259
  elements, 164
  family, 257, 258, 261
  gravitational field of, 236
  group, 236
  mean distance of, 239
  orbit of, 220, 236, 245, 251, 259
  perihelion of, 238, 239, 242, 245

K

Katmai eruption, 148
Krakatoa, 148

L

L(uyten) 40-109, 216
L 97-12, 216
L 153-31, 207
L 587-77, 211
L 879-2/3, 211
L 879-14, 207, 216
L 930-80, 207
L 1046-18, 211
Lagrangian surface, 68
  inner, 54, 62, 65, 83
Lagrangian point, inner, 55, 62
Lambert law, 159
LB 210, 216
LDS 275, 211, 216
LDS 749 B, 207
Leonids, 232
Lommel-Seeliger law, 159
Long-period variables, 287
LP 321-98, 210, 216
LP 357-186, 210
Lunar atmosphere, 188
Lunar ionosphere, 190
Lunik III, 154

M

M(essier) 3, 279
M 31, 286, 287
M 34, 215
M 36, 215
M 38, 215
M 39, 215
M 41, 215
M 67, 215, 293
M 92, 279
Magellanic clouds, 264, 266, 275, 280, 288, 301
  cepheids, 283
  distance of, 274
  dust, reddening properties of, 273
  dust, reddening and absorption by, 275
  dynamics of, 296
  emission nebulae in, 275, 276
  frequency distribution of colour excesses, 272
  large cloud, 265, 266, 267, 268, 271, 272, 275, 277, 278, 283, 288, 289, 294, 295, 296, 297, 298, 301
    clusters, 283
    external loop of, 269
    motions within, 296
    polarization of, 273
    variables, 282
  Me variables in, 301
  optical structure of, 265
  small cloud, 265, 267, 268, 271, 272, 275, 277, 283, 288, 289, 293, 296

cepheids, 283
motions within, 299
wing on, 269
spiral loops, 266
Mare Imbrium, 255
Mars, 160, 162, 180, 182, 225, 228, 231, 233, 234, 235, 236, 242, 245, 250, 261
asteroids, 246, 261
orbit of, 220
Mercury, 228, 233, 234
transits of, 166
Meteoritic accretion, 143
Meteoritic dust, 142
Moon, eclipses of, 100, 102, 113, 133, 179
catalogue of, 128
changes in the brightness of, 150
cone of umbra, 100
diffusion, illumination by, 120
disappearance (of the Moon) during, 146
earth-shine, 153
future eclipses, 103
geographic circumstances of, 115
meteorological influences on, 148
penumbra, 100, 102
penumbral cone, 100
photometry of, 124
shadow, flattening of, 137
shadow, increase of, 139
terrestrial shadow, 135, 141
theories of, 122, 123
tropospheric influences on, 145
umbra, 100, 102
Mt. Blanc, 133
Mt. Pelée, 148
Multiple meteor craters, 257

N

N Dor 1948, 287
N Hyi 1935, 286
Neptune, 221, 229, 232, 238, 239, 240
NGC 121, 279, 280, 284, 285, 288, 292, 293, 294
NGC 129, 215
NGC 333, 277
NGC 339, 279
NGC 361, 279
NGC 419, 279, 292, 293
NGC 458, 277
NGC 752, 215
NGC 1466, 279, 284
NGC 1511, 286
NGC 1783, 179, 288
NGC 1810, 277
NGC 1818, 277
NGC 1835, 280
NGC 1856, 283
NGC 1866, 277, 283
NGC 1978, 279, 284
NGC 2004, 277, 278
NGC 6365, 279
NGC 6885, 215
North America nebula, 205
Novae, 68, 75, 281, 286
dwarf, 43, 44, 45
(DI) Lac, 83
ordinary, 44
repeating, 44, 46

O

O-B associations, 44
Occultations of radio sources by the solar corona, 190
Occultations of stars by planets, 179
Orbital elements, 61
Orion nebula, 276
Orionids, 142
Ozone layer, 129, 130

P

P Cygni, 288
effect, 299
-type emission, 289
Period-luminosity relation, 281
Perseids, 142, 232
Pic-du-Midi, 133
Planetary atmospheres, action of, 90
Pleiades, 210, 215, 276, 277
Pluto, 221, 238, 239
Population I stars, 214, 288, 298
Population II cepheids, 274
Population II stars, 44, 208, 288
Praesepe, 67, 209, 210, 215
age of, 67
Procyon, companion to, 210

R

Radial velocities, 21-cm, 270
"Radio limb" of the Sun, 193
Rayleigh-Cabannes law, 94, 133
Rayleigh's atmosphere, 94, 96, 106, 109, 134, 148, 150
Rayleigh scattering, 22
Red shift, 213
Regulus, 162, 184
ρ Ophiuchi cloud, 205, 214
Roche limit, 243
Rocket effect, 260
Rocket soundings, 106
RR Lyrae variables, 78, 80, 208, 274, 279, 281, 284, 301
  apparent magnitudes of, 285
RU Peg, 56, 57, 61, 62, 63, 64
RV Tau variables, 301
RX And, 57, 60, 62, 64
RY Dor 1962, 287

S

S Dor, 277, 287, 289
St. Vincent, 148
Saturn, 228, 229, 232, 239
Seeliger's sector, 140
Shadow, actual, 91, 93, 108
Shadow, auxiliary, 91, 93, 106, 108, 163
Shadow, normal densities of, 108
Sirius, 200
  companion to, 200, 201, 205, 210, 211, 215
Sirius B, 213
Smithsonian Solar Observatory, 12
Solar corona, eclipse by, 192, 194
Solar image, formation of, 168
SS Aurigae, 57, 60, 62, 64
SS Cygni, 45, 47, 54, 55, 46, 57, 62, 63, 64, 65, 75
SS Cygni stars, 43, 44, 208
Statistical parallax, 64
Stellar perturbations, 241
SU UMa, 57
Sun, refraction images of, 115
Supernovae, slow, 287
Supernovae, type I, 44
Supernovae, type II, 44

T

T Aurigae, 70
T Corona Borealis, 46, 47, 54, 55, 56, 68, 70, 74, 75, 77, 83
T Leo, 57, 60
Taurids, 233
θ Car, 277
Transits of planets, 166
47 Tuc, 292
TX Cnc

U

U Geminorum, 44, 55, 57, 59, 60, 62, 64, 65, 66, 70
  stars, 43, 44, 56, 57, 63, 66, 73, 75, 78
  variables, 48, 58, 65, 66, 67, 68, 77, 83
Uranus, 229, 232
Ursa Major cluster, 215
UX UMa, 80, 82, 83
UZ Ser, 65

V

V 603 Aql, 70
Van Maanen's star, 205
Variable stars,
  AE Aqr, 54, 76, 83
  DI Lac, 68, 69, 83
  DQ Her, 47, 48, 49, 50, 51, 53, 54, 55, 68, 69, 70, 74, 75, 76, 80, 81, 82, 83
  ϵ Aur, 47
  η Aqr, 232
  η Car, 57, 287, 289
  EX Hya, 57, 62
  EY Cyg, 57, 62, 64
  GK Per, 68, 69, 70
  P Cyg, 288
  RR Lyr, 78, 80, 208, 274, 279, 281, 284, 301
  RU Peg, 56, 57, 61, 62, 63, 64
  RV Tau, 301
  RX And, 57, 60, 62, 64
  RY Dor, 287
  S Dor, 277, 287, 289
  SS Aur, 57, 60, 62, 64
  SS Cyg, 45, 47, 54, 55, 56, 57, 62, 63, 64, 65, 75
  SU UMa, 57

T Aur, 70
T CrB, 46, 47, 54, 55, 56, 68, 70, 74, 75, 77, 83
T Leo, 57, 60
θ Car, 277
TX Cnc, 67, 68
U Gem, 44, 55, 57, 59, 60, 62, 64, 65, 66, 70
UX UMa, 80, 82, 83
UZ Ser, 65
V 603 Aql, 70
VV Pup, 78, 79, 80, 81, 82, 83
W UMa, 65, 66, 68
WZ Sge, 52, 69, 70, 71, 72, 73, 74
Z Cam, 57, 60, 62, 64
Venus, 1, 122, 160, 162, 166, 180, 228, 232, 233, 234
  angular radius of, 165
  atmosphere os, 2, 17, 22, 23, 24, 25, 27, 29, 31, 40, 161, 162, 172, 175
  aureole, 171
    on the limb of, 169
  axis of rotation, 27, 173
  cusp extensions, 3, 5, 7, 8, 11, 15, 20, 39, 176
  cusps of, 17
    extent of, 177
  inferior conjunction of, 9, 36, 174
  occultation of Regulus by, 183
  orbit plane, 38
  refraction in the atmosphere, 167
  rotation of, 22
  transits of, 166, 167, 174, 177
  twilight phenomena of, 2, 29, 30
  upper scattering layer, 39
  visible surface of, 168
VV Pup, 78, 79, 80, 81, 82, 83

W

W UMa, 65, 66, 68
  stars, 65, 66, 67, 68
W 489, 207, 216
Whipple's mixture, 241
White dwarfs, 52, 54, 70, 199, 201, 209
  in clusters, 215
  masses of, 210
Wolf-Rayet stars, 289
WZ Sge, 52, 69, 70, 71, 72, 73, 74

Z

Z Cam, 57, 60, 62, 64
  stars, 44
Zodiacal dust, 255